Phytochemical Profiling of Iranian Plants, and ECD Calculation as Tool for Establishing the Absolute Configuration of New Natural Products

Inauguraldissertation

zur

Erlangung der Würde eines Doktors der Philosophie

vorgelegt der

Philosophisch-Naturwissenschaftlichen Fakultät

der Universität Basel

von

Samad Nejad Ebrahimi

aus Tabriz, Iran

Basel, 2013

Genehmigt von der Philosophisch-Naturwissenschaftlichen Fakultät
auf Antrag von

Prof. Dr. Matthias Hamburger
Prof. Dr. Jean-Luc Wolfender

Basel, den 22.5.2013

Prof. Dr. Jörg Schibler

Dekan

creative commons

Attribution-Noncommercial-No Derivative Works 2.5 Switzerland

---

You are free:

to Share — to copy, distribute and transmit the work

Under the following conditions:

Attribution. You must attribute the work in the manner specified by the author or licensor (but not in any way that suggests that they endorse you or your use of the work).

Noncommercial. You may not use this work for commercial purposes.

No Derivative Works. You may not alter, transform, or build upon this work.

- For any reuse or distribution, you must make clear to others the license terms of this work. The best way to do this is with a link to this web page.
- Any of the above conditions can be waived if you get permission from the copyright holder.
- Nothing in this license impairs or restricts the author's moral rights.

Your fair dealing and other rights are in no way affected by the above.

This is a human-readable summary of the Legal Code (the full license) available in German:
http://creativecommons.org/licenses/by-nc-nd/2.5/ch/legalcode.de

Disclaimer:
The Commons Deed is not a license. It is simply a handy reference for understanding the Legal Code (the full license) — it is a human-readable expression of some of its key terms. Think of it as the user-friendly interface to the Legal Code beneath. This Deed itself has no legal value, and its contents do not appear in the actual license. Creative Commons is not a law firm and does not provide legal services. Distributing of, displaying of, or linking to this Commons Deed does not create an attorney-client relationship.

Quelle: http://creativecommons.org/licenses/by-nc-nd/2.5/ch/deed.en Datum: 3.4.2009

To my wife,

Eli

“ If you cannot calculate something accurately, you probably don’ t understand it very well. ”

Lord Kelvin (1824-1907)

TABLE OF CONTENTS

List of abbreviations

96-DWP	96-Deep well plate
AC	Absolute configuration
B3LYP	Becke three-parameter exchange, Lee-Yang-Parr correlation
BLYP	Becke exchange, Lee-Yang-Parr correlation functional
BW	Boltzmann weighting
CAS	Central authentication service
CD	Circular dichroism
CE	COTTON effect
CI	Configuration interaction
CIS	CI with singles
COSY	Correlation spectroscopy (an NMR technique)
CPCM	The conductor-like polarizable continuum model
DNP	Dictionary of natural products
ECD	Electronic circular dichroism
ELSD	Evaporative light scattering detection
FDA	Food and drug administration
$GABA_A$	Gammamaniobutyric acid type A receptor
HF	Hartree Fock
HMBC	Heteronuclear multiple bond correlation (an NMR technique)
HPLC	High performance liquid chromatography
HSQC	Heteronuclear single-quantum correlation
HTS	High-throughput screening
IC_{50}	The half maximal inhibitory concentration
IHP	Iranian herbal pharmacopoeia
IR	Infrared spectroscopy
ITM	Iranian traditional medicine
MD	Molecular dynamics
MMFF	Molecular mechanics force field
MS	Mass spectrometry
NDA	New drug approval
NMR	Nuclear magnetic resonance spectroscopy
NOE	Nuclear Overhauser effect
NOESY	Nuclear Overhauser effect spectroscopy (an NMR technique)
NP	Natural product
OPLS	Optimized potentials for liquid simulations

OR	Optical rotation
ORD	Optical rotatory dispersion
PDA	Photo-diode array detector
PES	Potential energy surface
QM	Quantum mechanics
$\boldsymbol{R_{len}}$	Rotatory strength *R* in dipole length
$\boldsymbol{R_{vel}}$	Rotatory strength *R* in dipole velocity
SCRF	Self-consistent reaction field
TDDFT	Time dependent density functional theory
TOCSY	Total correlation spectroscopy (an NMR technique)
TOF	Time-of-flight
UV	Ultraviolet light spectrum
VCD	Vibrational circular dichroism
VIS	Visible light *spectrum*

Summary

Biosynthesis of secondary metabolites occurs by concerted multistep reactions in a biological (chiral) environment. Therefore, many natural products (NPs) are chiral molecules having one or several stereocenters. The biological activity of NPs and drug like molecules is generally dependent on the stereochemistry of a molecule. Thus NPs are uniquely predestined to interact with biomacromolecules, and this explains their importance as drug leads.

The complete structure elucidation of a new secondary metabolite involves determination of constitution, assignment of relative and, finally, absolute configuration. Constitution and relative stereochemistry of molecules can be typically derived from UV-Vis, MS and NMR spectral data. The *J*-based configurational analysis uses proton-proton couplings ($^3J_{HH}$) to assign the relative configuration of adjacent stereogenic centers in conformationally flexible molecules. The nuclear Overhauser effect (NOE) experiment is also extensively used, primarily, to define the stereochemistry within a molecule. Assignment of the absolute configuration of these chiral carbons is crucial to define the 3D structure of a molecule, and this can be a significant challenge in the structural elucidation of new metabolites.

Chiroptical methods such as electronic circular dichroism (ECD) have been used for assignment of absolute configuration since several decades, but were limited in their applicability. The rapidly developing computer technologies and a broad diversity of quantum chemical methods available now permit to study virtually any molecule by selecting the most appropriate method for each particular case, with regard to the desired accuracy, time consumption, and available computer resources. The progress in the areas of conformational analysis and quantum chemical calculation of molecular properties has widened the applicability of ECD in unambiguous determination of chiral molecules. This is especially valuable for the analysis of new molecular entities when chemical synthesis of the compound is not an option. The good agreements between the experimental and simulated ECD curves of these compounds provided the unambiguous configurational establishment.

The aim of the present work was phytochemical investigation of Iranian medicinal plants, in order to identify bioactive compounds responsible for inhibition of *Plasmodium falciparum*. About 120 plant extracts were prepared from 40 plants traditionally used in Iranian traditional medicine (ITM) to treat malaria and screened for *in vitro* activity against *P. falciparum.*

In a preliminary screen, the lipophilic extracts of *Artemisia persica*, *Salvia hydrangea*, *and Salvia sahendica* roots potently inhibited the growth of *P. falciparum* K1 strain. HPLC-based activity profiling led to localizing and identification of the active constituents of these plant extracts. Their structures were elucidated by a combination of powerful analytical methods such as HPLC-PDA-TOF-MS, and microprobe NMR. In order to determine the absolute configurations of isolated chiral compounds, quantum chemical calculation of ECD spectra in combination with experimental ECD studies were used. This methodology successfully applied to establish the ACs of structurally diverse and conformationally rigid or flexible molecules

including sesquiterpene coumarins, bisabolol sesquiterpenes, diterpenoids and complex isoprenoids with novel scaffolds.

Activity profiling of the active *n*-hexane extract from the roots of *Salvia sahendica* against malaria resulted in the identification of eight abietane-type diterpenoids. *In vitro* biological activities of isolated pure compounds were determined against *P. falciparum* L& strain and *Trypanosoma brucei rhodesiense* STIB 900 strain, and cytotoxicity in rat myoblast (L6) cells was determined. The IC_{50} values of the compounds ranged from 0.8 µM to over 8.8 µM against *P. falciparum*, and from 1.8 µM to over 32.3 µM against *T. brucei rhodesiense*. The cytotoxic IC_{50} values ranged from 0.5-15.5 µM. Selectivity indices for *P. falciparum* were from 0.1 to 18.2, and 0.1 to 1.2 for *T. brucei rhodesiense*. The absolute configuration of sahandol (**3**) and sahandone (**4**) were assigned by comparison of experimental and calculated ECD spectra and optical rotation values.

HPLC based activity profiling of the EtOAc extract of the aerial parts of *Artemisia persica* resulted in the isolation of a series of bisabolol oxide esters. Relative configurations of cyclohexenone/cyclohexene and tetrahydropyran moieties of **5**–**9** were established on the basis of $^{3}J_{H-H}$ coupling constants and NOE difference spectra. Absolute configurations of **5**–**9** were established by comparison of experimental ECD spectra with simulated ECD data for possible stereoisomers, by TDDFT. Assignment of AC by ECD calculation is possible even though relative stereochemistry cannot establish by NMR techniques due to the flexibility of the molecule. Bisaboloids **5**–**8** exhibited *in vitro* antimalarial activity against *Plasmodium falciparum*, with IC_{50} values ranging from 2.8 to 20.1 µM, and selectivity indices (SI) in L-6 cells of 3.7–11.9.

Hydrangenone (**15**), perovskone (**16**) and salvadione (**17**) three new triterpenoids with rare carbon skeletons were isolated from aerial parts and flowers of *Salvia hydrangea* endemic plant to Iran. These compounds indicated significance *in vitro* activity against *P. falciparum* with IC_{50} values 1.40, 0.18 and 1.43 µM, respectively and acceptable selectivity index in rat myoblast L-6 cells.

Zusammenfassung

Die Biosynthese von Sekundärmetaboliten findet innerhalb von konzentrierten, mehrstufigen Reaktionen in einer biologischen (chiralen) Umgebung statt. Aus diesem Grund, sind viele Naturstoffe (NPs) chirale Moleküle, die ein oder mehrere chirale Zentren aufweisen. Die biologische Aktivität von Naturstoffen und wirkstoffähnlichen Molekülen ist normalerweise abhängig von der Stereochemie des Moleküls. Deshalb sind Naturstoffe besonders prädestiniert mit Biomakromolekülen zu interagieren, das erklärt ihre Bedeutung als Wirkstoffe.

Eine vollständige Strukturaufklärung von Sekundärmetaboliten beinhaltet die Bestimmung des Aufbaus, die Bestimmung der relativen und schlussendlich der absoluten Molekülkonfiguration. Den Molekülaufbau und seine relative Stereochemie kann man üblicherweise mittels UV-Vis, MS und NMR Spektraldaten ableiten. Die *J*-basierte konfigurative Analyse nutzt Proton-Proton Kopplung ($^3J_{HH}$), um die relative Konfiguration von angrenzenden stereogenen Zentren in konformativ flexiblen Molekülen zu bestimmen. Das Kern-Overhauser-Effekt Experiment (NOE) wird in erster Linie umfangreich angewendet um die Stereochemie innerhalb der Moleküle zu definieren. Die Bestimmung der absoluten Konfiguration dieser chiralen Kohlenstoffe ist entscheidend für die molekulare dreidimensionale Strukturaufklärung, dies kann eine echte Herausforderung sein besonders bei der Strukturaufklärung von neuen Metaboliten.

Chiroptische Methoden wie elektronischer zirkularer Dichroismus (ECD) wurden schon vor Jahrzehnten für die absolute Konfiguration angewandt, sind aber in ihrer Anwendbarkeit limitiert. Die sich schnell entwickelnden computerunterstützten Technologien und eine umfassende Vielfalt von quantenchemischen Methoden erlauben virtuelle Studien eigentlich aller Moleküle unter Nutzung der geeigneten Methoden je nach Struktur die man untersucht, betreffend der erwünschten Präzision, Zeitverbrauch und verfügbaren Computerressourcen. Der Fortschritt in den Bereichen der Konfomationsanalyse und quantenchemische Berechnungen von molekularen Eigenschaften hat die Anwendbarkeit für ECD für die eindeutige Aufklärung von chiralen Strukturen erweitert. Das ist besonders wertvoll für die Analyse von neuen molekularen Einheiten, wenn die chemische Synthese des Stoffes keine Option darstellt. Die gute Übereinstimmung zwischen experimentellen und simulierten ECD-Kurven dieser Verbindungen führte zu der eindeutigen Strukturdarstellung.

Das Ziel der vorliegenden Arbeit ist die phytochemische Untersuchung von iranischen Medizinalpflanzen um bioaktive Verbindungen zu identifizieren die für die Hemmung von *Plasmodium falciparum* verantwortlich sind. Es wurden 120 Pflanzenextrakte aus 40 Pflanzen, die man in der iranischen traditionellen Medizin (ITM) gegen Malaria einsetzt, vorbereitet und für die *in vitro* Aktivität gegen *P. falciparum* gescreent.

In einem einführenden Screen hemmten die lipophilen Extrakte aus *Artemisia persica*, *Salvia hydrangea* und *Salvia sahendica* Wurzeln das Wachstum des *P. falciparum* K1-Stamms. Die HPLC-basierte Aktivitätsprofiling führte zur Lokalisierung und Identifizierung von aktiven Komponenten aus diesen Pflanzenextrakten. Ihre molekularen Strukturen wurden mittels analytischer Methoden wie HPLC-PDA-TOF-MS und NMR aufgeklärt. Um die absolute

Konfiguration (ACs) von isolierten chiralen Verbindungen zu bestimmen, wurden quantenchemische Berechnungen von ECD Spektren in Kombination mit experimentellen ECD Studien angewandt. Diese Methode wurde erfolgreich angewandt um die absoluten Konfigurationen von strukturell verschiedenen und konformativ starren oder flexiblen Molekülen zu ernitteln, einschliesslich Sesquiterpen Cumarine, Bisabolol-Sesquiterpene, Diterpenoide und komplexen Isoprenoiden mit neuartigen Baugerüsten.

Die Aktivitätsprofile der aktiven n-Hexan Extrakte aus Wurzeln von *Salvia sahendica* gegen Malaria zeigten acht abietane-typ Diterpenoide. Biologische *in vitro* Aktivität von isolierten reinen Verbindungen wurden gegen *P. falciparum* L& Stamm und *Trypanosoma brucei rhodesiense* STIB 900 Stamm bestimmt, ebenso wurde die Zytotoxizität in Myoblasten der Ratte (L6) bestimmt. Die IC_{50} Werte der Verbindungen reichten von 0.8 µM bis über 8.8 µM gegen *P. falciparum* und von 1.8 µM bis über 32.3 µM gegen *T. brucei rhodesiense*. Die zytotoxischen IC_{50} Werte reichten von 0.5-15.5 µM. Der Selektivitätsindex für *P. falciparum* war zwischen 0.1 und 18.2, und zwischen 0.1 und 1.2 für *T. brucei rhodesiense*. Die absolute Konfiguration von Sahandol (**3**) und Sahandone (**4**) wurde bestimmt durch den Vergleich von experimentellen und berechneten ECD Spektren und optischen Rotationswerten.

HPLC-basierte Aktivitätsprofile des EtOAc Extrakts der oberirdischen Teile der *Artemisia persica* führten zur Isolierung einer Reihe von Bisabololoxidestern. Die relative Konfiguration von Cyclohexenone/Cyclohexene und Tetrahydropyran Resten von **5-9** wurden ermittelt durch $^{3}J_{H-H}$ Kopplungkonstanten und NOE Differenzspektren. Die absolute Konfiguration von **5-9** wurden mittels TDDFT durch den Vergleich von experimentellen ECD Spektren mit simulierten ECD Daten für möglichen Stereoisomere ermittelt. Die Zuordnung der absoluten Konfiguration mittels ECD Berechnungen ist möglich obwohl die relative Stereochemie aufgrund der Flexibilität der Moleküle nicht per NMR ermittelt werden kann. Bisaboloide **5-8** zeigten *in vitro* Antimalaria-Aktivität gegen *Plasmodium falciparum* - die IC_{50} Werten reichten von 2.8 und 20.1 µM und der Selektivitätsindex (SI) in L-6 Zellen von 3.7-11.9.

Hydrangenone (**15**), Peroyskone (**16**) und Salvadione (**17**) sind drei neue Triterpenoide mit einem seltenen Kohlenstoffgerüst die aus den oberirdischen Teilen und Blüten von *Salvia hydrangea*, einer endemischen Pflanze im Iran, isoliert wurden. Diese Verbindungen zeigten signifikante *in vitro* Aktivität gegen *P. falciparum* mit IC_{50} Werten von 1.40, 0.18 and 1.43 µM, und einen akzeptablen Selektivitätindex in Myoblasten der Ratte (L-6).

1. Aim of the work

A large number of drugs are directly or indirectly derived from natural products, and the search for lead structures, notably for anticancer drugs, still heavily depends on natural product chemistry.[1, 2] NPs are uniquely predestined to interact with biomacromolecules, and this explains their importance as drugs leads. It is well known that the absolute configuration of natural or synthetic chiral substances has a remarkable role on their biological activity.[3] Actually, the building blocks of biological molecules (enzymes, proteins, carbohydrates, amino acids, etc.) and many secondary metabolites exist in nature in a single enantiomeric form. Due to different interactions between a chiral drug and its binding site, two enantiomers of a drug may have different effects. In this case, one enantiomer appear as pharmacologically active (e.g. *R*-salbutamol), whereas the other enantiomer is pharmacologically inactive (e.g. *S*-salbutamol),[4] and in the worst case some enantiomers are even toxic (e.g. Thalidomide). Since ligand-receptor interactions play a central role in life processes, a better understanding of chiroptical properties is critical for a complete study of biological activity on molecular basis.

The complete structure elucidation of a new secondary metabolite involves determination of constitution, assignment of relative and, finally, absolute configuration. Constitution and relative stereochemistry can be typically derived from UV-Vis, MS and NMR spectral data.[5] Determination of relative configuration of chiral elements is strictly related to determination of overall the molecular conformation. These features are determined by aid of NMR, by recording of three dimensional sensitive data like scalar *J*-coupling ($^3J_{HH}$ and $^3J_{CH}$), and NOE effects. However; NMR is unable to discriminate between two enantiomers. In order to solve this problem several methods have been proposed, chemical methods (total synthesis, derivatization, degradation) and X-Ray diffraction analysis being the most reliable ones. The first approach requires a long process for transforming the compound under study into one with a known absolute configuration. The diffraction technique, on the other hand, has strong limitations: the necessity of having single crystals, and the availability of expensive and complex equipment. Chiroptical methods such as optical rotation (OR), electronic circular dichroism (ECD) have been used for assignment of absolute configuration since several decades, but were limited in their applicability.[6, 7] Recent progress in computer technologies, the areas of conformational analysis and quantum chemical calculation has widened the applicability of chiroptical methods. Quantum chemical calculation of chiroptical methods like optical rotation ($[\alpha]_D$),[8] optical rotation dispersion (ORD),[8, 9] electronic circular dichroism (ECD)[10-13] and vibration circular dichroism (VCD)[14-16] represented a valuable tool to interpret experimental data and assignment of the absolute configuration of diverse structures of natural or synthetic compounds.

In our research group, HPLC-based activity profiling has been used as successful method for the rapid localization, dereplication, and characterization of bioactive NPs in extracts. This approach was successfully applied for the identification of new antiprotozoal substances, positive $GABA_{(A)}$ receptor modulators, and anti-HIV compounds.[17-24] The work shown here is an expansion of our group's plants screening, by exploring Iranian medicinal plants for the discovery of new antiprotozoal NPs with new scaffolds for the target. In this project over 120

plant extracts mainly from Lamiaceae and Asteraceae family from the Iranian flora were screened against *Plasmodium falciparum* K1 strain. These plants were selected based on ethnobotanical studies and taxonomical considerations. Promising extracts (threshold > 70% inhibition at 4.6 µg/ml) were separated by analytical scale HPLC. Whilst UV and MS data were recorded on-line, time-based microfractions for bioassay were collected via a T-splitter. LC-MS with an ion trap mass spectrometer was used for efficient dereplication of active compounds in the extracts. In a next step, constituents responsible for the activity within active extracts were identified and evaluated according to their lead potential. The aim was to isolate the most interesting molecules with the aid of diverse chromatographic methods and to fully elucidate their structure by means of spectrometric and spectroscopic methods. Structure elucidation was achieved by 1D and 2D NMR experiments. Relative configuration was established on the basis of $^{3}J_{H-H}$ coupling constants and NOE difference spectra. Finally, full assignment of isolated compounds were done by applying theoretical simulation of ECD spectra for attribution of the absolute configuration by applying *ab initio* approaches based on a time-dependent density functional theory (TDDFT).

The aim of thesis is to apply theoretical CD predictions to the assignment of the absolute configurations of optically active compounds. The necessity of the methods appeared when conventional empirical methods could not be applied for any of isolated new or known natural compounds. This approach was successfully applied for the assignment of the absolute configuration of structurally flexible molecules like the bisabololoxide derivatives (**5-9**), disesquiterpene and sesquiterpene coumarins (**10**-**12**) along with structurally rigid isoprenoids (**15-17**) with rare carbon skeleton. The AC of sahandone (**4**) was established by comparing of theoretical ECD and optical rotation with experimental values. The work presents a fast and smooth approach in the assignment of absolute configurations of chiral compounds isolated from natural sources (**Figure 1**).

In addition this method successfully applied for establishing AC of some other new NPs such as: terpenoids (mono, sesqui-, di-, sester, and triterpenes), abruquinones, alkaloids, and some phenolic compounds which will not be presented here.

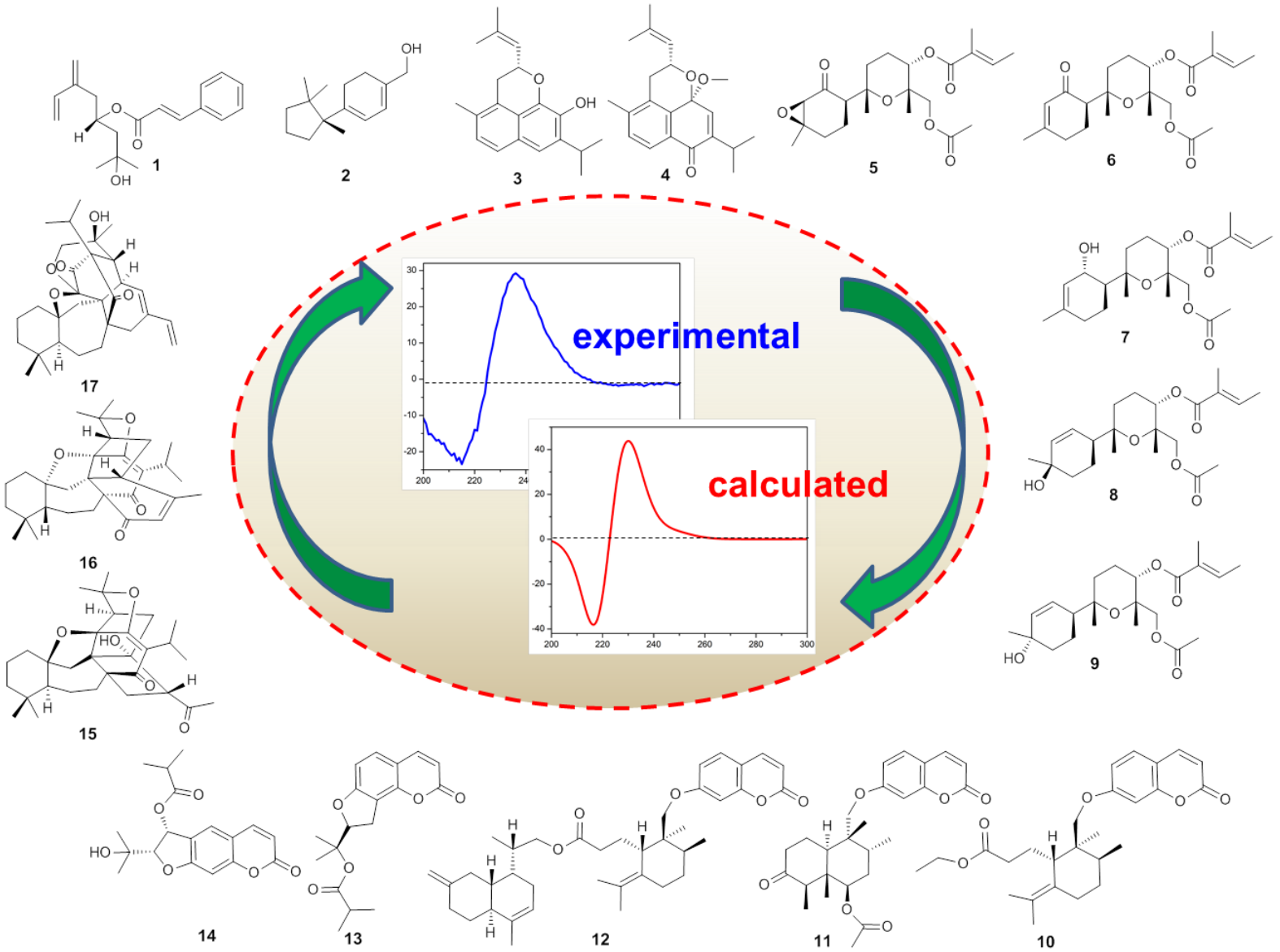

Figure 1. Overview of selected compounds that have been investigated during this work by quantum chemical calculations.

2. Introduction

2.1. Discovery of novel leads from natural sources

From ancient times, nature has inspired man to discover drugs to treat diseases. People in all over the world have been using herbal medicine for treating their illnesses and diseases. NPs have prepared the way for modern pharmacotherapy over last two centuries, and it is not surprising that 80 % of the world's populations is using plant derived medicines for basic health care.[2] Historically, nature has provided many ground-breaking drugs such as: penicillin from the fungus *Penicillium notatum*, morphine from the opium poppy (*Papaver somniferum*), or digoxin from the foxglove (*Digitalis purpurea*), paclitaxel from yew (*Taxus brevifolia)*, artemisinin from sweet wormwood (*Artemisia annua*), and vinblastine from Madagascar periwinkle (*Catharanthus roseus*). A significant number of natural product derived molecules are currently in clinical trials in therapeutic areas such as infectious, neurological, cardiovascular, metabolic, inflammatory, and cancer.[25]

In the last decades pharmaceutical drug discovery has moved from NPs to synthetic approaches. Combinatorial chemistry by aid of high throughput screening (HTS) techniques provides a rapid identification of a lead molecule against a given target. However NPs are differed from synthetic compounds. They are structurally more diverse and often exhibit specific biological activity because of spatial and structural complexity.[26] The abundance of synthetic compounds with limited chemical and functional diversity has refreshed interest in nature as excellent resource for the discovery of new hits to apply to the design of the next generation of drugs. Thus, NPs are still unique as both direct and indirect sources of leads to drugs against all classes of disease.[27-29]

Isolation of bioactive natural products

Natural extracts are highly complex mixtures containing hundreds to thousands of constituents. Within this mixture one or several compounds are responsible for pharmacological properties. Definitely the most challenging job in this context is localizing activity in the extract by bringing together biological data and chemo-analytical information in order to identify the active principles at an early stage.[26] This step is important in the discovery of bioactive constituents from natural sources due to inherent complexity of natural extracts. The identification of bioactive principles of natural extracts often failed, as the biological activity could not be enriched.[30] However, there are numerous examples like morphine, quinine, salicylic acid, physostigmine, digitalis glycosides, reserpine, or artemisinin, where the correlation between traditional use of a plant and therapeutically useful plant derived compounds was successfully established.[27] Recently, HPLC-based activity profiling has been used as one of the most successful approaches for tracking bioactive compounds in crude mixtures.[26, 31-35] It consists of fractionating bioactive extracts in 96-deep well plates (96-DWP) by means of analytical or semipreparative scale HPLC and subsequent assessment of the bioactivity in each fraction. In this manner, the activity can be assigned to chromatographic peaks and correlated with the spectroscopic information available on-line. Briefly, a minute amount of a bioactive extract is separated over analytical or semi-preparative HPLC and divided into microfractions which are to

be tested in the particular bioassay (Figure 2). Simultaneously, on-line or off-line chemical analysis allows direct allocation of the activity to single constituents. This is in contrast to the classical preparative approach of bioassay-guided isolation.[36, 37] An on-line HPLC-UV-MS system is the basic equipment for HPLC-based activity profiling since it provides UV-Vis absorbance spectrum, mass abundance, molecular mass, and even molecular formula in case of high resolution mass spectrometry (HR-MS) detectors in a single run.[38] Semi-quantitative information may also be obtained by hyphenated evaporative light scattering detection (ELSD).[36] Detailed structural information is achieved by NMR measurements of peak-resolved HPLC-fractions containing the compounds of interest.[39] Comparison of combined spectral data with natural products databases such as the Dictionary of Natural Products (DNP) allows rapid dereplication of interesting constituents. Hence, promising secondary metabolites can be distinguished from uninteresting ones. Based on these results, thorough investigations can be discontinued or further pursued by a large-scale isolation of compounds of interest.

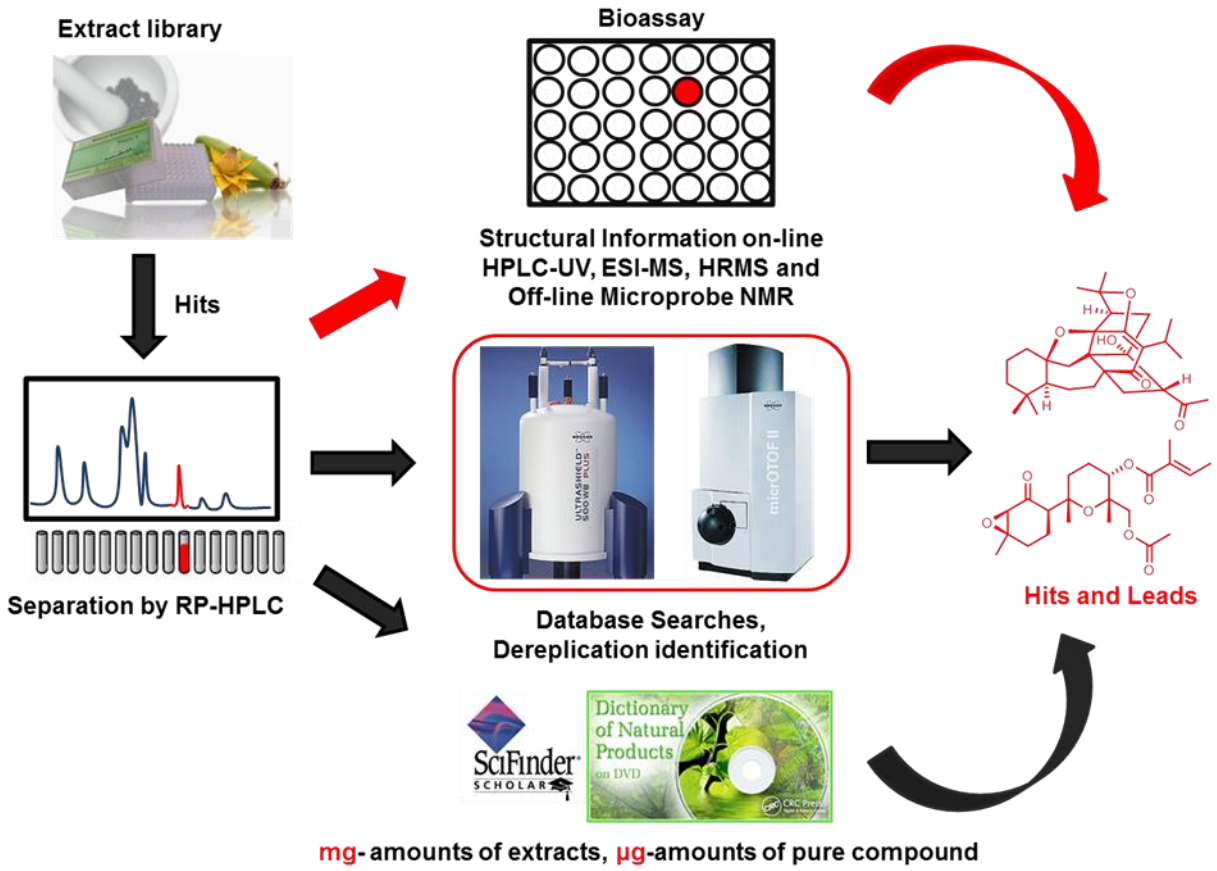

Figure 2. HPLC-based activity profiling approach of bioactive extract.[40]

Structure elucidation of natural products

In the past structure elucidation of NPs was extremely difficult. Nowadays a "standard" set of 1D and 2D NMR experiments, such as ^{1}H, ^{13}C, COSY, HSQC, HMBC, NOESY, on 400-500 MHz

spectrometers, in conjunction with high resolution mass spectrometric (HR-MS) data, is a routine approach to "small molecule" structure assignment with milligram, and even microgram quantities of sample. Hyphenation of HPLC separation with different spectroscopic detection methods such as PDA, MS offline- or online microflow NMR offers fast and precise methods for identification and structure elucidation of NPs.[41] A PDA detector provides a spectrum of a given compound, which allows relating them to classes of secondary metabolites with characteristic chromophores. The molecular formula, which can be deduced on-line using HPLC-MS with a time-of-flight (TOF) detector, is one of the most useful pieces of information for searching large databases such as CAS Registry and DNP. Ion trap MS analyzers are often coupled to HPLC and are suitable for MS^n experiments (repeated tandem mass spectrometry) which allows dereplication of active compounds at a very early stage of the discovery process, directly from crude extracts.[42]

A broad range of NMR experiments is available for the elucidation of the constitution and configuration of isolated molecules. One-dimensional ^{1}H-NMR and ^{13}C-NMR experiments, and two-dimensional homonuclear (^{1}H,^{1}H-COSY) and heteronuclear (^{1}H,^{13}C) correlation experiments such as HSQC and HMBC are standard in determining the covalent structure of a small molecule with limited signal overlap. For more complex structures with several overlapping spin systems, additional experiments like e.g. (^{1}H,^{1}H)-TOCSY or (^{1}H,^{13}C)-HSQC-TOCSY are recommended. While these experiments detect scalar couplings between two nuclei, NOESY and ROESY experiments provide stereochemical information by displaying through space correlations which provide information on the 3D-structure of a molecule. Combination of NOE based methods with molecular modeling are nowadays commonly used for assignment of the relative configuration of organic compounds. However, these experiments, only disclose the relative configuration, and complete spatial arrangements of groups need to be proven by methods for the determination absolute configuration. These methods will be addressed in chapter 2.4.

2.2. Iranian traditional medicine (ITM)

Plants have been used to alleviate and treat diseases since ancient times. In the history of the medicine of the Western world, Greeks contributed substantially to a rational use of herbal drugs. In the Middle Ages people from the Middle East took part in preserving the Greco-Roman expertise by adding their own resources, together with Chinese and Indian herbs.[43] They were not only responsible for accumulating all the existing information on medicine of the time, but also added to this knowledge their own keen observations, experimentation, and skills.[43] Iran has an long history of traditional medicine, and numerous historical references such as medical books and manuscripts with valuable information about medicinal plants are available in Iran.[44, 45] Iranian scholars played an important role in the conservation, combination, coordination and development of ideas and knowledge in ancient civilizations.[46] One of the main sources of medical and herbal knowledge of the ancient inhabitants of Iran is the Avesta (the holy book of the Zoroastrians, aka Zarathustrans). Many herbs were recorded in this book for various ailments. The Iranian academic centers like Jundishapur University (3rd century AD) were a gathering place for great scholars from different civilizations. This center had a large hospital, and an academy where the first international medical congress was held.[43] After appearance of Islam (1400 years ago), Iranian medical scientists saw two specific stages in in the advancement of medical sciences: a) the translation age, from 750-900 AD, when many graduates of *Jundishapur University* translated the corpus of Galenic and Hippocratic works; b) the golden age of creativity (900-1100 AD), which was the era of Iranian leading scholars in pharmacology and pharmacy such as Rhazes (850- 932) and Avicenna (980-1037).

Muhammad ibn Zakariyā Rāzī (Rhazes in Latin) (865-925 CE), a chemist, pharmacist, musician, physicist, philosopher, and great clinical physician was a leading figure in the field of medieval medicine.[47] He wrote his famous encyclopedia *Al-Hawi fi Tibb* (*The Continents of Rhazes)* in about 26 volumes.[45] Rhazes' book was based on his clinical approach. However, his writings did not make a strong impression on Western medical history as did Ibn Sina's (Avicenna, 980-1028) works. Avicenna, a Persian pharmacist and physician, contributed much to the science of pharmacy and medicine through a valuable book called "*Canon Medicinae*" regarded as "*The final codification of all Greco-Roman medicine*".[30] The book was more theoretical in its approach. Avicenna dedicated two of the five volumes of this book to pharmacy and pharmacology. In these two volumes he also mentioned the application of many drugs, most of them herbal.[44] He was also one of the first persons who introduced the concept of polymedicine (using multiple medications by a patient) in humoral theory, and he discussed the different effects of drugs from one person to another, which is considered an important factor in pharmacokinetics today.[44, 48, 49]

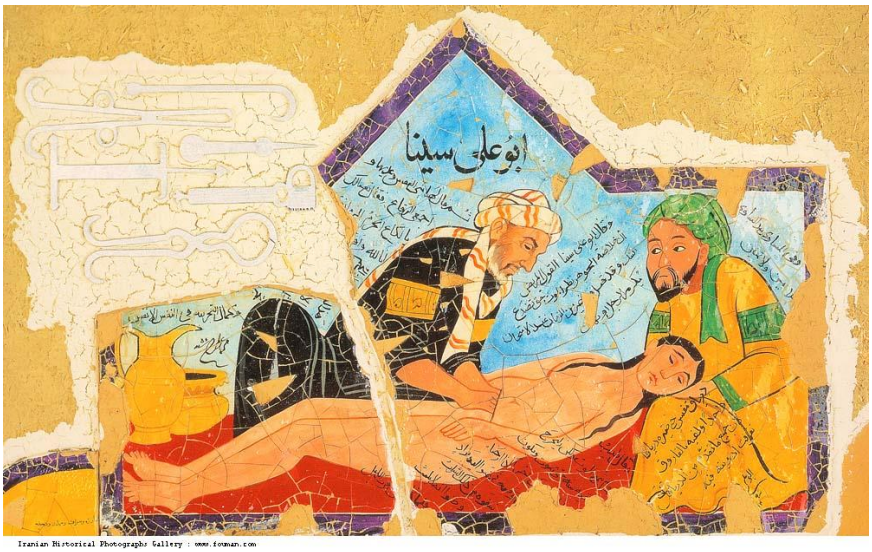

Figure 3. Canon Medicine, Avicenna operating on a woman, operation tools are displayed top-left. His Canon of Medicine was long a reference in the field. (picture provided from http://fouman.com)[50]

In this era numerous recipes of herbal formulations were written by different scientists. The oldest preserved Persian text on Materia Medica, *Ketāb al-abnīa ʿan ḥaqāʾeq al-adwīa (*Book of the Foundation of the True Properties of Remedies*)* was written by Abu-Mansur Mowaffaq Heravi around 980-90 CE.[51] Two popular pharmacopeias in Farsi have been used as main sources of traditional remedies by later physicians, traditional healers, and even traditional herbalists: (1) *Tuhfat al-Mu'minin* (The Gift of two Mumins) written by Muhammad Zaman e-Tunekabuni around 1669, and (2) *Makhzan al-adviyah* (The Storage of Medicaments) written by Muhammad husayn ibn al-Alavi al-Khurasani al-Shirazi in 1771 CE.[47]

Current situation of ethnomedicine in Iran

Modern Western medicine was introduced to Iranian in 1851 by establishing modern institutions of higher learning called "*Dar ul-Funun* (polytechnic institutes). When Western medicine was introduced, traditional medicine gradually lost ground and was finally excluded from the mainstream of the Iranian medico-pharmaceutical community. However, traditional medicine has survived through medical services rendered by unauthorized healers, sometimes even within urban areas that have well-equipped hospitals.[47] The herbal shop,"Attari", is a place for diagnostic, prescription and providing medical services (Figure 4). Some of these people have unique instructions on how to prepare herbal drugs. They use traditional experience to prepare herbal prescriptions and dispense them. Many Iranian people continue to consult these herbalist practitioners.

Figure 4. A typical herbal shop in Tehran, photo by Nastaran Dadjou (www.nasimonline.ir)

In recent years, the attitude of the Iranian population, as well as the medical and pharmaceutical authorities towards medicinal plants and herbal products has gradually improved. In this regard the *Iranian Herbal Pharmacopoeia* (IHP) has been published in 2002 by contribution of different pharmacy schools.[52] The IHP contains qualitative and therapeutic monographs for over 100 medicinal plants, and includes: definitions, scientific and common names, plant morphology, and plant parts recommended for use, geographical distribution of the plant in Iran and other countries, microscopic characteristics, constituents, medicinal applications, and pharmacological and toxicological information. The mission of the IHP is to promote the responsible use of herbal medicines, and to ensure that they are used with the highest possible degree of efficacy and safety.

Researches on different aspects of Iranian traditional medicine are increasing. Sixteen faculties of pharmacy (all have a department of pharmacognosy), and several research institutes on medicinal plant and ethnobotany all over Iran, investigate drugs of natural origin, usually with an emphasis on plant-derived drugs, and present various courses on medicinal herbs.[47] Research on medicinal plants plays an important role in education and promotion of herbal knowledge. Over the past two decades, in accordance with the new wave of medicinal plant usage, research activities have shown significant progress. Ethnobotanical information forms the starting point for many of these research activities. The results of these investigations have been published in respected international as well as domestic journals. The broad ranges of investigations carried out in these centers include phytochemical, pharmacological, and clinical studies on medicinal plants. The interests on research on different aspects Iranian herbal medicines are raising (Figure 5).

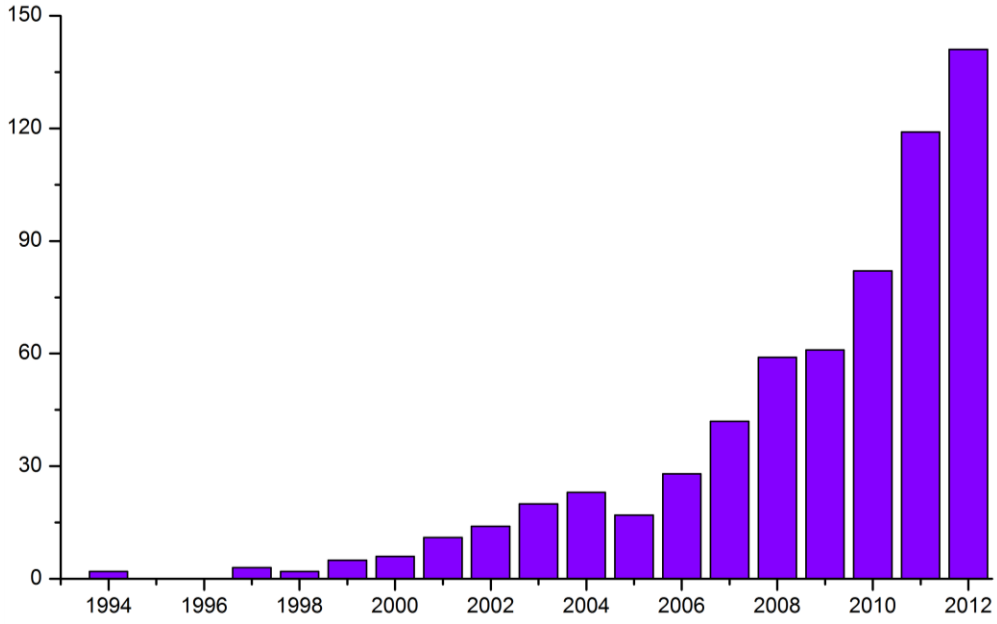

Figure 5. The number of indexed articles on herbal medicine by Iranian researchers. Source: ISI Web of Knowledge

Several studies have been published on uses of natural remedies in Iranian traditional medicine.[43, 53-55] One of the earliest ethnobotanical works is by Hopper and Field on useful plants and drugs of Iran and Iraq, which was a market survey of medicinal plants in Tehran, Esfahan and Baghdad markets.[56] Shokri and Safaian also presented a list of 210 medicinal plants used in Mazandaran province.[57] Several ethnobotanical surveys have documented uses in different parts of Iran such as: documentation of ethnobotanical information in the region of Turkmen Sahra in north part of Iran,[58] herbal remedies traditionally used in Kohghiluyeh va Boyer Ahmad province,[59] botanical drugs and preparations in the traditional medicine of west Azerbaijan.[60] Adhami investigated selected medicinal plants which have been used in Iranian traditional medicine for acetylcholinesterase inhibitory activity.[61] In other studies Sairafianpour [62]and Naghibi et al.[63] investigated ethnobotany and ethnopharmacology uses of plants with potential antiplasmodial properties.[62]

Biodiversity of the Iranian flora

Iran has a total surface area of 1.6 million km^2. The country is divided into five major climates including Mediterranean, Desert, Half-desert, Warm-Humid, Warm-Dry, and Mountainous climate regions. Except for the inland deserts and the lowlands along the Caspian Sea, Persian Gulf, and Gulf of Oman, about half of Iran is composed of high mountains. The main mountain chains are Alborz, Zagros, Kopet Dagh, Khorassan and Makran (Figure 6). Iran forms part of two biodiversity hotspots: the Caucasus and the Irano-Anatolian. Important terrestrial ecoregions for endemic species include the Zagros Mountains Forest Steppe and the Elburz Range Forest Steppe. The specific geographical situation of Iran, with its variable climates, makes it a unique

place with different ecosystems. Iran is a large country and - after Turkey- has the highest plant biodiversity in the Middle East. [64]

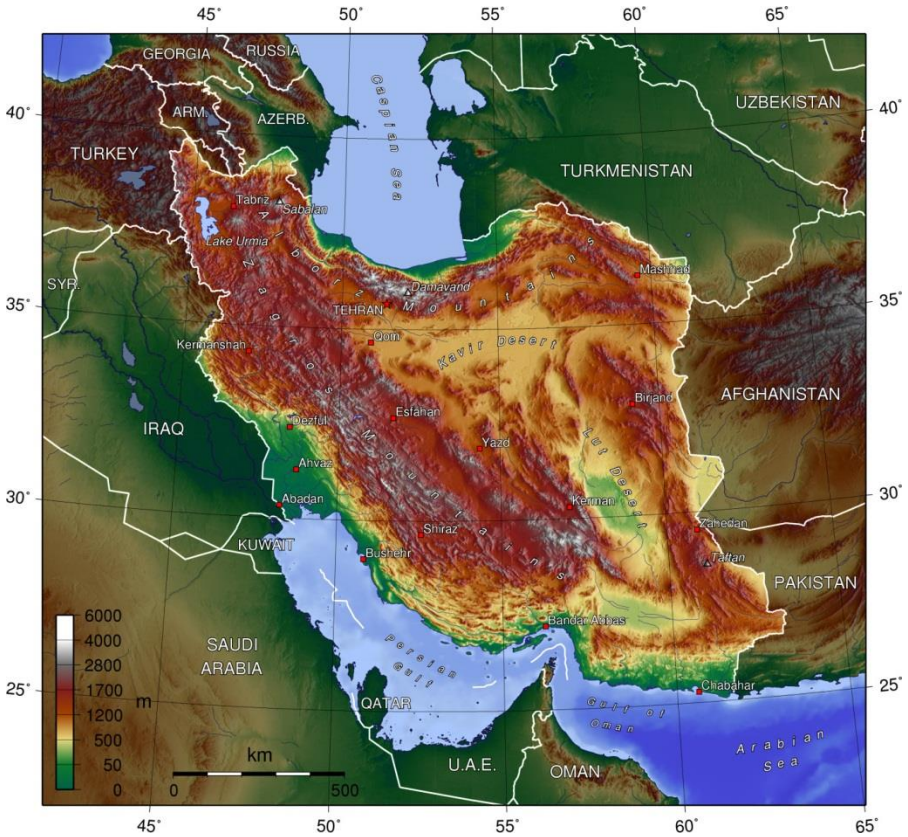

Figure 6. Topography map of Iran, main mountain ranges: the Alborz in central N, The Zagros from NW to SE. (Source: Wikipedia)

Due to the great number of its ecosystems and special climates, the Iranian flora consists of over 8000 spermatophytes plant species belonging to 167 families and 1200 genera. Of these, about 22% are endemic species belonging to 85 families. In total there are over 1700 endemic taxa in the country.[47, 65] Nearly 60% of the endemic species of Iran belong to the four families *Fabaceae* (394 species), *Asteraceae* (393 species), *Lamiaceae* (129 species) and *Apiaceae* (100 species). Genera with high number of endemic species within the Iranian flora are: *Astragalus*, *Cousinia*, *Nepeta*, *Onosma*, *Acantholimon*, and *Dionysia*.[66]

About 20 % of the Iranian flora consists of annual plant species. According to Raunkiær,[67] this figure for world's flora is 13%. When compared with the world flora, the Iranian flora is rich in annuals. Despite this, only 6.7% of Iran's endemic plant species are annuals. There is similar picture for tree, shrub, and sub-shrub species. Although 7.5% of the whole country is covered by forests, Iran has only seven endemic tree species. Six of these are from the *Rosaceae*, and one from the *Ulmaceae* families. With the exception of two species of the *Pyrus* genus which occur in the *Euxino-Hyrcanian* province, the remaining five species evolved within *Irano-Turanian*

boundaries. From a physiognomic view point, the vegetation of Iran is dominated by shrub and sub-shrub life forms, but only 6.9% of endemic species are shrubby plants. By contrast, 85 % of endemic species in Iran are herbaceous perennials (including 11% caespitose perennials).[65]

Selection and collection of plant material

The aim of this project was to screen medicinal plants from Iran for the discovery of new antiparasitic NPs with scaffolds new for the target. In this study different strategies were used to assemble extract libraries from the Iranian flora. The criteria for selecting plant species were based on folk medicinal uses, and indications of the presence of bioactive compounds with anti-fever properties. Some of the plant material was collected randomly, or in a targeted manner with a focus on chemotaxonomic considerations. A total of 40 different plants were selected from the Iranian flora, mainly from the Lamiaceae and Asteraceae families (Table 1).

The plant material was identified by Dr. Ali Sonboli from Department of Biology, Medicinal Plants and Drugs Research Institute, Shahid Beheshti University, Tehran, Iran. Voucher specimens had been deposited in Herbarium of Medicinal Plants and Drugs Research Institute (MPH). Dr. Sonboli also substantially contributed to the selection and collection of plant material.

Table 1. Plants collected for the screening against *Plasmodium falciparum*

Plant name	Family	Part
Heracleum persicum Desf.	Apiaceae	Fruits
Artemisia incana (L.) Druce	Asteraceae	Aerial parts
Artemisia persica Boiss.	Asteraceae	Aerial parts
Tanacetum balsamita subsp. *balsamitoides* (Sch.Bip.) Grierson	Asteraceae	Aerial parts
Tanacetum chiliophyllum (Fisch. & Mey.)	Asteraceae	Aerial parts
Tanacetum dumosum Boiss.	Asteraceae	Aerial parts
Tanacetum kotschyi Boiss.	Asteraceae	Aerial parts
Tanacetum pinnatum Boiss.	Asteraceae	Aerial parts
Tanacetum polycephalum Sch. Bip.	Asteraceae	Aerial parts
Tanacetum polycephalum subsp. *argyrophyllum* (K.Koch) Podlech	Asteraceae	Aerial parts
Tanacetum polycephalum subsp. Azerba	Asteraceae	Aerial parts
Tanacetum sonboli Mozaff.	Asteraceae	Aerial parts
Tanacetum stapfianum (Rech.f.) Podlech	Asteraceae	Aerial parts
Tanacetum tabrisianum (Boiss.) Sosn. & Takht.	Asteraceae	Aerial parts
Tanacetum tenuisectum (Boiss.) Podlech	Asteraceae	Aerial parts
Berberis vulgaris L.	Berberidaceae	Fruits
Buxus hyrcana Pojark.	Buxaceae	Leafs
Citrullus colocynthis (L.) Schrad.	Cucurbitaceae	Bark
Citrullus colocynthis (L.) Schrad.	Cucurbitaceae	Seeds
Hymenocrater elegans Bunge	Lamiaceae	Aerial parts
Hymenocrater bituminosus Fisch. & C.A.Mey.	Lamiaceae	Aerial parts
Lamium album L.	Lamiaceae	Aerial parts
Micromeria persica Boiss.	Lamiaceae	Aerial parts
Nepeta crispa Willd.	Lamiaceae	Aerial parts
Nepeta denudate Benth	Lamiaceae	Aerial parts
Nepeta hormozganica Jamzad	Lamiaceae	Aerial parts
Salvia aegyptiaca L.	Lamiaceae	Aerial parts
Salvia atropatana Bunge	Lamiaceae	Aerial parts
Salvia brachyantha (Bordz.) Pobed.	Lamiaceae	Aerial parts
Salvia ceratophylla L	Lamiaceae	Aerial parts
Salvia chloroleuca Rech.f. & Aellen	Lamiaceae	Aerial parts
Salvia hydrangea DC. ex Benth.	Lamiaceae	Aerial parts
Salvia sahendica Boiss. & Buhse	Lamiaceae	Aerial parts
Salvia sahendica Boiss. & Buhse	Lamiaceae	Roots
Stachys pilifera Benth.	Lamiaceae	Leafs
Otostegia persica (Burm.f.) Boiss.	Lamiaceae	Leafs
Stachys schtschegleevii Sosn. ex Grossh.	Lamiaceae	Leafs
Satureja khuzistanica Jamzad	Lamiaceae	Aerial parts
Satureja rechingeri Jamzad	Lamiaceae	Aerial parts
Nigella sativa L.	Ranunculaceae	Seeds
Rubia tinctorum L.	Rubiaceae	Roots

2.3. The challenge of absolute configuration

Stereoisomerism

Stereoisomerism arises because molecules having the same constitution may still differ, as isomers, in the spatial arrangements of their atoms. Stereoisomers which are related as object and nonsuperimposable mirror image are called *enantiomers* of *antipodes*, whereas those which are not so related are called *diastereomers.* The relationship between enantiomers simply resembles the relationship between right and left-handed helices. The screw sense (right or left) which characterizes a given dissymmetric conformation or helix is the chirality, a term which may be applied to any dissymmetric object or molecule and which refers to the handedness of given enantiomeric form.

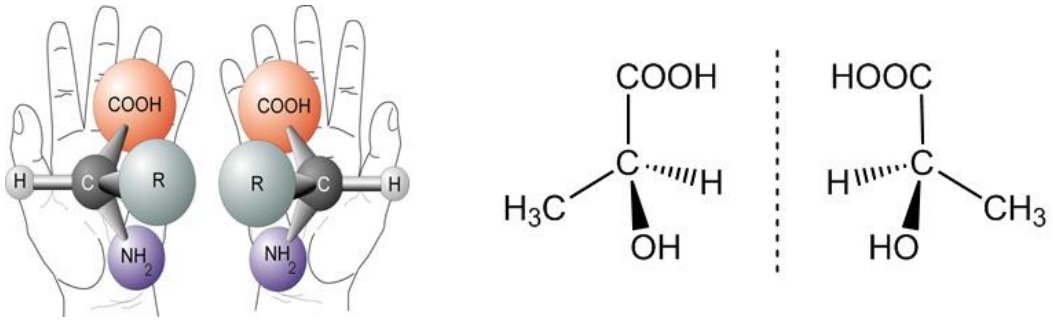

The concepts of *chirality* have been known since the 1870s, the time of fundamental statements by J. H. van't Hoff and J. A. Lebel, and even earlier when first experimental evidences were obtained by J. B. Biot and L. Pasteur. Pasteur manually separated crystals of sodium ammonium tartrate into two groups of crystals. Also, he recognized that solutions of one type of crystals – (+)-tartaric acid –rotated linearly polarized light to the right, whereas the other cristal form, the (-)-enantiomer, rotated it to the left. He was the first person who proposed that the source of natural optical activity is the molecular asymmetry. In 1904, Lord Kelvin introduced term of chirality on his lecture on Molecular Dynamics and the Wave Theory of Light:[68] " *.... I call any geometrical figure, or group of points, chiral, and say it has chirality, if its image in plane mirror, ideally realized, cannot be brought to coincide with itself.*"

In stereochemistry absolute configuration is the spatial arrangement of the atoms of a chiral molecular entity (or group) and its stereochemical description. In 1966, three chemists, R. S. Cahn (England), C. K. Ingold (England), and V. Prelog (Switzerland), devised a system of nomenclature of chiral molecules called *CIP system* or *CIP conventions*. In the CIP system of nomenclature, each chiral center in a molecule is assigned a prefix (*R* or *S*), depending to whether its configuration is right- or left-handed by giving a priority to each substituent on the stereogenic atom C_{abcd}.

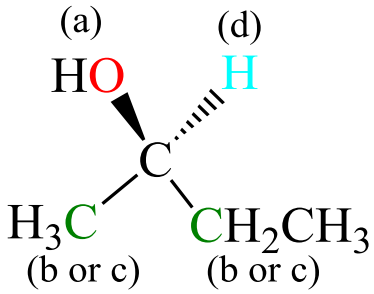

According to this system, one enantiomer of 2-butanol should be designated (*R*)-2-butanol and the other enantiomer should be designated (*S*)-2-butanol. [(*R*) and (*S*) are from the Latin words rectus and sinister, translated by right and left, respectively.]

The origin of optical activity- plane polarized light

Optical activity has its origins in microscopic phenomena, such as molecular structure and chromophores. It can be observed through macroscopic phenomena, such as chiroptical spectroscopic measurements. Light is an electromagnetic phenomenon. A beam of light consists of two mutually perpendicular oscillating fields: an oscillating electric field and an oscillating magnetic field (Figure 7). The oscillation of the electrical field occurs in all possible planes perpendicular to the direction of propagation (The same would be true of the magnetic field).

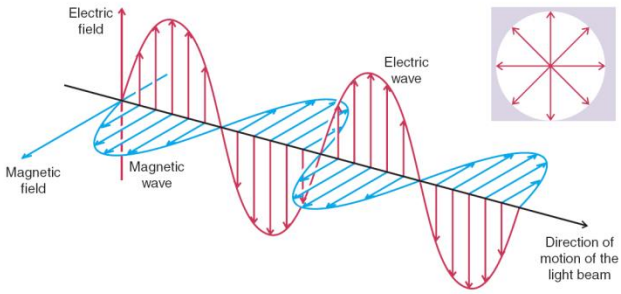

Figure 7. The oscillating electric and magnetic fields of a beam of ordinary light in one plane. The waves depicted here occur in all possible planes in ordinary light.[69]

When ordinary light is passed through a polarizer, the polarizer interacts with the electric field so that the electric field of the light that emerges from the polarizer (and the magnetic field perpendicular to it) is oscillating only in one plane. Such light is called *plane-polarized light*. When plane polarized light passes through an optically active sample, the light is rotated because of electronic interaction with the chiral molecules present, and the plane of light polarization emerging from the sample tube is rotated from the original plane of polarization (Figure 8). A second polarizer (analyzer) placed at the sample tube exit is rotated by the observer either clockwise or counterclockwise until the light intensity is greatest.[69]

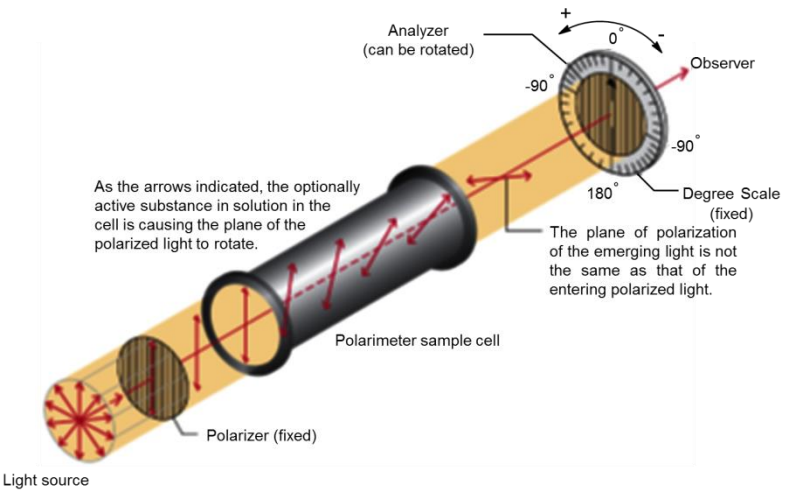

Figure 8. The principal working parts of a polarimeter and the measurement of optical rotation of chiral compounds using polarized light.[69]

If the analyzer is rotated in a clockwise direction, the rotation α (measured in degrees) is said to be positive (+). If the rotation is counterclockwise, the rotation is said to be negative (-). A substance that rotates plane-polarized light in the clockwise direction is also said to be *dextrorotatory*, and one that rotates plane-polarized light in a counterclockwise direction is said to be *levorotatory* (Latin: *dexter*, right, and *laevus*, left). Two enantiomers generate equal rotations magnitudes but opposite sign, and therefore can be easily distinguished. Polarimetry has traditionally been used for the analysis of the enantiomeric purity of chiral compounds with known specific rotations based on an equation (1).

$$[\alpha]_{\lambda}^{25} = \frac{[\alpha]}{cl} \qquad (1)$$

Where $[\alpha]_{\lambda}^{T}$ is the specific rotation, and [α] is the measured optical rotation in degrees; *l* is the length of the cuvette in dm; and *c* is the sample concentration in g/mL, for sample at a temrature T (given in degrees Celsius) and wavelength λ (in nm). The optical rotation value of a chiral compound depends on the wavelength of the linearly polarized light and the solvent, temperature, and sample concentration. The presence of small amounts of (chiral) impurities can significantly affect the accuracy of polarimetric measurements, in particular when compounds with small rotation angles are analyzed. Horeau and others have pointed out that, in the case of associating chiral analytes such as carboxylic acids, determination of the optical rotation for stereochemical analysis can be misleading. [70, 71] The optical rotation of a chiral compound does not always increase linearly with the enantiomeric purity, and is therefore not necessarily representative of the actual enantiomeric composition. It is important to notice that there is no simple relationship between the sign of the optical rotation of a chiral compound and its absolute configuration. Accordingly, polarimetry is generally not used for determination of absolute configurations unless a reference is available. Today's application of high level of quantum chemical calculation allows the prediction of a magnitude and sign of specific or molecular rotation with reasonable accuracy. [8, 15, 72]

Determination of absolute configuration

Available techniques for assigning absolute configurations (ACs) may be divided into two large categories, that are non chiroptical, so called, "chemical" methods (X-ray, NMR, synthesis) and spectroscopic, in particular chiroptical methods (OR, ORD, ECD, VCD). The latter ones permit to distinguish between stereoisomers in even sub-μg amounts without requiring great experimental efforts.

Non chiroptical methods

X-ray single crystal

The most widely known instrumental method for the determination of absolute configuration is X-ray crystallography. In 1951, Bijvoet used anomalous dispersion (Resonant Scattering) to solve the absolute structure of chiral compounds which contained elements with high imaginary resonant-scattering components.[73, 74] Bijvoet and his coworkers achieved the first experimental determination of the absolute configuration of sodium rubidium tartrate. In this compound rubidium atoms were the ones close to the absorption edge. The use of a *CuKα* radiation source has made absolute configuration assignments possible without introduction of a heavy atom in the molecule.[75] An essential precondition of using X-ray crystallography, however, still is the availability of crystals of suitable quality, [76] which sometimes appears to be a non-trivial task.

NMR techniques

NMR spectroscopy which is most frequently used technique for structural elucidation of compounds may also be applicable for the assignment of absolute configuration in two general approaches:[77-79]

a) Substrate analysis without derivatization (i.e., by the addition of a chiral solvating agent).
b) Analysis of the derivatives prepared from the substrate and the two enantiomers from a chiral derivatization agent.

In the first approach there is no covalent linkage between the substrate and the chiral "*reagent*", The two enantiomers must be available for comparison, and no clear-cut correlations between the absolute configuration and the NMR spectra can be established. The second and more common approach, involves derivatization of a pure enantiomer with the two enantiomers of a chiral agents, such as Mosher acid [α-methoxy- α -(trifluoromethyl)phenyl acetic acid],[78] O-methylatrolactic acid,[80] ADPD (5-amino-2,2-dimethyl-4-phenyl-1,3- dioxan),[81] or phosphorus-containing reagents.[82] In this approach an enantiomeric mixture can be converted to a pair of diastereomers, which can easily be distinguished by classical methods (Fig. 7). After derivatization the diastereomer, in which specific substituents are shielded by the aromatic group of the chiral shift reagent, will exhibit upfield chemical shifts for those substituents relative to the same substituents in the second diastereoisomer (Figure 9). This change in chemical shift values, due to the shielding effect of the aromatic group, is commonly

represented as a Δδ value, calculated for MTPA (methoxytrifluoromethylphenylacetic acid) esters as $\Delta\delta = \delta S - \delta R$ or $\Delta\delta = \delta R - \delta S$, while for MPA (methoxyphenylacetic ester) and other esters as $\Delta\delta = \delta R - \delta S$. To establish the absolute configuration, values of $\Delta\delta$ should be localized on the structure, and based on their arrangement the configuration can be concluded.

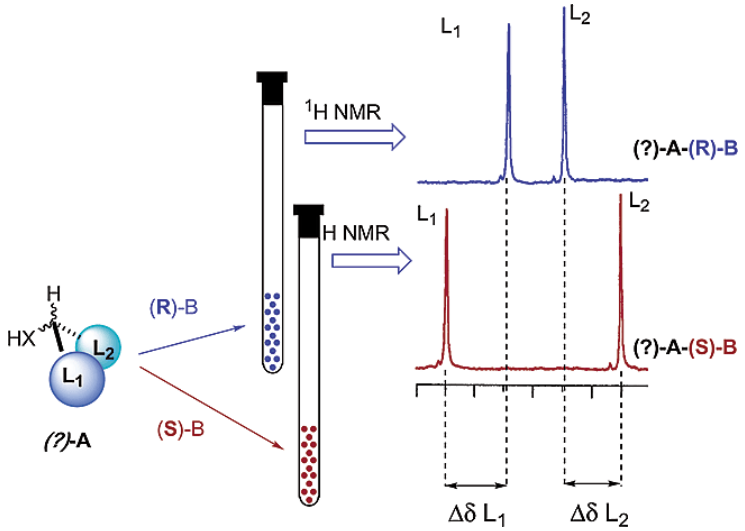

Figure 9. Typical ^{1}H NMR spectrum "Chiral derivatizing agents" showing variation on chemical shift of L-1 and L-2 resonances. Analysis of the chemical shifts of diastereomers ($\Delta\delta = \delta_S - \delta_R$) allowed the assignment of the absolute configuration of chiral alcohols, amines, and carboxylic acids.[78]

Partial to total synthesis

Total enantioselective synthesis has been used for the determination of absolute configurations of chiral compounds.[83-86] This method is a very effective and reliable, but sometimes also expensive and time-consuming. In this approach final configuration will confirm in stereochemical manner by using semi or total synthesis of chiral compounds from corresponding starting material.

Chemical degradation

Determination of ACs of chiral compound can be done by chemical degradation to optically active products suited for further comparison with authentic samples of known absolute configurations.[87, 88]

Chiroptical approaches

Spectroscopic measurements of chiroptical properties; such as optical rotation, optical rotatory dispersion (ORD), and circular dichroism (CD), represent excellent tools for the elucidation of the absolute configurations of chiral compounds. The main advantages of these methods are that they allow the rapid and unambiguous differentiation between stereoisomers without major experimental efforts and consume only small amounts of substance.

Optical rotatory dispersion (ORD)

Optical rotatory dispersion is the variation in the optical rotation of a substance with a change in the wavelength of light. Optical rotatory dispersion can be used to find the absolute configuration of chiral compounds. Biot found out that if the angle of rotation α (or $[\alpha]$ or $[\phi]$) can be measured as a function of the wavelength. Greater absolute values are obtained at shorter wavelengths (Figure 10). This behavior is described as "plain curve" (normal ORD), and in spectral regions that are remote from the absorption bands, it can be expressed by a Drude equation

$$[\phi] = \sum_i A_i(\lambda^2 - \lambda_i^2) \qquad (2)$$

(A_i and λ_i are constants).[89]

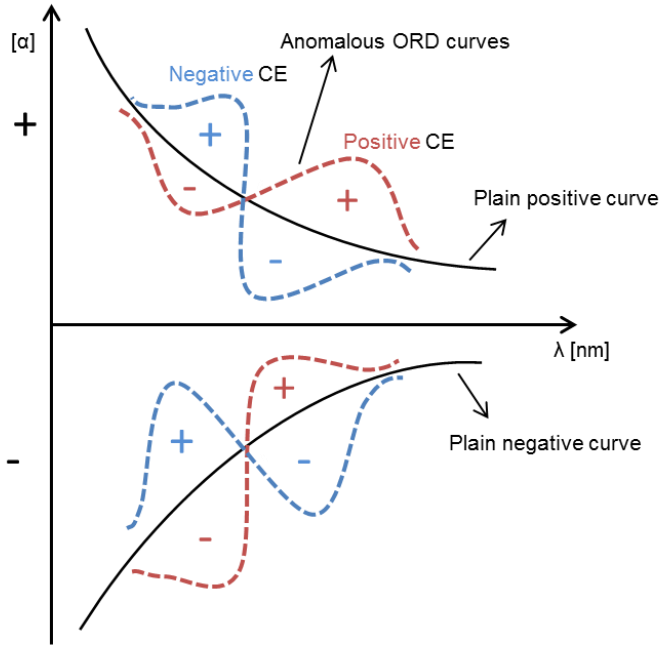

Figure 10. Typical ORD spectra: normal, plain curves (black) and anomalous ORD spectra, defined as positive (red) and negative (blue) COTTON effects (CE).[89]

Two types of ORD spectra are exist: the normal, plain curves (background rotation), which are characterized by a monotonic increase of $[\alpha]^T$ while the wavelength is decreased; and the anomalous spectra of dispersion, which are defined by reversal of direction and inflection in the curves around a maximum of an absorption band (Figure 10).[89] The presences of chromophores in vicinity of chiral element exhibit the anomalous behavior that has a maximum in the UV/vis region. The anomalous ORD is also described as a COTTON effect (CE) curve. In particular, a CE is called positive if the rotation magnitude first increases with a decreasing λ_i; conversely, the curve corresponds to a negative CE if the rotation value first decreases while going towards shorter wavelengths. It is remarkable that, for example an originally positive specific rotation $[\alpha]^T$ a two principal types of anomalous ORD spectra are possible (Figure 10).

Elucidation of the absolute configuration by using ORD spectroscopy is mainly based on the comparison of the ORD spectra of the examined molecule with the ORD curves of closely

related compounds of known configurations.[90] Furthermore, analogous to optical rotation, the ORD spectra can be predicted by quantum chemical calculations.[72]

Electronic circular dichroism (ECD)

UV-vis spectroscopy offers a way to understand the nature of ground and electronic states and the excitation process. Usually organic molecules adsorb light in the UV-vis region of an electromagnetic spectrum. The absorption of light in UV-vis spectroscopy associated with measuring both energy and probability of exciting a molecule from its ground electronic state to an electronically excited state. Circular dichroism (CD) as a unique type of UV-vis spectroscopy, which is sensitive only to chiral molecules, and can provide much information and a better understanding of the electronic structure. CD and UV-vis spectroscopy have their origins in the same photophysical process: raising an electronic ground state to an electronically excited state by movement of an electron. Consequently, their spectra closely resemble each other (Figure 11). However, CD involves measuring a difference in absorption; CD curves can take on either a positive or a negative bell shape. In contrast, UV-vis spectra are always positive. In UV-vis spectroscopy ordinary light is used.

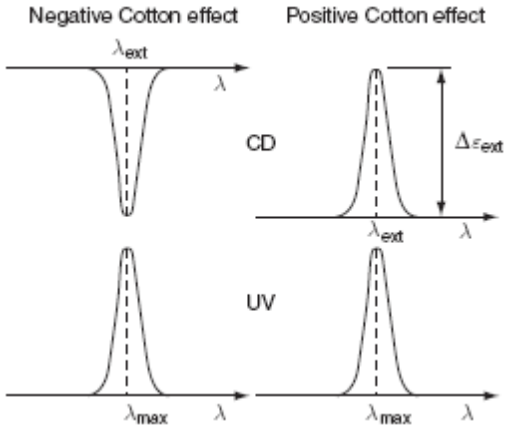

Figure 11. The general pattern of CD and UV spectra[10]

In CD spectroscopy light is anisotropic and circularly polarized, which is achieved by filtering ordinary light through a polarizer to give linearly polarized light. The linearly polarized light is then separated into its left and right circularly polarized components by passing it through a stress plate modulator. When difference in absorption of left and right circularly polarized light is non-zero ($\Delta A = A_L - A_R \neq 0$), circular dichroism can be measured for electronic transitions (Figure 12).

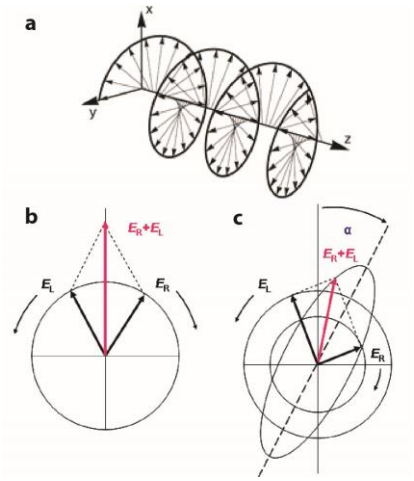

Figure 12. a) Left-circularly polarized light propagating in z-direction, b) Linear polarized light can be viewed as a superposition of opposite circular polarized light of equal amplitude and phase. (b): different absorption of the left- and right hand polarized component leads to ellipticity (CD). http://www.ruppweb.org/cd/cdtutorial.htm

In fact CD is the difference between the absorption coefficients for the left and right circularly polarized light. The original linearly polarized light is composed of left- and right –circularly polarized beams of equal intensity. However when these two oppositely polarized beams pass through a solution of chiral compounds their absorptions coefficients change and become unequal. The angle of θ of the ellipsoidally polarized transmitted light is defined as ellipticity angle (Figure 13).

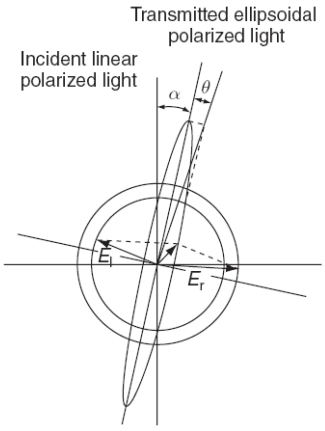

Figure 13. α rotation angle; θ, ellipticity angle; E_l and E_r, electric field vectors of left- and right-circularly polarized lights, respectively.

$$\tan\theta = \frac{\text{short axis of ellipsoid}}{long\ axis\ of\ ellipsoid} \quad (3)$$

The output of CD instruments is usually measured as ellipticity θ (in mdeg), Molar ellipticity [θ] is correlated to molar CD "$\Delta\varepsilon$" as follows: related to CD through θ (mdeg) = 3300 Δε.

$$\Delta\varepsilon = \varepsilon_l - \varepsilon_r \quad (4)$$

Where ε_l and ε_r are absorptions of left and right circularly polarized light, respectively.

In practice the following equation is used for obtaining molar CD Δε.

$$\frac{\theta}{33} = \Delta A = \Delta\varepsilon \times c' \times l' \qquad (5)$$

where ΔA is CD absorbance, c' is the molar concentration (mol solute/dm^3 solution), and l' the cell length (cm).

The equation (5) shows that CD can be measured only in correspondence to absorption bands. A a dichroic peak is also called a CE on account of Frank Albert Cotton (April 9, 1930 – February 20, 2007), the discoverer of the phenomenon. It is worth observing that CD is a signed quantity, because ε_l, may be smaller or larger than ε_r. It is easy to show that for each absorption band, the CD of two enantiomers are always exactly opposite.

Similarly as the ORD curve can be obtained, the measurement of the $\Delta\varepsilon$ value as a function of the wavelength λ leads to a CD spectrum. In general, the measured CD effect is directly associated with the ORD anomaly, since they both reflect the interaction of the polarized light with the same chiroptical chromophore. The maximum of the CD curve coincides with the wavelength of anomalous ORD crossover, and the sign of CE in ORD spectrum corresponds to that of CD (Figure 14).

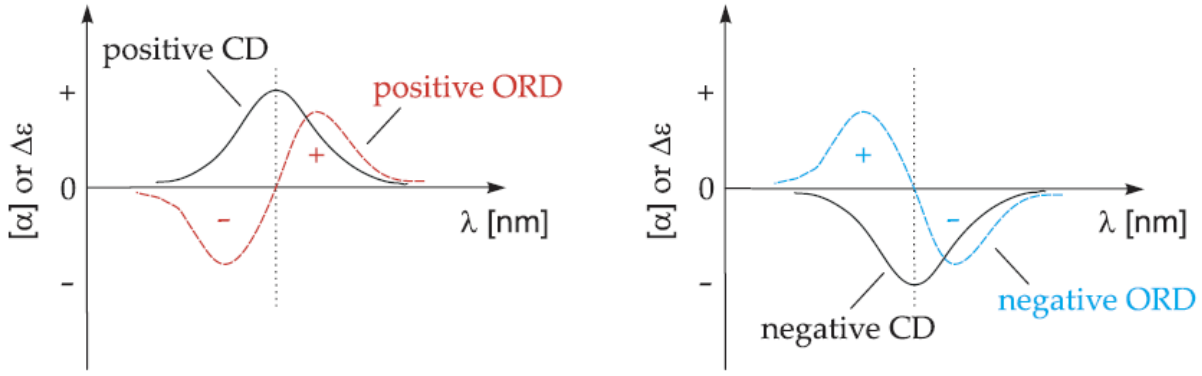

Figure 14. CD and ORD spectra describing (a) the positive and (b) negative CEs of a single electronic transition.[89]

Although both phenomena afford complementary information, CD spectroscopy has now completely replaced the ORD technique, because it provides better discrimination between overlapping bands, whereas the ORD curves often possess a fine structure due to molecular vibrations, which complicates the interpretation of the spectra.

Requirements for ECD phenomena

There are two requirements for a molecule or group of atoms in a molecule to exhibit a circular dichroism (CD) spectrum.

1) The first is the presence of a chromophore *i.e.*, a group that can absorb radiation by virtue of the electronic configuration of its resting or ground state at room temperature. The energy

absorbed results in a transition to a higher-energy or excited state, which has a different distribution of electrons around the nucleus. It can therefore interact with its environment in a way that differs from the ground state. A chromophore is a molecular moiety, responsible for one or more electronic transitions, allied to absorption bands in the UV or in the visible range. In the context of organic chemistry, it is usually a functional group or a combination of several groups with a more or less extended π electron system. A few common examples are depicted in Figure 15.

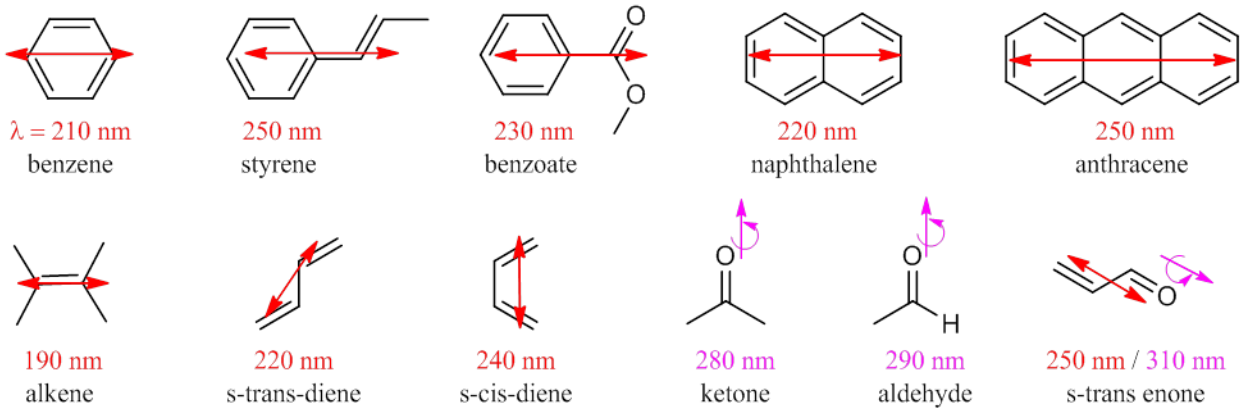

Figure 15. A few simple common organic chromophores with their main transitions; electric transition dipoles in red, magnetic in purple (last three structures).[10]

2) Close associated chromophores with, an optically asymmetric environment. For these reasons a crucial step which must precede any attempt in analyzing a CD spectrum requires a correct recognition of pertinent chromophoric unit(s). A careful estimation of similarity between two chromophores is an important issue, not only when we compare experimental data of different compounds, but also when we apply computational methods.

Solid state circular dichroism

Historically all chiroptical properties, $[\alpha]_T$, ORD, and ECD, have always been discussed as observables in solution. Although it usually requires more complex techniques, these effects can also be measured in both gas and solid states. Solid-state CD can provide information on solute–solvent interactions when compared with the solution spectra in various solvents. Solvent effect on the rotatory power is often the result on the formation of some kind of coordination between the solvent and the optically active molecules concerned in solution. This may affect the optical activity of the molecule by way of conformation alteration in the case of flexible compounds, or through vicinal effects. Furthermore, those conformations that are unstable in solution can be frozen in the crystalline state and then investigated.

Samples can be single crystals, microcrystals, or films. One big advantage for studying the CD of crystals is that the location of relevant atoms and molecules can be revealed through X-ray structure analysis. The ECD spectrum predicted for these well-defined, X-ray derived structures by using, e.g. quantum chemical calculations, can be compared with the experimental solid-state

ECD curve, thereby allowing an assignment of the absolute configuration. This is a rather new and not much investigated field of application of solid-state ECD spectroscopy.

Vibrational circular dichroism (VCD)

The vibrational circular dichroism (VCD) technique is infrared counterpart of ECD, and works in the same way as ECD. In the last few years many papers have described VCD for the determination of the AC in combination with high-level *ab initio* quantum chemical calculations. These methods likewise permit to determine the absolute configuration.[91-96] The first solution-phase measurements date back to the mid-1970s using a dispersive IR spectrometer.[97, 98] Today, measuring VCD over large spectral regions with a specially equipped Fourier Transformed Infrared (FT-IR) spectrometer is becoming more common practice. The main advantage of the vibrational chiroptical techniques with respect to ECD is their ability to distinguish equally well between the enantiomers irrespective of the presence of a chromophore, whereas in ECD, the presence of a chromophore is a fundamental precondition. In comparison with ECD curves, vibrational optical activity spectra contain much more transitions, through which the absolute stereochemistry can be determined. Also from the theoretical point of view, VCD spectra are easier to accurately calculate than ECD curves, since only ground electronic state properties have to be considered.[16, 99-101] CD in vibrational transitions, however, is a weak phenomenon, with magnitudes of typically around 10^{-5} absorbance units. Today, all VCD instruments are equipped with an FT-IR spectrometer. Because of the small magnitude of VCD it requires sophisticated modulation techniques for its observation.[102] Despite obvious advantages of VCD, the standard ECD, due to its wider availability, high sensitivity, and ease of handling, still remains the leading method.

Methods for interpretation of ECD spectra

The measured ECD spectra can be analyzed by using either empirical or semi-emprical relations, or it can be simulated by aid of quantum chemical calculation of ECD spectra and comparing with experimental data.

Empirical comparison of experimental ECD spectra

Determination of absolute configuration of a new natural or synthetic molecule can be easily deduced from a simple empirical comparison of the respective measured CD spectrum with the CD data of a previously obtained compound, for which the absolute stereostructure has been already defined. Furthermore, the comparison with the CD spectra of closely related substances of known configurations may also give hints at the configuration of the investigated molecule. It has to be mentioned that an unambiguous attribution of the absolute stereostructure is possible only if a reference compound possesses an identical chromophoric framework. The small modification and changes on the chromophor or conformation alterations may cause substantial changes in the CD spectrum and we are not allowed directly compare data.

Empirical rules

Up to now a number of *Sector Rules* have been postulated, to elucidate the absolute stereochemistry of various chiral molecules possessing an inherently achiral chromophore, such as benzene (*Quadrant Rule*), carbonyl (*Octant rule*), or alkene (*Diene Rule*). The basic idea of these rules is that the sign of a CE associated with a specific transition is considered to be very sensitive to contributions from all substituents ("*perturbers*") in a chromophore surrounding. These contributions are assessed by dividing the 3D space around the chromophore into sectors characterized by empirically attributed signs.

For compounds having a single chromophore (carbonyl, aryl, diene, enone, *etc.*), qualitative approaches such as sector and helicity rules have been developed. They link the sign of the ECD CEs allied to the main electronic transitions of the chromophore to the AC. These approaches, although widely employed, often present some ambiguity and can lead to incorrect assignments. ECD spectra are sensitive to conformation and chromophores, since small modifications in the Structure of the chromophore or even minor conformational alterations may cause substantial changes in the ECD spectrum. For this reason, although qualitative methods are often the "first" choice for their simplicity and rapidity, they sometimes need to be supported by more rigorous computational analysis.[7]

The carbonyl chromophore – Octant rule

The oldest and most popular sector rule is the so-called "*octant rule*," allowing us to assign the AC of saturated ketones by the sign of the CE allied to the n → π∗ transition of the carbonyl around 300 nm. [1, 7, 103] Although it was originally proposed on empirical grounds,[104] it was later supported by theoretical studies on the origin of the ketone n → π∗ CE. [105] The carbonyl group is characterized by a weak magnetic dipole transition (n → π*) around 300 nm. The *n* and *π*-orbitals define three orthogonal nodal planes, as shown in Figure 16, two of which are also symmetry planes. Overall, they divide the space into eight sectors called octants, which are associated with the signs of contribution to the CD (300 nm) depicted in the Figure 16.

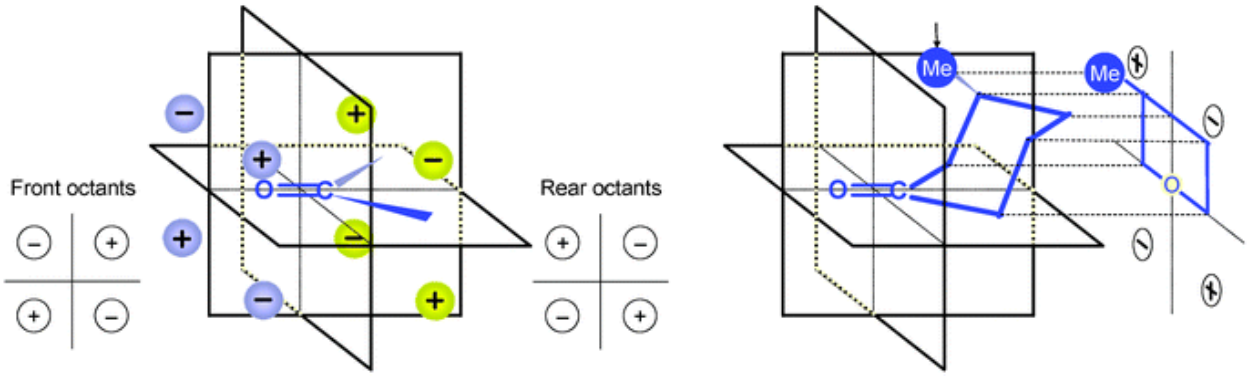

Figure 16. Saturated ketone octant rule; Left: the nodal planes of the chromophore define 8 octants; the signs of the contributions to the CD of the band around 300 nm are shown. Right: how the projection in the rear octant is built for (*R*)-3-methylcyclohexanone ($\Delta\varepsilon_{max}$ = +0.57 at 284 nm).[10]

Figure 1 shows application of the octant rule is (*R*)-3-methylcyclohexanone. In Octant rule, all space surrounding the carbonyl group is divided up to eight octants, and the octant occupied by a particular perturber determines the sign of its contribution to rotatory strength of the n → π* transition. In order to apply the octant rule to determine the AC of a ketone, the conformation of the latter must be known. A major problem arises when the molecule shows an equilibrium of several conformations, since the octant rule only allows predicting the sign of the n → π* band for each conformer but not its intensity. For this reason the octant rule has usually been applied to cyclic, conformationally defined ketones. Another problem of the octant rule concerns the priority assessment of substituents that fall in different octants (opposite signed).

Dienes and *trans*-enones

Dienes and enones form a class of chromophores that can be helical due to non-planarity of the π-bond system. The conformations of these molecules may be conveniently described by considering their helicities. 1,3-Dienes can exist in two planar conformations defined as *S*-trans and *S*-cis and an infinite number of nonplanar, skewed forms, traditionally called cisoid or transoid, depending on the conformation of the nearer planar form.

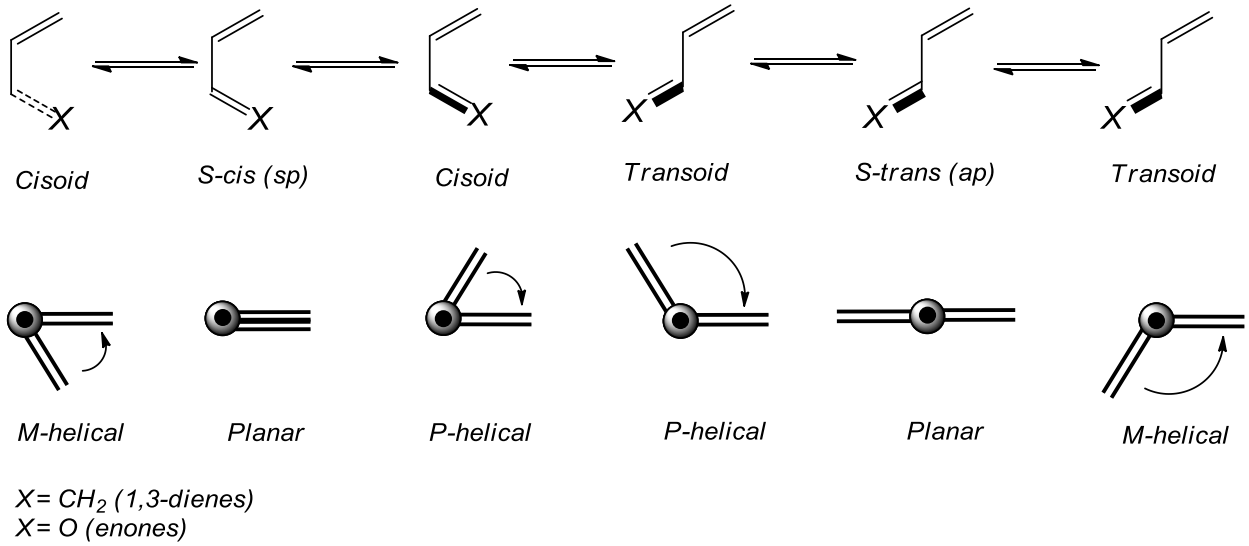

Figure 17. a) Possible planar and nonplanar conformations of 1,3-dienes and enones and b) definition of *M*- and *P*-helicities in the cases of cisoid and transoid 1,3-dienes.[7]

The electronic transitions of 1,3-dienes and enones are reflections of their structures (Figure 17). Conjugated 1,3-dienes show absorption in the 220-280 nm range (π →π* transitions) depending on the possible substitution and ring size. The degree of electron delocalization determines intensity and energy of the low-energy π –π* electronic transition in the diene chromophore. When the diene is skewed, an inherently chiral chromophor is present. The corresponding absolute configuration is correlated with the sign of CE by means of the diene helicity rule. Calculation shows that *p* helicity is correlated with positive CE, and *M* helicity give rise to negative CE. Exceptions to the rule are found especially when the double bonds are not homoannular.

The semiempirical *exciton chirality*

Exciton Chirality was used for first time in 1969 by Harada and Nakanishi for determination AC of adjacent hydroxyl groups. The sign of strong CE from π→π* transition of the glycol dibenzoate derivatives used for the determination of the configuration from the.[106, 107] When two chromophores are in close spatial proximity to one another, and so disposed that a chiral array results, interaction (dynamic coupling) between the individual chromophores gives rise to distinctive CE couplets, often called exciton coupling in the ECD spectrum, from which the configuration of the chiral array may be easily deduced. However, current method has been frequently applied in an empirical manner, in fact it is based on a non-empirical coupled oscillator [108, 109] and on group polarizability[110] theories. Molecules possess two or more well-separated, strongly absorbing chromophores, the movement of an electron creates the oscillating transition dipoles localized on each chromophore which can spatially interact by dipole - dipole coupling in a symmetric and antisymmetric manner. This gives rise to a split of the energy level of the excited state (Δλ, Davydov splitting), resulting in a broadening of the respective UV absorption band. The CD band corresponding to this transition becomes bisignate (Figure 18a). The intensity of such a CD split is inversely proportional to the square of the inter-chromophoric distance.[111]

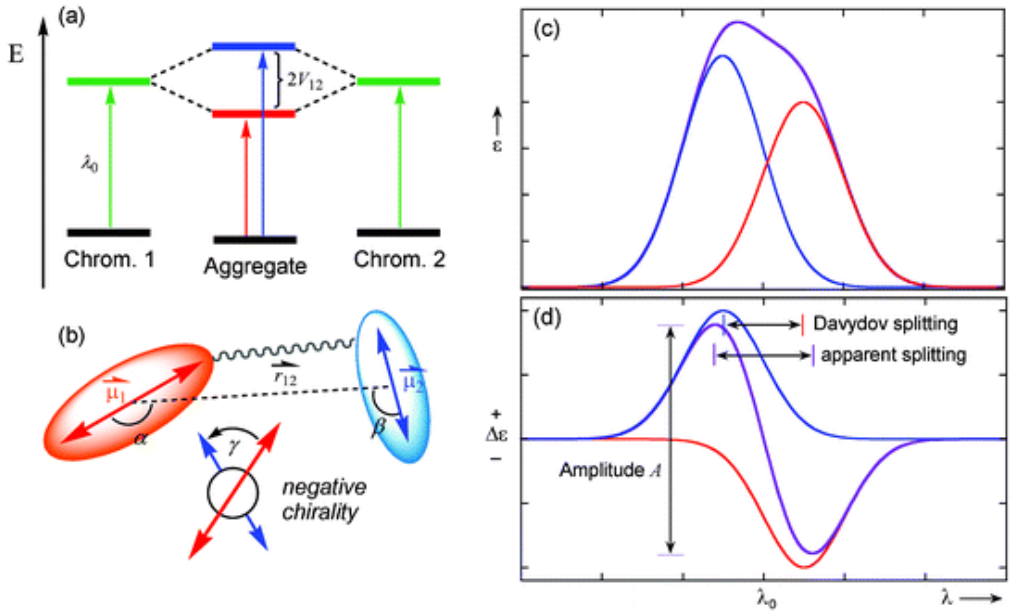

Figure 18. (a) Exciting splitting of two chromophores with negative chirality, (b) representing of geometrical parameters necessary is for predicting CD, (c) expected UV absorption and (d) CD spectra.[10]

According to the Harada and Nakanishi's Exciton Chirality Rule,[112] when the relevant transition moments are oriented to form a positive (+) torsion angle (positive chirality), the long wavelength component of the associated exciton couplet can be expected to exhibit a positive CE. When they are oriented to form a negative (-) torsion angle (negative chirality), the long wavelength CE is negative (Figure 18b).

2.4. AC through quantum chemical calculation

The past decade has witnessed revolutionary advancements in the area of quantum mechanical calculations of ECD as well as other molecular chiroptical properties such as VCD, ORD and OR. The use of TDDFT method, followed by a comparison with the experimental data, represents a powerful tool for the unambiguous determination of the AC of chiral molecules.[76, 112, 113]

In particular, chiroptical data such as ECD, VCD spectra and OR values are extremely sensitive to the overall molecular geometry in terms of both conformation and configuration. Any solution CD spectrum amounts to the sum of contributions from all populated conformations; therefore the set of input structures to be considered in the calculation must be representative of the whole conformational ensemble. Whenever a molecular property is predicted by theory, and used for comparison with the experiment, it is crucial to employ a correct input structure. "Correct" means it must represent possible and true structure (or structures) responsible for the observed property.

In 1993, Bringmann and co-workers developed a Boltzmann approach for the assignment of ACs of NPs, in particular by employing semiempirical QM and TDDFT calculations of ECD spectra for first time (Figure 19). [114] Comparison of calculated and experimentally measured ECD spectra provides an excellent and efficient analytical tool for the assignment of the AC of chiral compounds.[1, 13, 39, 76]

From a practical point of view the concept of "ECD calculations" implies three general steps:

1- Conformational search and energy minimization of a chiral molecule
2- Calculation of the rotatory and oscillator strengths
3- Treatment of the obtained values, leading to the simulation of the ECD and UV curves, which are then compared with the experimental data.

A conformational analysis is normally started with a rapid computational procedure, based on Monte Carlo or molecular dynamics approaches at a low level of theory, such as molecular mechanics (MM).[115] These conformational search routines provide a set of structures that are further optimized at a higher level of theory, usually density functional theory (DFT) or other *ab initio* methods. After a reliable set of input structures has been generated with an initial arbitrary AC, ECD calculations must be run on all minima within a certain energy threshold (2–3 kcal/mol) that is, with significant population (>3 – 5%) at the working temperature (normally, 298 or 300 K).

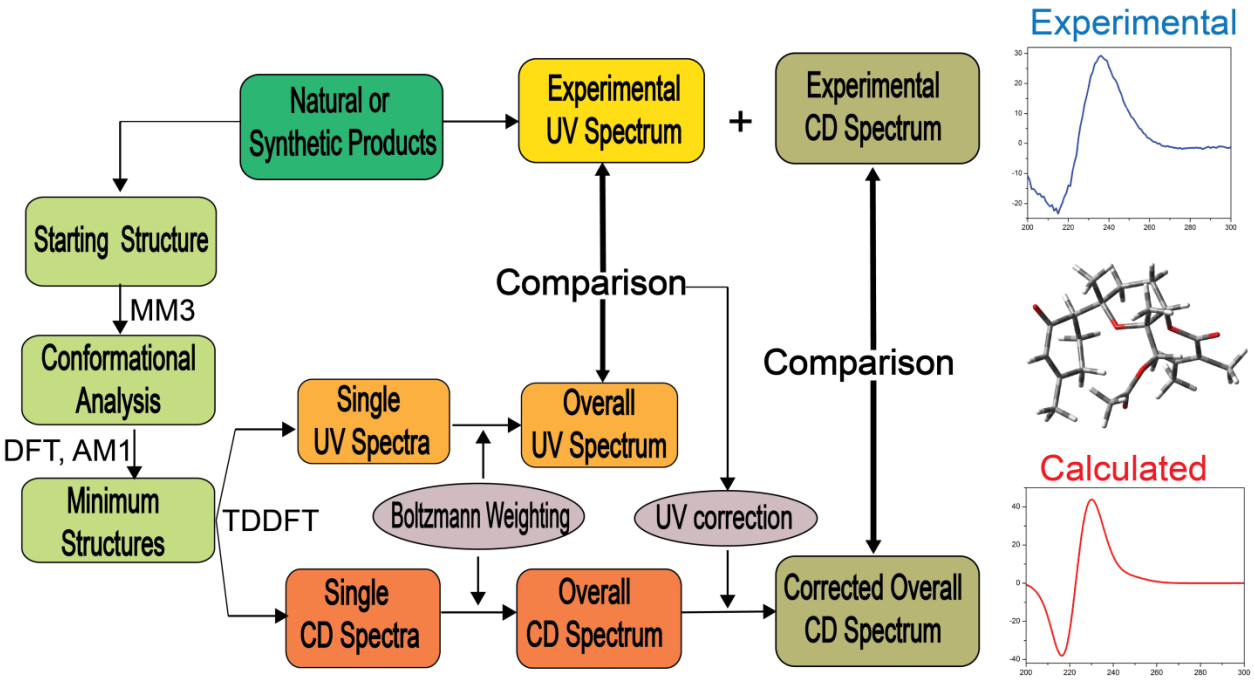

Figure 19: The principal approaches for the assignment of absolute configuration of chiral compounds by quantum chemical ECD calculations in combination with experimental ECD measurements; the conformation-dependent chiroptical behavior is interpreted by conformational analysis.[39] Adapted from Reference 39.

Thereafter, a weighted average of all computed ECD spectra is estimated according to the Boltzmann weights at the working temperature. Reliable populations can be obtained by single point calculations at a higher calculation level which used for geometry optimizations. Furthermore, internal energies should be corrected with zero-point vibrational and entropy terms to afford true free energies. Finally, the weighted average ECD is compared with the experimental ECD spectrum: If the agreement is good with either the calculated ECD (for the initially assumed AC) or its mirror image (i.e., for the opposite AC), the configuration may be assigned.

Conformational analysis

ECD investigations can normally only distinguish between stereoisomers with a sufficient chiroptical differentiation, i.e. usually between enantiomers, whose CD curves are fully opposite. A reliable prediction of ECD requires a thorough conformational analysis. The signs of predicted ECD bands can vary among different conformers (with the same absolute configuration).Therefore it is important that all predominant conformations are identified. In the case of more than one stereogenic element, the relative configuration has to be known in advance by other methods (e.g., by X-ray diffraction or NMR).

In the earlier days, conformational analysis used to be conducted manually by constructing the structures of different possible conformers, and optimizing their geometries. This laborious task can now be automated, using commercial conformational analysis programs, which include

SPARTAN,[116] SYBYL,[117] CONFLEX,[118] HYPERCHEM,[119] and MACROMODEL.[120] These programs generate conformers by rotating atoms around different bonds or by wagging chosen atoms, and they use molecular mechanics force constants to optimize their structures. These rotations can be selected systematically (using rules predefined within the software) or randomly (Monte Carlo method). In addition, molecular mechanics force constants are associated with classically defined bonds (single, double, etc.), and rotations can occur only around single bonds. Therefore the starting structural definitions that are entered as input into the molecular mechanics-based conformational analysis programs are to be identified with classical bonds.[7]

Geometry optimization (minimization)

The geometry of a molecule determines many of its physical and chemical properties. In this regard it is very important to know the precise geometry of a molecule when running the computation. In computational chemistry we are specifically concerned with optimizing bond angles (degrees), bond distances (angstroms), and dihedral angles (degrees). The arrangement of atoms in the molecules and more specifically the electrons around the atom determine the energy level of that molecule. In fact, the energy of a molecular system varies even with small changes in its structure. This is why geometry is so important when performing calculations. The objective of geometry optimization is to find the configuration of minimum energy of the molecule, because this is where the molecule is most stable and most likely to be found in nature. One way to observe the effect of different geometries on energy level is to calculate a potential energy surface (PES). The PES is just a mathematical relationship correlating the particular molecular structure and its single point energy, and describes how the energy of the molecule in a particular state varies as a function of the structure of the molecule.[121] A PES (Figure 20) can be visualized as a hilly landscape, with valleys, peaks, and mountain passes. Geometry optimization usually attempts to locate minima on the PES, thereby predicting equilibrium structures of molecular systems. Optimization can also locate transition structures. Geometry optimization begins at the molecular structure specified as input, and steps along potential energy surfaces. It computes the energy. The procedure calculates the wave function and the energy at a starting geometry and then proceeds to search a new geometry of a lower energy. This is repeated until the lowest energy geometry is found. In the final, minimum energy geometry the force on each atom is zero.

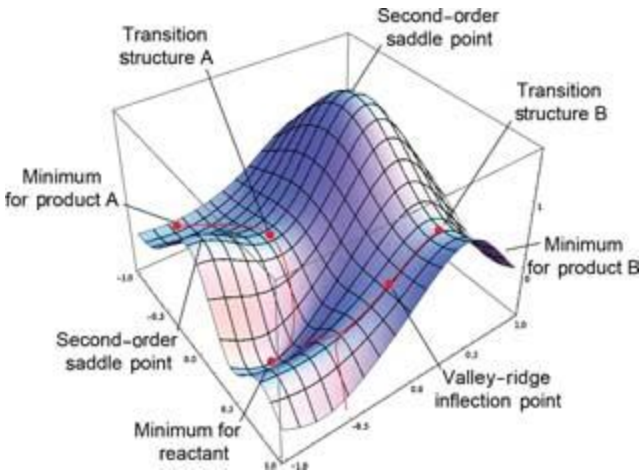

Figure 20. Model potential energy surface showing minima, transition structures, second-order saddle points, reaction paths, and a valley ridge inflection point.[121]

The energies calculated with molecular mechanics methods are not accurate, but as long as a large energy window are used to identify the possible conformations, the conformers generated by molecular mechanics can serve as a reasonable set of starting conformers for further optimization at a higher level of theory, for example . by means of the density functional theory (DFT), mainly with use of the B3LYP or the BLYP functional, often together with the resolution of identity (RI) approximation and with use of a split-valence double-zeta basis set such as 6–31G** to locate all minimum conformers that are significantly populated at ambient temperature.

Basis set

A basis set is a mathematical description of the orbitals of a system, which is used for the approximate theoretical calculation or modeling. It is a set of basic functional building blocks that can be stacked or added to have the features that we need. It was John C. Slater who first turned to orbital computation using basis sets, known as Slater Type Orbitals (STOs).[122]

The electron cloud of an atom in the molecule is usually perturbed in comparison with the isolated atom. The common way to solve this problem is to introduce polarization functions into the basis set. The polarization function have a higher angular quantum number and so correspond to *p* orbitals for hydrogen and *d* orbitals for the first- and second-row elements. Polarization functions denoted in Pople's sets by an asterisk. For example 6-31G* refers to 6-31G basis set with polarization functions on the heavy atoms (non-hydrogen). The 6-31G** indicates polarization functions on heavy atoms and hydrogen or helium.

For example, the 6-31G code means, that the inner shells are represented by "1" contraction constructed from 6 primitives and the valence shell is represented by double zeta with an "inner" contraction constructed from 3 and an "outer" constructed from 1 primitive.[122]

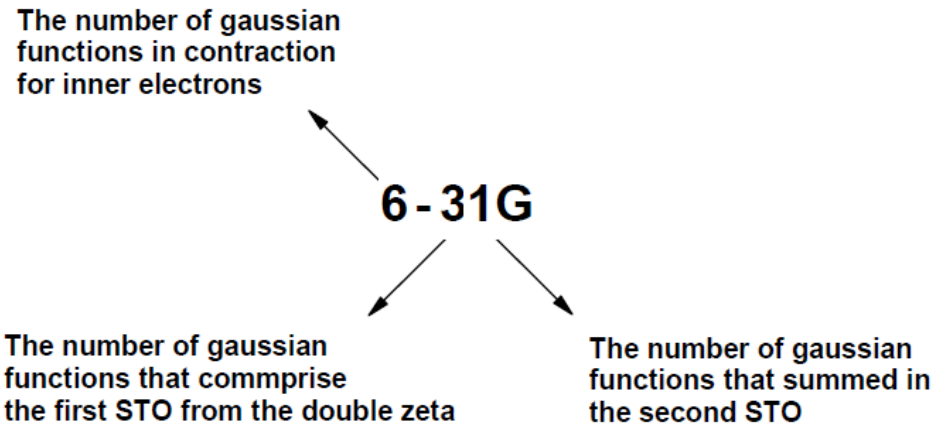

To properly describe the species such as anions and molecules containing lone pairs, additional diffuse functions are used. These basis sets are denoted '+'; thus 6-31+G contain an additional single set of diffuse s-and p-type Gaussian functions. 6-31++G indicates diffuse functions included for hydrogen as well as for heavy atoms.

As soon as a basis set is specified, the software will then compute the energy and the gradient at that point, and decide if it has reached a stopping point (convergence). It then varies the geometry based on the size of the gradient. The self-consistent field (SCF) calculations are done, by calculation of new integrals and the system will reach to a new energy and gradient. These steps are repeated until the software reaches convergence and finds a stationary point. Finally, these energetically favorable minimum structures are then subjected to the actual calculations of excited states.[123]

Computing chiroptical properties

Assuming that one or several optimized structures for the system of interest are available, the next task is then to compute the chiroptical response property (See Figure 19 for a flow chart of computational tasks leading up to the point of chiroptical computations). The main goal in CD spectroscopy is determination of the rotatory strength and the intensity of an absorption band (oscillator strength) ranging from wavelengths λ_1 to λ_2 given (in cgs units) by

$$R = 2.297 \times 10^{-39} \int_{\lambda_1}^{\lambda_2} \frac{\Delta\epsilon(\lambda)}{\lambda} \, \mathrm{d}\lambda \qquad (6)$$

For a transition between states Ψ_0 (ground state) and $|\Psi_i$ (excited state), it is theoretically defined as

$$\begin{aligned} R_{0i} &= Im(\langle\Psi_0|\hat{\mu}|\Psi_i\rangle\langle\Psi_0|\hat{m}|\Psi_i\rangle) \\ &= |\overrightarrow{\mu_{0i}}|\cdot|\overrightarrow{m_{0i}}|\cdot\cos(\overrightarrow{\mu_{0i}}, \overrightarrow{m_{0i}}). \end{aligned} \qquad (7)$$

Where, μ and $\hat{m}$ are the electric and magnetic dipole operators, respectively. An inspection of the equation (7) shows that the electric and magnetic transition dipole moments $\vec{\mu}_{01}$and $\vec{m}_{0i}$ as well as the angle between both moments has to be determined. The sign of theoretical ECD response (R) depends on the relative orientation of two transition moment vectors. Therefore, an accurate prediction of rotatory strengths represents a significantly more demanding task than the calculation of oscillator strengths.

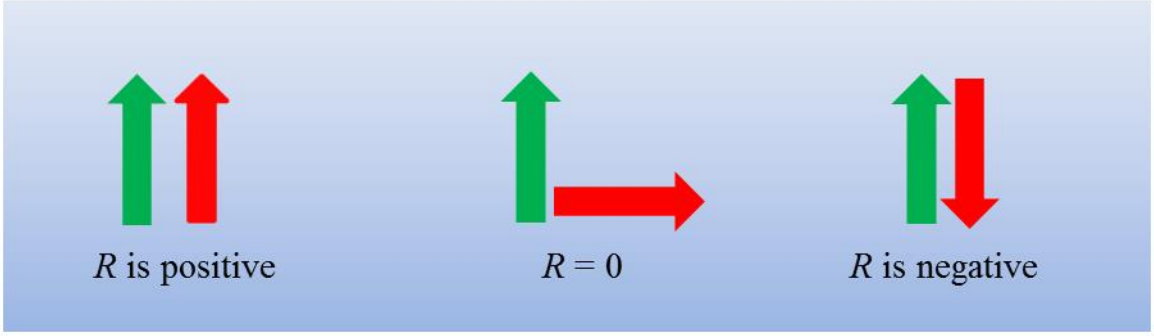

TDDFT together with coupled cluster (CC) theory are the most popular functions used to simulate a reliable ECD. Nevertheless, the TDDFT, has been considered to provide the best balance between accuracy and computational cost, hence being the most frequently used method of choice. However, in the case of highly conjugated π system, TDHF is preferred over TDDFT since the later method overestimated the extent of conjugation. Precise TDDFT-based ECD predictions can be obtained using B3LYP functional and moderate to large basis sets depending on the system such as 6-31G(d), 6-311+G(2d,2p), aug-cc-pVTZ, etc. To obtain a more optimal correlation with the experimental trace, some case studies show variation in the choice of hybrid functional (BPW91, BHLYP). Up to now, a high computational level which has been used for ECD calculation is a hybrid method called TDDFT/MRCI (where MR stands for multi-reference and CI for configuration-interaction). In this method the electron correlation is considered, and provides even more reliable ECD predication, but is expensive and highly time consuming and at the moment cannot applied for big systems.[7, 13, 14, 72, 89, 124]

Simulation of the band-shape curves

In practice, predictions of at least 10 excited states are necessary to simulate an ECD spectrum over a typically measured range (200-800 nm). Both Lorentzian and Gaussian bandshapes have been utilized for simulating the theoretical ECD trace. Normally simulation of the band-shape of curves Δε (λ) and ε(λ) from the bar spectra is performed by utilizing a Gaussian distribution. Thus, for each *k*th electronic excitation centered at the wavelength λ_k the Gaussian shape function is constructed according to expression (Eq. 8), followed by the addition of these Gausses over the whole wavelength range λ to provide the final CD curve Δε(λ), or the UV spectrum ε(λ) when pursuing equation (Eq. 9).

$$\Delta\varepsilon(\lambda) = \frac{16\pi^2 N_A \lambda R_{0k}}{6909\hbar c} \cdot \frac{1}{\sigma\sqrt{2\pi}} \exp\left[-\frac{(\lambda-\lambda_k)^2}{2\sigma^2}\right] \qquad (8)$$

$$\varepsilon(\lambda) = \frac{4\pi^2 N_A \lambda D_{0k}}{6909\hbar c} \cdot \frac{1}{\sigma\sqrt{2\pi}} \exp\left[-\frac{(\lambda-\lambda_k)^2}{2\sigma^2}\right] \qquad (9)$$

In these equations, σ is the exponential half-width, i.e., half the width of the CD or UV band at 1/e height, which is used as an adjustable parameter for reproducing the experimental CD or UV features.

Dependence of the shape of predicted CD spectrum on the σ value is represented in Figure 21. The detailed CD spectrum is obtained in smaller σ values, whereas larger σ values make the smoother and broader spectrum (Figure 21). In this thesis to simulate CD spectra the half width ranged from 0.15 eV to 0.2 eV.

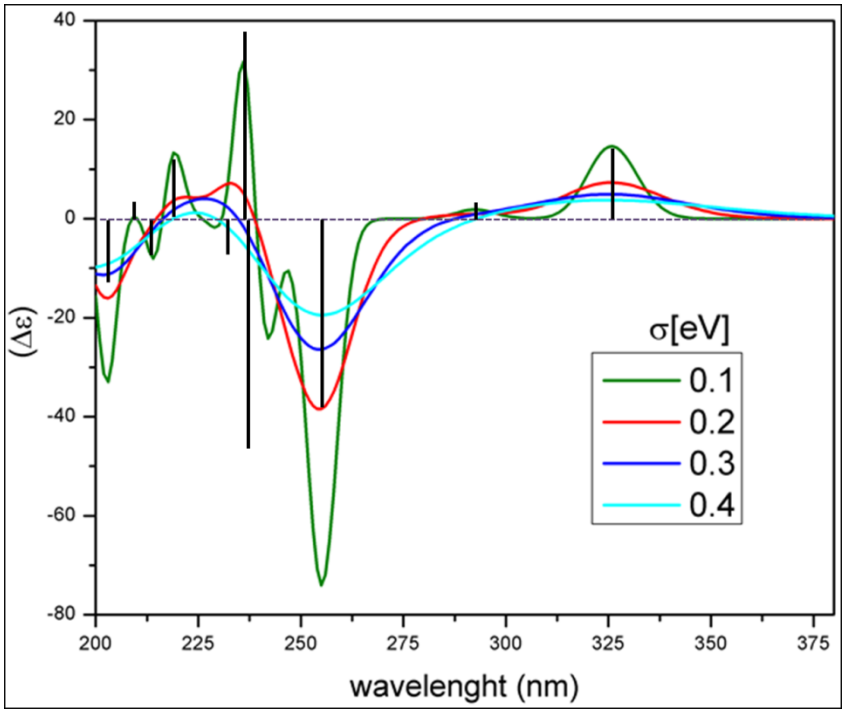

Figure 21. Influence of *σ* on the shape of a simulated "Gauss"

Obtaining of the overall spectra

The next step is the summing up of the single spectra of the individual conformers to provide the overall CD or UV spectrum. For the conformers obtained from the conformational analysis, adding up is carried out in accordance with the Boltzmann statistics. Thus, the contribution of the

particular single spectrum to the overall one is estimated by calculating the weighting factor *fi* for each *i*th conformer in the dependence on its relative energy *ΔEi* with respect to the global minimum structure (Eq. 10).[13, 89]

$$f_i = \frac{e^{-\frac{\Delta E_i}{k_B T}}}{\sum_i^{N_{conf}} e^{-\frac{\Delta E_i}{k_B T}}} \qquad (10)$$

Here, k_B is the Boltzmann constant T is the absolute temperature, and N_{conf} is the number of all conformers considered.

$$CD_{overall} = \sum_i^{N_{conf}} f_i . CD_i \qquad \text{and} \qquad UV_{overall} = \sum_i^{N_{conf}} f_i . UV_i$$

The overall CD or UV spectrum is then obtained as the weighted average of the single spectra (Figure 22).

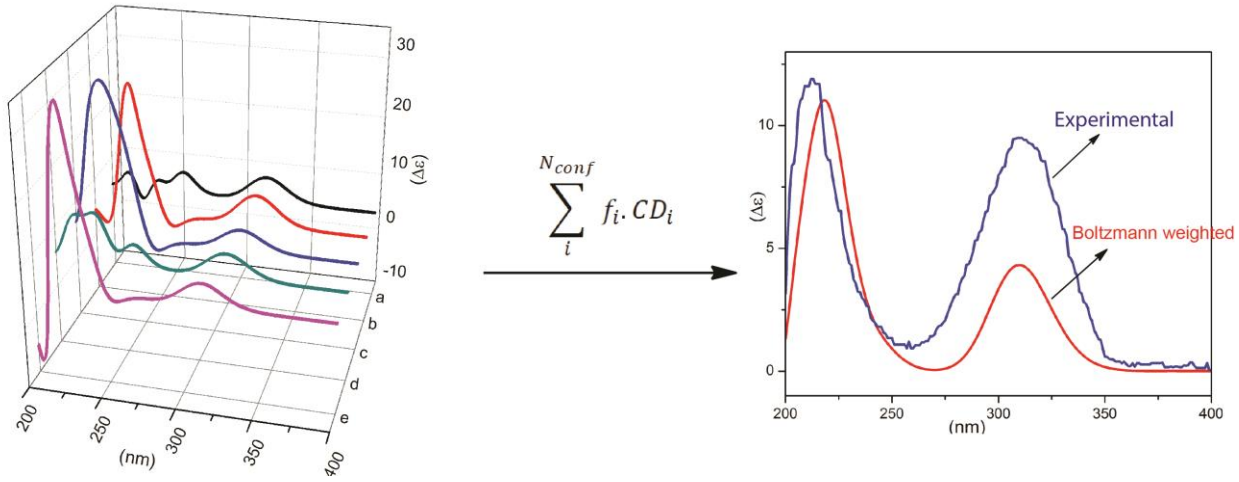

Figure 22. Representation for Boltzmann weighting, single calculated CD spectra of all possible conformers (right), overlaid experimental and calculated Boltzmann weighted CD spectrum (left).

Matching of experimental spectra

To figure out systematic error of used methods, the calculated UV spectrum is compared with the experimental UV curve in order to estimate the accuracy of the calculations. Generally, semiempirical methods provide overestimated result and the calculated spectrum has to be red-shifted to reproduce the measured curve, whereas the TDDFT calculations often provide underestimate transition energies, so that a correcting blue shift is required to match the experimental UV spectrum (Figure 23). Finally, the assignment of the absolute configuration of

chiral compound will done after UV correction by comparison of corrected theoretical CD spectrum with the measured curve.[89]

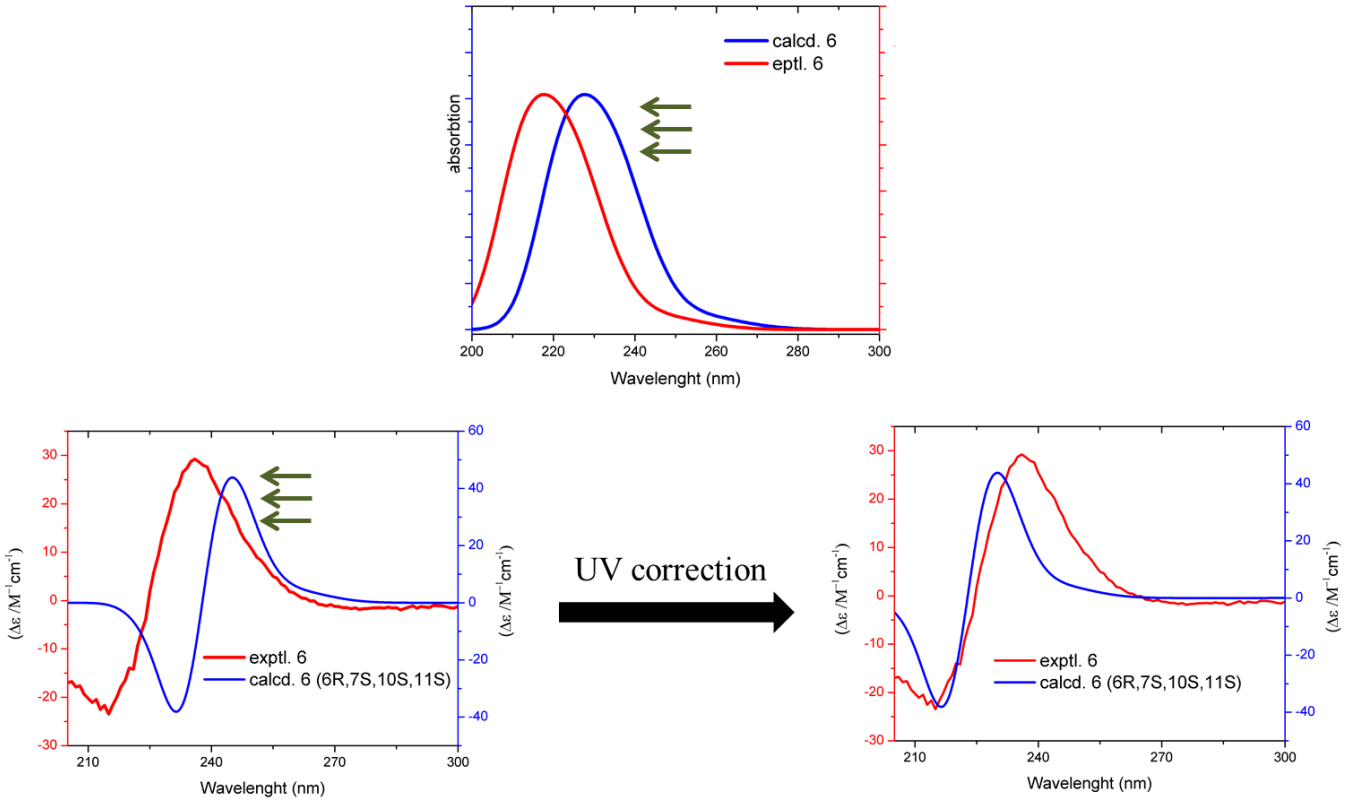

Figure 23: Principle of a UV correction

References

1. Pescitelli, G.; Kurtan, T.; Florke, U.; Krohn, K., Absolute Structural Elucidation of Natural Products-A Focus on Quantum-Mechanical Calculations of Solid-State CD Spectra. *Chirality* **2009,** *21*, E181-E201.
2. Newman, D. J.; Cragg, G. M., Natural products as sources of new drugs over the last 25 years. *Journal of Natural Products* **2007,** *70*, 461-477.
3. McConathy, J.; Owens, M. J., Stereochemistry in Drug Action. *Prim Care Companion J Clin Psychiatry* **2003,** *5*, 70-73.
4. Westerhof, F. J.; Zuidhof, A. B.; Kok, L.; Meurs, H.; Zaagsma, J., Effects of salbutamol and enantiomers on allergen-induced asthmatic reactions and airway hyperreactivity. *Eur Respir J* **2005,** *25*, 864-72.
5. Petrovic, A. G.; Navarro-Vazquez, A.; Lorenzo Alonso-Gomez, J., From Relative to Absolute Configuration of Complex Natural Products: Interplay Between NMR, ECD, VCD, and ORD Assisted by ab initio Calculations. *Current Organic Chemistry* **2010,** *14*, 1612-1628.
6. Nakanishi, K. o.; Berova, N.; Woody, R., *Circular dichroism : principles and applications*. VCH: New York, N.Y., 1994; p xvii, 570 p.
7. Berova, N., *Advances in chiroptical methods*. Wiley: Hoboken, NJ, 2012.
8. Stephens, P. J.; Pan, J. J.; Devlin, F. J.; Krohn, K.; Kurtán, T., Determination of the Absolute Configurations of Natural Products via Density Functional Theory Calculations of Vibrational Circular Dichroism, Electronic Circular Dichroism, and Optical Rotation: The Iridoids Plumericin and Isoplumericin. *The Journal of Organic Chemistry* **2007,** *72*, 3521-3536.
9. Polavarapu, P. L., Protocols for the analysis of theoretical optical rotations. *Chirality* **2006,** *18*, 348-356.
10. Berova, N.; Di Bari, L.; Pescitelli, G., Application of electronic circular dichroism in configurational and conformational analysis of organic compounds. *Chem Soc Rev* **2007,** *36*, 914-931.
11. Allenmark, S. G., Chiroptical methods in the stereochemical analysis of natural products. *Nat Prod Rep* **2000,** *17*, 145-155.
12. Warnke, I.; Furche, F., Circular dichroism: electronic. *Wires Comput Mol Sci* **2012,** *2*, 150-166.
13. Bringmann, G.; Bruhn, T.; Maksimenka, K.; Hemberger, Y., The Assignment of Absolute Stereostructures through Quantum Chemical Circular Dichroism Calculations. *Eur J Org Chem* **2009**, 2717-2727.
14. Petrovic, A. G.; Navarro-Vazquez, A.; Alonso-Gomez, J. L., From Relative to Absolute Configuration of Complex Natural Products: Interplay Between NMR, ECD, VCD, and ORD Assisted by ab initio Calculations. *Current Organic Chemistry* **2010,** *14*, 1612-1628.
15. Stephens, P. J.; Devlin, F. J.; Pan, J. J., The determination of the absolute configurations of chiral molecules using vibrational circular dichroism (VCD) spectroscopy. *Chirality* **2008,** *20*, 643-663.
16. Drabowicz, J.; Zajac, A.; Lyzwa, P.; Stephens, P. J.; Pan, J. J.; Devlin, F. J., Determination of the absolute configurations of isotopically chiral molecules using vibrational circular dichroism (VCD) spectroscopy: the isotopically chiral sulfoxide, perdeuteriophenyl-phenyl-sulfoxide. *Tetrahedron-Asymmetr* **2008,** *19*, 288-294.
17. Hata, Y.; Zimmermann, S.; Quitschau, M.; Kaiser, M.; Hamburger, M.; Adams, M., Antiplasmodial and Antitrypanosomal Activity of Pyrethrins and Pyrethroids. *Journal of Agricultural and Food Chemistry* **2011,** *59*, 9172-9176.
18. Kim, H. J.; Baburin, I.; Zaugg, J.; Ebrahimi, S. N.; Hering, S.; Hamburger, M., HPLC-based Activity Profiling - Discovery of Sanggenons as GABAA Receptor Modulators in the Traditional Chinese Drug Sang bai pi (Morus alba Root Bark). *Planta Med* **2012,** *78*, 440-7.

19. Rueda, D. C.; Zaugg, J.; Quitschau, M.; Reich, E.; Hering, S.; Hamburger, M., Discovery of GABA(A) Receptor Modulator Aristolactone in a Commercial Sample of the Chinese Herbal Drug "Chaihu" (Bupleurum chinense Roots) Unravels Adulteration by Nephrotoxic Aristolochia manshuriensis Roots. *Planta Med* **2012,** *78*, 207-210.
20. Slusarczyk, S.; Zimmermann, S.; Kaiser, M.; Matkowski, A.; Hamburger, M.; Adams, M., Antiplasmodial and Antitrypanosomal Activity of Tanshinone-Type Diterpenoids from Salvia miltiorrhiza. *Planta Med* **2011,** *77*, 1594-1596.
21. Vidal, V.; Potterat, O.; Louvel, S.; Hamy, F.; Mojarrab, M.; Sanglier, J.-J.; Klimkait, T.; Hamburger, M., Library-Based Discovery and Characterization of Daphnane Diterpenes as Potent and Selective HIV Inhibitors in Daphne gnidium. *Journal of Natural Products* **2012,** *75*, 414-419.
22. Zaugg, J.; Ebrahimi, S. N.; Smiesko, M.; Baburin, I.; Hering, S.; Hamburger, M., Identification of GABA A receptor modulators in Kadsura longipedunculata and assignment of absolute configurations by quantum-chemical ECD calculations. *Phytochemistry* **2011,** *72*, 2385-95.
23. Zimmermann, S.; Kaiser, M.; Brun, R.; Hamburger, M.; Adams, M., Cynaropicrin: The First Plant Natural Product with In Vivo Activity against Trypanosoma brucei. *Planta Med* **2012,** *78*, 553-6.
24. Adams, M.; Zimmermann, S.; Kaiser, M.; Brun, R.; Hamburger, M., Protocol for HPLC-based Activity Profiling for Natural Products with Activities against Tropical Parasites. *Nat Prod Commun* **2009,** *4*, 1377-1381.
25. Newman, D. J.; Cragg, G. M., Natural products as sources of new drugs over the 30 years from 1981 to 2010. *Journal of Natural Products* **2012,** *75*, 311-335.
26. Potterat, O., Targeted approaches in natural product lead discovery. *Chimia* **2006,** *60*, 19-22.
27. Petersen, F.; Amstutz, R., *Natural compounds as drugs*. Birkhäuser: Basel ; Boston, 2008.
28. Rollinger, J. M.; Langer, T.; Stuppner, H., Strategies for efficient lead structure discovery from natural products. *Current Medicinal Chemistry* **2006,** *13*, 1491-1507.
29. Pfisterer, P. H.; Wolber, G.; Efferth, T.; Rollinger, J. M.; Stuppner, H., Natural Products in Structure-Assisted Design of Molecular Cancer Therapeutics. *Current Pharmaceutical Design* **2010,** *16*, 1718-1741.
30. Butler, M. S.; Newman, D. J., Mother Nature's gifts to diseases of man: the impact of natural products on anti-infective, anticholestemics and anticancer drug discovery. *Prog Drug Res* **2008,** *65*, 1, 3-44.
31. Potterat, O.; Hamburger, M., Natural products in drug discovery - Concepts and approaches for tracking bioactivity. *Current Organic Chemistry* **2006,** *10*, 899-920.
32. Challal, S.; Bohni, N.; Buenafe, O. E.; Esguerra, C. V.; de Witte, P. A. M.; Wolfender, J.-L.; Crawford, A. D., Zebrafish Bioassay-guided Microfractionation for the Rapid in vivo Identification of Pharmacologically Active Natural Products. *Chimia* **2012,** *66*, 229-232.
33. Queiroz, E. F.; Wolfender, J.-L.; Hostettmann, K., Modern Approaches in the Search for New Lead Antiparasitic Compounds from Higher Plants. *Current Drug Targets* **2009,** *10*, 202-211.
34. Wolfender, J.-L.; Queiroz, E. F., New Approaches for Studying the Chemical Diversity of Natural Resources and the Bioactivity of their Constituents. *Chimia* **2012,** *66*, 324-329.
35. Nicoli, R.; Martel, S.; Rudaz, S.; Wolfender, J.-L.; Veuthey, J.-L.; Carrupt, P.-A.; Guillarme, D., Advances in LC platforms for drug discovery. *Expert Opinion on Drug Discovery* **2010,** *5*, 475-489.
36. Potterat, O.; Hamburger, M., Natural products in drug discovery - concepts and approaches for tracking bioactivity. *Curr. Org. Chem.* **2006,** *10*, 899-920.
37. Potterat, O., Targeted approaches in natural product lead discovery. *Chimia* **2006,** *60*, 19-22.
38. Koehn, F. E., High impact technologies for natural products screening. *Prog Drug Res* **2008,** *65*, 175, 177-210.
39. Bringmann, G.; Gulder, T. A. M.; Reichert, M.; Gulder, T., The online assignment of the absolute configuration of natural products: HPLC-CD in combination with quantum chemical CD calculations. *Chirality* **2008,** *20*, 628-642.
40. Potterat, O.; Hamburger, M., Concepts and technologies for tracking bioactive compounds in natural product extracts: generation of libraries, and hyphenation of analytical processes with bioassays. *Nat Prod Rep* **2013**.

41. Wolfender, J.-L., HPLC in Natural Product Analysis: The Detection Issue. *Planta Medica* **2009,** *75*, 719-734.
42. Zaugg, J. Discovery of New Scaffolds for GABAA Receptor Modulators from Natural Origin. Universität Basel, Basel, 2011.
43. Gorji, A.; Ghadiri, M. K., History of epilepsy in Medieval Iranian medicine. *Neurosci Biobehav R* **2001,** *25*, 455-461.
44. Sina., I., *Al-Qanun Fi'l Tibb. English Translation of the Critical Arabic Text.* Jamia Hamdard Printing Press: New Delhi, 1998.
45. Razi, A.-B. M. h. i. Z., *Kitab al-Hawii fi al-tibb*. 1955.
46. Ancient Iranian medicine. http://en.wikipedia.org/wiki/Ancient_Iranian_medicine (March, 2013),
47. Adhami, H. R., Mesgarpour B, Farsam H., Herbal medicine in Iran. *The Journal of the American Botanical Council (HerbalGram)* **2007,** *74*, 34-43.
48. Darmani, N., Avicenna: the prince of physician and a giant in pharmacology. *The Journal of Islamic Medical Association of North America* **1995,** *26*, 78-81.
49. Faridi, P.; Roozbeh, J.; Mohagheghzadeh, A., Ibn-Sina's life and contributions to medicinal therapies of kidney calculi. *Iran J Kidney Dis* **2012,** *6*, 339-45.
50. http://fouman.com/Y/Image/History/Samanid_Avicenna_Qanun_Medicine.jpg (March, 2013),
51. Encyclopedia of Iranica. http://www.iranicaonline.org/articles/abu-mansur-mowaffaq-b-ali-heravi-fl-ca-980-90 (Januery, 2013),
52. Ghasemi Dehkordi N.A., S. S. E., Ghanadi A.R., Amanzadeh Y., Azadbakht M., Asghari Gh.R., Amin Gh.R., Haji Akhoundi A.,Taleb A.M, *Iranian Herbal Pharmacopoeia*. Ministry of Health and Medical Education: Tehran, 2004.
53. Naghibi, F., Mosaddegh, M; Mohammadi Motamed M; Ghorbani A,, Labiatae Family in folk Medicine in Iran: from Ethnobotany to Pharmacology. *The Iranian Journal of Pharmaceutical Research* **2005,** *4*, 63-79.
54. Gorji, A., Pharmacological treatment of headache using traditional Persian medicine. *Trends Pharmacol Sci* **2003,** *24*, 331-4.
55. Khaleghi Ghadiri, M.; Gorji, A., Natural remedies for impotence in medieval Persia. *Int J Impot Res* **2004,** *16*, 80-3.
56. Hooper, D.; Field, H., *Useful plants and drugs of Iran and Iraq / by David Hooper. With notes by Henry Field*. Chicago,, 1937.
57. Shokri, M. S., N., The study of medicinal plants in mazandaran (Northeran Iran). *Acta Hort. (ISHS)* **1993,** *333*, 165-174.
58. Ghorbani, A., Studies on pharmaceutical ethnobotany in the region of turkmen sahra, north of Iran - (Part 1): general results. *J. Ethnopharmacol.* **2005,** *102*, 58-68.
59. Mosaddegh, M.; Naghibi, F.; Moazzeni, H.; Pirani, A.; Esmaeili, S., Ethnobotanical survey of herbal remedies traditionally used in Kohghiluyeh va Boyer Ahmad province of Iran. *J. Ethnopharmacol.* **2012,** *141*, 80-95.
60. Miraldi, E.; Ferri, S.; Mostaghimi, V., Botanical drugs and preparations in the traditional medicine of West Azerbaijan (Iran). *J. Ethnopharmacol.* **2001,** *75*, 77-87.
61. Adhami, H.-R. Bioassay guided isolation of compounds with acetylcholinesterase inhibitory activity from selected medicinal plants used in Iranian Traditional Medicine. University of Vienna, Vienna, 2012.
62. Sairafianpour, M. Iranian Medicinal Plants and Antiparasitic Compounds; from Ethnobotany to Contemporary Scientific Evidence. The Royal Danish School of Pharmacy, 2002.
63. Esmaeili, S.; Naghibi, F.; Mosaddegh, M.; Sahranavard, S.; Ghafari, S.; Abdullah, N. R., Screening of antiplasmodial properties among some traditionally used Iranian plants. *J. Ethnopharmacol.* **2009,** *121*, 400-404.
64. Animals and Plants Unique to Iran. http://Intreasures.com/iran.html (February, 2013),
65. Jalili, A.; Jamzad, Z., *Red data book of Iran: a preliminary survey of endemic, rare and endangered plant species in Iran*. Research Institute of Forests and Rangelands: 1999.

66. Noroozi, J.; Akhani, H.; Breckle, S. W., Biodiversity and phytogeography of the alpine flora of Iran. *Biodivers Conserv* **2008,** *17*, 493-521.

67. Raunkiær, C.; Gilvert-Carter, H.; Fausbøll, A.; Tansley, A. G., *The life forms of plants and statistical plant geography*. The Clarendon press: Oxford,, 1934; p xvi, 632 p.

68. Whyte, L. L., Chirality. *Nature* **1958,** *182*, 198-198.

69. Solomons, T. W. G.; Fryhle, C. B., *Organic chemistry*. 10th ed.; Wiley: Hoboken, NJ, 2011.

70. Horeau, A.; Guette, J. P., Diastereoisomer Interactions of Liquid-Phase Antipodes. *Tetrahedron* **1974,** *30*, 1923-1931.

71. Horeau, A., Enantiomer Interactions in Solution . Effect on Rotatory Power, Optical Purity and Enantiomeric Purity. *Tetrahedron Lett* **1969**, 3121.

72. Stephens, P. J.; Pan, J. J.; Devlin, F. J.; Cheeseman, J. R., Determination of the Absolute Configurations of Natural Products Using TDDFT Optical Rotation Calculations: The Iridoid Oruwacin. *Journal of Natural Products* **2008,** *71*, 285-288.

73. Bijvoet, J. M.; Peerdeman, A. F.; Vanbommel, A. J., Determination of the Absolute Configuration of Optically Active Compounds by Means of X-Rays. *Nature* **1951,** *168*, 271-272.

74. Flack, H. D., The use of X-ray crystallography to determine absolute configuration (II). *Acta Chim Slov* **2008,** *55*, 689-691.

75. Flack, H. D.; Bernardinelli, G., The use of X-ray crystallography to determine absolute configuration. *Chirality* **2008,** *20*, 681-690.

76. Li, X. C.; Ferreira, D.; Ding, Y. Q., Determination of absolute configuration of natural products: theoretical calculation of electronic circular dichroism as a tool. *Current Organic Chemistry* **2010,** *14*, 1678-1697.

77. Wenzel, T. J., *Discrimination of chiral compounds using NMR spectroscopy*. Wiley-Interscience: Hoboken, N.J., 2007; p xxiii, 549 p.

78. Seco, J. M.; Quiñoá, E.; Riguera, R., The Assignment of Absolute Configuration by NMR. *Chemical Reviews* **2004,** *104*, 17-118.

79. Seco, J. M.; Quiñoá, E.; Riguera, R., Assignment of the Absolute Configuration of Polyfunctional Compounds by NMR Using Chiral Derivatizing Agents. *Chemical Reviews* **2012,** *112*, 4603-4641.

80. Kowalczyk, R.; Skarzewski, J., O-Methylatrolactic acid as a new reagent for determination of the enantiomeric purity and absolute configuration of chiral alcohols and amines. *Tetrahedron-Asymmetr* **2006,** *17*, 1370-1379.

81. Enders, D.; Thomas, C. R.; Runsink, J., 5-Amino-4-aryl-2,2-dimethyl-1,3-dioxans: application as chiral NMR shift reagents and derivatizing agents for acidic compounds. *Tetrahedron-Asymmetr* **1999,** *10*, 323-326.

82. Chauvin, A. S.; Bernardinelli, G.; Alexakis, A., Determination of the absolute configuration of chiral cyclic alcohols using diamine derivatizing agents by P-31 NMR spectroscopy. *Tetrahedron-Asymmetr* **2006,** *17*, 2203-2209.

83. Fuerstner, A.; Fluegge, S.; Larionov, O.; Takahashi, Y.; Kubota, T.; Kobayashi, J. i., Total synthesis and biological evaluation of amphidinolide V and analogues. *Chemistry-a European Journal* **2009,** *15*, 4011-4029.

84. Nilewski, C.; Carreira, E. M., Recent Advances in the Total Synthesis of Chlorosulfolipids. *Eur J Org Chem* **2012**, 1685-1698.

85. Tadano, K.-i., Natural Product Synthesis Featuring Intramolecular Diels-Alder Approaches - Total Syntheses of Tubelactomicins and Spiculoic Acid A. *Eur J Org Chem* **2009**, 4381-4394.

86. Umezawa, T.; Matsuda, F., Stereoselective Total Syntheses of Chlorosulfolipids. *Journal of Synthetic Organic Chemistry Japan* **2011,** *69*, 1122-1133.

87. Bringmann, G.; God, R.; Schaffer, M., An improved degradation procedure for determination of the absolute configuration in chiral isoquinoline and beta-carboline derivatives. *Phytochemistry* **1996,** *43*, 1393-1403.

88. Bringmann, G.; Geuder, T.; Rubenacker, M.; Zagst, R., Acetogenic isoquinoline alkaloids .22. Afacile degradation procedure for determination of absoluteconfiguration in 1,3-dimethyltetraquinolines and dihydroisoquinolines. *Phytochemistry* **1991,** *30*, 2067-2070.

89. Maksimenka, K. Absolute Configuration by Circular Dichroism Quantum Chemical CD Calculations. Die Julius-Maximilians-Universität Würzburg, 2010.

90. Mitscher, L. A.; Park, Y. H.; Clark, D.; Beal, J. L., Anti-Microbial Agents from Higher-Plants - Anti-Microbial Isoflavonoids and Related Substances from Glycyrrhiza-Glabra L Var Typica. *Journal of Natural Products* **1980,** *43*, 259-269.

91. Studying Chirality with Vibrational Circular Dichroism http://www.gaussian.com/g_whitepap/vcd.htm (February, 2013),

92. Kuppens, T.; Herrebout, W.; Van Der Veken, B.; Corens, D.; De Groot, A.; Doyon, J.; Van Lommen, G.; Bultinck, P., Elucidation of the absolute configuration of JNJ-27553292, a CCR2 receptor antagonist, by vibrational circular dichroism analysis of two precursors. *Chirality* **2006,** *18*, 609-20.

93. Yang, G.; Tran, H.; Fan, E.; Shi, W.; Lowary, T. L.; Xu, Y., Determination of the Absolute Configurations of Synthetic Daunorubicin Analogues Using Vibrational Circular Dichroism Spectroscopy and Density Functional Theory. *Chirality* **2010,** *22*, 734-743.

94. Devlin, F. J.; Stephens, P. J.; Figadere, B., Determination of the absolute configuration of the natural product klaivanolide via density functional calculations of Vibrational Circular Dichroism (VCD). *Chirality* **2009,** *21*, E48-E53.

95. Uncuta, C.; Ion, S.; Gherase, D.; Bartha, E.; Teodorescu, F.; Filip, P., Absolute Configurational Assignment in Chiral Compounds through Vibrational Circular Dichroism (VCD) Spectroscopy. *Revista De Chimie* **2009,** *60*, 86-98.

96. Nafle, L. A., Vibrational circular dichroism: A new tool for the solution-state determination of the structure and absolute configuration of chiral natural product molecules. *Natural Product Communications* **2008,** *3*, 451-466.

97. Faulkner, T. R.; Moscowit.A; Holzwart.G; Hsu, E. C.; Mosher, H. S., Infrared Circular-Dichroism of carbon-hydrogen and carbon-deuterium stretching modes - calculations. *J Am Chem Soc* **1974,** *96*, 252-253.

98. Nafie, L. A.; Keiderling, T. A.; Stephens, P. J., Vibrational Circular-Dichroism. *J Am Chem Soc* **1976,** *98*, 2715-2723.

99. Mazzanti, A.; Casarini, D., Recent trends in conformational analysis. *Wiley Interdisciplinary reviews-computational molecularscience* **2012,** *2*, 613-641.

100. Magyarfalvi, G.; Tarczay, G.; Vass, E., Vibrational circular dichroism. *Wires Comput Mol Sci* **2011,** *1*, 403-425.

101. Gobi, S.; Magyarfalvi, G., Reliability of computed signs and intensities for vibrational circular dichroism spectra. *Phys Chem Chem Phys* **2011,** *13*, 16130-16133.

102. Kuppens, T.; Bultinck, P.; Langenaeker, W., Determination of absolute configuration via vibrational circular dichroism. *Drug Discovery Today: Technologies* **2004,** *1*, 269-275.

103. Lightner, D. A.; Gurst, J. E., *Organic conformational analysis and stereochemistry from circular dichroism spectroscopy*. Wiley-VCH: New York, 2000; p xiii, 487 p.

104. Kaizaki, S.; Azuma, N.; Fuyuhiro, A., First solid state synthesis of the racemic compound and enantiomer of dinuclear Lambda,Lambda-di-mu-hydroxo-bis[bis((1S,2S)-1,2-trans-cyclohexanediamine)chromium(III)] and Delta,Delta-di-mu-hydroxo-bis[bis((1R,2R)-1,2-trans-cyclohexanediamine)chromium(III)] bromides. *Inorg Chim Acta* **1998,** *274*, 210-214.

105. Ama, T.; Hidaka, J.; Shimura, Y., Optical Resolution of a Heteropolymolybdate Anion. *B Chem Soc Jpn* **1970,** *43*, 2654-&.

106. Harada, N.; Nakanish.K, A Method for Determining Chiralities of Optically Active Glycols. *J Am Chem Soc* **1969,** *91*, 3989-&.

107. Harada, N.; Nakanish.K; Tatsuoka, S., A Method for Determining Chirality of 2 Aromatic Chromophores and Absolute Configurations of Chromomycin A3 and Related Antibiotics. *J Am Chem Soc* **1969,** *91*, 5896-&.

108. Moffitt, W., Optical Rotatory Dispersion of Helical Polymers. *J Chem Phys* **1956,** *25*, 467-478.

109. Moffitt, W.; Fitts, D. D.; Kirkwood, J. G., Critique of the Theory of Optical Activity of Helical Polymers. *P Natl Acad Sci USA* **1957,** *43*, 723-730.

110. Kirkwood, J. G., On the theory of optical rotatory power. *J Chem Phys* **1937,** *5*, 479-491.

111. Harada, N.; Chen, S.-M. L.; Nakanishi, K., Quantitative definition of exciton chirality and the distant effect in the exciton chirality method. *J Am Chem Soc* **1975,** *97*, 5345-5352.

112. Pescitelli, G.; Di Bari, L.; Berova, N., Conformational aspects in the studies of organic compounds by electronic circular dichroism. *Chem Soc Rev* **2011,** *40*, 4603-4625.

113. Autschbach, J., Computing chiroptical properties with first-principles theoretical methods: Background and illustrative examples. *Chirality* **2009,** *21*, E116-E152.

114. Bringmann, G.; Gulden, K. P.; Busse, H.; Fleischhauer, J.; Kramer, B.; Zobel, E., Circular-dichroism of naphthyltetrahydroisoquinoline alkaloids - calculation of CD Spectra by semiempirical methods. *Tetrahedron* **1993,** *49*, 3305-3312.

115. Cramer, C. J., *Essentials of computational chemistry : theories and models*. 2nd ed.; Wiley: Chichester, West Sussex, England ; Hoboken, NJ, 2004; p 596.

116. Spartan Model. http://www.wavefun.com/ (February, 2013),

117. Molecular Modeling from Sequence through Lead Optimization, SYBL-X. http://www.tripos.com/ (February, 2013),

118. High Performance Confrmation Analysis. http://www.conflex.us/ (February, 2013),

119. HyperChem, Molecular Modeling,. http://www.hyper.com/ (February, 2013),

120. MacroModel: Versatile, full-featured program for molecular modeling. http://www.schrodinger.com/ (February, 2013),

121. Schlegel, H. B., Geometry optimization. *Wiley Interdisciplinary Reviews: Computational Molecular Science* **2011,** *1*, 790-809.

122. Stanislav, I. Elucidation of chemical phenomena by means of computational chemistry. University of Basel, , basel, 2005.

123. Geometry Optimization Lab. http://www.shodor.org/chemviz/optimization/teachers/background.html (March, 2013),

124. Stephens, P. J.; Devlin, F. J.; Pan, J. J., The determination of the absolute configurations of chiral molecules using vibrational circular dichroism (VCD) spectroscopy. *Chirality* **2008,** *20*, 643-663.

3. Results and discussion

3.1. Abietane diterpenoids from *Salvia sahendica* - antiprotozoal activity and determination of their absolute configurations

Samad Nejad Ebrahimi, Stefanie Zimmermann, Janine Zaugg, Martin Smiesko, Reto Brun, Matthias Hamburger

Planta Med. 2013 Jan; 79(2):150-6. doi: 10.1055/s-0032-1328063

HPLC-based activity profiling *n*-hexane extract from roots of *Salvia sahendica* led to the identification of seven known and one new abietane-type diterpenoid which inhibited the growth of *P. falciparum* K1 strain. Structure elucidation was achieved by analysis of spectroscopic data including 1D and 2D NMR. The absolute configuration of sahandol (7) and sahandone (8) were assigned by comparison of experimental ECD spectra with calculated ECD data, using time-dependent density functional theory and methanol as the solvent. *In vitro* biological activity against *P. falciparum* and *Trypanosoma brucei rhodesiense* STIB 900 strain and cytotoxicity in rat myoblast (L6) cells were determined. The IC_{50} values of the compounds ranged from 0.8 μM to over 8.8 μM against *P. falciparum*, and from 1.8 μM to over 32.3 μM against *T. brucei rhodesiense*. The cytotoxic IC_{50} values ranged from 0.5-15.5 μM. Selectivity indices for P. falciparum were 0.1 to 18.2, and 0.1 to 1.2 for *T. brucei rhodesiense*.

Extraction of plant material, isolation, recording and interpretation of analytical data for structure elucidation (HPLC-PDA-ESI-MS and 1D and 2D-NMR optical rotation, ECD), quantum chemical calculations ECD spectra and optical rotation (some advice from Martin Smiesko and Janine Zaugg), writing of the manuscript draft, and preparation of figures were my contributions to this publication. Antiprotozoal tests were done by Stefanie Zimmermann.

Samad Ebrahimi

Abietane Diterpenoids from *Salvia sahendica* – Antiprotozoal Activity and Determination of Their Absolute Configurations

Authors Samad N. Ebrahimi[1,2], Stefanie Zimmermann[1,3], Janine Zaugg[1], Martin Smiesko[4], Reto Brun[3], Matthias Hamburger[1]

Affiliations The affiliations are listed at the end of the article

Key words
- *Salvia sahendica*
- Lamiaceae
- diterpenes
- *Plasmodium falciparum*
- *Trypanosoma brucei rhodesiense*

Abstract

In a screening of Iranian plants for antiprotozoal activity, an *n*-hexane extract of the roots of *Salvia sahendica* potently inhibited the growth of *Plasmodium falciparum* K1 strain. Subsequent HPLC-based activity profiling led to the identification of seven known and one new abietane-type diterpenoid. Structure elucidation was achieved by analysis of spectroscopic data including 1D and 2D NMR. The absolute configuration of sahandol (**7**) and sahandone (**8**) were assigned by comparison of experimental ECD spectra with calculated ECD data, using time-dependent density functional theory and methanol as the solvent. *In vitro* biological activity against *P. falciparum* and *Trypanosoma brucei rhodesiense* STIB 900 strain and cytotoxicity in rat myoblast (L6) cells were determined. The IC_{50} values of the compounds ranged from 0.8 µM to over 8.8 µM against *P. falciparum*, and from 1.8 µM to over 32.3 µM against *T. brucei rhodesiense*. The cytotoxic IC_{50} values ranged from 0.5–15.5 µM. Selectivity indices for *P. falciparum* were 0.1 to 18.2, and 0.1 to 1.2 for *T. brucei rhodesiense.*

Abbreviations

TDDFT:	time-dependent density functional theory
ECD:	electronic circular dichroism
CE:	Cotton effect
SCRF:	self-consistent reaction field
CPCM:	conductor-like polarizable continuum model
MPLC:	medium-pressure liquid chromatography
NP:	normal phase
OR:	optical rotation
R_{vel}:	rotatory strength R in dipole velocity
R_{len}:	dipole length
MMFF	Merck molecular force field

Supporting information available online at http://www.thieme-connect.de/ejournals/toc/plantamedica

received June 27, 2012
revised October 31, 2012
accepted Nov. 17, 2012

Bibliography
DOI http://dx.doi.org/10.1055/s-0032-1328063
Published online January 8, 2013
Planta Med 2013; 79: 150–156

ISSN 0032-0943

Correspondence
Prof. Matthias Hamburger
Division of Pharmaceutical Biology
University of Basel
Klingelbergstrasse 50
4056 Basel
Switzerland
Phone: + 41 61 267 14 25
Fax: + 41 61 267 14 74
matthias.hamburger@unibas.ch

Introduction

Salvia is the largest genus of the Lamiaceae family, with over 900 species found throughout the world. It is represented in the Iranian flora by 58 species, of which 17 are endemic [1]. Some of these species have been used as medicinal, aromatic, and ornamental plants [2,3]. For Iranian *Salvia* species, such as *S. leriifolia, S. hydrangea, S. macrosiphon*, and *S. viridis*, antibacterial, antifungal, antiplasmodial, and antibacterial properties have been reported [4–6]. *Salvia* species are particularly rich in diterpenoids, and they are responsible for various biological activities of these plants. *Salvia sahendica* Boiss. & Buhse is used in Iranian folk medicine as antibacterial and antifungal, and for treatment of dyspepsia [7]. Its essential oil composition as well as antibacterial and antioxidant activities have been studied [8]. Previous phytochemical studies of the aerial parts of *S. sahendica* led to identification of sesterterpenes, nor-sesterterpenes, and nor-diterpenes [9,10], whereas rearranged abietane diterpenoids have been reported from the roots [11].

In recent years we successfully applied HPLC-based activity profiling for the rapid localization, dereplication, and characterization of bioactive natural products in extracts. This approach was successfully applied for the identification of new anti-protozoal substances, positive GABA(A) re-

ceptor modulators, and anti-HIV compounds [12–19]. Continuing in our screening of medicinal plants for the discovery of new antiparasitic natural products with scaffolds new for the target, we recently screened over 150 plant extracts mainly from the Labiatae and Asteraceae families from the Iranian flora. These plants were selected based on ethnobotanical studies and taxonomical considerations. One of the most active extracts against *P. falciparum* K1 was a *n*-hexane extract of the roots of *S. sahendica* that inhibited parasites by 70% when tested at a concentration of 0.85 µg/mL. HPLC-based activity profiling was used to identify the active constituents in the extract. Here we report on the isolation and identification of anti-protozoal compounds from roots of *S. sahendica* and also on determination of the absolute configuration of compounds **7** and **8** by simulation of ECD spectra using TDDFT calculation.

Material and Methods

General experimental procedures

Optical rotations were measured using a JASCO P-2000 automatic digital polarimeter. ECD spectra were recorded in MeOH (16 µg/mL) on an AVIV CD spectrometer model 62ADS and analyzed with the AVIV 60DS V4.1 software. NMR spectra were recorded at a target temperature of 18 °C on a Bruker Avance III 500 MHz spectrometer operating at 500.13 MHz for ^{1}H and 125.77 MHz for ^{13}C. A 1-mm TXI microprobe with a z-gradient was used for ^{1}H-detected experiments. ^{13}C-NMR spectra were recorded with a 5-mm BBO probe head with z-gradient. Spectra were analyzed using Bruker TopSpin 2.1 software. HRESI-MS spectra in positive and negative ion modes were recorded on a Bruker microTOF ESI-MS system with a scan range of *m/z* 200–1500. MS calibration was performed using a reference solution of sodium formate 0.1% in isopropanol-water (1 : 1) containing 5 mM sodium hydroxide. The typical mass accuracy was ± 3 ppm. HyStar 3.0 software (Bruker Daltonics) was used for data acquisition and processing. HPLC separations were performed on an Agilent 1100 series HPLC system consisting of a quaternary low-pressure mixing pump with degasser module, column oven, PDA detector, and autosampler. For MPLC, a Buchi Sepacore system consisting of a control unit C-620, a fraction collector C-660, and two pump modules C-605 was used. Waters SunFire C18 (3.5 µm, 3.0 × 150 mm) and SunFire® Prep C18 (5 µm, 30 × 150 mm) columns were used for analytical HPLC and preparative RP-HPLC, respectively. HPLC solvents contained 0.1% HCO_2H for separations. NP column chromatography was carried out on silica gel (Merck, 40–63 µm; 460 × 50 mm). Pre-coated silica gel 60 F_{254} plates (Merck) were used for TLC. Detection was at 254 and 366 nm or by spraying with anisaldehyde sulfuric acid reagent and subsequently heating (120 °C for 5 min). $CDCl_3$ (100 Atom% D) for NMR was purchased from Armar Chemicals. Solvents used for extraction, open column chromatography, and MPLC were of technical grade and were purified by distillation.

Plant material

The roots of *Salvia sahendica* Boiss. & Buhse were collected in September 2009 from Sardrood-Tabriz (East Azarbaijan Province, Iran). The plant material was identified by Dr. Ali Sonboli, and a voucher specimen (MPH-848) has been deposited at the Herbarium of the Department of Biology, Medicinal Plants and Drugs Research Inistitute, Shahid Beheshti University, Tehran, Iran.

Microfractionation for activity profiling

Aliquots of 350 µg of *n*-hexane extract from the extract library (35 µL of 10 mg/mL solution in DMSO) were separated on a SunFire C18 column (5 µm, 10 × 150 mm; Waters) with 0.1% formic acid in H_2O (solvent A) and MeCN (solvent B) using the following gradient: 80% B to 100% B in 30 minutes, hold for 10 min. The flow rate was 0.4 mL/min. Thirty-two one-minute fractions were collected in 96-well deep well plates. The plates were dried in a GeneVac EZ-2 Plus evaporator and submitted to bioassay.

Extraction and isolation

The dried root samples were ground with a Retsch ZM1 mill. The powdered roots (1.3 kg) were extracted at room temperature with *n*-hexane (3 × 5 L). The extract was concentrated under reduced pressure at a temperature around 40 °C to give 22.5 g of a dark red residue. A portion (13.0 g) of the *n*-hexane extract was separated by MPLC on silica gel (Merck, 40–63 µm; 460 × 50 mm). The column was eluted with a gradient of *n*-hexane/CH_2Cl_2 (100/0 to 0/100%) over 150 min, followed by CH_2Cl_2/MeOH (100/0 to 0/100%) over 160 min. The flow rate was 20 mL/min. One-minute fractions were collected and pooled into 14 fractions (Fr 1–14) according to similar composition as assessed by TLC (Merck silica gel 60F254, mobile phase *n*-hexane/EtOAc 8 : 2): Fr 1 (340 mL, 0.12 g), Fr 2 (380 mL, 0.22 g), Fr 3 (500 mL, 1.5 g), Fr 4 (400 mL, 0.75 g), Fr 5 (300 mL, 0.35 g), Fr 6 (460 mL, 1.8 g), Fr 7 (800 mL, 3.5 g), Fr 8 (280 mL, 0.25 g), Fr 9 (460 mL, 0.25 g), Fr 10 (320 mL, 0.35 g), Fr 11 (400 mL, 0.45 g), Fr 12 (500 mL, 1.0 g), Fr 13 (400 mL, 0.3 g), and Fr 14 (600 mL, 0.45 g). Compounds **1** and **2** (2.8 g) were obtained as a mixture in a red precipitate from Fr 7. An aliquot (100 mg) of this mixture was separated by column chromatography with $AgNO_3$-impregnated silica gel (40–63 µm; 200 × 20 mm). Elution with *n*-hexane-EtOAc (80 : 20) afforded pure **1** (35 mg, > 98% [^{1}H-NMR]) and **2** (40 mg > 98% [^{1}H-NMR]). A step gradient separation of a portion of Fr 6 (700 mg) using a mixture of *n*-hexane-EtOAc [8 : 2 (200 mL) → 7 : 3 (100 mL) → 6 : 4 (200 mL) → 5 : 5 (150 mL) → 4 : 6 (120 mL) → 1 : 9 (200 mL) → 0 : 10 (200 mL) on silica gel (40–63 µm; 400 × 20 mm)] afforded seven subfractions (Fr 6–1 to Fr 6–7). A portion of subfraction Fr 6–4 (200 mg) was further purified by preparative RP-HPLC (MeCN-H_2O, 75 : 25 → 90 : 10 in 35 min; flow rate 20 mL/min, detection at 280 nm) to afford **3** (6.0 mg, t_R = 24.5, > 97.5% [^{1}H-NMR]), **4** (3 mg, t_R = 30.7, > 98% [^{1}H-NMR]), and **5** (47 mg, t_R = 32.5, > 99% [^{1}H-NMR]). A portion (50 mg) of Fr 6–5 was purified by preparative RP-HPLC (MeCN-H_2O, 85 : 15 → 0 : 100 in 30 min; flow rate 20 mL/min, detection at 280 nm) to afford **8** (17 mg, t_R = 20.5, > 96% [^{1}H-NMR]). A portion of Fr 4 (200 mg) was purified by preparative RP-HPLC (MeCN-H_2O, 80 : 20 → 0 : 100 in 40 min; flow rate 20 mL/min, detection at 280 nm) to afford **7** (125 mg, t_R = 35.5, > 98.5% [^{1}H-NMR]). Compound **6** (90 mg, > 99% [^{1}H-NMR]) precipitated as yellowish needles during evaporation of Fr 9.

Antiplasmodial and antitrypanosomal assay

Testing for antiplasmodial and antitrypanosomal activity and determination of cytotoxicity was done as previously reported [18, 19]. Cytotoxicity was determined using rat skeletal myoblast L6 cells. Assays were performed in three independent experiments as duplicates. IC_{50} values were calculated from sigmoidal growth inhibition curves. Melarsoprol (Arsobal®, purity > 95%; Sanofi-Aventis) and artesunate® (purity > 95%; Mepha) were used as reference drugs (details on the bioassays are provided as Supporting Information).

Conformational analysis, geometrical optimization, and ECD calculation

Conformational analyses of compounds **7** and **8** were performed with Schrödinger MacroModel 9.1 software (Schrödinger, LLC) using the MMFFs (Merck Molecular Force Fields) force field in H_2O. Conformers occurring within a 2 kcal/mol energy window from the particular global minimum were chosen for the gas-phase geometrical optimization and energy calculation using the density functional theory (DFT) with the B3LYP functional and the 6–31 G** basis-set as implemented with the Gaussian 09 program package [20]. Vibrational analysis was performed at the same level to confirm stability of the minima. Time-dependent density function theory calculation at the TD-DFT/B3LYP/6–31 G** level in the gas phase and in MeOH using the SCRF with the CPCM was employed to calculate excitation energy (denoted by wavelength in nm) and R_{vel} and R_{len} forms. ECD curves were calculated based on rotatory strengths using half bandwidth of 0.2 eV with conformers of **7** and **8** using SpecDis version 1.53 [21]. The OR calculations were carried out with TDDFT/GIAO methodology using PBE0/6–31 G++ (2d,2p) in the $CHCl_3$ (SCRF/CPCM) [22, 23]. The ECD spectra and optical rotation values were constructed based on the Boltzmann-weighting according to their population contribution.

Table 1 ^{1}H and ^{13}C-NMR spectral data of sahandol (**7**) ($CDCl_3$, *J* in Hz).

Position	δ_H	δ_C
1α	2.97 dd (16.4, 10.8)	32.5
1β	3.12 dd (16.4, 3.1)	
2	4.93 ddd (10.8, 8.5, 3.1)	73.2
3	5.53 brd (8.5)	124.4
4	–	136.4
5	–	129.2
6	7.12 d (8.4)	125.1
7	7.53 d (8.4)	126.5
8	–	124.5
9	–	120.2
10	–	125.3
11	–	138.0
12	–	138.6
13	–	136.2
14	7.24 s	115.9
15	3.44 sep (6.6)	27.9
16	1.37 d (6.6)	22.7
17	1.35 d (6.6)	22.8
18	1.81 d (1.5)	18.5
19	1.86 d (1.5)	25.8
20	2.37 s	18.4
OH	5.80 s	–

Isolates

Sahandol (**7**): yellowish oil, $[\alpha]_D^{24} = -56.5$ (*c* 0.8, $CHCl_3$); UV (MeOH): λ_{max} (log ε) 244 (3.72), 312 (3.12), 342 (3.25); CD (MeOH, *c* = 0.3 mM, 0.1 cm): $[\theta]_{221} = -26802$, $[\theta]_{247} = +36265$, $[\theta]_{309} = -6556$, $[\theta]_{337} = +1267$; ^{1}H-NMR ($CDCl_3$, 500 MHz) and ^{13}C-NMR ($CDCl_3$,125 MHz), see **Table 1**; HREIMS *m/z* 297.1855 $[M + H]^+$, calcd. for $C_{20}H_{24}O_2$, 296.1776.

Sahandone (**8**): yellow gummy material, $[\alpha]_D^{24} = -198.1$ (*c* 0.06, MeOH); UV (MeOH): λ_{max} (log ε) 243 (3.83), 342 (3.48); CD (MeOH, *c* = 0.05 mM, 1.0 cm): $[\theta]_{210} = -109493$, $[\theta]_{243} = +27913$, $[\theta]_{259} = -2863$, $[\theta]_{340} = +26180$, $[\theta]_{386} = -28252$; ^{1}H-NMR ($CDCl_3$, 500 MHz) and ^{13}C-NMR ($CDCl_3$,125 MHz), see Supporting Information.

Supporting information

^{1}H-NMR- ^{13}C-NMR spectra of compounds **7** and **8**, calculated ECD spectra, optical rotation values of conformers of compounds **7** and **8**, and details for the bioassay can be found as Supporting Information available online.

Results and Discussion

In a library-based medium-throughput screening of 150 extracts prepared from Iranian plants against the chloroquine-resistant *P. falciparum* K1 strain, an *n*-hexane extract of *S. sahendica* roots produced 70% inhibition at a test concentration of 0.85 µg/mL. The antiplasmodial activity was localized with the aid of HPLC-based activity profiling using a previously validated protocol [19]. The analytical HPLC chromatogram (210–700 nm) and the corresponding activity profiling of the time-based microfractionation (32 microfractions of 60 s each) are shown in **Fig. 1 A** and **B**, respectively. The highest activities were found in fractions 23, 19, and 13 (79, 69, and 43% inhibition, respectively). Targeted preparative isolation of active compounds was subsequently achieved by a combination of normal phase MPLC and preparative RP-HPLC. In total, seven known abietane diterpenoids, sahandinone (**1**), 12-deoxy-salvipisone (**2**), 12-deoxy-6,7-dehydroroyleanone (**3**), Δ^9-ferruginol (**4**), ferruginol (**5**), 7α-acetoxyroyleanone (**6**), sahandone (**8**), and one new diterpene, sahandol (**7**), were identified by HR-ESIMS, 1D and 2D NMR spectroscopy, and by comparison with published data (**Fig. 2**) [11, 24–26].

Compound **7** was obtained as yellow oil. The molecular formula of $C_{20}H_{24}O_2$ was deduced from HRESI-TOFMS (*m/z* 297.1855 $[M + H]^+$, calcd. 296.1776) and accounted for 9 degrees of unsaturation. The UV spectrum in MeOH showed absorption maxima at 244, 312, and 342 nm and was indicative of a highly conjugated naphthalene system [27]. The ^{1}H-NMR spectrum (**Table 1**, **Fig. 1S**) showed resonances of five methyl groups at δ_H 2.37 (s), 1.86 (d, 1.5 Hz), 1.81 (d, 1.5 Hz), 1.37 (d, 6.6 Hz), and 1.35 (d, 6.6 Hz), three aromatic and one olefinic proton resonating at δ_H 7.53 (d, 8.4 Hz), 7.24 (s), 7.12 (d, 8.4 Hz), and 5.53 (brd, 8.5 Hz), two deshielded diastereotopic methylene protons [δ_H 3.12 (dd, 16.4, 3.1 Hz), 2.97 (dd, 16.4, 10.8 Hz)], one methine proton [δ_H 3.44, (sep, *J* = 6.6 Hz)], and a signal of a deshielded proton at δ_H 4.93, (ddd, 10.8, 8.5, 1.5 Hz). The ^{13}C-NMR spectrum exhibited 20 signals. Of these, 10 signals for sp^2-carbons could be assigned to a naphthalene system, while the other 2 sp^2-carbon resonances were attributed to olefinic carbons. In addition, the spectrum showed 8 saturated sp^3-carbons which were attributed to one oxygen bearing C-atom, a methylene group, one methine, and five methyl groups. The protonated carbons and their attached protons were correlated with the aid of an HSQC spectrum. The presence of an isopropyl group as a substituent of an aromatic ring was highly reminiscent of an abietane skeleton. Further analysis of ^{1}H-^{1}H COSY and HMBC spectra of compound **7** established a 4,5-seco-rearranged abietane diterpenoid skeleton (**Fig. 3**). HMBC correlations between H-15 and C-13, C-12, and C-14 confirmed the attachment of the isopropyl moiety at C-13. Correlations between CH_3-20 and C-5 and C-10, and between H-6 and C-5 established the attachment of CH_3-20 at C-7. The key HMBC correlations of H-2 (δ 4.93) with C-11 (136.2) and C-1 (32.5) indicated that the aromatic moiety was linked to C-2 by an ether bridge. HMBC cross signals between H-2 and C-3, and H-3 and C-1 corroborated the position of a vinyl group at C-

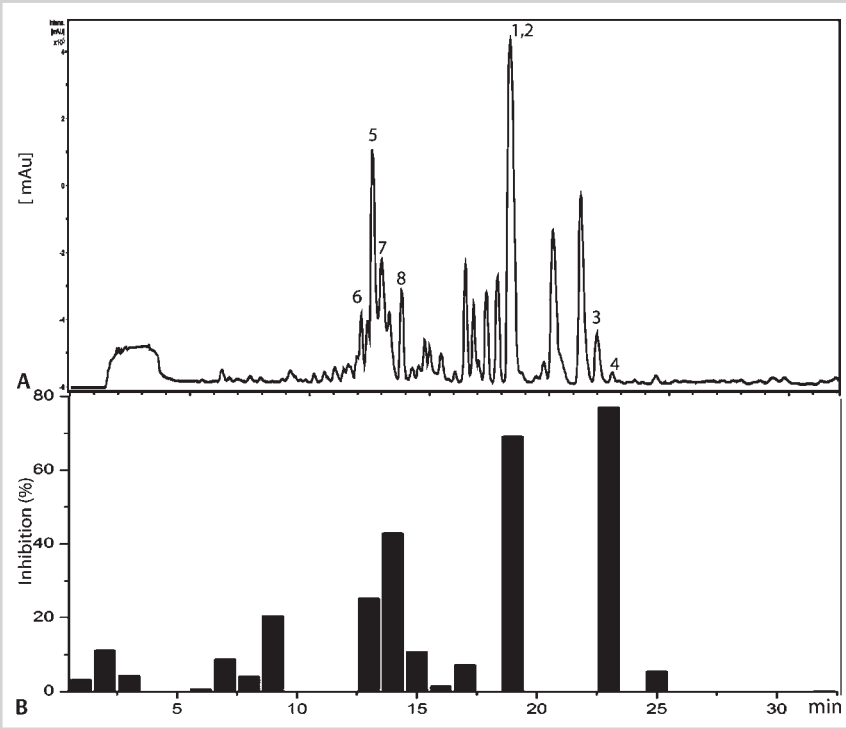

Fig. 1 HPLC-UV chromatogram (254 nm) of the *n*-hexane extract (**A**) and antiplasmodial activity of microfractions (**B**).

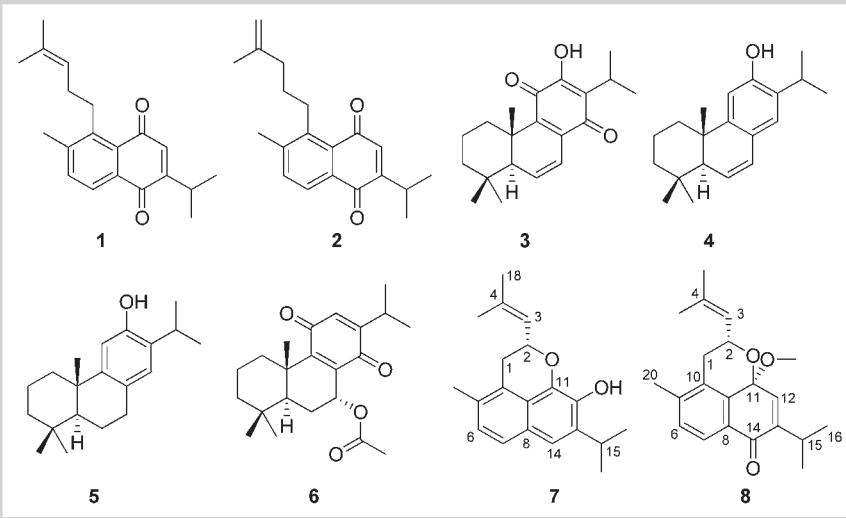

Fig. 2 Structures of diterpenes **1**–**8**.

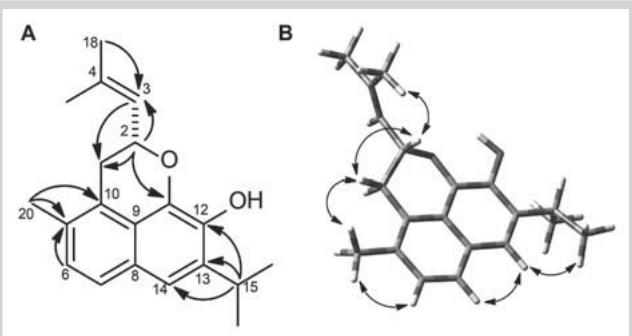

Fig. 3 **A** Key HMBC correlations; **B** key NOESY correlations in the DFT-optimized structure of the most stable conformer of **7**.

2. Detailed analysis of vicinal coupling constants in the ^{1}H-NMR spectrum and NOESY measurements was employed to characterize the heterocyclic ring. Vicinal couplings of H-2/H1α (J = 10.8) and H-2/H1β (J = 3.1) corresponded to the dihedral angles of 180 and 60°, respectively. Hence, H-2 was in an axial orientation, and the oxene ring showed a half chair conformation.

Since compound **7** contained only one stereogenic center, two stereoisomers (2*R* and 2*S*) were possible. A conformation analysis of the 2*R*-stereoisomer using the MMFFs method found six conformers within a 2 kcal/mol energy window from the particular global minimum. These conformers were subjected to geometrical optimization and energy calculation by the DFT/B3LYP/6–31 G** basis set in the gas phase. Vibrational frequency analysis was carried out to confirm minima. No imaginary frequencies were found. Conformation analysis using relative free energy re-

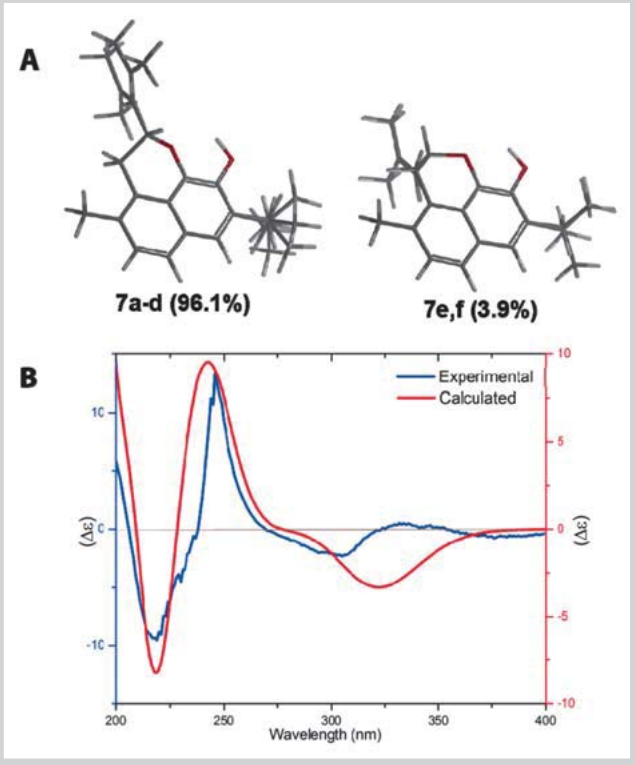

Fig. 4 **A** Superimposed lowest energy conformers (within 2 kcal/mol range from the global minimum) of (*R*)-sahandol (**7**). Conformers obtained from the conformational search were recalculated using DFT at the B3LYP/6–31 G** level in the gas phase. Compound **7** showed two core conformers which differed in the orientation of H-2 (axial, 96.1%; equatorial, 3.9%). **B** Comparison of experimental and calculated ECD spectra of **7**. The calculations were performed with TDDFT at the B3LYP/6–31 G** level with MeOH as the solvent.

vealed the presence of six stable conformers (**Fig. 4A**). The superimposed structures showed two core conformers (96.1 and 3.9%, respectively) and minor differences arising from the rotation of the isopropyl and vinyl moieties. ECD spectra of optimized conformes were calculated by TDDFT-B3LYP/6–31 G** and MeOH as solvent (SCRF/CPCM). The averaged spectrum resulting from Boltzmann weighting of ECD spectra for individual conformers showed a positive CE at 245 nm and two negative CE at 220 and 320 nm. Comparison of experimental and calculated ECD spectra showed an excellent fit with the data calculated for the 2*R*-stereoisomer (**Fig. 4B**). In particular, the negative CE at 220 nm and the positive CE at 245 nm matched with the pattern of the experimental spectrum. Comparison between the experimental (−56.50) and calculated (−35.99) optical rotation gave the same sign and a similar magnitude for the 2*R*-stereoisomer (**Table 1S**). Compound **7** is a new natural product and was named (2*R*)-sahandol.

Sahandone (**8**) had been previously isolated from roots of *S. sahendica* [11]. Its relative stereochemistry was at that time proposed on the basis of 2D NMR studies including ROESY data. Due to cross signals between H-2, the methoxy group, and Hα-1 in the ROESY spectrum, the relative configuration was proposed as (2*S**,11*S**). We compared optical rotation, ^{1}H and ^{13}C-NMR data of our compound with the original substance and found them to be identical. We also measured a NOESY spectrum of **8** and found similar correlations as initially reported. In the context of this study, we re-examined the compound to establish its absolute configuration. **Fig. 5B** shows the experimental ECD spectrum of **8** in MeOH. The stereocenter at C-11 is close to the naphthalenone chromophore, whereas the second stereocenter C-2 is remote from this portion of the molecule and close to the vinyl chromophore. Hence, the spectrum is dominated by $\pi\rightarrow\pi^*$ transitions of the aromatic and vinyl chromophores. We calculated the ECD spectrum of the (2*S*,11*S*)-stereoisomer for a comparison

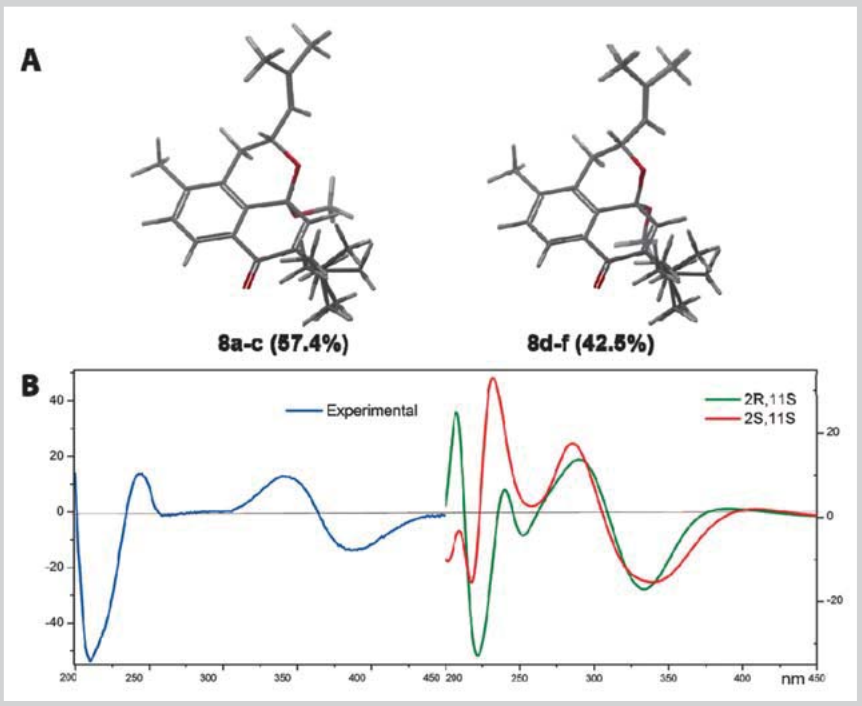

Fig. 5 **A** Superimposed lowest energy conformers (within 2 kcal/mol range from the global minimum) of (2*R*,11*S*)-sahandone (**8**). Conformers obtained from the conformational search were recalculated using DFT at the B3LYP/6–31 G** level in the gas phase. Compound **8** shows one core conformer, two differing orientations of the methoxy group (**8a–c** and **8d–f**, respectively). **B** Comparison of experimental and calculated ECD spectra for two stereoisomers [(2*S*,11*S*) and (2*R*,11*S*)] of **8**. The calculations were performed with TDDFT at the B3LYP/6–31 G** level and MeOH as solvent.

Table 2 *In vitro* activity of compounds **1–8** against *P. falciparum* K1, *T. brucei rhodesiense* STIB 900, and L6-cells.

No	Compound	IC_{50} (SEM)[a]	SI	IC_{50} (SEM)	SI	IC_{50} (SEM)
		P. falciparum		*T. brucei rhodesiense*		L6-cells
1	12-Deoxy-salvipisone	8.8 ± 0.1	0.1	2.5 ± 0.1	0.2	0.5 ± 0.1
2	Sahandinone	5.1 ± 0.1	0.1	1.8 ± 0.1	0.2	0.4 ± 0.1
3	12-Deoxy-6,7-dehydroroyleanone	17.8 ± 0.4	0.6	32.3 ± 0.3	0.9	10.7 ± 0.4
4	Δ^9-Ferruginol	0.9 ± 0.1	18.2	12.8 ± 0.1	1.2	15.5 ± 0.3
5	Ferruginol	0.9 ± 0.1	15.6	28.1 ± 0.1	0.5	14.6 ± 0.4
6	7α-Acetoxyroyleanone	1.3 ± 0.3	0.1	2.9 ± 0.1	0.1	0.2 ± 0.1
7	Sahandol	4.7 ± 0.1	3.3	18.4 ± 0.1	0.8	15.3 ± 0.7
8	Sahandone	17.2 ± 0.9	0.7	19.5 ± 0.1	0.6	11.9 ± 1.0
	Artemisinin	0.004				
	Melarsoprol			0.004		
	Podophyllotoxin					0.02

[a] Values are expressed in μM. Each value corresponds to the mean ± standard error of the mean from at least three independent bioassays. SI = Selectivity index (IC_{50} in L6 cells (cytotoxicity) divided by IC_{50} against *P. falciparum* and *T. brucei rhodesiense*)

with the experimental ECD data. A conformational search revealed 13 conformers within a 2 kcal/mol energy window from the particular global minimum (**Fig. 9S A**). Geometrical optimization and energy calculation followed by calculation of ECD spectra were performed as described above (**Fig. 5B**). The calculated data showed a negative and a positive CE at 340 and 300 nm, respectively, which fitted with the experimental data. However, the fit of the calculated ECD spectrum in the region 200–250 nm was not satisfactory. Hence, we calculated the ECD spectrum for the (2*R*,11*S*) stereoisomer. Six conformers differing in orientation of the isopropyl and methoxy moieties were found within a 2 kcal/mol energy window from the particular global minimum (**Fig. 5A**). The averaged ECD spectrum for the (2*R*,11*S*)-stereoisomer and experimental data were in good agreement. In particular, the negative CEs at 350 and 220 nm along with positive CEs at 250 and 300 nm matched with the ECD pattern of **8** (**Fig. 5B**). Differences between calculated and experimental spectra were apparently due to minor differences between calculated and solution conformers [17]. However, the differences to the calculated spectrum of the (2*S*,11*S*)-stereoisomer were not such as to unambiguously exclude it. We therefore calculated optical rotation values for both stereoisomers and compared them with the experimental data. The averaged $[\alpha]_D$ of the (2*R*,11*S*) and (2*S*,11*S*)-stereoisomers were −164.1 and −97.2°, respectively (**Table 1S** and **2S**), while the experimental value was −198.1° (the optical rotation previously reported for **8** was −202° [11]). Taking into account the good agreement between calculated and experimental ECD spectra and optical rotation values and considering the biosynthetic relationship between **7** and **8**, we concluded that sahandone (**8**) had the (2*R*,11*S*)-configuration. The NOESY cross-peaks between H-2, the methoxy group, and Hα-1, which led to the previous stereochemical assignment, are compatible with both stereoisomers, given the size of the methoxy group and its rather free rotation. The natural occurrence of compound **8** was confirmed by HPLC-MS analysis (RP-18 with H_2O/MeCN) of a crude *n*-hexane extract.

Compounds **1**-**8** were tested for their *in vitro* antiplasmodial, antitrypanosomal, and cytotoxic activities (**Table 2**). Ferruginol (**5**), Δ^9-ferruginol (**4**), and 7-acetoxy royleanone (**6**) were the most active antiplasmodial compounds, followed by sahandol (**7**), sahandinone (**2**), 12-deoxy-salvipisone (**1**), and sahandone (**8**). The IC_{50} values against *P. falciparum* ranged from 0.9 to 17.8 μM, and cytotoxicity from 0.2 to 15.5 μM, respectively. Thus, the selectivity indices were between 0.1 and 18.2. Compounds **1, 2**, and **3** were the most active against trypanosomes (IC_{50} values of 2.5, 1.8, and 2.9 μM, respectively) but were also the most cytotoxic diterpenoids of this series (IC_{50} values of 0.4, 0.5, and 0.2 μM, respectively) and, hence, exhibited nonselective toxicity.

Acknowledgements

Thanks to the Ministry of Science, Research, and Technology of Iran (MSRT) for a Ph.D. fellowship No 24/87100055 (S.N.E). Support from the Swiss National Science Foundation through grant 205320_126888/1 (to M.H.) is gratefully acknowledged. Thanks are due to Dr. Ali Sonboli for the identification of the plant material and Ms. T. Schulthess (University of Basel) for technical assistance with measurement of UV and CD spectra. We thank Mehdi N. Ebrahimi for his help in the collection of the plant material.

Conflict of Interest

The authors declare no conflict of interest.

Affiliations

[1] Division of Pharmaceutical Biology, University of Basel, Basel, Switzerland
[2] Department of Phytochemistry, Medicinal Plants and Drugs Research Institute, Shahid Beheshti University, G.C., Tehran, Iran
[3] Department of Medical Parasitology and Infection Biology, Swiss Tropical and Public Health Institute and University of Basel, Basel, Switzerland
[4] Division of Molecular Modeling, University of Basel, Basel, Switzerland

References

1 *Mozaffarian V.* A dictionary of Iranian plant names, 3rd edition. Tehran: Farhang Moaser; 1996
2 *Habibi Z, Eftekhar F, Samiee K, Rustaiyan A.* Structure and antibacterial activity of new labdane diterpenoid from *Salvia leriaefolia*. J Nat Prod 2000; 63: 270–271
3 *Naghibi F, Mosaddegh M, Motamed SM, Ghorbani A.* Labiatae family in folk medicine in Iran: from ethnobotany to pharmacology. Iranian J Pharm Res 2005; 2: 63–79
4 *Rustaiyan A, Masoudi S, Tabatabaei-Anaraki M.* Terpenoids from Iranian *Salvia* species. Nat Prod Commun 2007; 2: 1031–1042
5 *Atta-ur-Rahman FRS, editor.* Studies in natural products chemistry. Amsterdam: Elsevier; 2008
6 *Farimani MM, Taheri S, Ebrahimi SN, Bahadori MB, Khavasi HR, Zimmermann S, Brun R, Hamburger M.* Hydrangenone, a new isoprenoid with

an unprecedented skeleton from *Salvia hydrangea*. Org Lett 2011; 14: 166–169

7 *Esmaeili MA, Sonboli A, Kanani MR, Sadeghi H. Salvia sahendica* prevents tissue damages induced by alcohol in oxidative stress conditions: Effect on liver and kidney oxidative parameters. J Med Plants Res 2009; 3: 276–283

8 *Salehi P, Sonboli A, Ebrahimi SN, Yousefzadi M.* Antibacterial and antioxidant activities of the essential oils and various extracts of *Salvia sahendica* in different phenological stages. Chem Nat Compd 2007; 43: 328–330

9 *Moghaddam FM, Zaynizadeh B, Ruedi P.* Salvileucolide methylester, a sesterterpene from *Salvia sahendica*. Phytochemistry 1995; 39: 715–716

10 *Moghaddam FM, Farimani MM, Seirafi M, Taheri S, Khavasi HR, Sendker J, Proksch P, Wray V, Edrada R.* Sesterterpenoids and other constituents of *Salvia sahendica*. J Nat Prod 2010; 73: 1601–1605

11 *Jassbi AR, Mehrdad M, Eghtesadi F, Ebrahimi SN, Baldwin IT.* Novel rearranged abietane diterpenoids from the roots of *Salvia sahendica*. Chem Biodivers 2006; 3: 916–922

12 *Hata Y, Zimmermann S, Quitschau M, Kaiser M, Hamburger M, Adams M.* Antiplasmodial and antitrypanosomal activity of pyrethrins and pyrethroids. J Agric Food Chem 2011; 59: 9172–9176

13 *Kim HJ, Baburin I, Zaugg J, Ebrahimi SN, Hering S, Hamburger M.* HPLC-based activity profiling – discovery of sanggenons as $GABA_A$ receptor modulators in the traditional Chinese drug sang bai pi (*Morus alba* root bark). Planta Med 2012; 78: 440–447

14 *Rueda DC, Zaugg J, Quitschau M, Reich E, Hering S, Hamburger M.* Discovery of $GABA_A$ receptor modulator aristolactone in a commercial sample of the Chinese herbal drug "chaihu" (*Bupleurum chinense* roots) unravels adulteration by nephrotoxic *Aristolochia manshuriensis* roots. Planta Med 2012; 78: 207–210

15 *Slusarczyk S, Zimmermann S, Kaiser M, Matkowski A, Hamburger M, Adams M.* Antiplasmodial and antitrypanosomal activity of tanshinone-type diterpenoids from *Salvia miltiorrhiza.* Planta Med 2011; 77: 1594–1596

16 *Vidal V, Potterat O, Louvel S, Hamy F, Mojarrab M, Sanglier JJ, Klimkait T, Hamburger M.* Library-based discovery and characterization of daphnane diterpenes as potent and selective HIV inhibitors in *Daphne gnidium*. J Nat Prod 2012; 75: 414–419

17 *Zaugg J, Ebrahimi SN, Smiesko M, Baburin I, Hering S, Hamburger M.* Identification of $GABA_A$ receptor modulators in *Kadsura longipedunculata* and assignment of absolute configurations by quantum-chemical ECD calculations. Phytochemistry 2011; 72: 2385–2395

18 *Zimmermann S, Kaiser M, Brun R, Hamburger M, Adams M.* Cynaropicrin: the first plant natural product with *in vivo* activity against *Trypanosoma brucei*. Planta Med 2012; 78: 553–556

19 *Adams M, Zimmermann S, Kaiser M, Brun R, Hamburger M.* Protocol for HPLC-based activity profiling for natural products with activities against tropical parasites. Nat Prod Commun 2009; 4: 1377–1381

20 *Frisch MJ, Trucks GW, Schlegel HB, Scuseria GE, Robb MA, Cheeseman JR, Scalmani G, Barone V, Mennucci B, Petersson GA, Nakatsuji H, Caricato M, Li X, Hratchian HP, Izmaylov AF, Bloino J, Zheng G, Sonnenberg JL, Hada M, Ehara M, Toyota K, Fukuda R, Hasegawa J, Ishida M, Nakajima T, Honda Y, Kitao O, Nakai H, Vreven T, Montgomery JA, Peralta JE, Ogliaro F, Bearpark M, Heyd JJ, Brothers E, Kudin KN, Staroverov VN, Kobayashi R, Normand J, Raghavachari K, Rendell A, Burant JC, Iyengar SS, Tomasi J, Cossi M, Rega N, Millam JM, Klene M, Knox JE, Cross JB, Bakken V, Adamo C, Jaramillo J, Gomperts R, Stratmann RE, Yazyev O, Austin AJ, Cammi R, Pomelli C, Ochterski JW, Martin RL, Morokuma K, Zakrzewski VG, Voth GA, Salvador P, Dannenberg JJ, Dapprich S, Daniels AD, Farkas O, Foresman JB, Ortiz JV, Cioslowski J, Fox DJ.* Gaussian 09, Revision A02. Wallingford: Gaussian, Inc.; 2009

21 *Bruhn T, Schaumlöffel A, Hemberger Y, Bringmann G.* SpecDis version 153. Würzburg: University of Würzburg; 2012

22 *Srebro M, Govind N, de Jong WA, Autschbach J.* Optical rotation calculated with time-dependent density functional theory: the OR45 benchmark. J Phys Chem A 2011; 115: 10930–10949

23 *McCann DM, Stephens PJ.* Determination of absolute configuration using density functional theory calculations of optical rotation and electronic circular dichroism: chiral alkenes. J Org Chem 2006; 71: 6074–6098

24 *Rodríguez B.* ^{1}H and ^{13}C NMR spectral assignments of some natural abietane diterpenoids. Magn Reson Chem 2003; 41: 741–746

25 *González AG, Aguiar ZE, Grillo TA, Luis JG.* Diterpenes and diterpene quinones from the roots of *Salvia apiana*. Phytochemistry 1992; 31: 1691–1695

26 *Rustaiyan A, Samadizadeh M, Habibi Z, Jakupovic J.* Two diterpenes with rearranged abietane skeletons from *Zhumeria majdae*. Phytochemistry 1995; 39: 163–165

27 *Lin LZ, Cordell GA, Lin P.* De-O-ethylsalvonitin and salprionin, 2 further diterpenoids from *Salvia prionitis*. Phytochemistry 1995; 40: 1469–1471

Supporting Information

Abietane Diterpenoids from *Salvia sahendica* - Antiprotozoal Activity and Determination of Their Absolute Configurations

Samad N. Ebrahimi[1,2], Stefanie Zimmermann[1,3], Janine Zaugg[1], Martin Smiesko[4], Reto Brun[3], Matthias Hamburger[1]

Affiliation

[1] Division of Pharmaceutical Biology, University of Basel, Basel, Switzerland

[2] Department of Phytochemistry, Medicinal Plants and Drugs Research Institute, Shahid Beheshti University, G. C., Tehran, Iran

[3] Department of Medical Parasitology and Infection Biology, Swiss Tropical and Public Health Institute and University of Basel, Basel, Switzerland

[4] Division of Molecular Modeling, University of Basel, Basel, Switzerland

Correspondence

Prof. Matthias Hamburger

Division of Pharmaceutical Biology

University of Basel

Klingelbergstrasse 50

CH-4056 Basel, Switzerland

Phone: +41/61/267/1425; Fax: +41/61/267/1474

matthias.hamburger@unibas.ch

Spectral data of sahandone (8)

^{1}H NMR (500 MHz, $CDCl_3$) δ 7.08 (1H, d, J = 7.6 Hz, H-6), 6.95 (1H, d, J = 7.3 Hz, H-7), 6.87 (1H, s, H-12), 5.48 (1H, dq, J = 8.5, 1.1 H-3), 5.01 (ddd, J = 13.1, 8.9, 4.4 Hz, H-2), 3.24 (s, O-CH_3), 2.95 (sep, J = 7.0 Hz, H-15), 2.68 (dd, J = 17.0, 4.3 Hz, H_β-1), 2.53 (dd, J = 17.1, 11.1 Hz, H_α-1), 2.19 (s, H-20), 1.80 (d, J = 1.1 Hz, CH_3-18), 1.78 (d, J = 1.1 Hz, CH_3-19), 1.15 (d, J = 7.0 Hz, CH_3-16), 1.14 (d, J = 7.0 Hz, CH_3-17). ^{13}C NMR (125 MHz, $CDCl_3$) δ 30.9 (CH_2-1), 65.4 (CH-2), 125.0 (CH-3), 136.2 (C-4), 136.7 (C-5), 130.5 (CH-6), 126.4 (CH-7), 128.4 (C-8), 132.3 (C-9), 133.5 (C-10), 93.6 (C-11), 135.7 (CH-12), 140.2 (C-13), 195.5 (C-14), 27.2 (CH-15), 22.1 (CH_3-16), 21.4 (CH_3-17), 25.9 (CH_3-18), 18.4 (CH_3-19), 18.9 (CH_3-20), 50.3 (O-CH_3).

Micro-fractionation and processing for bioassay

Fractions of 60 sec each starting from minute 0.00 were collected on a FC 204 fraction collector (Gilson) into deep well plates (ScreenMate 96 well; Matrix Technology) during the run and dried in a GeneVac EZ-2 Plus evaporator (Genevac Ltd.) at 40°C using the pre-installed “HPLC-fractions” vacuum settings. Typical evaporation time was 24 h.

The dried microfractions were dissolved in 5 µL of DMSO and then diluted with 95 µL of PBS buffer (137 mM NaCl, 10 mM phosphate, 2.7 mM KCl, pH 7.4). This gave the stock solution which could be used for any of the three assays.

Antiplasmodial assay against *Plasmodium falciparum* strain K1

A modification of the [3H]-hypoxanthine incorporation assay was used for determining intra-erythrocytic inhibition of parasite growth [1, 2]. Infected erythrocytes (100 µL per well with

2.5% hematocrit and 0.3% parasitemia) were added to each drug plate in duplicates. The second test concentration was a six fold dilution of this. After 48 h incubation, 0.5 μCi of [3H]hypoxanthine in 50 μL medium was added, and plates were incubated for an additional 24 h. Parasites were harvested onto glass-fiber filters, and radioactivity was counted using a Betaplate liquid scintillation counter (Wallacand). The results were recorded as counts per minute (cpm) per well at each drug concentration and expressed as percentage of the untreated controls. IC_{50}s were estimated by linear interpolation [4].

Antitrypanosomal assay against *Trypanosoma brucei rhodesiense*

Minimum essential medium (50 μL), supplemented according to Baltz et al. [5] with 2 mercaptoethanol and 15% heat-inactivated horse serum, was added to each well of a 96-well microtiter plate [6]. 2000 *T. brucei rhodesiense* STIB 900 bloodstream forms in 45 μL of medium were added to each well, and the plate incubated at 37°C under a 5% CO_2 atmosphere for 72 h. 10 μL of resazurin solution (12.5 mg resazurin dissolved in 100 mL distilled water) was then added to each well, and incubation continued for a further 2–4 h. The plate was then read in a Spectramax Gemini XS microplate fluorometer (Molecular Devices Cooperation) using an excitation wavelength of 536 nm and emission wavelength of 588 nm. Fluorescence development was measured and expressed as percentage of the control. Data were transferred into the graphic programme Softmax Pro (Molecular Devices) which calculated IC_{50} values.

Cytotoxicity assay

The cytotoxicity assay was performed using the Alamar Blue assay [6] described above with rat skeletal myoblasts (L6-cells) seeded in 100 μL RPMI 1640 in 96-well micro titer plates (4000

cells/well). After 24 h the medium was removed and replaced by 100 μL of fresh RPMI 1640 with or without a serial threefold drug dilution. Podophyllotoxin (purity > 95%; Sigma-Aldrich) was used as the reference drug. After 70 h of incubation under a humidified 5% CO_2 atmosphere, 10 μL of the Alamar blue was added to all wells. The plates were incubated for an additional 2 h. A Spectramax Gemini XS micro plate fluorescence reader (Molecular Devices) was used to read the plates using an excitation wavelength of 536 nm and an emission wavelength of 588 nm. The IC_{50}s were calculated from the sigmoidal growth inhibition curves using Softmax Pro software (Molecular Devices).

References

1. *Adams M, Zimmermann S, Kaiser M, Brun R, Hamburger M.* A protocol for HPLC-based activity profiling for natural products with activities against tropical parasites. Nat Prod Commun 2009; 10: 1377-1381
2. *Adams M, Plitzko I, Kaiser M, Brun R, Hamburger M.* 3-methoxy carpachromene- A new tetracyclic flavonol from *Pistacia atlantica* with antiplasmodial activity. Phytochem Lett 2009; 2: 159-162
3. *Adams M, Christen M, Plitzko I, Zimmermann S, Brun R, Kaiser M, Hamburger M.* Antiplasmodial lanostanes from *Ganoderma lucidum* mushroom. J Nat Prod 2010; 73: 897-900
4. *Kunert O, Swamy R, Kaiser M, Presser A, Buzzi S, Appa Rao AVN, Schühly W.* Antiplasmodial and leishmanicidal activity of biflavonoids from Indian *Selaginella bryopteris*. Phytochem Lett 2009; 2: 171-174

5. *Baltz T, Baltz D, Giroud C, Crockett J*. Cultivation in a semi-defined medium of animal infective forms of *Trypanosoma brucei, T. equiperdum, T.evansi, T. rhodesiense* and *T. gambiense*. EMBO J 1985; 4: 1273–1277
6. *Räz B, Iten M, Grether-Bühler Y, Kaminsky R, Brun R.* The Alamar Blue assay to determine drug sensitivity of African trypanosomes (*T. b. rhodesiense* and *T. b. gambiense*) *in vitro*. Acta Trop 1997; 68: 139–147

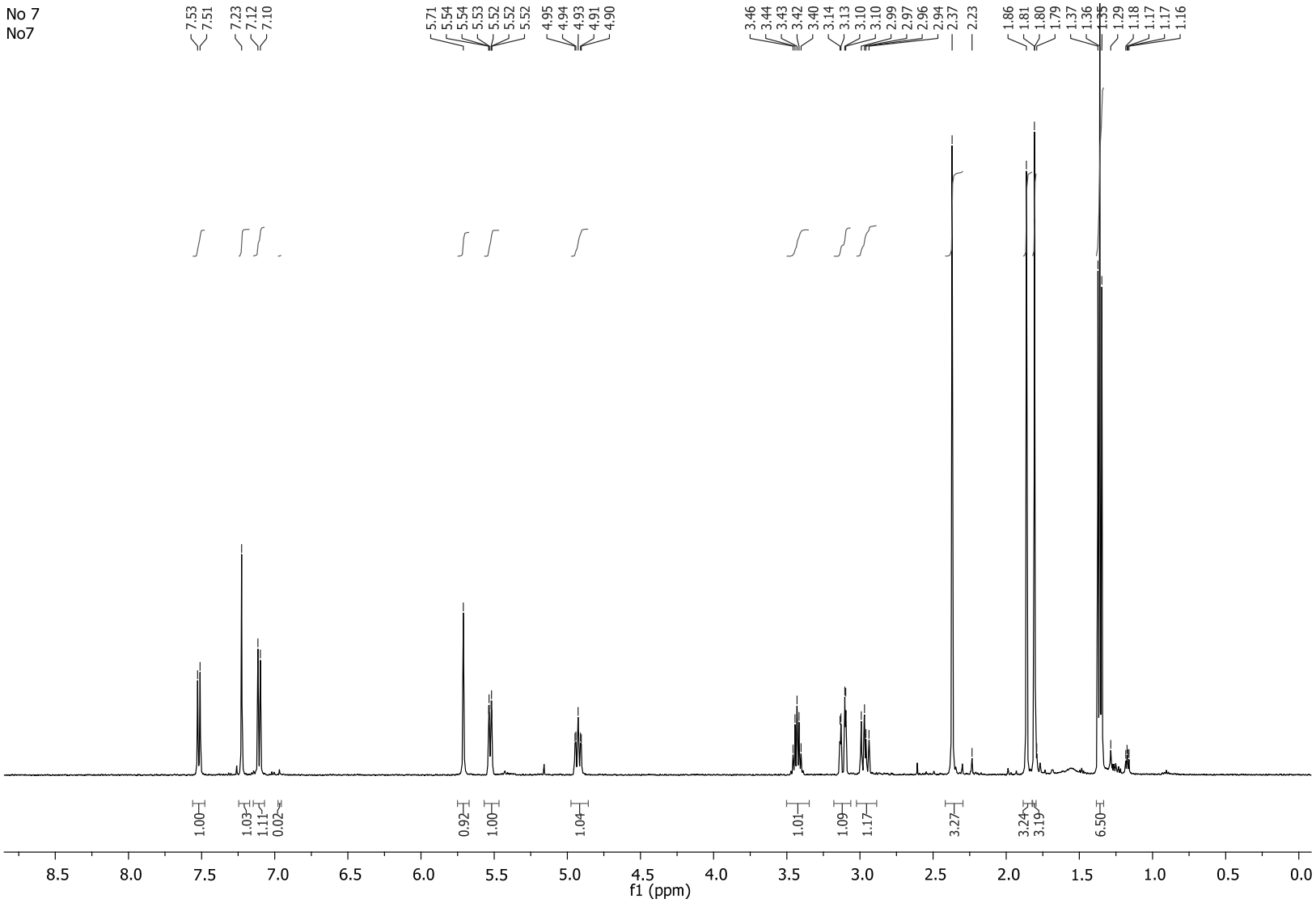

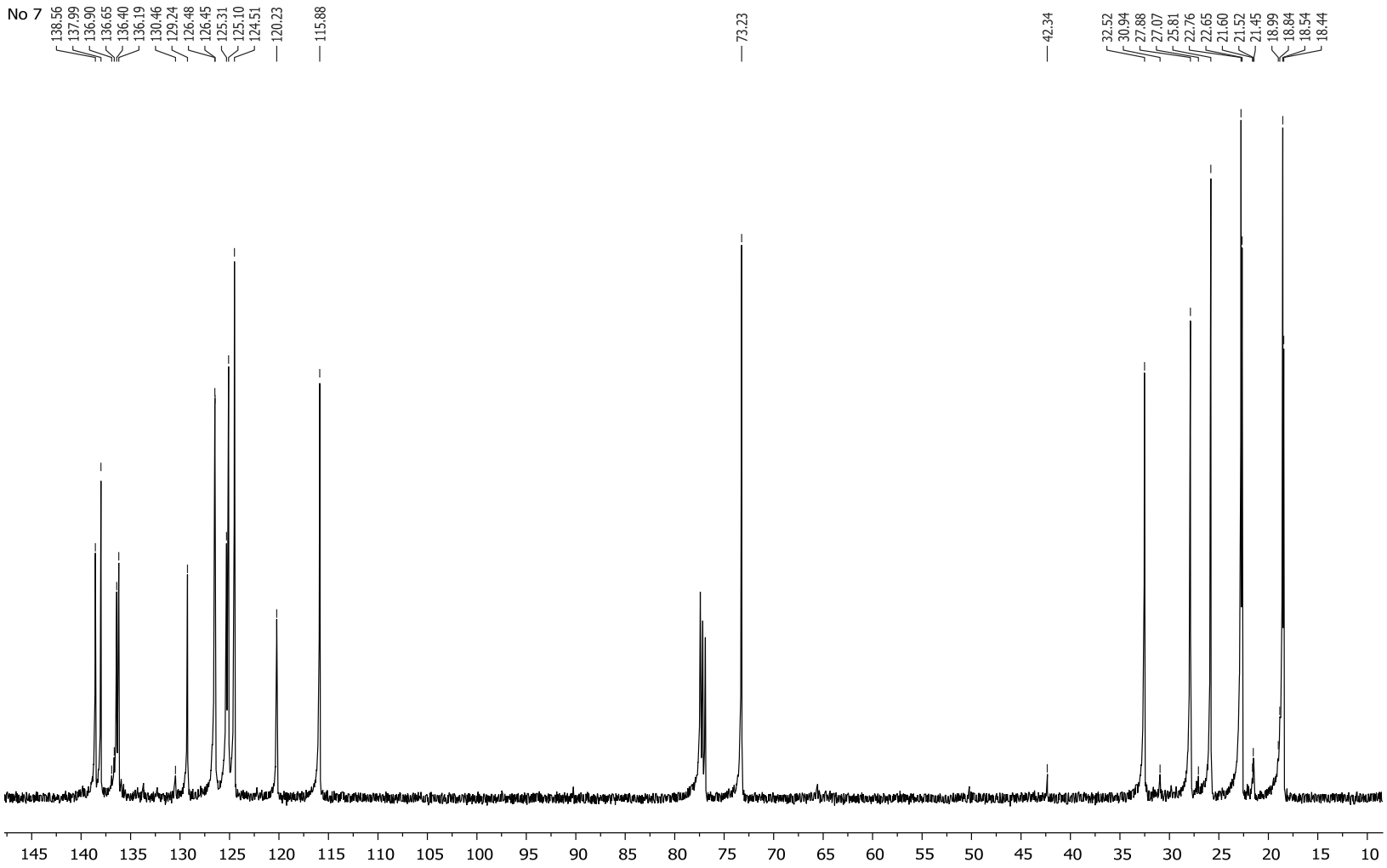

Fig. 2S ^{13}C NMR spectrum of sahandol (**7**) in $CDCl_3$.

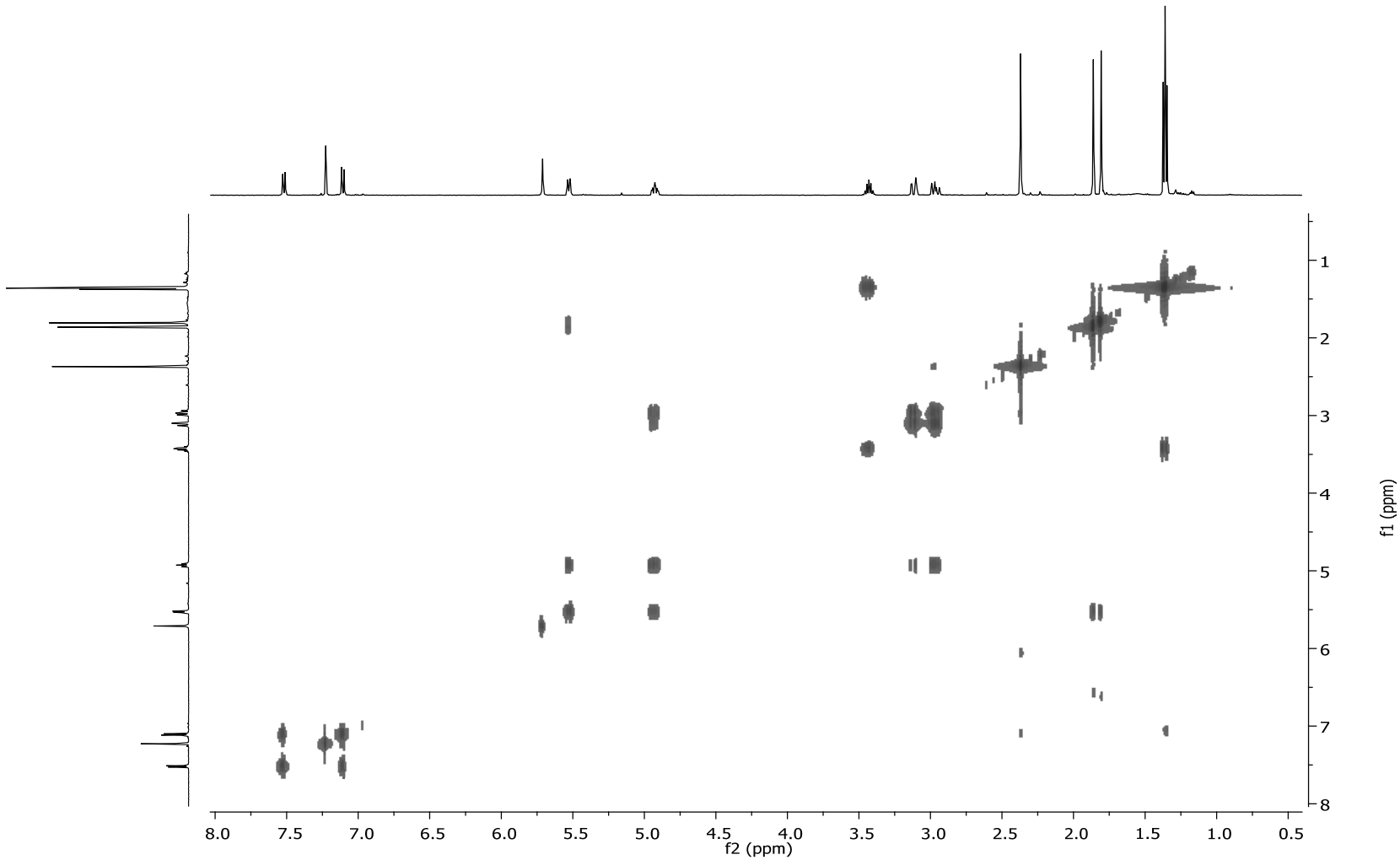

Fig. 3S ^{1}H-^{1}H COSY NMR spectrum of sahandol (**7**) in $CDCl_3$.

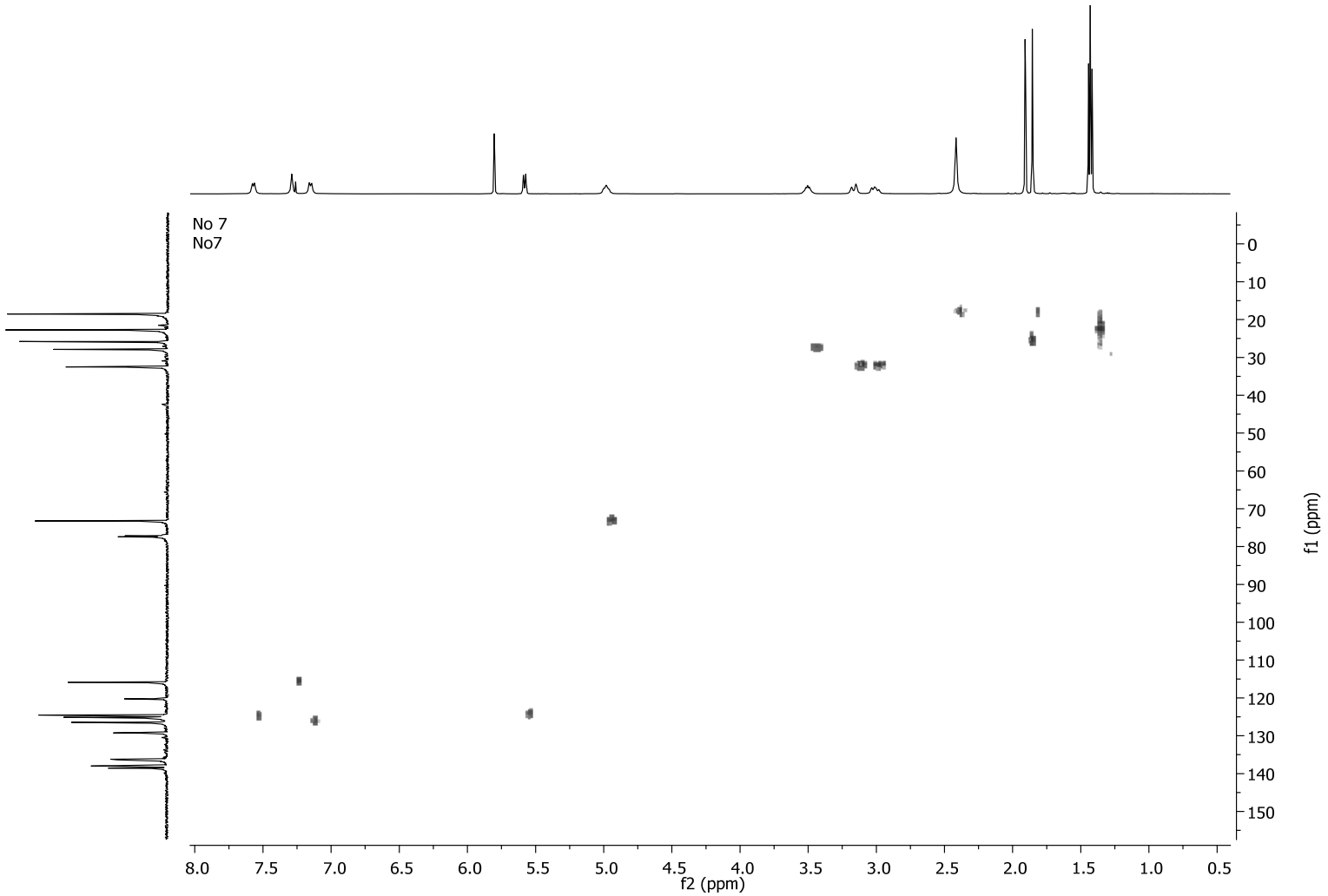

Fig. 4S HSQC NMR spectrum of sahandol (**7**) in $CDCl_3$.

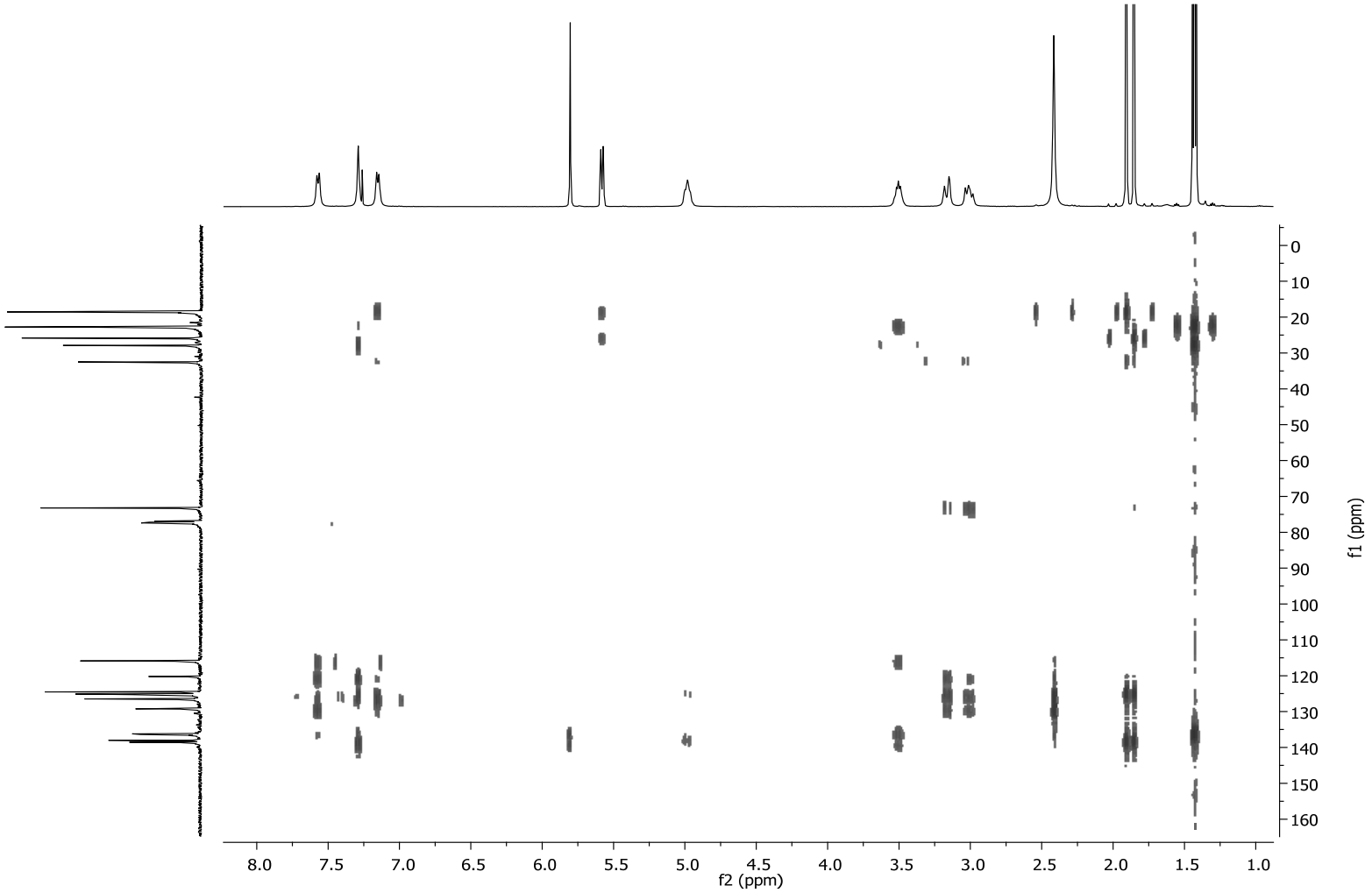

Fig. 5S HMBC NMR spectrum of sahandol (**7**) in $CDCl_3$.

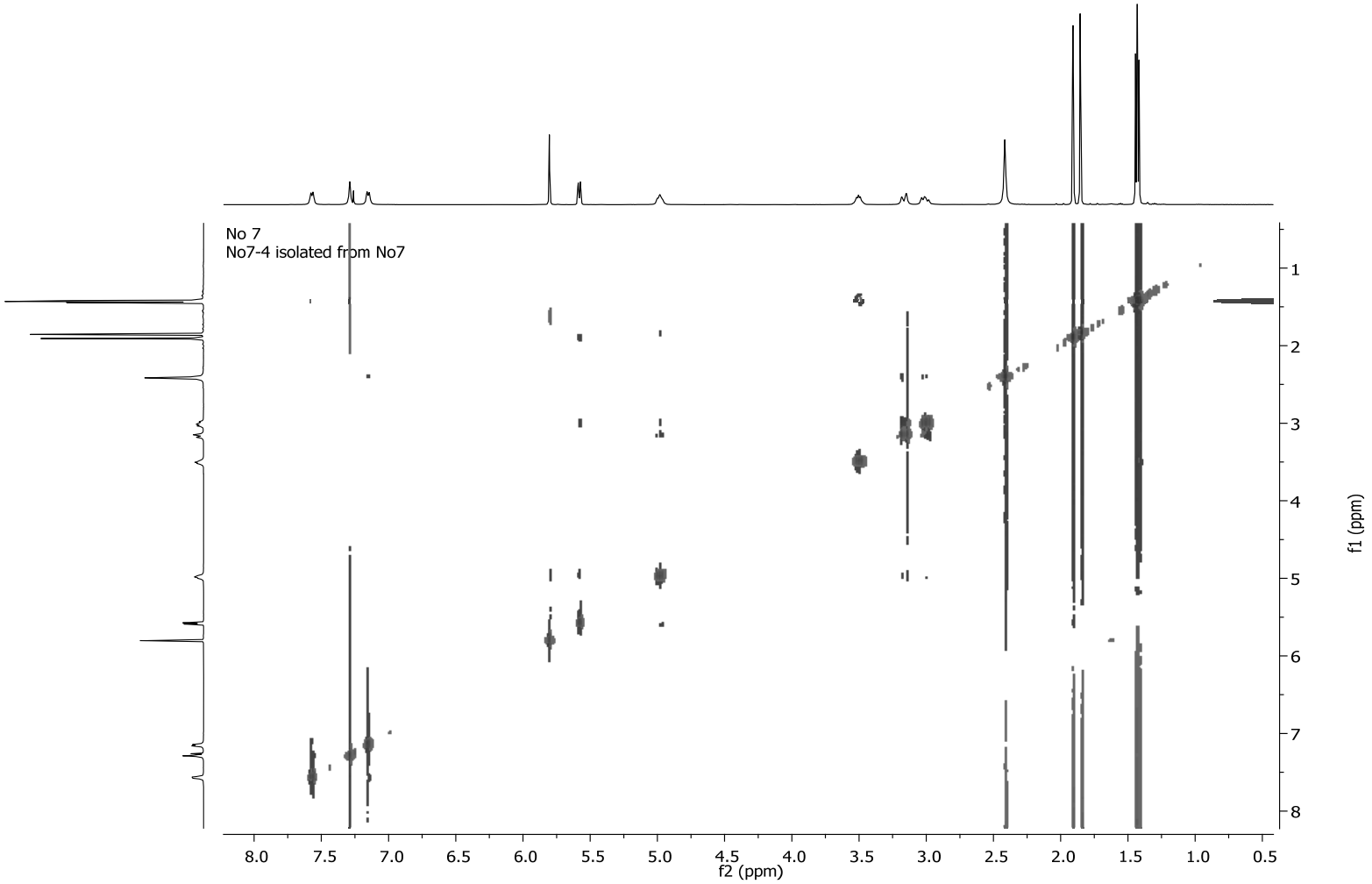

Fig. 6S NOESY NMR spectrum of sahandol (**7**) in $CDCl_3$.

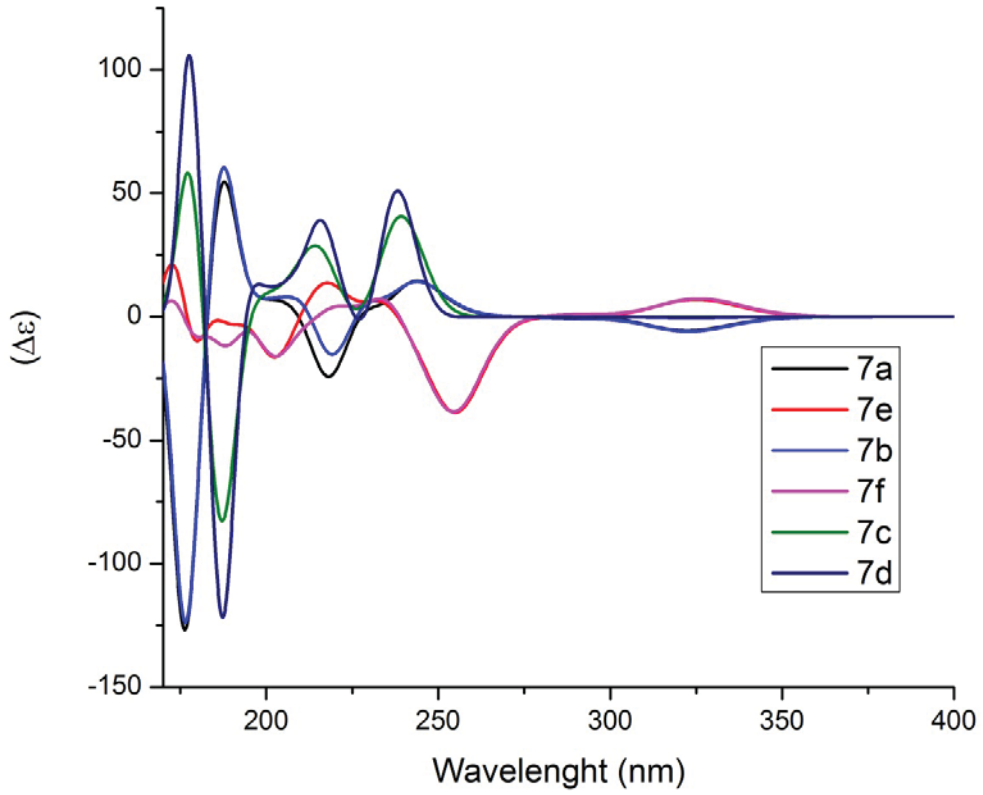

Fig. 7S Comparison of the computed ECD spectra for the six lowest energy conformers of (2*R*)-**7**. The calculations were performed with TDDFT at the B3LYP/6-31G(d,p) level using the CPCM solvent continuum model with methanol as the solvent.

Table 1S Calculated OR values for the six lowest energy conformers of (2*R*)-**7** and the conformational average compared to experimental $[\alpha]_D$.

Conformer	Population (%)	$[\alpha]_D$
7a	48.5	-62.26
7b	44.4	-15.02
7c	1.0	+188.88
7d	2.2	+202.92
7e	0.7	-150.10
7f	3.1	-131.33
Conformational average		**-35.99**
Experimental		**-56.50**

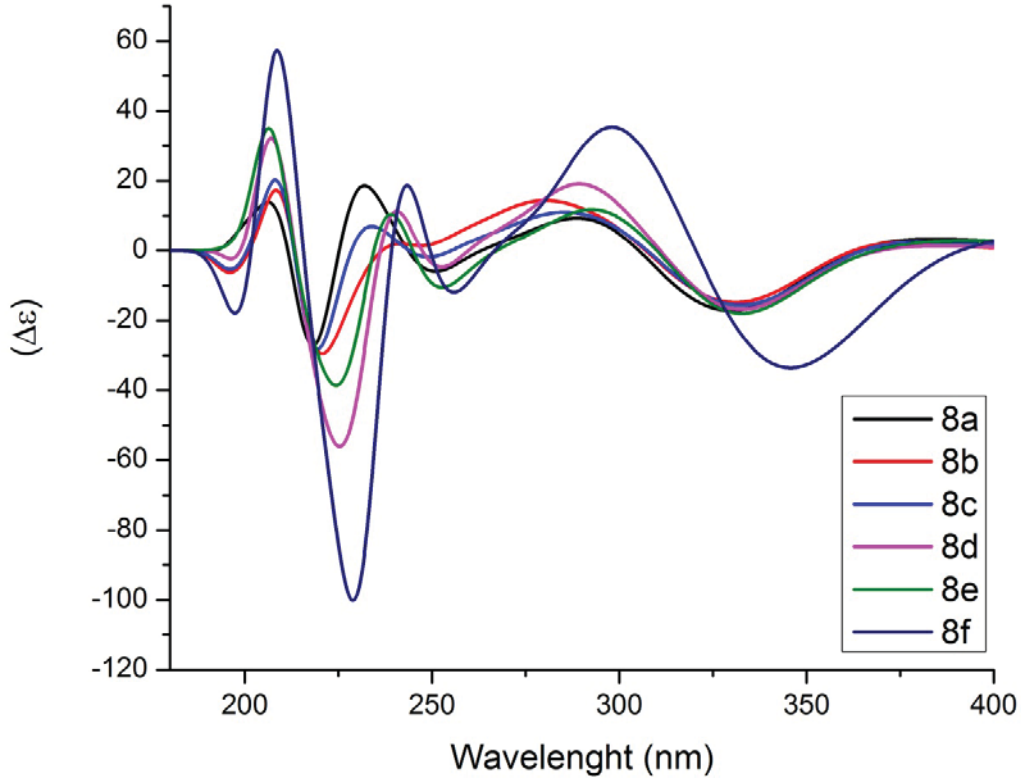

Fig. 8S Comparison of the computed ECD spectra for the six lowest energy conformers of (2*R*,11*S*)-**8**. The calculations were performed with TDDFT at the B3LYP/6-31G(d,p) level using the CPCM solvent continuum model with methanol as the solvent.

Table 2S Calculated OR values for the six lowest energy conformers of (2*R*, 11*S*)-**8**, and the conformational average compared to experimental $[\alpha]_D$.

Conformer	Population (%)	$[\alpha]_D$
8a	24.3	-118.5
8b	21.7	-96.8
8c	11.3	-104.1
8d	16.5	-221.5
8e	17.9	-255.8
8f	8.0	-239.9
Conformational average		**-164.1**
Experimental		**-198.1**

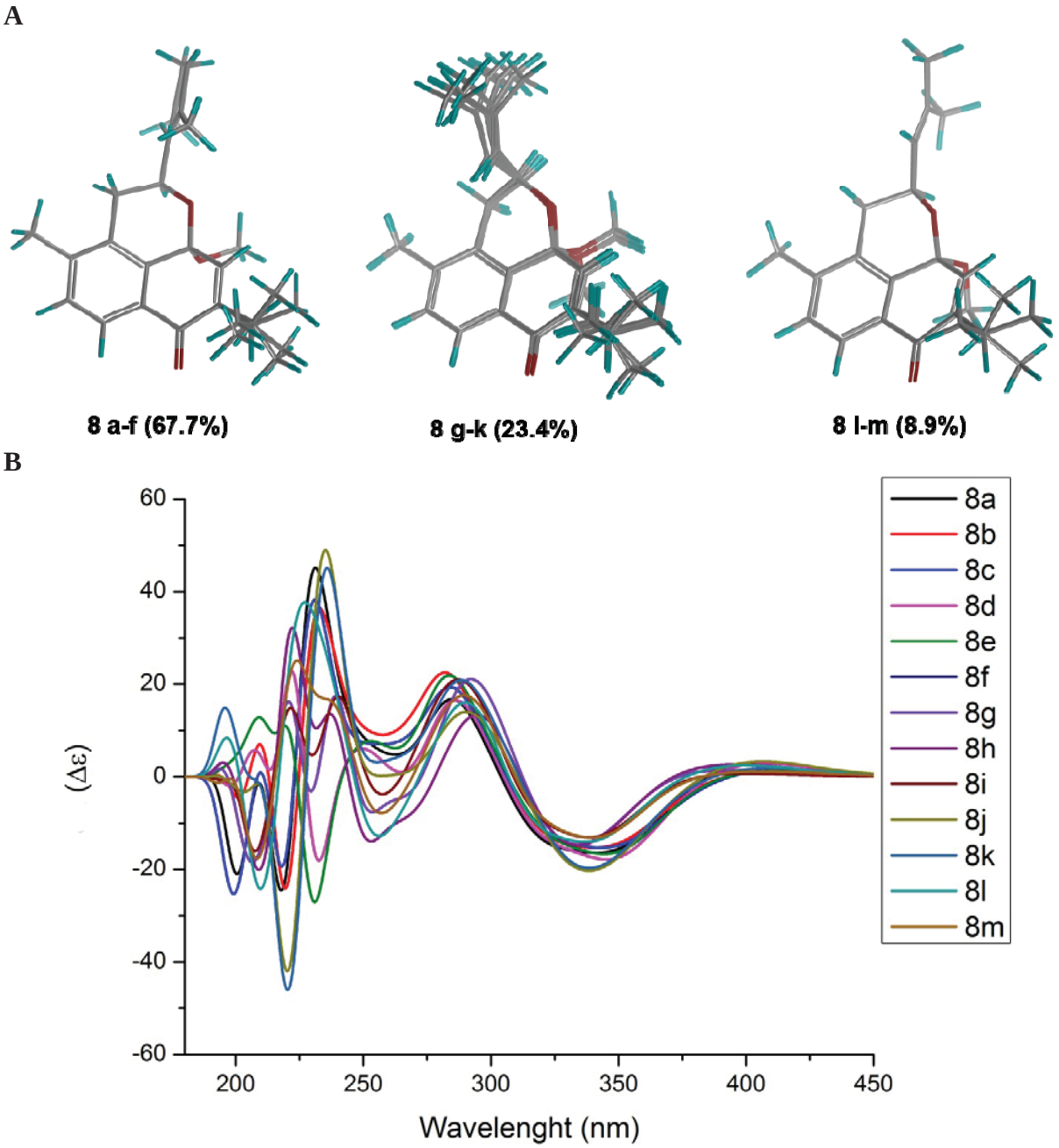

Fig. 9S A) Superimposed lowest energy conformers (within 2 kcal/mol range from the global minimum) of (2*S*,11*S*)-sahandone (**8**). Conformers obtained from the conformational search were re-calculated using DFT at the B3LYP/6-31G** level in the gas phase. **B**) Comparison of the computed ECD spectra for the six energy lowest conformers with a (2*S*,11*S*) configuration. The calculations were performed with TDDFT at the B3LYP/6-31G(d,p) level using the CPCM solvent continuum model with methanol as the solvent.

Table 3S Calculated OR values for the six lowest energy conformers of (2*S*,11*S*)-**8**, and the conformational average compared to experimental $[\alpha]_D$.

Conformer	Population (%)	$[\alpha]_D$
8a	28.3	-80.28
8b	23.1	-71.2
8c	13.0	-93.0
8d	1.4	-219.00
8e	1.2	-221.2
8f	5.3	-78.6
8g	2.6	-110. 8
8h	2.9	-156.2
8i	4.8	-62.5
8j	4.8	-254.2
8k	4.0	-218.0
8l	5.3	-78.5
8m	2.4	-75.0
Conformational average		**-97.2**
Experimental		**-198.1**

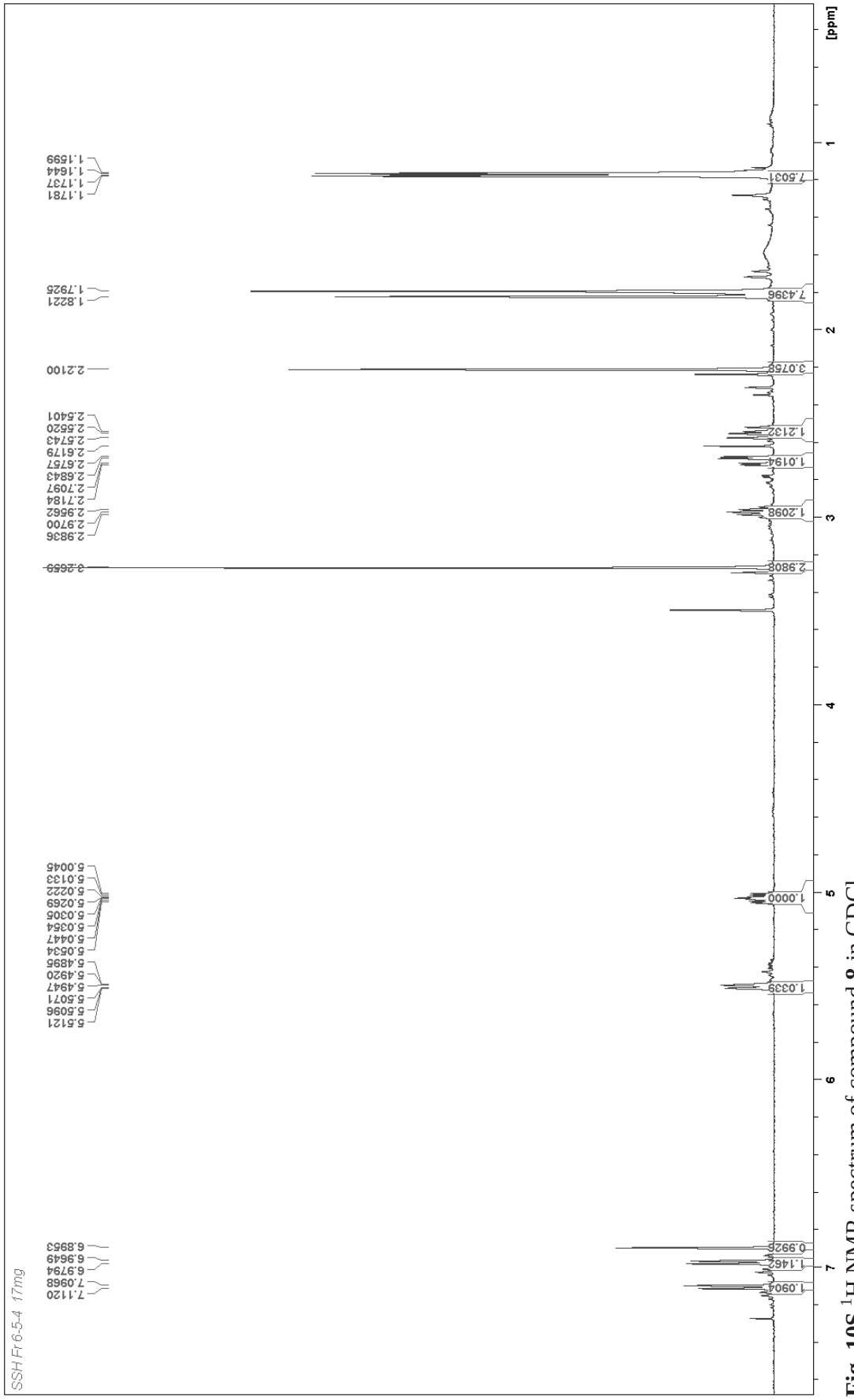

Fig. 10S ^{1}H NMR spectrum of compound **8** in $CDCl_3$.

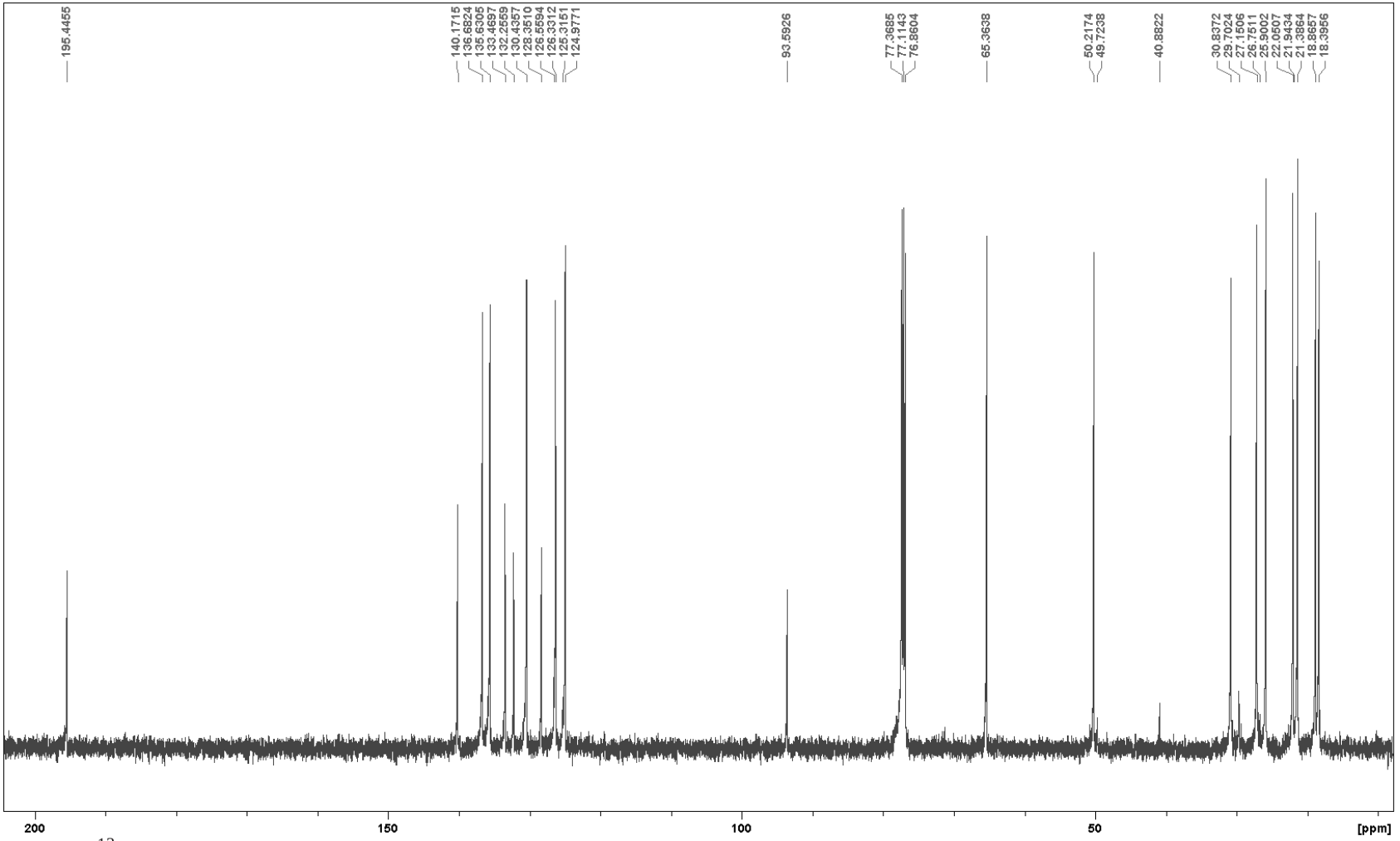

Fig. 11S ^{13}C NMR spectrum of compound **8** in $CDCl_3$.

3.2. Bisabololoxide derivatives from *Artemisia persica*, and determination of their absolute configurations by ECD

Fahimeh Moradi-Afrapoli, Samad Nejad Ebrahimi, Martin Smiesko, Melanie Raith, Stefanie Zimmermann, Farsad Nadjafi, Reto Brun , Matthias Hamburger

Phytochemistry (2012), http://dx.doi.org/10.1016/j.phytochem.2012.08.017

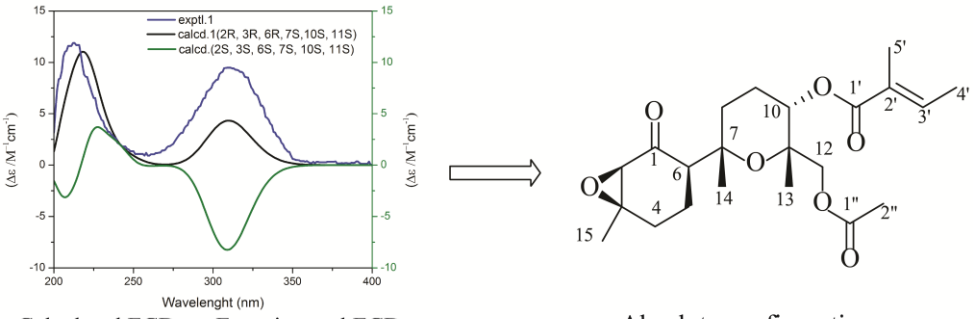

HPLC based activity profiling enabled the identification five new bisabololoxide derivatives from an EtOAc extract of *Artemisia persica*. Structures were elucidated by mass spectrometry and microprobe NMR. The absolute configuration of the compounds **1**-**5** was determined by ECD supported by *in silico* base simulation of ECD spectra. Bisaboloids **1**-**4** exhibited *in vitro* antimalarial activity against *Plasmodium falciparum*, with IC50 values ranging from 2.8 to 20.1 µM, and selectivity indices (SI) in L-6 cells of 3.7–11.9.

Extraction of plant material for isolation, isolation of compounds (major part was done by Fahimeh Moradi), HPLC microfractionation, recording and interpretation of analytical data for structure elucidation (mass spectrometry, microprobe NMR, optical rotation, ECD), data analysis, experimental measurement and quantum-chemical calculation of ECD spectra, taking part in writing of the manuscript, and preparation of figures were my contribution to this publication. Antimalarial tests were done by Stefanie Zimmermann.

Samad Ebrahimi

Phytochemistry 85 (2013) 143–152

Contents lists available at SciVerse ScienceDirect

Phytochemistry

journal homepage: www.elsevier.com/locate/phytochem

Bisabololoxide derivatives from *Artemisia persica*, and determination of their absolute configurations by ECD

Fahimeh Moradi-Afrapoli [a,1], Samad Nejad Ebrahimi [b,c,1], Martin Smiesko [d], Melanie Raith [b], Stefanie Zimmermann [b,e], Farsad Nadjafi [f], Reto Brun [e], Matthias Hamburger [b,*]

[a] Department of Pharmacognosy, Faculty of Pharmacy, Mazandaran University of Medical Sciences, Sari, Iran
[b] Division of Pharmaceutical Biology, University of Basel, Klingelbergstrasse 50, 4056 Basel, Switzerland
[c] Department of Phytochemistry, Medicinal Plants and Drugs Research Institute, Shahid Beheshti University, G. C., Evin, Tehran, Iran
[d] Division of Molecular Modeling, University of Basel, Klingelbergstrasse 50, 4056 Basel, Switzerland
[e] Department of Medical Parasitology and Infection Biology, Swiss Tropical and Public Health Institute, Basel, Switzerland
[f] Department of Agriculture, Medicinal Plants and Drugs Research Institute, Shahid Beheshti University, G. C., Evin, Tehran, Iran

ARTICLE INFO

Article history:
Received 11 June 2012
Received in revised form 24 August 2012
Available online 23 September 2012

Keywords:
Artemisia persica
Plasmodium falciparum
TDDFT
Absolute configurations
Bisabololoxide

ABSTRACT

Five antiplasmodial bisabololoxide sesquiterpene diesters were isolated from an EtOAc extract of the aerial parts of *Artemisia persica* following an HPLC-time-based activity profiling of the extract. Structure elucidation was achieved by 1D and 2D NMR experiments. Relative configurations of cyclohexenone/cyclohexene and tetrahydropyran moieties of **1**–**5** were established on the basis of $^3J_{H-H}$ coupling constants and NOE difference spectra. Stereochemical correlation of the two rings, and assignment of absolute configuration of **1**–**5** were achieved by comparison of experimental ECD spectra with simulated ECD data for possible stereoisomers, by using time dependent density function theory (TDDFT). Bisaboloids **1**–**4** exhibited *in vitro* antimalarial activity against *Plasmodium falciparum*, with IC_{50} values ranging from 2.8 to 20.1 μM, and selectivity indices (SI) in L-6 cells of 3.7–11.9.

1. Introduction

The genus *Artemisia* belongs to the Asteraceae family and comprises more than 400 species. Several *Artemisia* species have been used in various traditional and folk medicines as a treatment for fever and malaria (Ortet et al., 2008; Tu, 2011). From the traditional Chinese herb *Artemisia annua*, artemisinin was isolated and served as lead for today's most effective antimalarial drugs (Meshnick et al., 1996). In Iran, *Artemisia* species with the local name of "*Dermaneh*" are distributed all over the country (Mozaffarian, 2007). They have been traditionally used for treatment of intermittent fever and chills which are the main symptoms of malaria (Biruni, 2004; Hoseyni, 1997; Mirjalili et al., 2007; Razi, 2006; Rustaiyan and Masoudi, 2011). *Artemisia persica* Boiss. is an indigenous plant that grows mainly in the Zagros mountains, south-western, southern and central parts of Iran (Ghahreman, 1978–2005).

HPLC-based activity profiling is a miniaturized and rapid approach for the localization, dereplication, and characterization of bioactive natural products in extracts (Potterat and Hamburger, 2006), which we have successfully applied to discovery of new anti-protozoal compounds (Adams et al., 2010, 2011, 2009; Slusarczyk et al., 2011; Zimmermann et al., 2012). We here report on the identification of new antiplasmodial sesquiterpenes by this HPLC-based approach, and on the assignment of relative and absolute stereochemistries by a combination of NMR spectroscopy and electronic circular dichroism (ECD) measurements and calculations. In particular, on a series of bisabolol oxide esters we demonstrate the assignment of absolute configuration by ECD calculation for compounds in which relative stereochemistry of two discrete parts of the molecule but not of its entirety could be established by NMR.

2. Results and discussion

In screening for new antiparasitic natural products from plants of the Iranian flora (Farimani et al., 2011, 2012), an EtOAc extract of *A. persica* tested active against the chloroquine-resistant *Plasmodium falciparum* K1 strain (77% inhibition at a test concentration of 0.8 μg/ml). The antiplasmodial activity was localized with the aid of HPLC-time-based activity profiling using a previously validated protocol (Adams et al., 2009). Briefly, 350 μg of extract was separated by analytical gradient HPLC, UV and MS data recorded on-line, while time-based microfractions for bioassay were

* Corresponding author. Tel.: +41 612671425; fax: +41 612671474.
E-mail address: matthias.hamburger@unibas.ch (M. Hamburger).
[1] These authors contributed equally to this work.

0031-9422/$ - see front matter © 2012 Elsevier Ltd. All rights reserved.
http://dx.doi.org/10.1016/j.phytochem.2012.08.017

collected *via* a T-splitter. The HPLC-MS trace and corresponding activity profile are shown in Fig. 1a and b, respectively. Fraction 26 (R_t 25–26 min) contained a major peak of activity. The LC-MS^n and off-line microprobe NMR data of the fraction revealed that the active peak was composed of several compounds. Preparative isolation of new sesquiterpene diesters **1**–**5** (Fig. 2) in the active time-window was achieved by a combination of normal-phase medium pressure liquid chromatography (MPLC) and semi-preparative RP-HPLC. Structures were established by ESI-TOF-MS, 1D and 2D NMR experiments. The relative configurations in the two rings were established by analysis of vicinal coupling constants and NOE experiments, while the absolute configuration was determined by comparison of experimental ECD data with calculated spectra of possible stereoisomers.

Compound **1** was obtained as colorless oil. Its molecular formula of $C_{22}H_{32}O_7$ (HRESIMS m/z 431.2039 $[M+Na]^+$; calcd. 431.2046) accounted for 7° of unsaturation. The ^{1}H NMR spectrum (500 MHz, C_6D_6, Table 1) showed resonances attributable to six methyl groups, an olefinic methine (δ 6.96), two deshielded diastereotopic methylene protons at δ 4.35 (d, J_{gem} = 10.3 Hz) and 3.94 (d, J_{gem} = 10.3 Hz), and protons of two oxygen-bearing methines (δ 4.99, 2.94). The signal at δ 6.96 (qq, J = 7.0, 1.1 Hz) and two vinylic

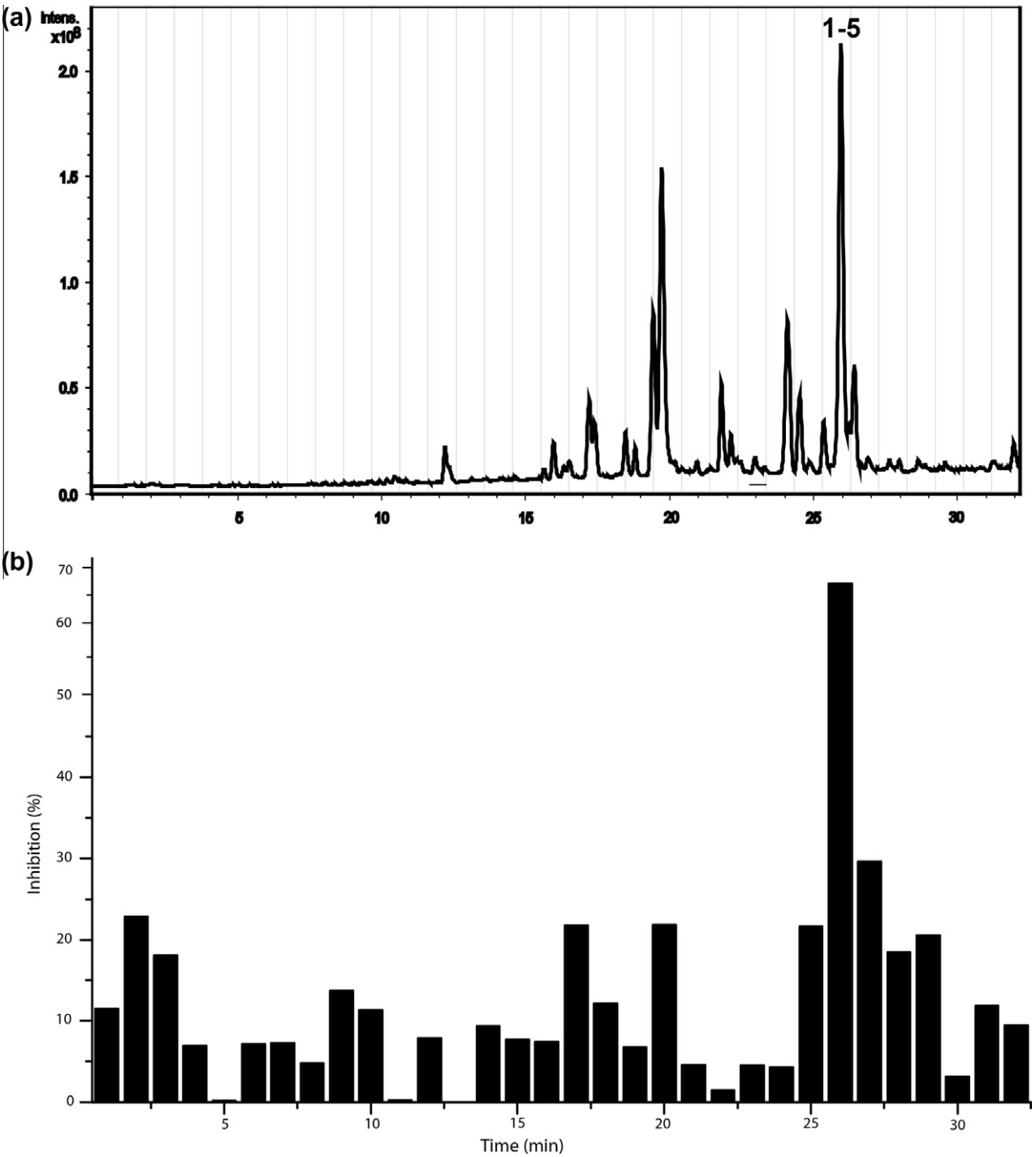

Fig. 1. HPLC-MS trace (ESI positive, TIC m/z 200–1500) of the EtOAc extract (a), and antiplasmodial activity of the one-minute microfractions (b).

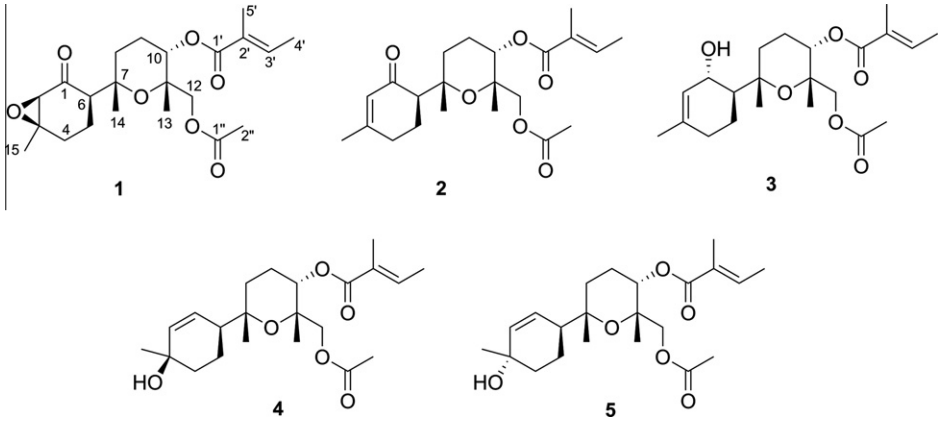

Fig. 2. Structures of sesquiterpene diesters 1–5.

Table 1
^{1}H NMR data (500 MHz) of sesquiterpene diesters **1**–**5**.

No.	**1**[a]	**2**[a]	**2**[b]	**3**[a]	**4**[a]	**5**[a]
1	–	–	–	4.59 (br *d*, 9.8)	6.04 (br *d*, 10.0)	5.90 (*dd*, 10.5, 2.0)
2	2.94 (*s*)	5.77 (br *s*)	5.88 (br *s*)	5.64 (br *s*)	5.74 (*dd*, 10.0, 2.4)	5.74 (*ddd*, 10.5, 2.5, 1.6)
3	–	–	–	–	–	–
4α	1.26 (*ddd*, 4.0, 13.0, 13.0)[c]	1.84[d]	2.17[c]	1.67 (*ddd*, 17.0, 12.4, 3.5)[c]	1.81 (*ddd*, 13.0, 4.0, 4.0)[c]	1.56 (*dddd*, 13.2, 4.5, 3.4, 1.6)[c]
4β	1.69 (*ddd*, 4.0, 4.0, 13.0)[c]		2.26 (*ddd*, 18.2, 4.4, 4.4)[c]	1.86 (*dd*, 17.0, 5.0, 2.2)[c]	1.39 (*ddd*, 13.0, 13.0, 4.0)[c]	1.77 (*dddd*, 13.2, 13.2, 4.5, 2.5)[c]
5α	1.76[d]	2.31[d]	2.44 (*dddd*, 13.2, 4.4, 4.4, 4.4)[c]	1.34 (*dddd*, 13.0, 3.5, 2.2, 2.2)[c]	1.47 (*dddd*, 13.0, 13.0, 11.0, 4.0)[c]	1.17 (*dddd*, 13.2, 13.2, 10.7, 3.4)[c]
5β	1.91 (*dddd*, 4.0, 13.0, 13.0, 13.0)[c]	1.64[d]	1.85 (*dddd*, 13.2, 11.5, 11.5, 4.4)[c]	1.06 (*dddd*, 13.0, 13.0, 12.4, 5.0)[c]	1.55 (*dddd*, 8.0, 3.0, 4.0, 4.0)[c]	1.65 (*dddd*, 13.2, 4.5, 4.5, 8.0)[c]
6	2.06 (*dd*, 6.0, 13.0)[c]	2.31[d]	2.51(*dd*, 4.4, 11.5)[c]	1.69 (*ddd*, 13.0, 9.0, 2.2)[c]	2.05 (*ddd*, 11.0, 8.0, 2.4)[c]	2.20 (*dddd*, 10.7, 8.0, 2.0, 1.6)[c]
7	–	–	–	–	–	–
8α	1.90 (*ddd*, 4.0, 4.0, 13.5)[c]	1.93 (*ddd*, 13.6, 13.2, 4.2)[c]	2.10 (13.2, 13.2, 2.2)[c]	0.80 (*ddd*, 3.5, 3.5, 13.3)[c]	0.92[d]	0.89[d]
8β	2.00[d]	2.36 (*ddd*, 13.6, 3.5, 3.5)[c]	2.34 (*ddd*, 13.2, 4.4, 4.4)[c]	1.87[d]	1.71[d]	1.68[d]
9α	1.74[d]	1.74[d]	1.90[d]	1.72[d]	1.71[d]	1.71[d]
9β		1.84[d]	2.15[d]			
10	4.99 (*dd*, 3.2, 3.2)	5.02 (*dd*, 3.0, 3.0)	5.14 (*dd*, 2.3, 3.7)	4.92 (*dd*, 3.0, 3.0)	4.99 (*dd*, 2.5, 2.5)	5.01 (*dd*, 3.0, 3.0)
11	–	–	–	–	–	–
12a	3.94 (*d*, 10.3)	3.94 (*d*, 10.4)	4.07 (*d*, 10.5)	3.94 (*d*, 10.7)	4.00 (*d*, 10.4)	3.92 (*d*, 10.4)
12b	4.35 (*d*, 10.3)	4.34 (*d*, 10.4)	4.41 (*d*, 10.5)	4.28 (*d*, 10.7)	4.29 (*d*, 10.4)	4.38 (*d*, 10.4)
13	1.11 (*s*)	1.16 (*s*)	1.39 (*s*)	1.10 (*s*)	1.17 (*s*)	1.19 (*s*)
14	1.14 (*s*)	1.23 (*s*)	1.37 (*s*)	1.08 (*s*)	1.04 (*s*)	1.00 (*s*)
15	0.95 (*s*)	1.39 (*s*)	1.75 (br *s*)	1.61 (br *s*)	1.25 (br *s*)	1.23 (*s*)
1′	–	–	–	–	–	–
2′	–	–	–	–	–	–
3′	6.96 (*qq*, 7.0, 1.1)	6.90 (*qq*, 7.2, 1.2)	7.04 (*qq*, 7.0, 1.2)	7.08 (*qq*, 1.2, 7.1)	7.00 (*qq*, 7.1, 1.1)	6.99 (*qq*, 7.2, 1.2)
4′	1.39 (*qd*, 7.0, 1.1)	1.38 (*dq*, 7.2, 1.2)	1.64 (*qd*, 7.0, 1.2)	1.43 (*qd*, 1.2, 7.1)	1.44 (*qd*, 7.1, 1.1)	1.42 (*qd*, 7.2, 1.2)
5′	1.82 (*qd*, 1.1, 1.1)	1.78 (br *s*)	1.90 (*qq*, 1.2, 1.2)	1.84 (br *s*)	1.83 (br *s*)	1.82 (*qd*, 1.2, 1.2)
1″	–	–	–	–	–	–
2″	1.69 (*s*)	1.70 (*s*)	2.02 (*s*)	1.69 (*s*)	1.71 (*s*)	1.70 (*s*)
OH	–	–	–	4.31 (*s*)	–	5.00 (*s*)

[a] In C_6D_6.
[b] In pyridine-d_5.
[c] Signals were resolved by 1D selective TOCSY experiments.
[d] Multiplet signals.

methyls at δ 1.39 (*qd*, *J* = 7.0, 1.1 Hz) and 1.82 (*qd*, *J* = 1.1, 1.1 Hz) formed a discrete spin system indicative of a tigloyl moiety. The ^{13}C NMR spectrum (Table 2) showed 22 carbon signals which were resolved through a DEPT experiment into six methyl, five methylene, four methine, and seven quaternary carbons. Additional resonances of a ketone carbonyl (δ 206.2) and two ester carbonyls (δ 167.0, 170.1) were observed, whereas six carbon signals at δ 75.9 (C), 74.7 (C), 68.9 (CH), 68.7 (CH_2), 63.7 (CH), and 61.8 (C) were assigned to oxygen bearing sp^3 carbons. The protonated carbons and their attached protons were correlated by an HSQC spectrum. Based on the correlations observed in ^{1}H–^{1}H COSY and HMBC spectra (Fig. 3) compound **1** was found to be a bisabololoxide derivative. HMBC correlations from Me-13 to C-11, C-12, and from Me-14 to C-6, C-7, and C-8 confirmed the location of Me-13 at C-11 and Me-14 at C-7, respectively. Correlations between Me-15 and C-2, C-3, C-4 indicated that the methyl group was located at C-3. Correlations between H-6 and C-7, C-8, and C-14 confirmed the linkage of rings A and B *via* the C6–C7 bond. An HMBC cross peak

Table 2
^{13}C NMR data of compounds **1**–**5** (125 MHz, C_6D_6).

No.	1	2	3	4	5
1	206.2 (C)	198.7 (C)	68.2 (CH)	130.8 (CH)	128.5 (CH)
2	63.7 (CH)	128.7 (CH)	126.9 (CH)	135.1 (CH)	136.8 (CH)
3	61.8 (C)	159.8 (C)	134.2 (C)	66.6 (C)	68.3 (C)
4	28.8 (CH_2)	31.7 (CH_2)	30.8 (CH_2)	37.7 (CH_2)	38.9 (CH_2)
5	18.0 (CH_2)	23.9 (CH_2)	23.4 (CH_2)	20.1 (CH_2)	22.6 (CH_2)
6	59.4 (CH)	58.9 (CH)	52.8 (CH)	48.9 (CH)	48.7 (CH)
7	75.9 (C)	75.5 (C)	79.7 (C)	75.4 (C)	75.6 (C)
8	30.2 (CH_2)	30.4 (CH_2)	23.5 (CH_2)	24.6 (CH_2)	24.7 (CH_2)
9	20.9 (CH_2)	20.9 (CH_2)	20.3 (CH_2)	20.4 (CH_2)	20.4 (CH_2)
10	68.9 (CH)	69.3 (CH)	68.8 (CH)	68.6 (CH)	68.5 (CH)
11	74.7 (C)	74.9 (C)	75.2 (C)	74.1 (C)	74.4 (C)
12	68.7 (CH_2)	68.9 (CH_2)	68.5 (CH_2)	68.4 (CH_2)	68.3 (CH_2)
13	24.1 (CH_3)	24.2 (CH_3)	23.3 (CH_3)	23.5 (CH_3)	23.6 (CH_3)
14	22.6 (CH_3)	21.7 (CH_3)	25.4 (CH_3)	24.5 (CH_3)	24.0 (CH_3)
15	21.8 (CH_3)	23.6 (CH_3)	23.0 (CH_3)	30.2 (CH_3)	28.3 (CH_3)
1′	167.0 (C)	167.0 (C)	166.5 (C)	166.7 (C)	166.6 (C)
2′	129.5 (C)	129.7 (C)	128.9 (C)	129.2 (C)	129.6 (C)
3′	137.5 (CH)	137.3 (CH)	138.0 (CH)	137.5 (CH)	137.4 (CH)
4′	14.4 (CH_3)	14.3 (CH_3)	14.1 (CH_3)	14.1 (CH_3)	14.0 (CH_3)
5′	12.6 (CH_3)	12.6 (CH_3)	12.1 (CH_3)	12.2 (CH_3)	12.1 (CH_3)
1″	170.1 (C)	170.2 (C)	169.5 (C)	169.8 (C)	169.7 (C)
2″	20.7 (CH_3)	20.7 (CH_3)	20.2 (CH_3)	20.4 (CH_3)	20.4 (CH_3)

between the methyl group at δ 1.69 (H-2″) and the carbonyl at δ 170.1 (C-1″) corroborated the presence of an acetoxy moiety which was attached at C-12 (HMBC correlation of C-1″ (δ 170.1) with H-12a and H-12b (δ 3.94 and 4.35, respectively)). The tigloyl moiety was attached to C-10, as indicated by a cross peak between H-10 (δ 4.99) and the carbonyl group at δ 167.0. Hence, compound **1** was found to be a sesquiterpene diester. In the ^{1}H NMR spectrum, overlapping signals in the range of δ 1.5–2.0 were deconvoluted with the aid of 1D selective TOCSY experiments. Excitation of H-6 led to detection of H-4α, H-4β, H-5α, and H-5β in ring A, while excitation of H-10 revealed that H-9, H-8α, and H-8β formed a spin system in ring B (Supporting information).

The relative configurations of the cyclohexanone and tetrahydropyran portions of **1** were derived from vicinal coupling constants and by NOE difference measurements (Fig. 3). H-4α/H-5β and H-5β/H-6 ($^3J_{H-H}$ = 13.0 Hz) had both *trans*-diaxial orientations, with dihedral angles of ca. 180°. In a NOE difference experiment, presaturation of the H-6 resonance led to enhancement of H-2 and H-4α. Therefore, ring A adopted an envelope conformation with H-4α, H-5β, and H-6 in axial positions, corresponding to two possible absolute configurations of ring A (2*R*,3*R*,6*R* or 2*S*,3*S*,6*S*). The vicinal coupling constants between H-9α/H-10 and H-9β/H-10 (both $^3J_{H-H}$ = 3.2 Hz) corresponded to dihedral angles of ca. 60°. Hence, H-10 had to be in an equatorial position. Presaturation of H-10 in an NOE difference experiment resulted in enhancement of Me-13 and Me-14, while irradiation of Me-13 led to enhancement of H-9. Thus, Me-13 and Me-14 were both located in the axial position and in a cofacial orientation with H-10. Consequently, ring B had a chair conformation with two possible configurations (7*S*,10*S*,11*S* or 7*R*,10*R*,11*R*). Since rings A and B were linked through a rotatable C6–C7 bond, relative stereochemical correlation of the cyclohexanone and the tetrahydropyran portions of the molecule was not possible through NOE data. Hence, four stereoisomers were conceivable at that point, namely 2*R*,3*R*,6*R*,7*S*,10*S*,11*S*, 2*S*,3*S*,6*S*,7*S*,10*S*,11*S*, 2*R*,3*R*,6*R*,7*R*,10*R*,11*R* or 2*S*,3*S*,6*S*,7*R*,10*R*,11*R*. The absolute configuration of **1** was finally established by measurement of the ECD spectra and comparison with calculated ECD data calculated using time dependent density function theory (TDDFT) method. For that purpose, we selected two stereoisomers, 2*R*,3*R*,6*R*,7*S*,10*S*,11*S* and 2*S*,3*S*,6*S*,7*S*,10*S*,11*S*,

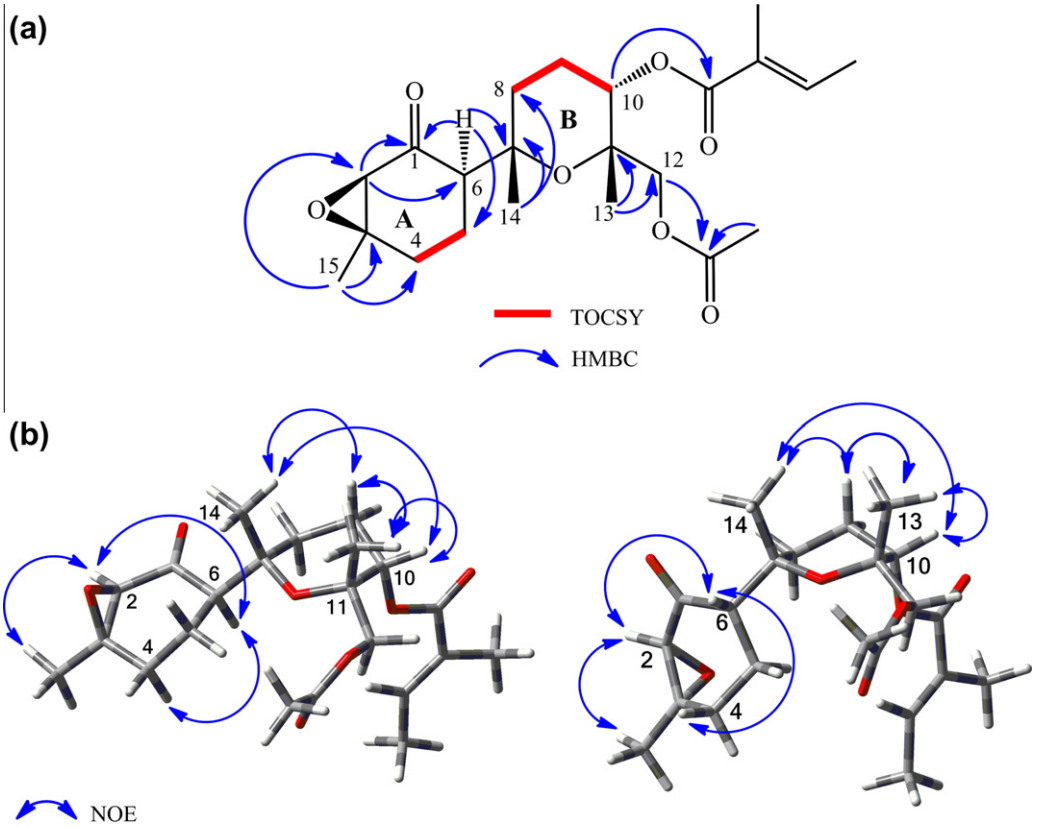

Fig. 3. 1D-TOCSY and key HMBC correlations observed for **1** (a), and key NOE correlations of DFT-optimized conformer of two possible stereoisomers, 2*R*,3*R*,6*R*,7*S*,10*S*,11*S* (left), and 2*S*,3*S*,6*S*,7*S*,10*S*,11*S* (right) (b).

since the other two would be enantiomeric and thus would show mirror images of the ECD spectra. Conformational analysis of the two stereoisomers revealed five and six conformers, respectively, within a 1 kcal/mol energy window from the particular global minimum. These conformers were subjected to geometrical optimization and energy calculation using density function theory (DFT) with the Becke's nonlocal three parameter exchange and correlation functional, and the Lee–Yang–Parr correlation functional level (B3LYP) using the 6-31G** basis set in the gas-phase. Vibrational frequency calculations were carried out to confirm these minima. No imaginary frequencies were found. Conformational analysis using relative free energies indicated the presence of five and six stable conformers, respectively (Fig. 4, Fig. S17).

ECD spectra of the conformers were calculated by the TDDFT (time-dependent density functional theory) method at B3LYP/6-31G** with MeOH as the solvent, using the SCRF (Self-consistent reaction field) method with the CPCM (*Conductor*-like *polarizable* continuum) model. For the 2*R*,3*R*,6*R*,7*S*,10*S*,11*S* stereoisomer, the ECD spectrum resulting from Boltzmann weighting of ECD spectra for individual conformers (Fig. 5a) showed two positive cotton effects (CE) around 220 and 320 nm. There was excellent agreement of the overall patterns of the calculated and experimental ECD spectra. The positive CE at around 320 nm was likely due to an $n \rightarrow \pi^*$ transition of the ketone group. The calculated ECD spectrum of the 2*S*,3*S*,6*S*,7*S*,10*S*,11*S* stereoisomer (Fig. 5a) was distinctly different from the experimental data, with two negative and one positive CEs at 210, 320, and 225 nm, respectively. Hence, the 2*R*,3*R*,6*R*,7*S*,10*S*,11*S* configuration of **1** was confirmed, and all other three possible stereoisomers could be ruled out.

Compound **2** was obtained as colorless oil. The molecular formula of $C_{22}H_{32}O_6$ was deduced from HRESIMS (*m*/*z* 415.2090 $[M+Na]^+$, calcd. 415.2097). Based on 1D- and 2D-NMR data (Tables 1 and 2) and comparison with **1**, compound **2** was also found to be a bisabololoxide derivative. Notable differences were only found in the signals attributable to ring A. In the ^{13}C NMR spectrum, the olefinic carbons C-2 and C-3 were observed at δ 128.7 and 159.8, respectively, indicative of a replacement of the C-2, C-3 epoxy moiety by a double bond. The carbonyl carbon (C-1) was shifted to higher field (δ 198.7) due to conjugation with the C-2, C-3 double bond. In the ^1H NMR spectrum, the vinylic proton H-2 appeared downfield at δ 5.77. The H-6 signal overlapped with that of H-5α (δ 2.31). Measurement in pyridine-d_5 resolved the overlap (Table 1). Vicinal coupling constants derived from ^1H NMR and selective TOCSY spectra, and NOE difference measurements in pyridine-d_5 were used to define the relative configurations of rings A and B, respectively (Fig. 6a). Vicinal coupling constants of H-5β/H-6 (J = 11.5 Hz) and H-5α/H-6 (J = 4.4 Hz) corresponded to dihedral angles of ca. 150° and 40°, respectively. Hence, H-6 was in an axial orientation. Ring A contained only one stereocenter (6*R* or 6*S*). The vicinal coupling constants of H-9α/H-10 (J = 2.3 Hz) and H-9β/H-10 (J = 3.7 Hz) corresponded to dihedral angles of 60–70° and indicated that H-10 was equatorial. Key NOEs observed for ring B (Fig. 6b) were similar to those of **1**. Hence, four stereoisomers (6*R*,7*R*,10*R*,11*R*, 6*R*,7*S*,10*S*,11*S*, 6*S*,7*R*,10*R*,11*R* or 6*S*,7*S*,10*S*,11*S*) were possible for **2**. A conformational search for the 6*R*,7*S*,10*S*,11*S* stereoisomer yielded five conformers within 1 kcal/mol from the global minimum.

The conformers were subjected to geometrical optimization (DFT/B3LYP/6-31G**) in gas phase followed by analysis of vibrational modes. The superimposed conformers showed differences arising from rotation around the C-6/C-7 bond, and from orientation of ester moieties (Fig. 7, Fig. S19). The ECD spectra of conformers were calculated (TDDFT/B3LYP/6-31G**) with MeOH as the solvent (SCRF/CPCM). The average spectrum resulting from Boltzmann weighting of ECD spectra for individual conformers showed a positive CE at 230 nm along with a negative CE at 215 nm. On the other hand, the simulated ECD spectrum of the 6*S*,7*S*,10*S*,11*S* stereoisomer showed a negative CE at 230 nm and two positive CEs at 243 and 215 nm. The experimental ECD spectrum of **2** showed a positive CE at 236 nm along with a negative CE at 213 nm. The positive CE at around 240 nm was likely due to a $\pi \rightarrow \pi^*$ transition of α,β-unsaturated carbonyl group. Comparison of the experimental ECD spectrum revealed an excellent fit with the data calculated for the 6*R*,7*S*,10*S*,11*S* stereoisomer (Fig. 5b), and we thus concluded that the absolute configuration of compound **2** was 6*R*,7*S*,10*S*,11*S*.

Compound **3** was obtained as colorless oil. The molecular formula of $C_{22}H_{34}O_6$ was deduced from HRESIMS (*m*/*z* 417.2285 $[M+Na]^+$, calcd. 417.2253). 1D and 2D NMR data of compound **3** (Table 1) were in part similar to those of **1** and **2**, indicating a sesquiterpene diester structure with an identical ring B. Notable differences were found with resonances attributable to ring A. In the ^{13}C NMR spectrum, the signals of C-1 and C-3 appeared at δ 68.2 and 134.2, respectively, and C-6 was located at δ 52.8 due to an allylic alcohol instead of the carbonyl group at C-1. In the ^1H NMR spectrum an additional signal was observed at δ 4.59 (H-1, *br d*, 9.8 Hz). Overlapping signals in the range of 1–2 ppm were resolved by 1D selective TOCSY experiments into discrete spin systems and supported the proposed structure of **3**. H-2 appeared as a broad singlet, indicative of a dihedral angle ($\phi_{H1,C1,C2,H2}$) of 70–80° and, hence, of a pseudo-axial orientation of H-1. The vicinal coupling of H-1/H-6 (J = 9.8 Hz) and H-5β/H-6 (J = 13.0 Hz) corresponded to dihedral angles of approx. 140° and 150–160°, respectively. Hence, H-6 was in an axial orientation. Close inspection of the splitting pattern of all protons on ring A indicated a pseudo-chair conformation. Given the conformational flexibility of ring A, there was some uncertainty regarding its relative configuration. Therefore, we performed a conformational analysis of **3** with three of the four possible configurations (1*S*,6*S*, 1*S*,6*R*, 1*R*,6*S*, 1*R*,6*R*) for ring A, whereby the absolute configuration of ring B was identical with that in **1** and **2** (7*S*,10*S*,11*S*).

The ECD spectrum of **3** in MeOH showed a negative CE around 205 nm and two positive CEs at 221 and 232 (shoulder) nm. The negative CE at 205 nm was likely due to a $\pi \rightarrow \pi^*$ transition of

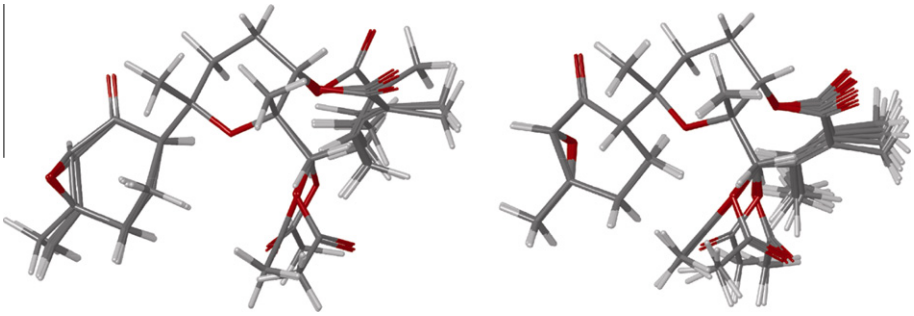

Fig. 4. Low energy conformers of the 2*R*,3*R*,6*R*,7*S*,10*S*,11*S* (left; five conformers within a 1 kcal/mol range from the global minimum) and 2*S*,3*S*,6*S*,7*S*,10*S*,11*S* stereoisomers (right; six conformers) of **1**. The calculations were performed in the gas phase with DFT at the B3LYP/6-31G** level.

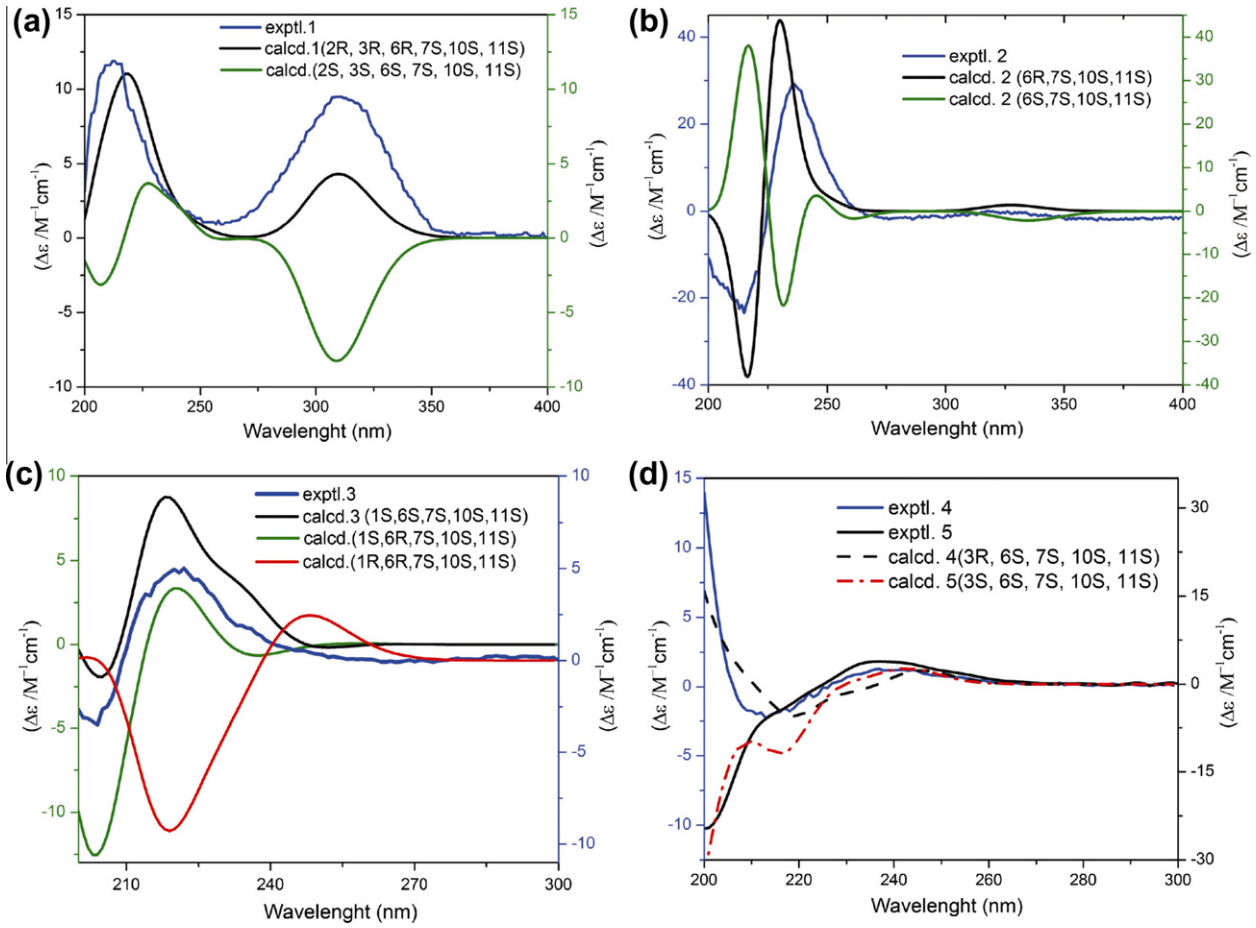

Fig. 5. Comparison of experimental spectra with those calculated for relevant stereoisomers of 1–**5**. The calculations were performed with TDDFT at the B3LYP/6-31G** level with MeOH as the solvent.

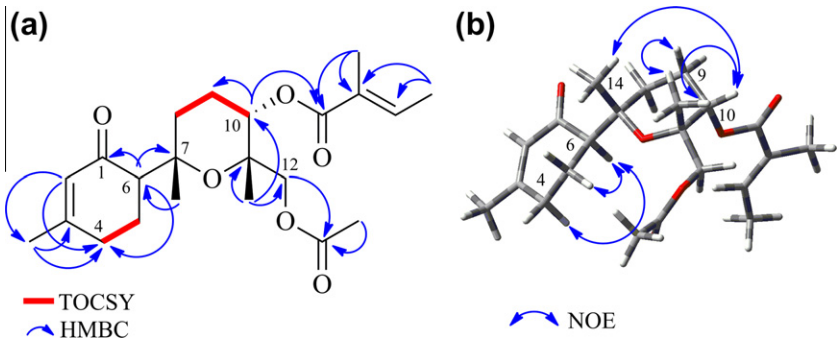

Fig. 6. (a)1D-TOCSY and key HMBC correlations; (b) key NOE correlations of the DFT-optimized structure of the most stable conformer of **2** (6*R*,7*S*,10*S*,11*S* stereoisomer).

olefinic group of ring A, while the positive CE around 236 nm resulted from the $\pi \rightarrow \pi^*$ transition of the ester moiety in ring B. The ECD spectra for three stereoisomers (1*S*,6*S*,7*S*,10*S*,11*S*, 1*S*,6R,7S,10S,11S, and 1*R*,6*R*,7*S*,10*S*,11*S*) were calculated with TDDFT at the B3LYP/6-31G** level and MeOH as solvent. The simulated ECD spectrum of the 1*S*,6*S*,7*S*,10*S*,11*S* stereoisomer showed a negative CE at 205 nm and two positive CEs at 220 and 230 (shoulder) and, thus, was in excellent agreement with the experimental data. The ECD spectrum of the 1*R*,6*R* stereoisomer was distinctly different, with a negative CE at 220 nm and a positive CE around 250 nm. The 1*S*,6*R* stereoisomer exhibited a negative CE around 205 and a positive CE at 220. In addition, conformational analysis of the 1*S*,6*R*,7*S*,10*S*,11*S* configuration revealed that H-1 would be in an equatorial orientation in the stable conformers. This, in turn, would result in dihedral angles and coupling constants ($\phi_{H1,C1,C2,H2}$) of 40°, $^3J_{H1-H2}$ 8 Hz) differing from those observed in NMR data of compound **3**. On the basis of these observations we concluded that the absolute configuration of **3** was 1*S*,6*S*,7*S*,10*S*,11*S*.

Compounds **4** and **5** had the same molecular formula $C_{22}H_{32}O_6$ (based on HRESIMS data) and very similar NMR spectroscopic data (Tables 1 and 2). Ring B in **4** and **5** was identical with compounds **1**–**3**. In compound **4**, a double bond was located between C-1 (δ 130.8) and C-2 (δ 135.1) of ring A, and C-3 (δ 66.6) was substituted by a hydroxyl and a methyl moiety (δ 1.25). Vicinal coupling constants of H-1/H-6 (<2.0 Hz) and H-5α/H-6 (11.0 Hz) were

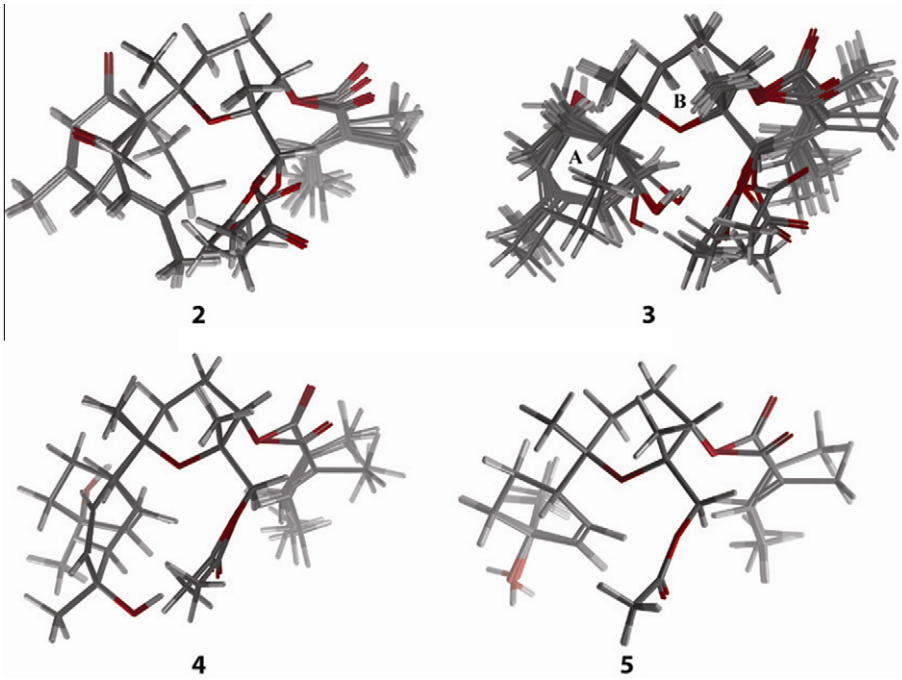

Fig. 7. Superimposed lowest energy conformers (within 1 kcal/mol range from the global minimum) of **2**–**5**. Conformers obtained from the conformational search were re-calculated using DFT at the B3LYP/6-31G** level in the gas phase. Compound **2** (6*R*,7*S*,10*S*,11*S*) showed two core conformers which differed in the orientation of ring A, **3** (1*S*,6*S*,7*S*,10*S*,11*S*) showed six conformers, and epimers **4** (3*R*,6*S*,7*S*,10*S*,11*S*) and **5** (3*S*,6*S*,7*S*,10*S*,11*S*) showed five and five conformers, respectively.

indicative of dihedral angles of 70–80° and 140–150° and, hence, of a pseudo-axial orientation of H-6. H-4β/H-5α showed a vicinal coupling constant of 13 Hz and thus were in a *trans*-diaxial relationship. In a 1D NOE difference experiment, presaturation of H-6 resulted in enhancement of H-4β and H-5β, while irradiation of Me-15 enhanced H-4α and H-4β (Fig. 8). Hence, Me-15 was in a pseudo-equatorial orientation, and ring A adopted a pseudo-chair conformation with two probable configurations (3*R*,6*S* or 3*S*,6*R*). In compound **5**, the splitting pattern of the protons on ring A indicated a pseudo-chair conformation with H-4β and H-5α in axial, and H-6 in pseudo-axial orientation as in **4** (Table 1). Small differences in ^{1}H NMR shifts were observed for ring A, in particular for H-4α (δ 1.81 in **4**, δ 1.56 in **5**), H-4β (δ 1.39 in **4**, δ 1.77 in **5**) and H-5α (δ 1.47 in **4**, δ 1.17 in **5**). ^{13}C NMR chemical shifts of C-1, 2, 3, 4, 5, and Me-15 in **4** and **5** were comparable (Table 2). **A** diagnostic difference was detected by NOE difference experiments. In **5**, presaturation of Me-15 led to an enhancement of H-4α but not H-4β (Fig. 8). Thus, Me-15 had to be in a pseudo-axial position. Ring A of **5** adopted a pseudo-chair conformation, with two possible configurations (3*R*,6*R* or 3*S*,6*S*). Hence, **4** and **5** were epimers.

The experimental ECD spectra of **4** showed positive CEs at 202 and 243 nm, and a negative CE at 210 nm, while **5** showed negative CEs at 202 and 210 nm, and a positive CE at 243 nm. Calculated ECD spectra for the 3*R*,6*S*,6*R*,7*S*,10*S*,11*S* and 3*S*,6*S*,7*S*,10*S*,11*S* stereoisomers showed excellent fit with the experimental data of **4** and **5**, respectively (Fig. 5), whereas the calculated ECD spectrum of the 3*R*,6*R*,7*S*,10*S*,11*S* and 3*S*,6*R*,7*S*,10*S*,11*S* stereoisomers were distinctly different (data not shown). Consequently, **4** and **5** were confirmed to be 3*R* and 3*S* epimers, respectively.

Antiplasmodial activity of **1**–**5** and cytotoxicity in murine L6 cells were assessed, and selectivity indices (SI) were calculated as an indicator of differential toxicity towards the parasite (Table 3).

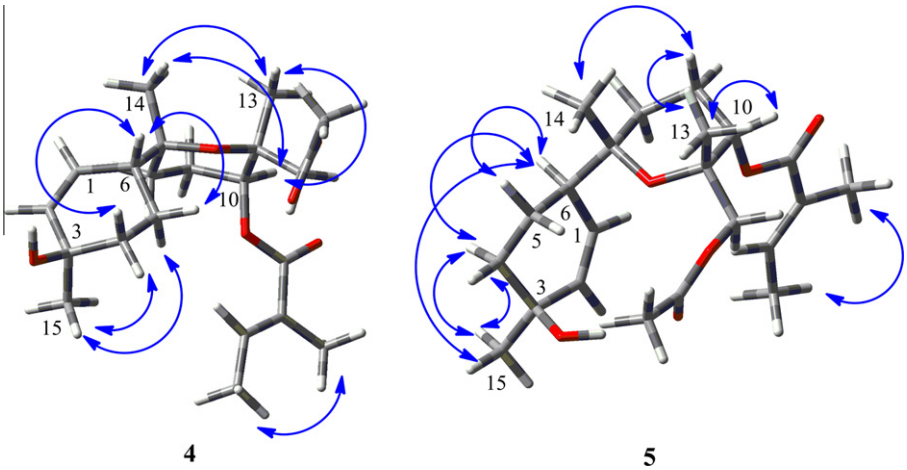

Fig. 8. Key NOE correlations of DFT-optimized of the most stable conformers of **4** (left) and **5** (right).

Table 3
Antiplasmodial and cytotoxic activities (IC_{50} values[a]) of Compounds **1**–**5**.

Compound	*P. falciparum*	L-6 cells	SI
1	2.8 ± 0.4	10.4 ± 1.0	3.7
2	14.9 ± 1.7	90.9 ± 8.5	6.1
3	20.1 ± 0.7	88.4 ± 7.4	4.4
4	19.1 ± 2.2	>227.3	11.9
5	NA[b]	–	–
Artesunate	0.002		
Podophyllotoxin		0.021	

[a] Values are expressed in μM. Each value corresponds to the mean ± standard error of the mean from at least three independent bioassays.
[b] Not active at >20 μM, SI = Selectivity index (IC_{50} in L6 cells (cytotoxicity) divided by IC_{50} against *P. falciparum*).

Epoxide **1** was the most active compound, but showed only very moderate selectivity (IC_{50} 2.8 μM; SI 3.7). Compounds **2**, **3**, and **4** showed moderate inhibition, with IC_{50} values ranging from 14.9 to 20.1 μM, and SI values between 6 and 12. Compound **5** was not active at the concentrations tested.

3. Conclusions

Bisabololoxides are a rather rare type of sesquiterpenoids. Their occurrence appears limited to some sections of the family Asteraceae. Bisaboloxide A is one of the main constituents in the essential oil of German chamomile (*Matricaria recutita*) (Ogata et al., 2010; Salamon et al., 2010). In the genus *Artemisia*, derivatives of bisabololoxide A have only been reported from *Artemisia abrotanum* and *Artemisia lucentica* (*Artemisia hispanica*). (Cubukcu et al., 1990), (Marco et al., 1997; Mericli et al., 1988; Sanz et al., 1989). However, these compounds were monoesters bearing an acetyl group at C-10. Compounds **1**–**5** bear an additional ester moiety at C-12 and, hence, an additional stereocenter in ring A. Relative stereochemistry and absolute configuration of simple bisaboloids have been established in part, and this was achieved either by synthesis from known compounds and comparison of optical rotation values, or with the aid of NMR shifts reagents (Delay and Ohloff, 1979; Flaskamp et al., 1981a,b).

We here performed the first ECD analysis of bisaboloids. We confirmed that the absolute configurations at C-7 and C-10 in **1**–**5** were identical with those of bisabolol oxide (Franke and Schilcher, 2005). Most important though, we demonstrated that the absolute configuration could be established with the aid of ECD calculation in cases where relative stereochemical correlation of two portions of a molecule was not known. In the case of compounds **1**–**5**, calculated lowest energy conformers of the possible stereoisomers were sufficiently different to result in distinctly different ECD spectra after Boltzmann weighting. Comparison of ECD curves obtained for individual conformers of a compound showed that even subtle conformational differences may lead to substantial changes of the chiroptical properties (see Supporting information). Consequently, the quality of predicted ECD data critically depends on a careful conformational analysis. There are extremely few cases where calculation of ECD spectra established the absolute configuration of molecules with unknown relative stereochemical correlation of flexibly linked molecular portions. To our knowledge, this approach was successfully used for the simple sesquiterpenoid cycloabisequine A (Yang et al., 2009), whereas in microdiplodiasone some degree of uncertainty remained about the absolute configuration of one of the stereocenters (Siddiqui et al., 2011). It was not successful in cases such as the aflaquinolones where the ECD-relevant stereocenters in the two molecular portions were too remote from each other to produce distinguishable ECD spectra of stereoisomers (Neff et al., 2012). Given that numerous natural products possess flexibly linked moieties with stereocenters, the ECD approach described here for this series of bisaboloxides may be more widely applicable in natural products chemistry.

4. Experimental section

4.1. General experimental procedures

Optical rotations were measured using a JASCO P-2000 automatic digital polarimeter. NMR spectra were recorded at target temperature 18 °C on a Bruker Avance III 500 MHz spectrometer operating at 500.13 MHz for ^{1}H, and 125.77 MHz for ^{13}C. A 1 mm TXI-microprobe with a z-gradient was used for 1H-detected experiments; ^{13}C NMR spectra were recorded with a 5 mm BBO-probe head with z-gradient. Spectra were analyzed using Bruker TopSpin 2.1 software. HRESIMS spectra in positive and negative ion modes were recorded on a Bruker microTOF ESI-MS system with a scan range of *m*/*z* 200–1500. ECD spectra were recorded in MeOH (400 μg/ml) on an AVIV CD spectrometer model 62ADS and analyzed with the AVIV 60DS V4.1 software. HPLC separations were performed on an Agilent 1100 series HPLC system consisting of a quaternary low-pressure mixing pump with degasser module, column oven, PDA detector, and an autosampler. For medium-pressure liquid chromatography (MPLC) a Buchi Sepacore system consisting of a control unit C-620, a fraction collector C-660, and two pump modules C-605 was used. The MPLC unit was controlled with the Sepacore Control software (version 1.0.3000.1). Waters SunFire C18 (3.5 μm, 3.0 × 150 mm) and SunFire® Prep C18 (5 μm, 10 × 150 mm) columns were used for analytical HPLC and semipreparative RP-HPLC, respectively. HPLC solvents contained 0.1% HCO_2H for analytical separations. NP-Column chromatography was carried out on silica gel (70–230 and 230–400 mesh; Merck). Pre-coated silica gel 60 F_{254} plates (Merck) were used for TLC. Detection was at 254 and 366 nm (CAMAG), or by spraying with anisaldehyde sulfuric acid reagent and subsequent heating (120 °C for 5 min). C_6D_6 (100 Atom% D) and pyridine-d_5 (100 Atom%) for NMR was purchased from Armar Chemicals. Solvents used for extraction, open column chromatography, and MPLC were of technical grade and purified by distillation.

4.2. Plant material

The aerial parts of *Artemisia persica* Boiss. (110 g) were collected from Botanical Garden of Ferdowsi University of Mashhad, Iran. The plant material was identified by Mr. M. R. Joharchi, Research Center for Plant Sciences Ferdowsi University of Mashhad, Mashhad, Iran. A voucher specimen (44518) has been deposited at the Herbarium of the Research Center for Plant Sciences Ferdowsi University of Mashhad.

4.3. Microfractionation for activity profiling

Aliquots of 350 μg of EtOAc extract (35 μl of 10 mg/ml soln. in DMSO) were separated on a SunFire® C18 column (5 μm, 10 × 150 mm; Waters) with 0.1% formic acid in water (solvent A) and acetonitrile (solvent B) using the following gradient: 10% B to 100% B in 30 minutes, hold for 10 min. The flow rate was 0.4 ml/min. Thirty-two one-minute fractions were collected in 96-well deep well plates. The plates were dried in a GeneVac EZ-2 Plus evaporator and submitted to bioassay.

4.4. Extraction and isolation procedures

The grounded plant material (100 g) was successively percolated with *n*-hexane, EtOAc and MeOH. The EtOAc extract (2.3 g)

was separated by NP-MPLC on silica gel (24 × 5 cm *i.d.*, 230–400 mesh) using a linear gradient *n*-hexane-EtOAc 100:0 → 0:100 in 6 h, followed by EtOAc–MeOH 100:0 → 0:100) in 5 h. Flow rate was 5 ml/min. Eleven fractions (F_1–F_{11}) were combined on the basis of TLC patterns. Fractions were also monitored by HPLC-PDA-ESIMS analysis and compared with the activity and LC-MS profiles in order to localize the bioactive compounds. They were found in F_5 and F_7. F_5 (32.0 mg) was subjected to semi-preparative RP-HPLC using gradient of H_2O–MeCN (80:20 to 0:100%) as mobile phase. Flow rate was 4 ml/min, and detection at 254 and 210 nm). Compounds **1** (t_R = 25, 2.0 mg) and **2** (t_R = 26, 1.5 mg) were obtained. The single peak (t_R = 45) in the active time window of F_7 (65.0 mg) was obtained by semi-preparative RP-HPLC (H_2O–MeOH, 70:30 to 0:100%, flow rate 4 ml/min, detection at 254 and 210 nm) as subfraction F_{7-1} (15 mg). F_{7-1} was separated on a silica gel column (20 × 1 cm, 0.040 × 0.063 μm) with *n*-hexane-EtOAc (7:3) into compounds **3** (7.4 mg), **4** (1.8 mg) and **5** (1.0 mg).

4.5. Conformational analysis, geometrical optimization, and ECD calculation

Conformational analysis of compounds **1**–**5** was performed with Schrödinger MacroModel 9.1 software (Schrödinger, LLC, New York) using the OPLS 2005 (Optimized Potential for Liquid Simulations) force field in H_2O. Conformers occurring within 1 kcal/mol energy window from the particular global minimum, were chosen for the gas-phase geometrical optimization and energy calculation using the density function theory (DFT) with the B3LYP functional and the 6-31G** basis-set as implemented in the gas-phase with the Gaussian 03 program package (Frisch et al., 2004). Vibrational analysis was formed at the same level to confirm stability of minima. Time dependent density function theory TD-DFT/B3LYP/6-31G** in the gas phase and in MeOH using the "self-consistent reaction field" method (SCRF) with the conductor-like polarizable calculation model (CPCM) was employed to calculate excitation energy (denoted by wavelength in nm) and rotatory strength *R* in dipole velocity (R_{vel}) and dipole length (R_{len}) forms. ECD curves were calculated based on rotatory strengths using half bandwidth of 0.2 eV with conformers of **1**–**5**. The spectra were constructed based on the Boltzmann-weighting according to their population contribution.

4.6. Spectral data

4.6.1. Compound (*1*)

Colorless oil, $[\alpha_D^{24}]$ + 62.5 (*c* 0.8, MeOH); CD (MeOH, c = 1.0 mM, 0.1 cm): $[\theta]_{214}$ = +12555, $[\theta]_{310}$ = +9810; UV (λ_{max} 213 nm); ^{1}H NMR (C_6D_6, 500 MHz) and ^{13}C NMR (C_6D_6,125 MHz) see Tables 2 and 3, respectively; HRESIMS *m*/*z* 431.2039 $[M+Na]^+$, calcd. for $C_{22}H_{32}O_7$, 431.2046.

4.6.2. Compound (*2*)

Colorless oil, $[\alpha_D^{24}]$ + 34.3 (*c* 3.9, MeOH); CD (MeOH, c = 1.0 mM, 0.1 cm): $[\theta]_{213}$ = −19415, $[\theta]_{236}$ = +30820; UV (λ_{max} 213 nm); ^{1}H NMR (C_6D_6, 500 MHz) and ^{13}C NMR (C_6D_6,125 MHz) see Tables 2 and 3, respectively; HRESIMS *m*/*z* 415.2090 $[M+Na]^+$, calcd. for $C_{22}H_{32}O_6$, 415.2097.

4.6.3. Compound (*3*)

Colorless oil, $[\alpha_D^{24}]$ + 25.3 (*c* 10.0, MeOH); CD (MeOH, c = 1.0 mM, 0.1 cm): $[\theta]_{205}$ = −2483, $[\theta]_{221}$ = +5685, $[\theta]_{232}$ = +2222; UV (λ_{max} 213 nm); ^{1}H NMR (C_6D_6, 500 MHz) and ^{13}C NMR (C_6D_6,125 MHz) see Tables 2 and 3, respectively; HRESIMS *m*/*z* 417.2285 $[M+Na]^+$, calcd. for $C_{22}H_{34}O_6$, 417.2253.

4.6.4. Compound (*4*)

Colorless oil, $[\alpha_D^{24}]$ − 9.0 (*c* 5.6, MeOH); CD (MeOH, c = 1.0 mM, 0.1 cm): $[\theta]_{202}$ = +4764, $[\theta]_{210}$ = −8743, $[\theta]_{243}$ = + 911; UV (λ_{max} 213 nm); ^{1}H NMR (C_6D_6, 500 MHz) and ^{13}C NMR (C_6D_6,125 MHz) see Tables 2 and 3, respectively; HRESIMS *m*/*z* 417.2281 $[M+Na]^+$, calcd. for $C_{22}H_{34}O_6$, 417.2253.

4.6.5. Compound (*5*)

Colorless oil, $[\alpha_D^{24}]$ − 29.7 (*c* 3.7, MeOH); CD (MeOH, c = 1.0 mM, 0.1 cm): $[\theta]_{202}$ = −13575, $[\theta]_{210}$ = −5101, $[\theta]_{243}$ = + 1517; UV (λ_{max} 213 nm); ^{1}H NMR (C_6D_6, 500 MHz) and ^{13}C NMR (C_6D_6,125 MHz) see Tables 2 and 3, respectively; HRESIMS *m*/*z* 417.2277 $[M+Na]^+$, calcd. for $C_{22}H_{34}O_6$, 417.2253.

4.7. Biological assays

4.7.1. Antiplasmodial assay

Antiplasmodial activity of extracts and pure compounds were determined against *P. falciparum* strain K1 (resistant to chloroquine and pyrimethamine), using a modified [3H]-hypoxanthine incorporation assay as previously described. Artesunate served as a positive control. Assays were run in three independent experiments in duplicates. IC_{50} values were calculated from sigmoidal growth inhibition curves (Adams et al., 2009).

4.7.2. Cytotoxicity assay

Cytotoxicity was determined using rat skeletal myoblast L6 cells. Pure substances were tested as previously described, and podophyllotoxin was used as a positive control. Tests were run in three independent experiments in duplicates. IC_{50} values were calculated from sigmoidal growth inhibition curves (Adams et al., 2009).

Acknowledgements

F. M. A. is grateful for a research fellowship from Ministry of Health and Medical Education of Iran. S. N. E. thanks the Ministry of Science, Research, and Technology of Iran (MSRT) for a Ph.D. fellowship (No. 24/87100055). Support from the Swiss National Science Foundation through Grant 205320_126888/1 (to M.H.) is gratefully acknowledged. We thank Ms. T. Schulthess for technical assistance with measurement of UV and CD spectra.

Appendix A. Supplementary data

Supplementary data associated with this article can be found, in the online version, at http://dx.doi.org/10.1016/j.phytochem.2012.08.017.

References

Adams, M., Christen, M., Plitzko, I., Zimmermann, S., Brun, R., Kaiser, M., Hamburger, M., 2010. Antiplasmodial lanostanes from the *Ganoderma lucidum* mushroom. J. Nat. Prod. 73, 897–900.

Adams, M., Gschwind, S., Zimmermann, S., Kaiser, M., Hamburger, M., 2011. Renaissance remedies: antiplasmodial protostane triterpenoids from *Alisma plantago-aquatica* L. (Alismataceae). J. Ethnopharmacol. 135, 43–47.

Adams, M., Zimmermann, S., Kaiser, M., Brun, R., Hamburger, M., 2009. Protocol for HPLC-based activity profiling for natural products with activities against tropical parasites. Nat. Prod. Commun. 4, 1377–1381.

Biruni, M., 2004. Kitab al-saydana. Iranian Academy of Persian Language and Literature, Tehran.

Cubukcu, B., Bray, D.H., Warhurst, D.C., Mericli, A.H., Ozhatay, N., Sariyar, G., 1990. In vitro antimalarial activity of crude extracts and compounds from *Artemisia abrotanum* L. Phytother. Res. 4, 203–204.

Delay, F., Ohloff, G., 1979. Syntheses and absolute-configuration of (E)-alpha-bisabolenes and (Z)-alpha-bisabolenes. Helv. Chim. Acta 62, 369–377.

Farimani, M.M., Bahadori, M.B., Taheri, S., Ebrahimi, S.N., Zimmermann, S., Brun, R., Amin, G., Hamburger, M., 2011. Triterpenoids with rare carbon skeletons from

Salvia hydrangea: antiprotozoal activity and absolute configurations. J. Nat. Prod. 74, 2200–2205.
Farimani, M.M., Taheri, S., Ebrahimi, S.N., Bahadori, M.B., Khavasi, H.R., Zimmermann, S., Brun, R., Hamburger, M., 2012. Hydrangenone, a new isoprenoid with an unprecedented skeleton from *Salvia hydrangea*. Org. Lett. 14, 166–169.
Flaskamp, E., Nonnenmacher, G., Isaac, O., 1981a. On the diastereoisomerism of natural and synthetic alpha-bisabolols. Z. Naturforsch. B 36, 114–118.
Flaskamp, E., Nonnenmacher, G., Zimmermann, G., Isaac, O., 1981b. On the stereochemistry of the bisaboloids from *Matricaria chamomilla* L. Z. Naturforsch. B 36, 1023–1030.
Franke, R., Schilcher, H., 2005. Chamomile: Industrial Profiles. Taylor & Francis, Boca Raton.
Frisch, M.J., Trucks, H.B., Schlegel, H.B., Scuseria, G.E., Robb, M.A., Cheeseman, J.R., Montgomery Jr., J.A., Vreven, T., Kudin, K.N., Burant, J.C., Millam, J.M., Iyengar, S.S., Tomasi, J., Barone, V., Mennucci, B., Cossi, M., Scalmani, G., Rega, N., Petersson, G.A., Nakatsuji, H., Hada, M., Ehara, M., Toyota, K., Fukuda, R., Hasegawa, J., Ishida, M., Nakajima, T., Honda, Y., Kitao, O., Nakai, H., Klene, M., Li, X., Knox, J.E., Hratchian, H.P., Cross, J.B., Bakken, V., Adamo, C., Jaramillo, J., Gomperts, R., Stratmann, R.E., Yazyev, O., Austin, A.J., Cammi, R., Pomelli, C., Ochterski, J.W., Ayala, P.Y., Morokuma, K., Voth, G.A., Salvador, P., Dannenberg, J.J., Zakrzewski, V.G., Dapprich, S., Daniels, A.D., Strain, M.C., Farkas, O., Malick, D.K., Rabuck, A. D., Raghavachari, K., Foresman, J.B., Ortiz, J.V., Cui, Q., Baboul, A.G., Clifford, S., Cioslowski, J., Stefanov, B.B., Liu, G., Liashenko, A., Piskorz, P., Komaromi, I., Martin, R.L., Fox, D.J., Keith, T., Al-Laham, M.A., Peng, C.Y., Nanayakkara, A., Challacombe, M., Gill, P.M.W., Johnson, B., Chen, W., Wong, M.W., Gonzalez, C., Pople, J.A., 2004. Gaussian 03, Revision E.01. Gaussian, Inc., Wallingford CT.
Ghahreman, A., 1978–2005. Flora of Iran. Research Institute of Forests and Rangelands, Tehran.
Hoseyni, M.M., 1997. Tohfe-ye-hakim moemen. Ketabforoushi-e-Mahmoodi, Tehran.
Marco, J.A., SanzCervera, J.F., GarciaLliso, V., Batlle, N., 1997. Sesquiterpene lactones from *Artemisia lucentica*. Phytochemistry 45, 755–763.
Mericli, A.H., Cubukcu, B., Jakupovic, J., Ozhatay, N., 1988. Alpha-bisabololoxide derivatives from *Artemisia abrotanum*. Planta Med., 463–464.
Meshnick, S.R., Taylor, T.E., Kamchonwongpaisan, S., 1996. Artemisinin and the antimalarial endoperoxides: from herbal remedy to targeted chemotherapy. Microbiol. Rev. 60, 301–315.
Mirjalili, M.H., Tabatabaei, S.M.F., Hadian, J., Ebrahimi, S.N., Sonboli, A., 2007. Phenological variation of the essential oil of *Artemisia scoparia* Waldst. et Kit from Iran. J. Essent. Oil Res. 19, 326–329.
Mozaffarian, V., 2007. A Dictionary of Iranian Plant Names. Farhang Moaser, Tehran.
Neff, S.A., Lee, S.U., Asami, Y., Ahn, J.S., Oh, H., Baltrusaitis, J., Gloer, J.B., Wicklow, D.T., 2012. Aflaquinolones A–G: secondary metabolites from marine and fungicolous isolates of *Aspergillus* spp.. J. Nat. Prod. 75, 464–472.
Ogata, I., Kawanai, T., Hashimoto, E., Nishimura, Y., Oyama, Y., Seo, H., 2010. Bisabololoxide A, one of the main constituents in German chamomile extract, induces apoptosis in rat thymocytes. Arch. Toxicol. 84, 45–52.
Ortet, R., Prado, S., Mouray, E., Thomas, O.P., 2008. Sesquiterpene lactones from the endemic cape verdean *Artemisia gorgonum*. Phytochemistry 69, 2961–2965.
Potterat, O., Hamburger, M., 2006. Natural products in drug discovery – concepts and approaches for tracking bioactivity. Curr. Org. Chem. 10, 899–920.
Razi, M.Z., 2006. Al-Havi. Academy of Medical Sciences of Iran, Tehran.
Rustaiyan, A., Masoudi, S., 2011. Chemical constituents and biological activities of Iranian *Artemisia* species. Phytochem. Lett. 4, 440–447.
Salamon, I., Ghanavati, M., Abrahimpour, F., 2010. Potential of medicinal plant production in Iran and variability of chamomile (*Matricaria recutita* L.) essential oil quality. J. Essent. Oil Bearing Plants 13, 638–643.
Sanz, J.F., Barbera, O., Marco, J.A., 1989. Sesquiterpene lactones from *Artemisia hispanica*. Phytochemistry 28, 2163–2167.
Siddiqui, I.N., Zahoor, A., Hussain, H., Ahmed, I., Ahmad, V.U., Padula, D., Draeger, S., Schulz, B., Meier, K., Steinert, M., Kurtan, T., Florke, U., Pescitelli, G., Krohn, K., 2011. Diversonol and blennolide derivatives from the endophytic fungus *Microdiplodia* sp.: absolute configuration of diversonol. J. Nat. Prod. 74, 365–373.
Slusarczyk, S., Zimmermann, S., Kaiser, M., Matkowski, A., Hamburger, M., Adams, M., 2011. Antiplasmodial and antitrypanosomal activity of tanshinone-type diterpenoids from *Salvia miltiorrhiza*. Planta Med. 77, 1594–1596.
Tu, Y.Y., 2011. The discovery of artemisinin (qinghaosu) and gifts from Chinese medicine. Nat. Med. 17, 1217–1220.
Yang, X.W., Ding, Y., Li, X.C., Ferreira, D., Shen, Y.H., Li, S.M., Wang, N., Zhang, W.D., 2009. Cycloabiesesquine A, a unique sesquiterpenoid from *Abies delavayi*. Chem. Commun. (Camb), 3771–3773.
Zimmermann, S., Kaiser, M., Brun, R., Hamburger, M., Adams, M., 2012. Cynaropicrin: the first plant natural product with in vivo activity against *Trypanosoma brucei*. Planta Med. 78, 553–556.

Supporting information

Bisabololoxide derivatives from *Artemisia persica*, and determination of their absolute configurations by ECD

Fahimeh Moradi-Afrapoli [a,1] Samad Nejad Ebrahimi [b,c,1] Martin Smiesko [d], Melanie Raith [b], Stefanie Zimmermann [b,e], Farsad Nadjafi [f], Reto Brun [e], Matthias Hamburger [b,*]

[a] Department of Pharmacognosy, Faculty of Pharmacy, MazandaranUniversity of Medical Sciences, Sari, Iran.

[b] Division of Pharmaceutical Biology, University of Basel, Klingelbergstrasse 50, 4056 Basel, Switzerland.

[c] Department of Phytochemisty, Medicinal Plants and Drugs Research Institute, Shahid Beheshti University, G. C., Evin, Tehran, Iran.

[d] Division of Molecular Modeling, University of Basel, Klingelbergstrasse 50, 4056 Basel, Switzerland.

[e] Department of Medical Parasitology and Infection Biology, Swiss Tropical and Public Health Institute, Basel, Switzerland.

[f] Department of Agriculture, Medicinal Plants and Drugs Research Institute, Shahid Beheshti University, G. C., Evin, Tehran, Iran.

[1] These authors contributed equally to this work

*Corresponding author. Tel.: +41 612671425; fax: +41 612671474.

E-mail address: matthias.hamburger@unibas.ch (M. Hamburger)

Figure S1: ^{1}H-NMR spectrum of compound **1**(500MHz, Benzene-*d6*)

Figure S2: DEPT-Q spectrum of compound **1**(125 MHz, Benzene-*d6*)

Figure S3: ^{1}H-^{1}H COSY spectrum of compound **1**

Figure S4: HSQC-DEPT spectrum of compound **1**

Figure S5: HMBC spectrum of compound **1**

Figure S6: 1D-Selective TOCSY spectra of compound **1**

Figure S7: Expanded 1D-Selective TOCSY spectra of compound **1**

Figure S8: ^{1}H-NMR spectrum of compound **2** (500MHz, Benzene-*d6*)

Figure S9: DEPT-Q spectrum of compound **2** (125 MHz, Benzene-*d6*)

Figure S10: ^{1}H-NMR spectrum of compound **2** (500MHz, Pyridine-*d5*)

Figure S11: ^{1}H-NMR spectrum of compound **3** (500MHz, Benzene-*d6*)

Figure S12: DEPT-Q spectrum of compound **3** (125 MHz, Benzene-*d6*)

Figure S13: ^{1}H-NMR spectrum of compound **4** (500MHz, Benzene-*d6*)

Figure S14: DEPT-Q spectrum of compound **4** (125 MHz, Benzene-*d6*)

Figure S15: ^{1}H-NMR spectrum of compound **5** (500MHz, Benzene-*d6*)

Figure S16: DEPT-Q spectrum of compound **5** (125 MHz, Benzene-*d6*

Figure S17. Minimized conformers of **1** in the gas phase using DFT at the B3LYP/6-31G∗ level: compound **1**, showing five conformers in 1 kcal/mol range from the global minimum

Figure S18: Calculated ECD spectra of the minimized conformers of **1**

Figure S19. Minimized conformers of **2** in the gas phase using DFT at the B3LYP/6-31G∗ level: compound **2**, showing fiveconformers in 1 kcal/mol range from the global minimum

Figure S20: Calculated ECD spectra of the minimized conformers of **2**

Figure S21. Minimized conformers of **3** in the gas phase using DFT at the B3LYP/6-31G∗ level: compound **3**, showing six conformers in 1 kcal/mol range from the global minimum

Figure S22: Calculated ECD spectra of the minimized conformers of **3**

Figure S23. Minimized conformers of **4** in the gas phase using DFT at the B3LYP/6-31G∗ level: compound **3**, showing six conformers in 1 kcal/mol range from the global minimum

Figure S24. Minimized conformers of **5** in the gas phase using DFT at the B3LYP/6-31G∗ level: compound **5**, showing six conformers in 1 kcal/mol range from the global minimum

Figure S25: Calculated ECD spectra of the minimized conformers of **4** and **5**

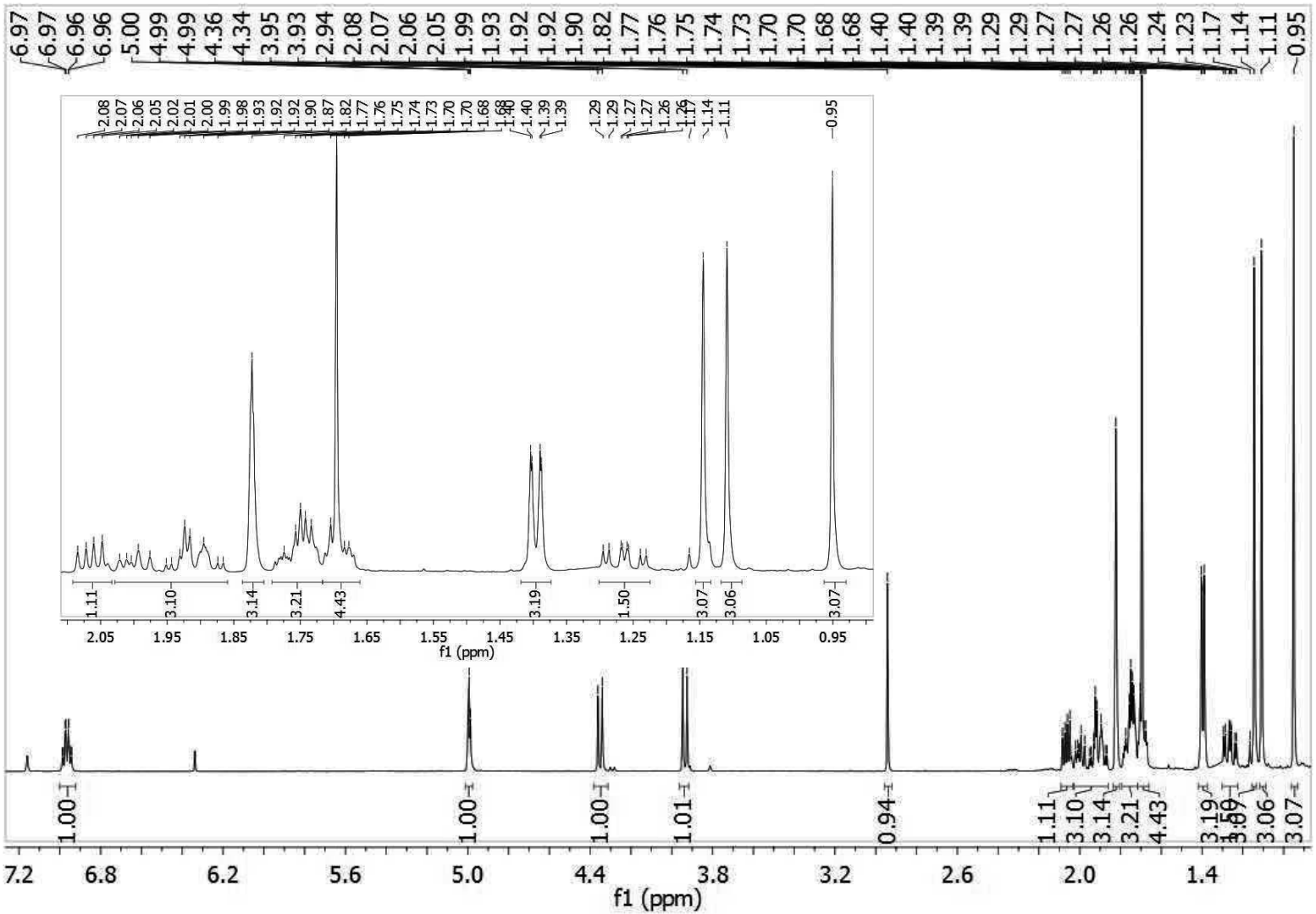

Figure S1: ^{1}H-NMR spectrum of compound **1**(500MHz, Benzene-*d6*)

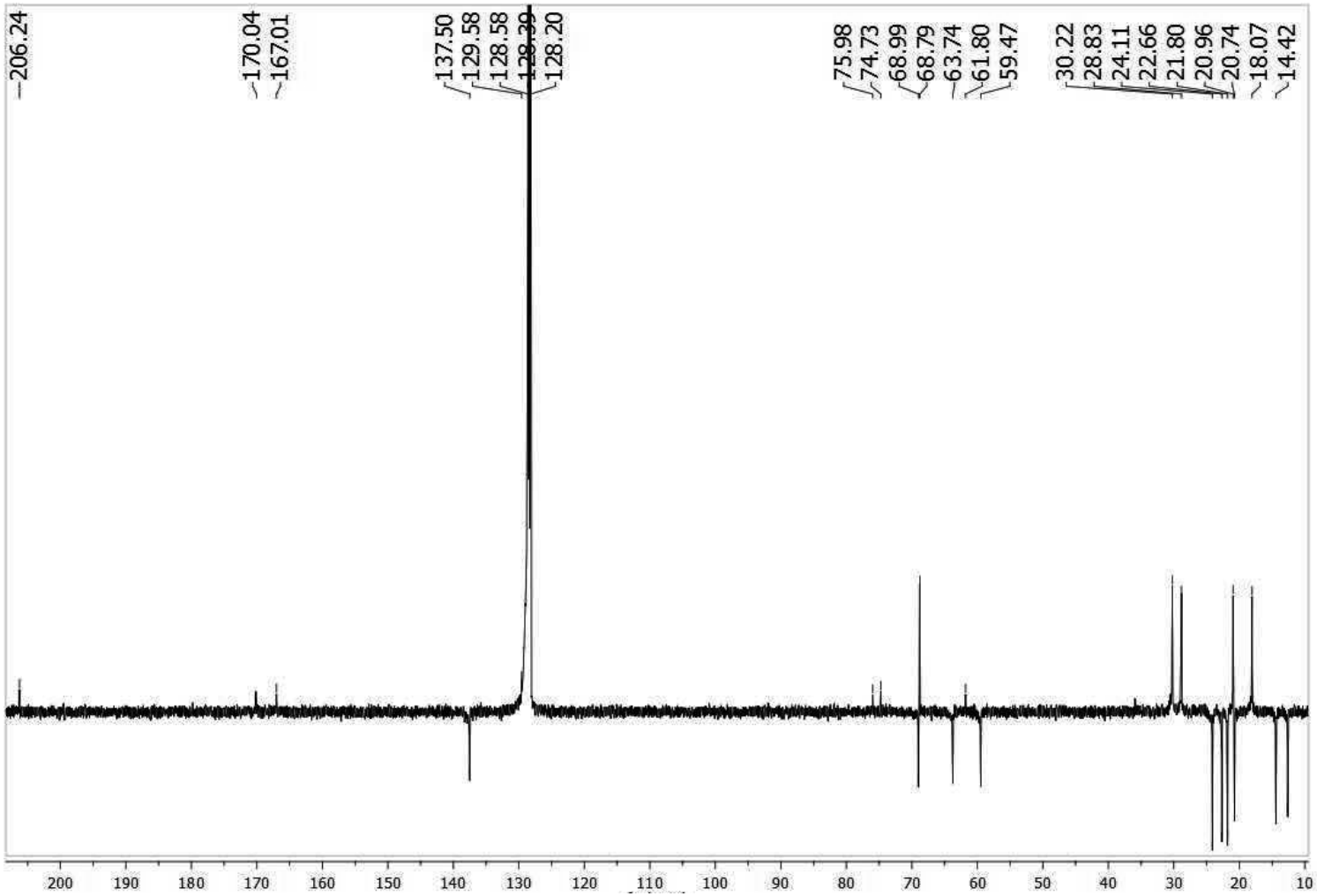

Figure S2: DEPT-Q spectrum of compound **1**(125 MHz, Benzene-*d6*)

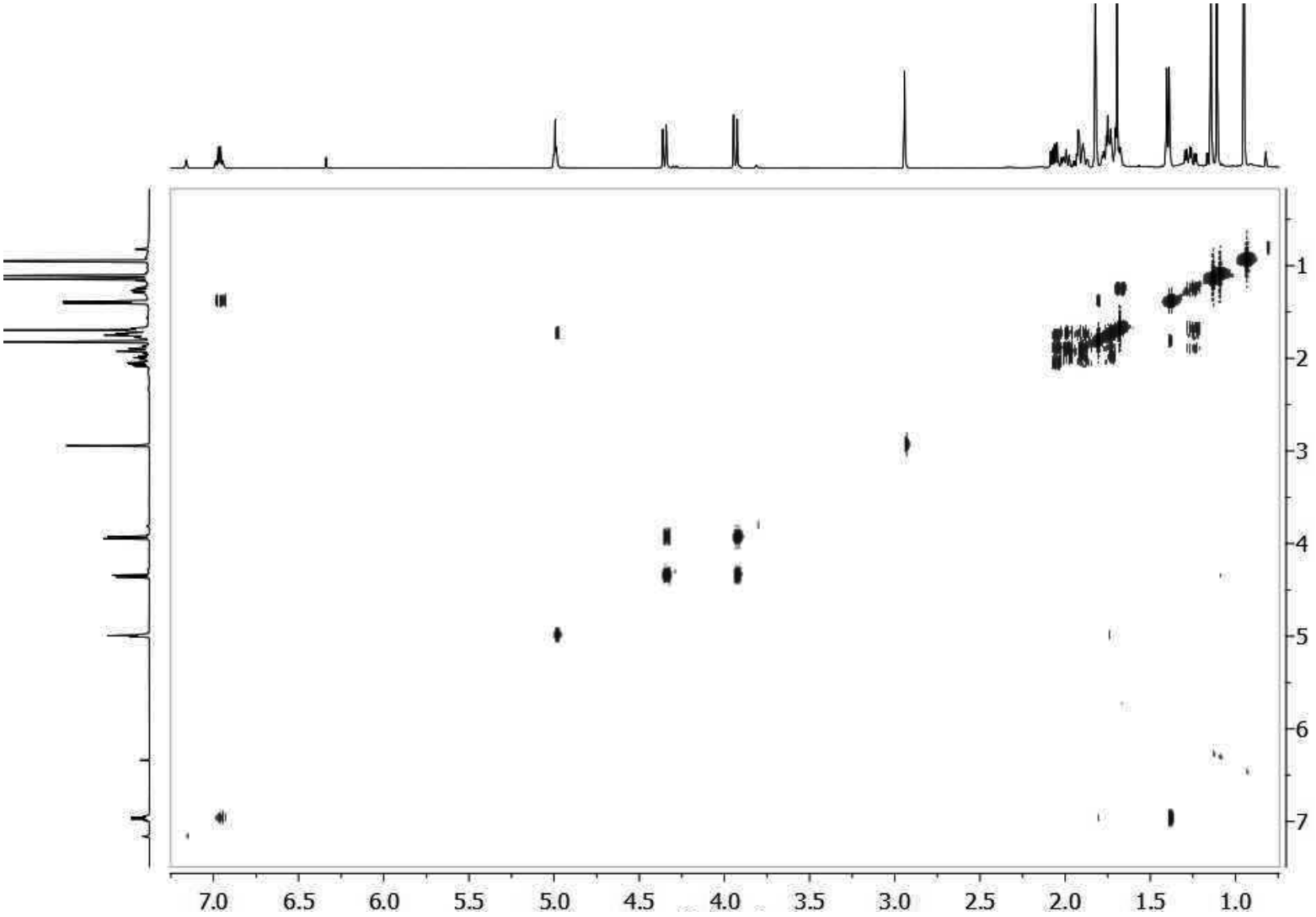

Figure S3: ^{1}H-^{1}H COSY spectrum of compound **1**

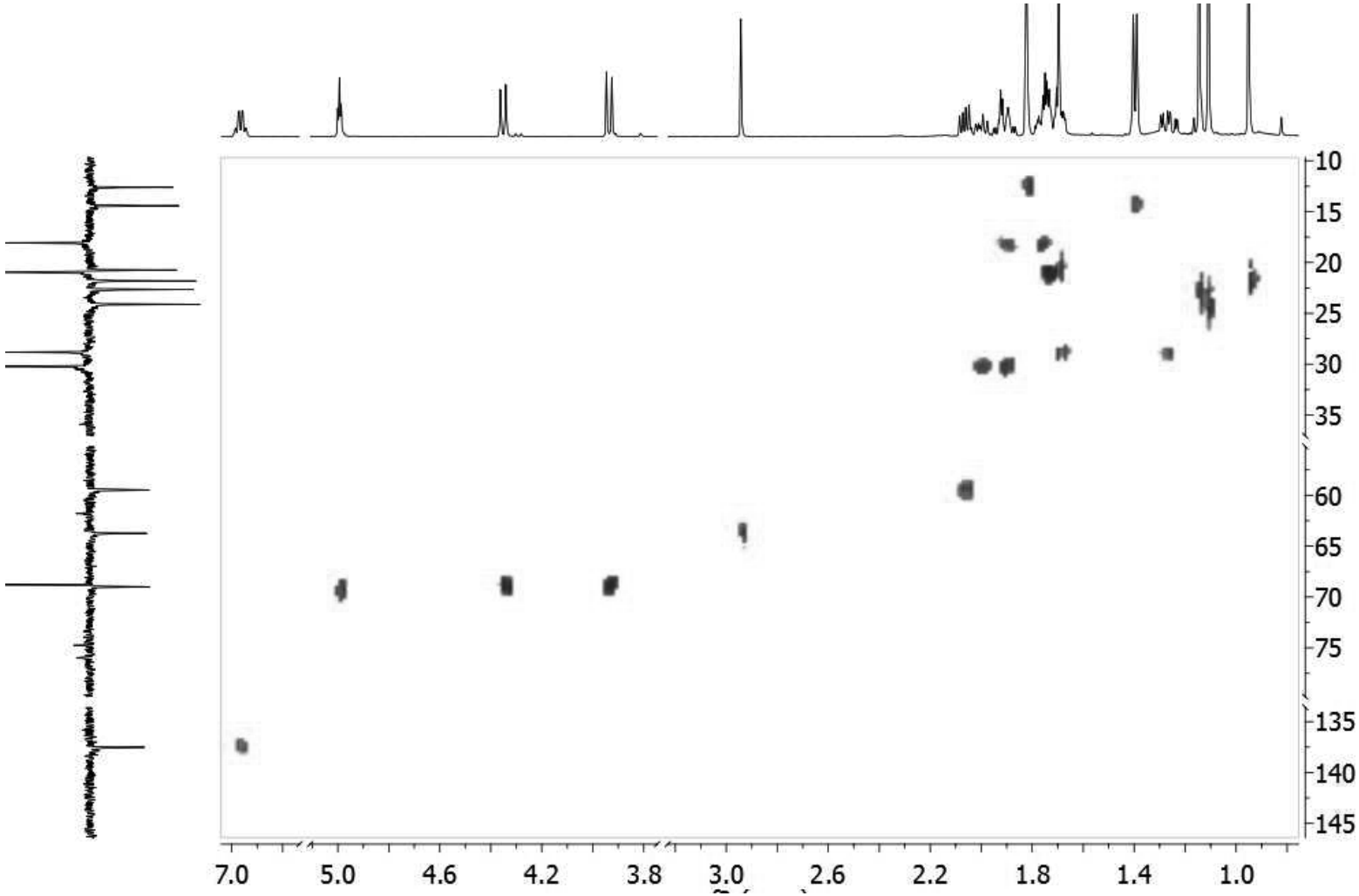

Figure S4: HSQC-DEPT spectrum of compound **1**

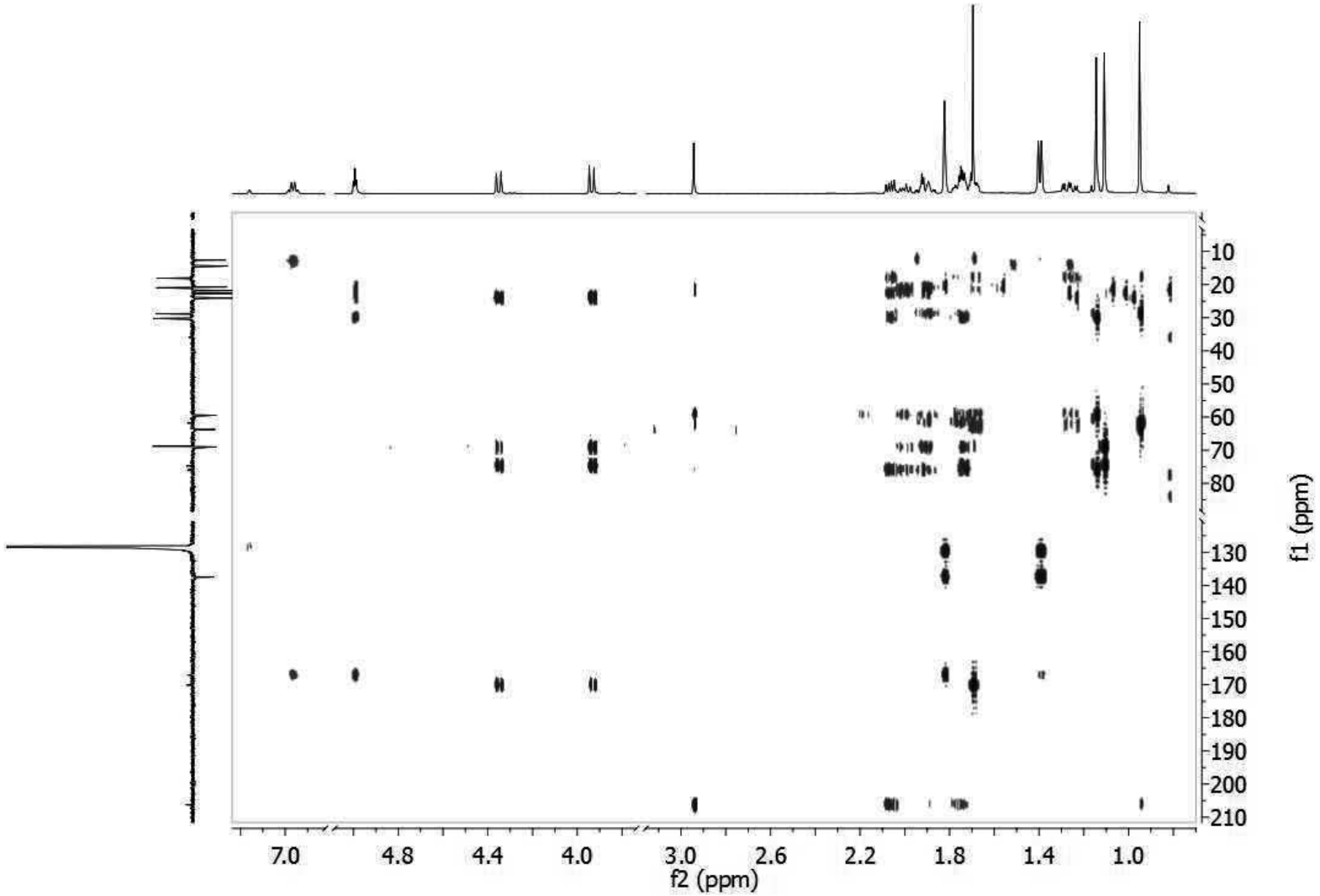

Figure S5: HMBC spectrum of compound **1**

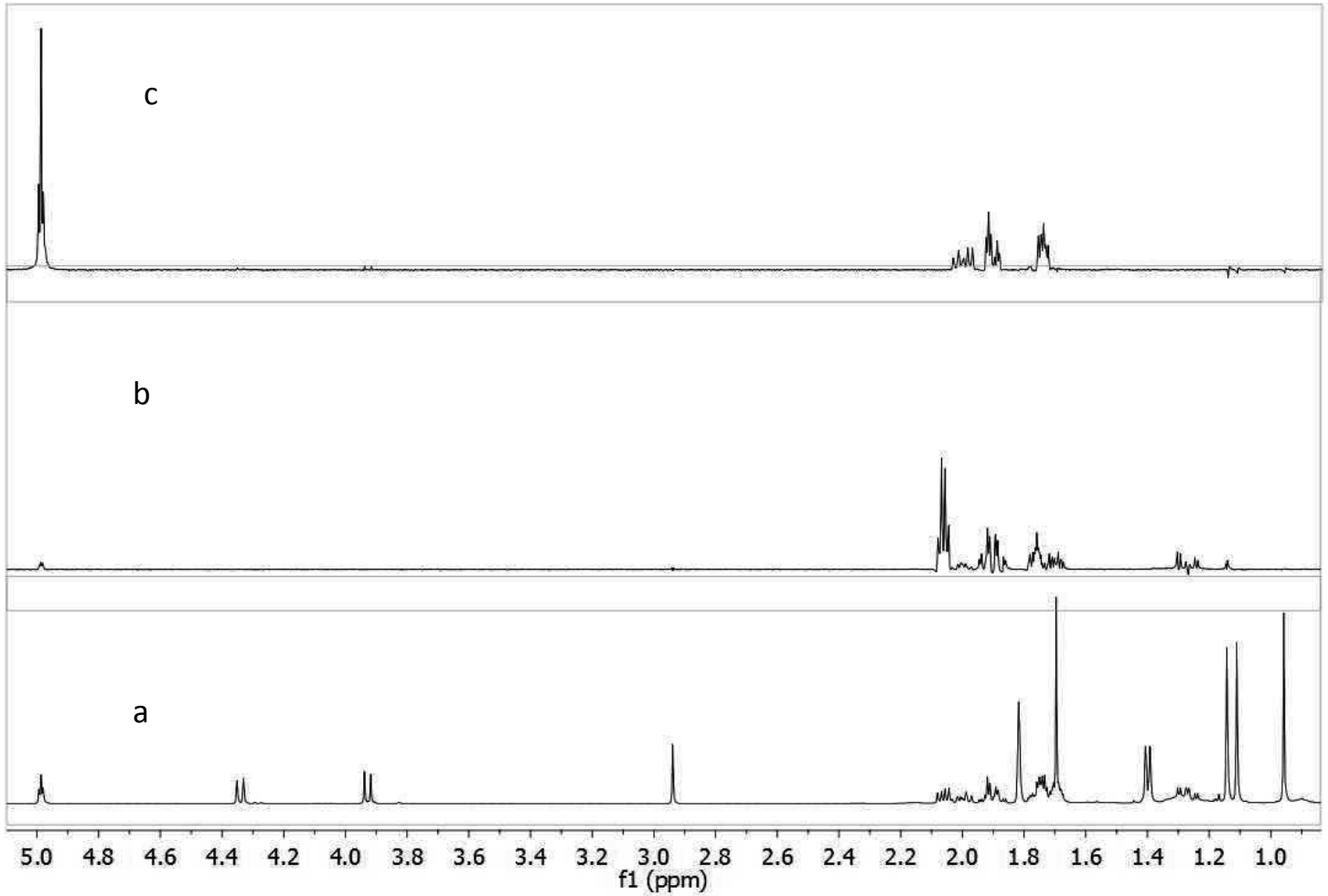

Figure S6: 1D-Selective TOCSY spectra of compound **1**; a) The whole ^{1}H-NMR spectrum, b) Excitation of H-10 resulted in detection of H-9, H-8α, and H-8β (a spin system in ring B), c) Excitation of H-6 led to detection of H-4α, H-4β, H-5α, and H-5β (a spin system in ring A).

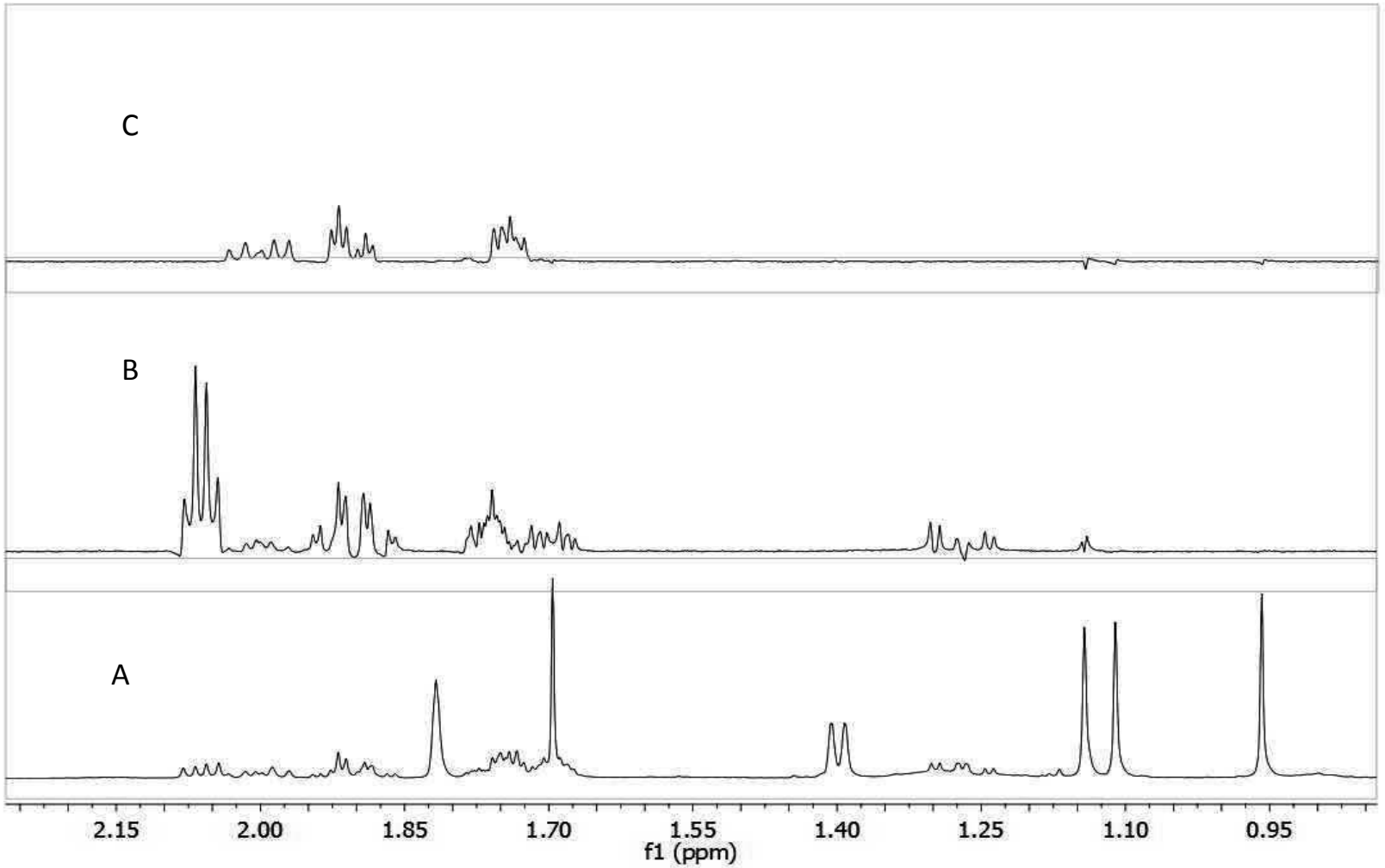

Figure S7: Expanded 1D-Selective TOCSY spectra of compound **1** (0.9-2.15 ppm); a) ^{1}H-NMR spectrum, b) Selective xcitation of H-10, c) Selective xcitation of H-6

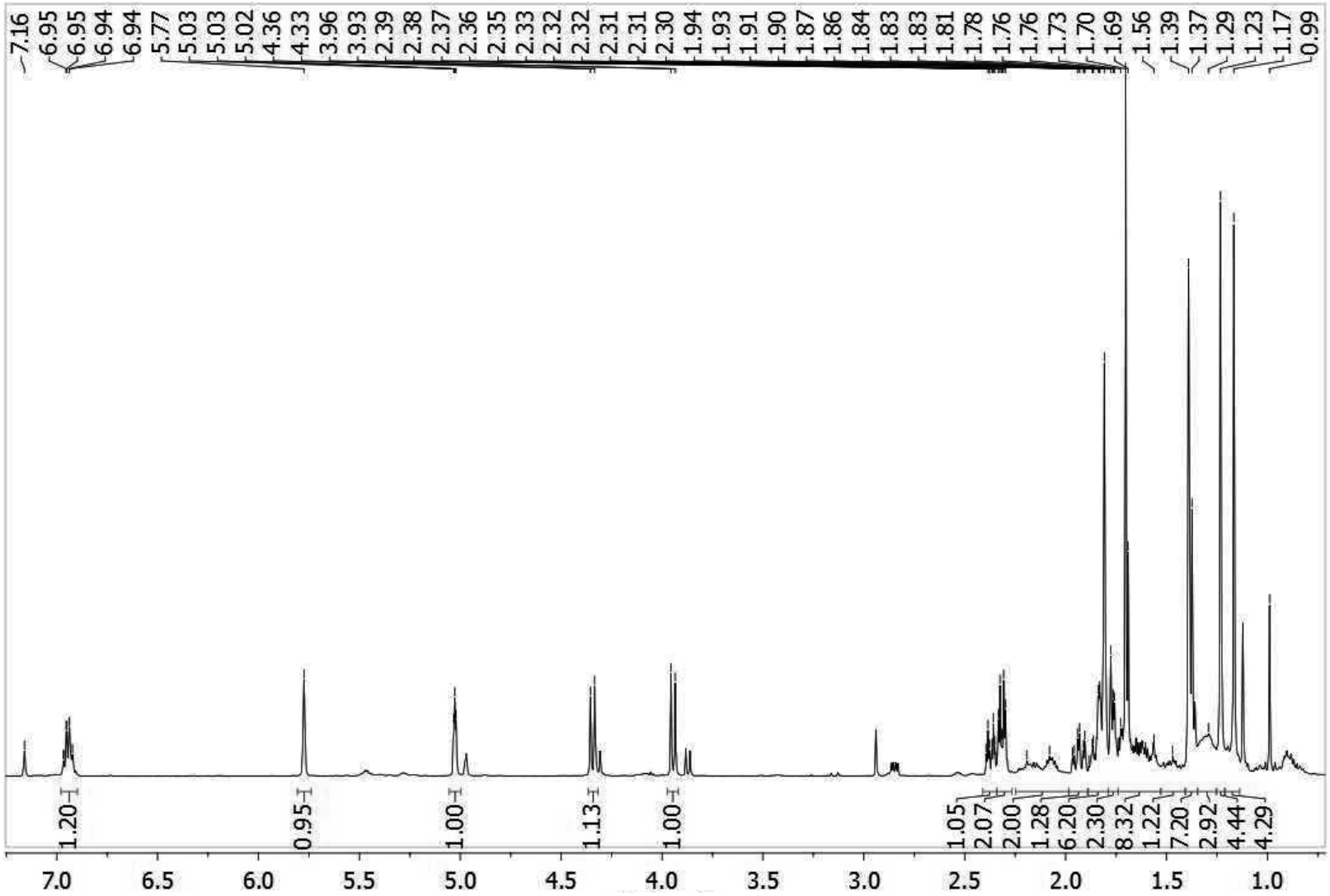

Figure S8: ^{1}H-NMR spectrum of compound **2** (500MHz, Benzene-*d6*)

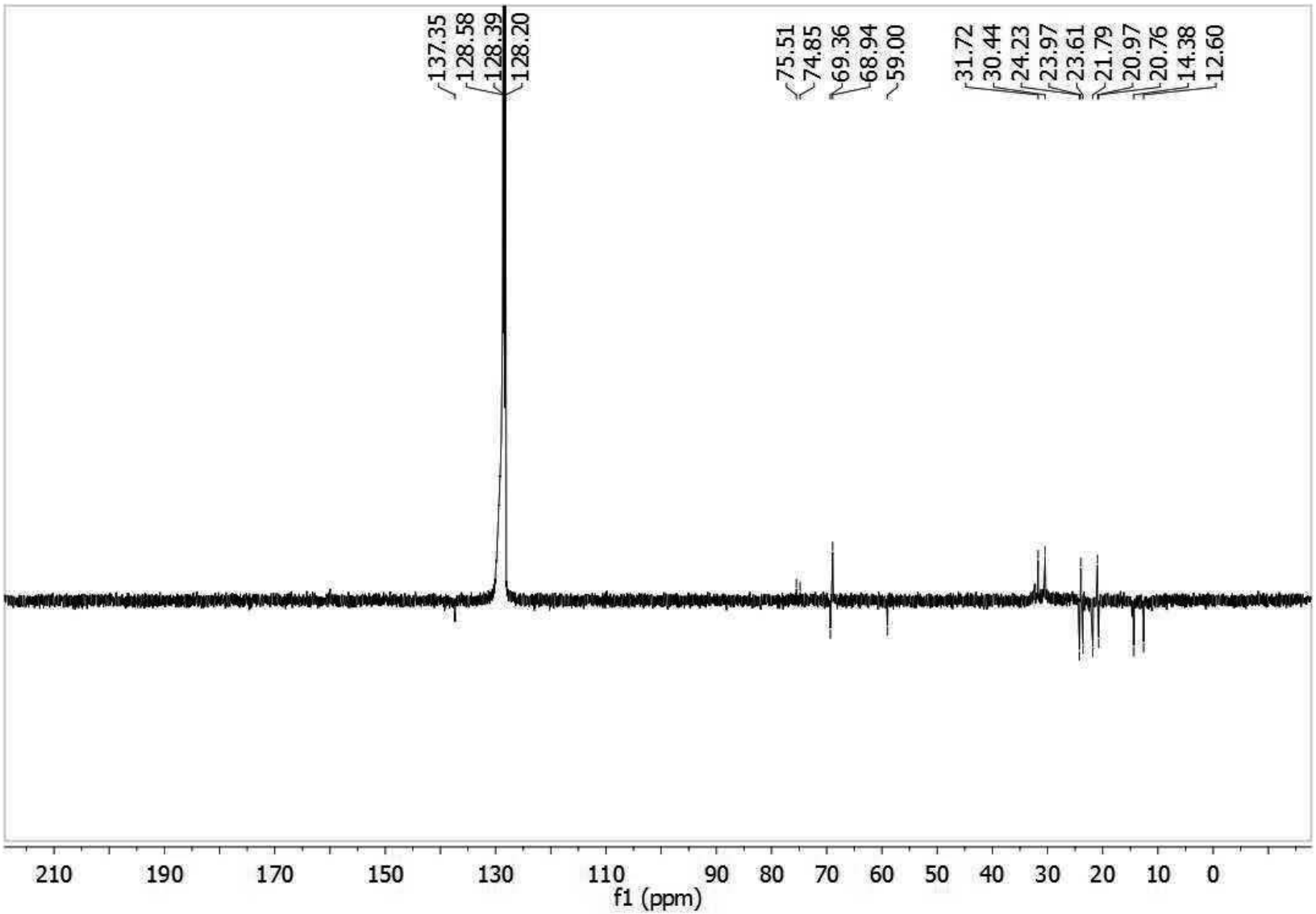

Figure S9: DEPT-Q spectrum of compound **2** (125 MHz, Benzene-*d6*)

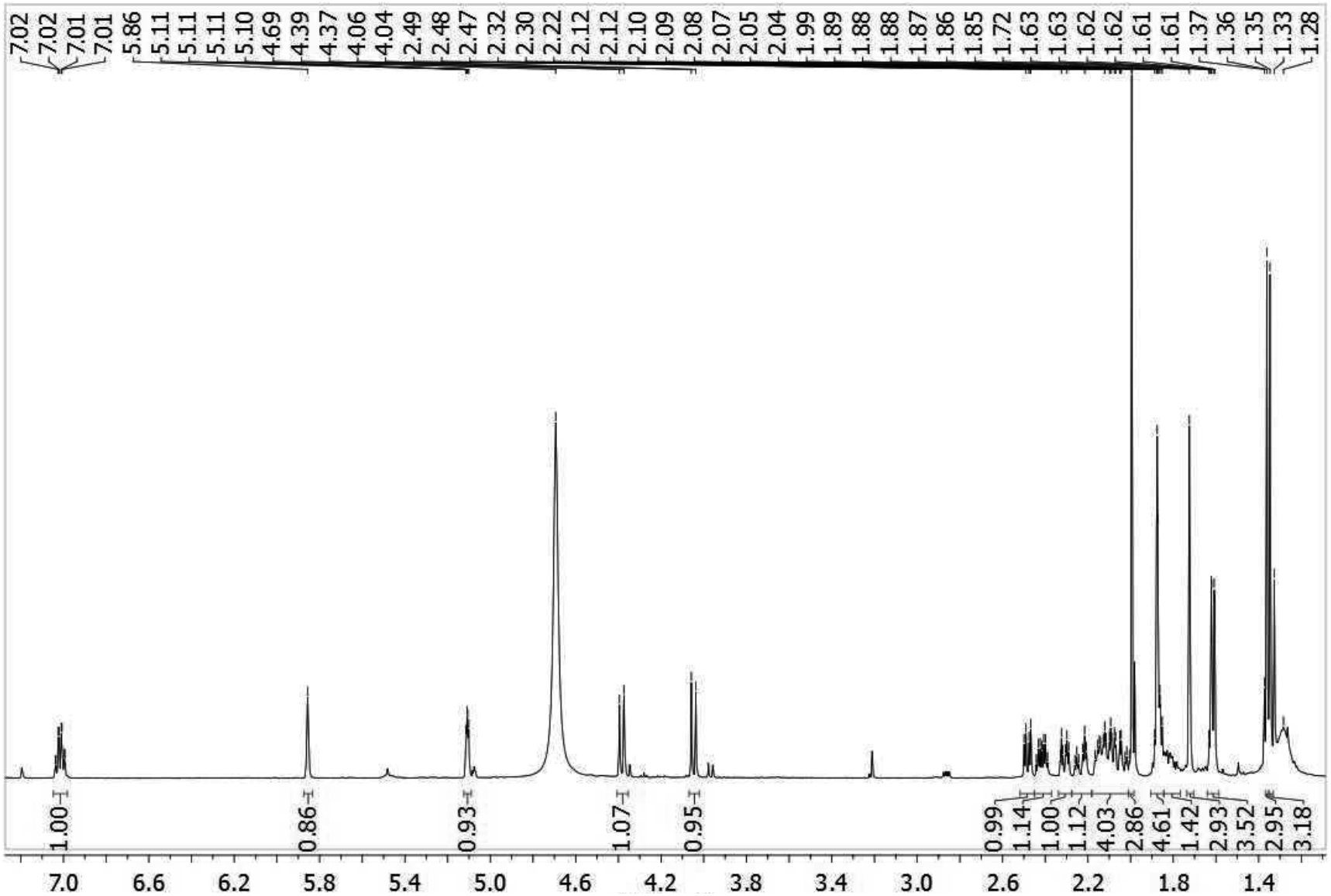

Figure S10: ^{1}H-NMR spectrum of compound **2** (500MHz, Pyridine-*d5*)

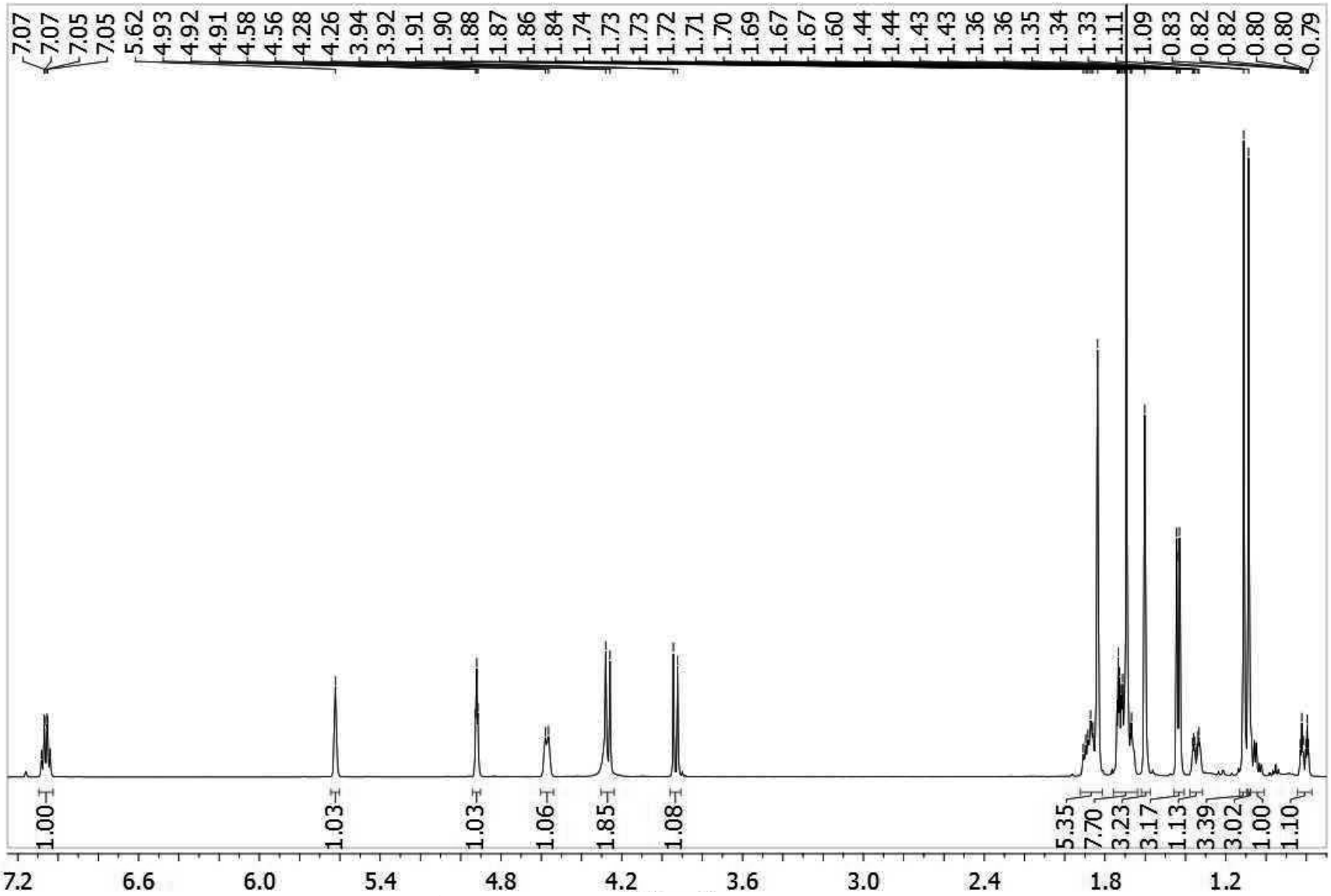

Figure S11: ^{1}H-NMR spectrum of compound **3** (500MHz, Benzene-*d6*)

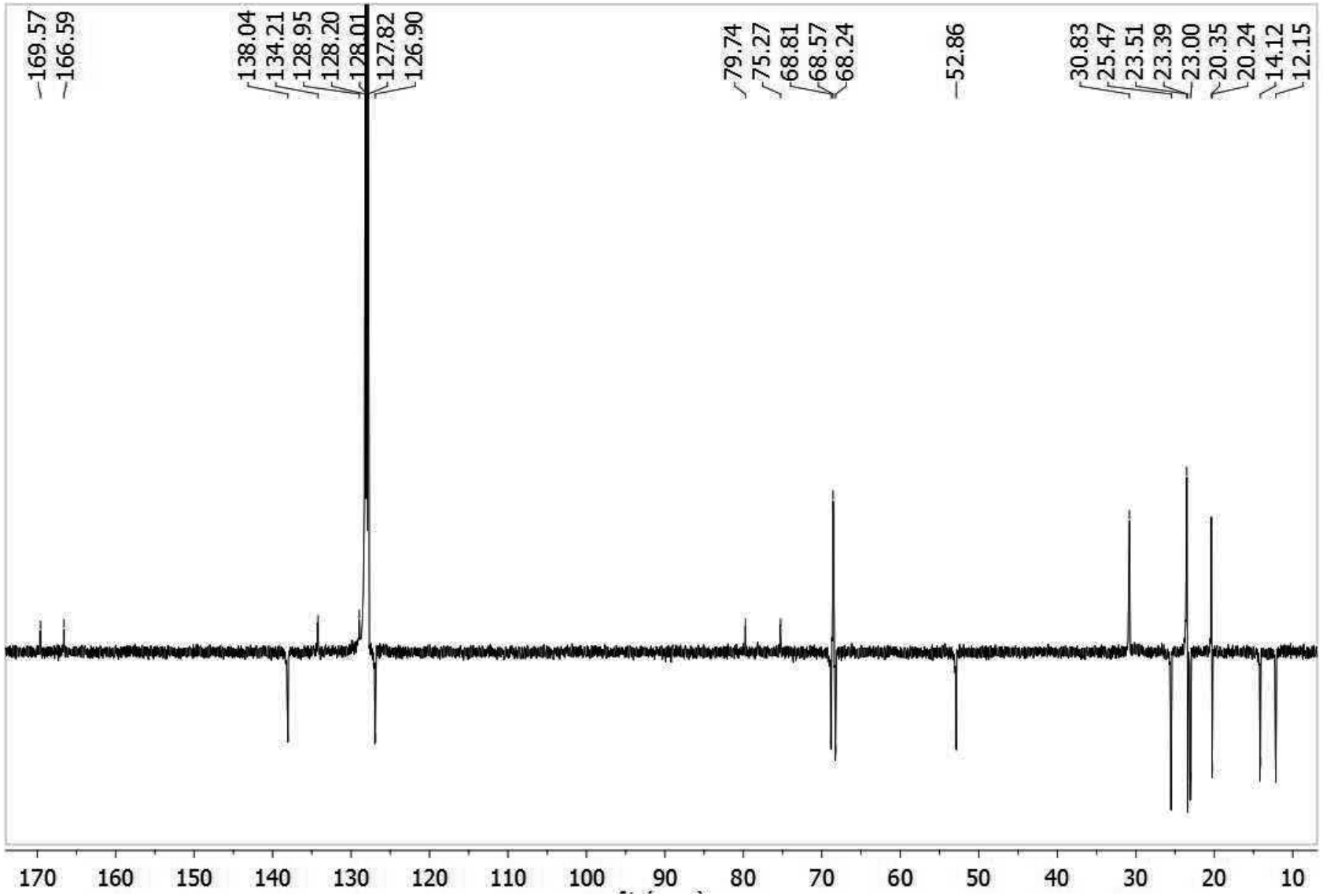

Figure S12: DEPT-Q spectrum of compound **3** (125 MHz, Benzene-*d6*)

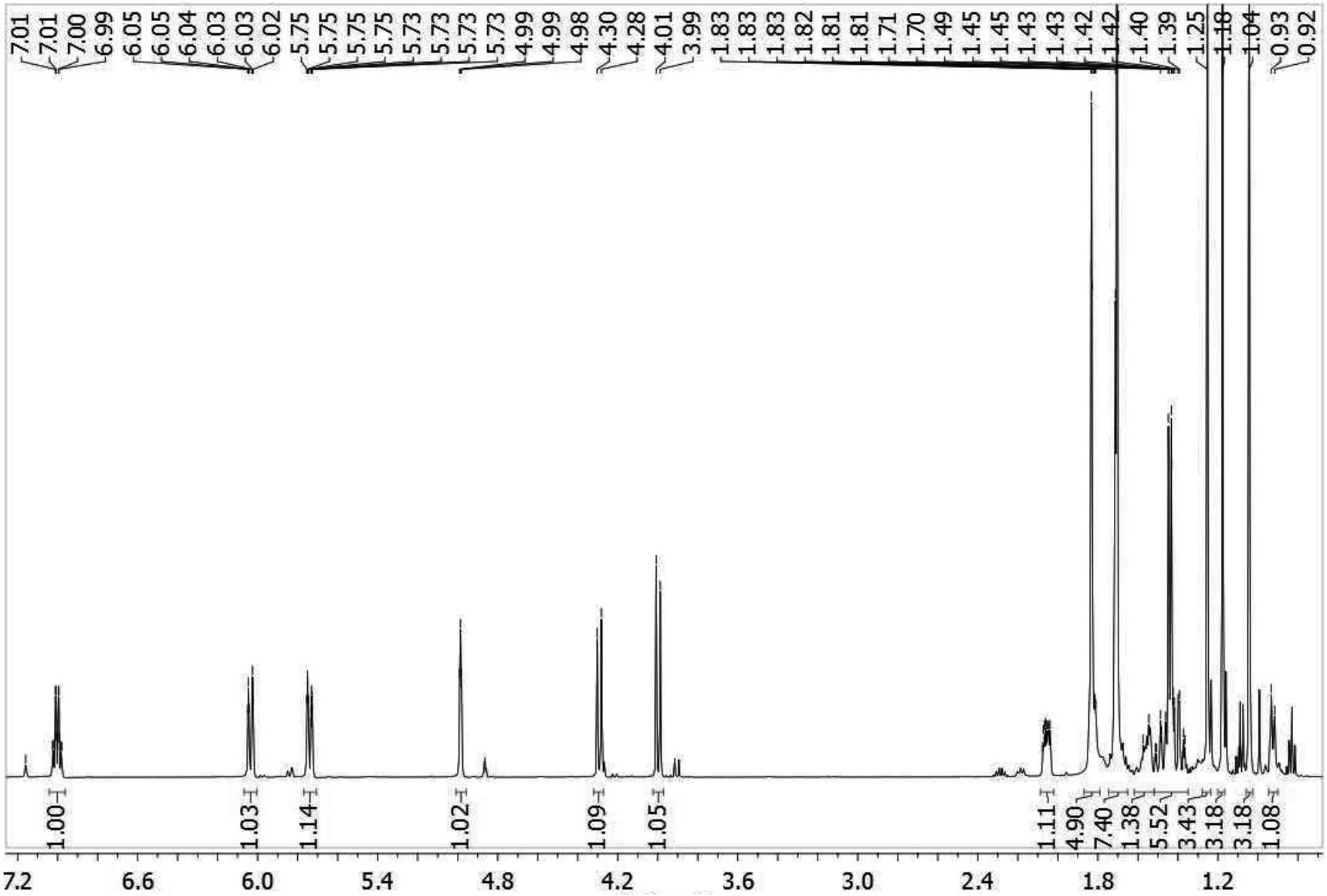

Figure S13: ^{1}H-NMR spectrum of compound **4** (500MHz, Benzene-*d6*)

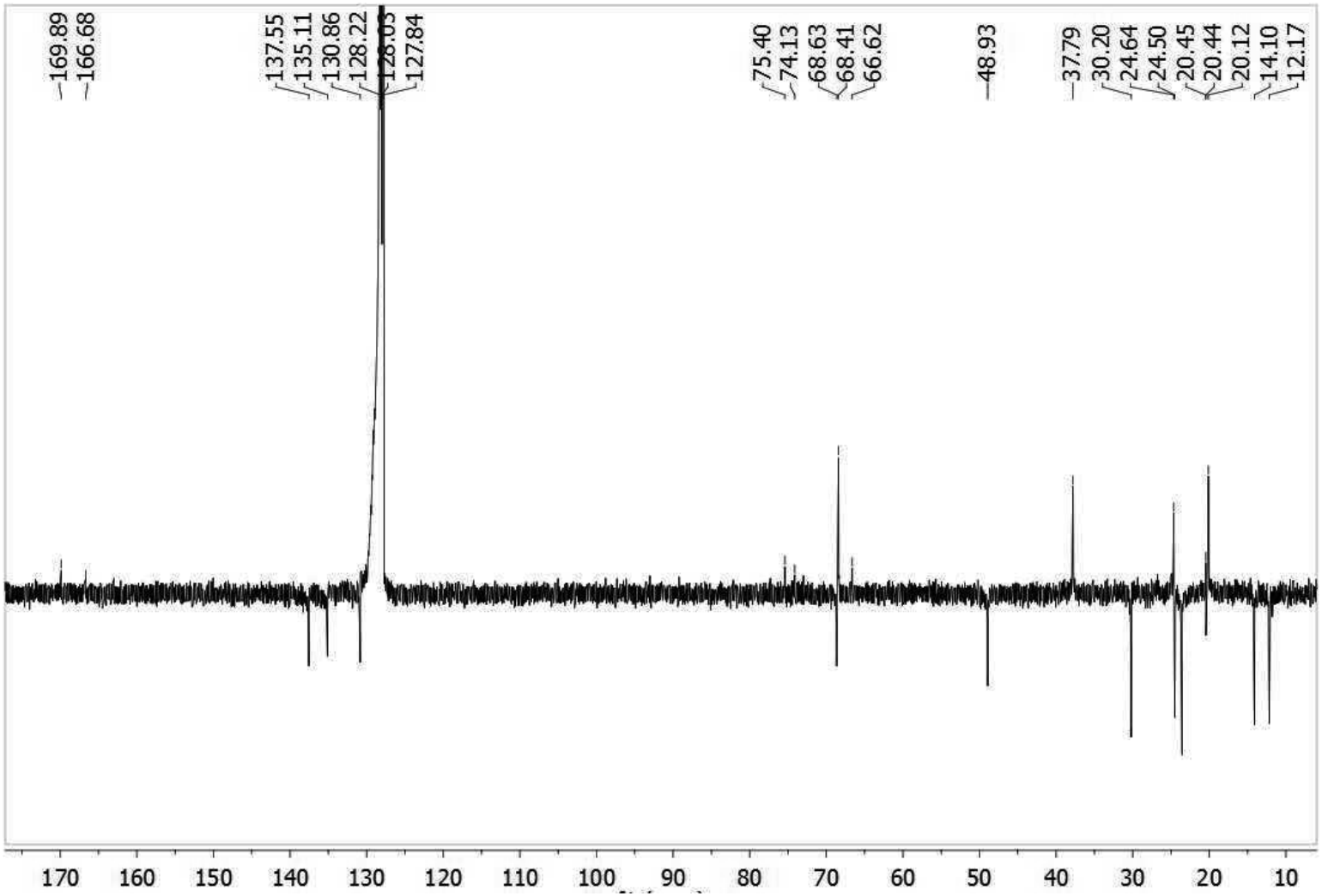

Figure S14: DEPT-Q spectrum of compound **4** (125 MHz, Benzene-*d6*)

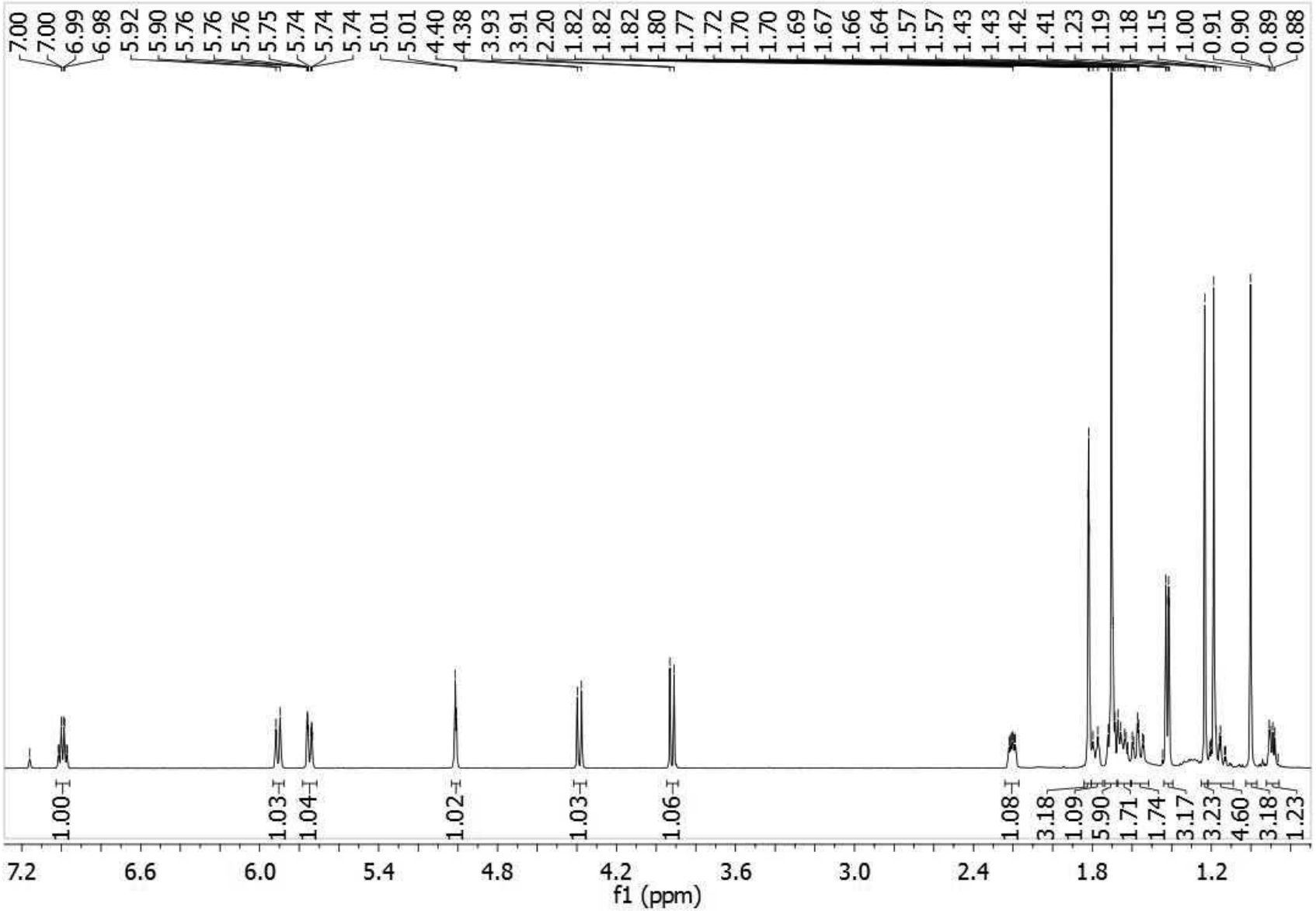

Figure S15: ^{1}H-NMR spectrum of compound **5** (500MHz, Benzene-*d6*)

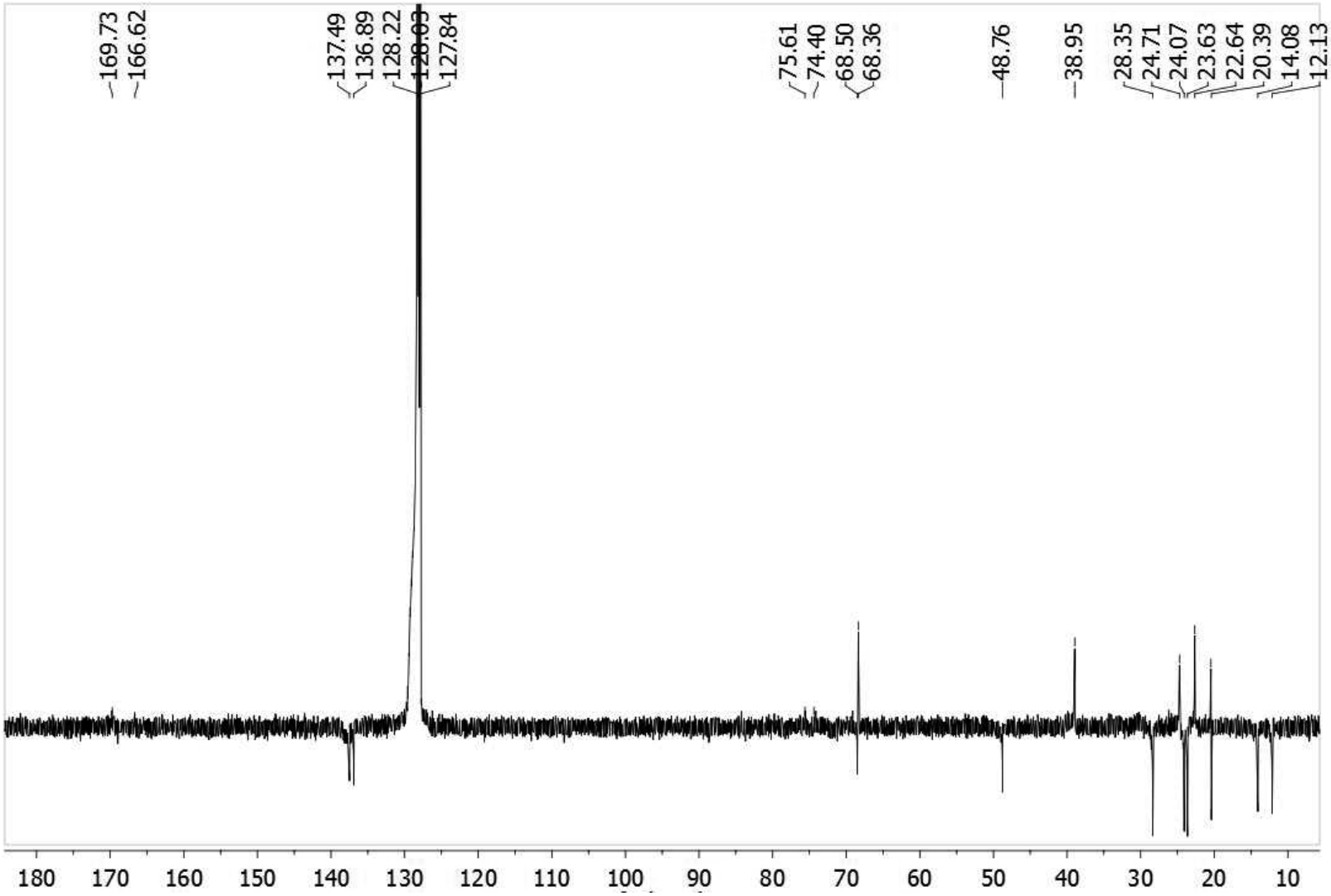

Figure S16: DEPT-Q spectrum of compound **5** (125 MHz, Benzene-*d6*)

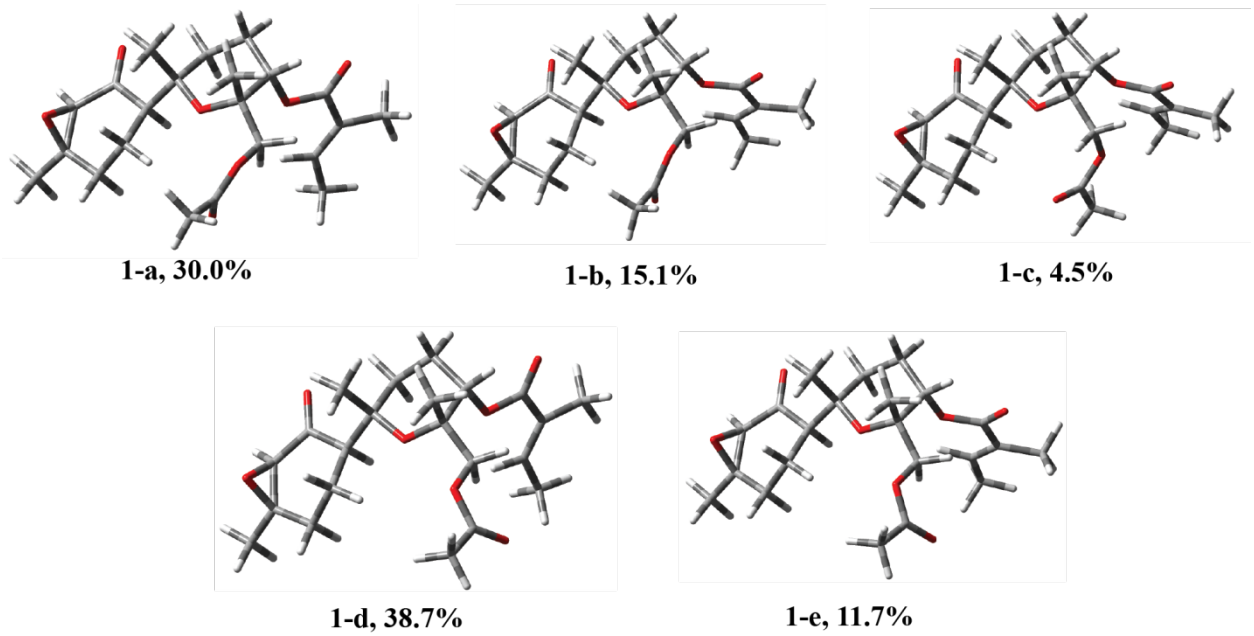

Figure S17. Minimized conformers of **1** in the gas phase using DFT at the B3LYP/6-31G∗ level: compound **1**, showing five conformers in 2 kcal/mol range from the global minimum.

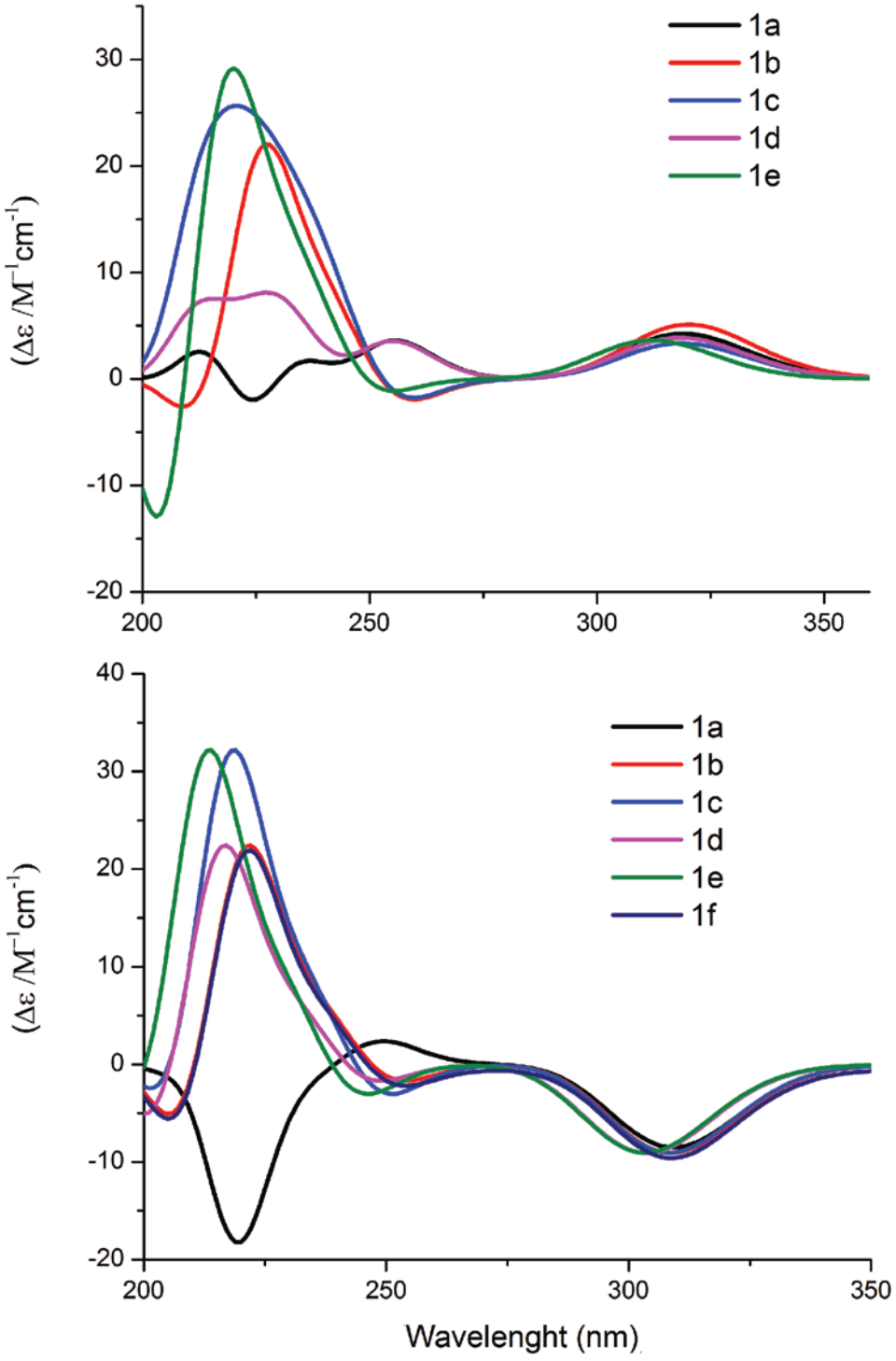

Figure S18. Calculated ECD spectra of the minimized conformers of **1** in MeOH (DFT/B3LYP/6-31G**); 2*R*,3*R*,6*R*,7*S*,10*S*,11*S* (top) 2*S*,3*S*,6*S*,7*S*,10*S*,11*S* (down)

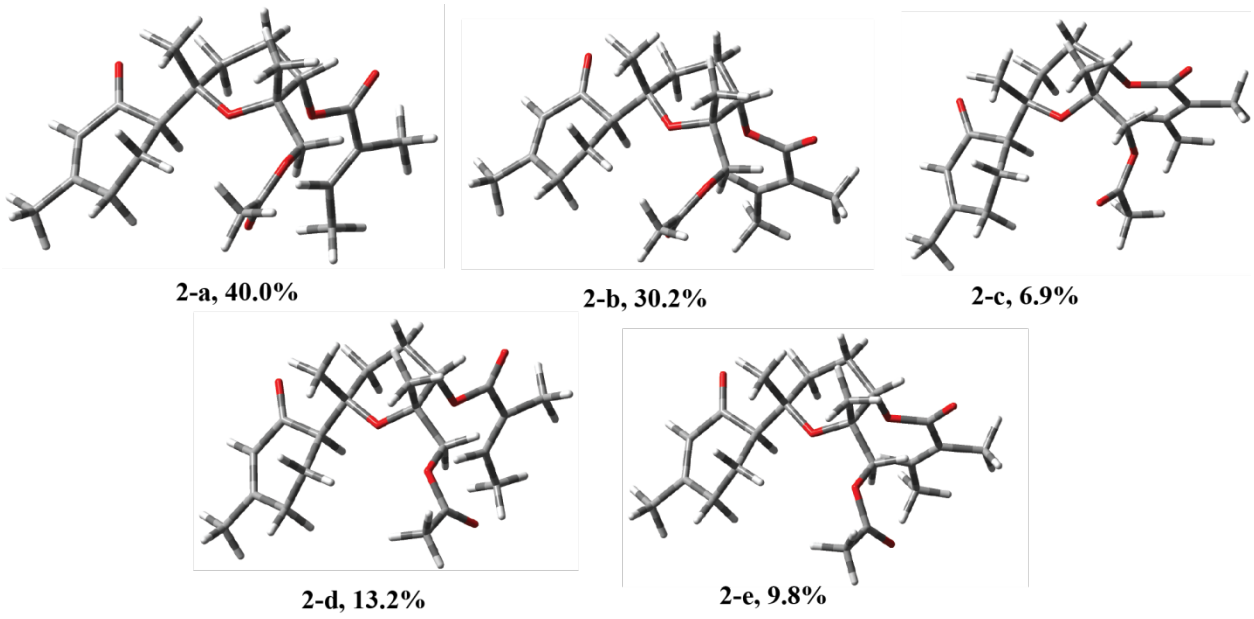

Figure S19. Minimized conformers of **2** in the gas phase using DFT at the B3LYP/6-31G∗ level: compound **2**, showing five conformers in 2 kcal/mol range from the global minimum.

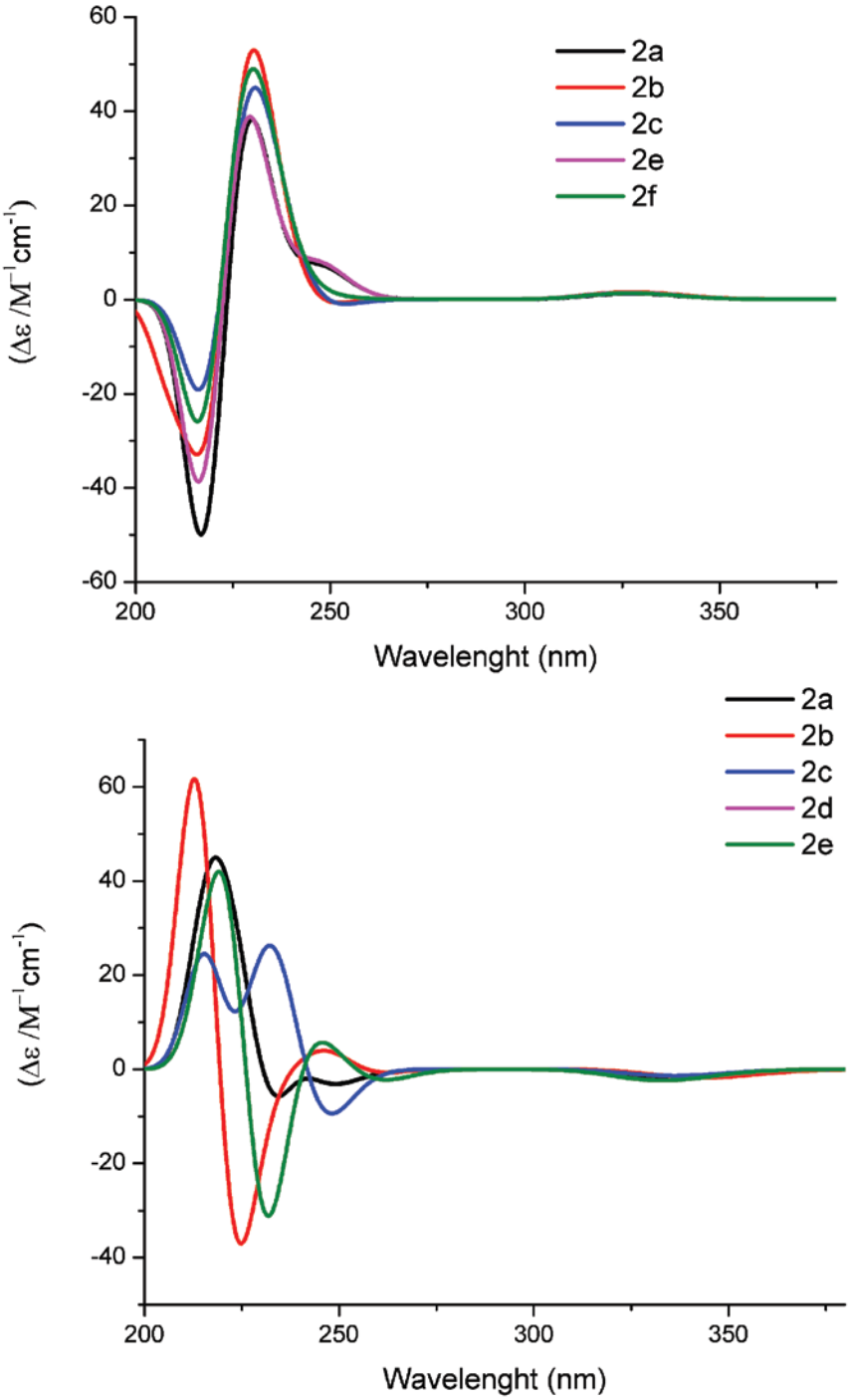

Figure S20. Calculated ECD spectra of the minimized conformers of **2** in MeOH (DFT/B3LYP/6-31G**); 6*R*,7*S*,10*S*,11*S* (top) 6*S*,7*S*,10*S*,11*S* (down)

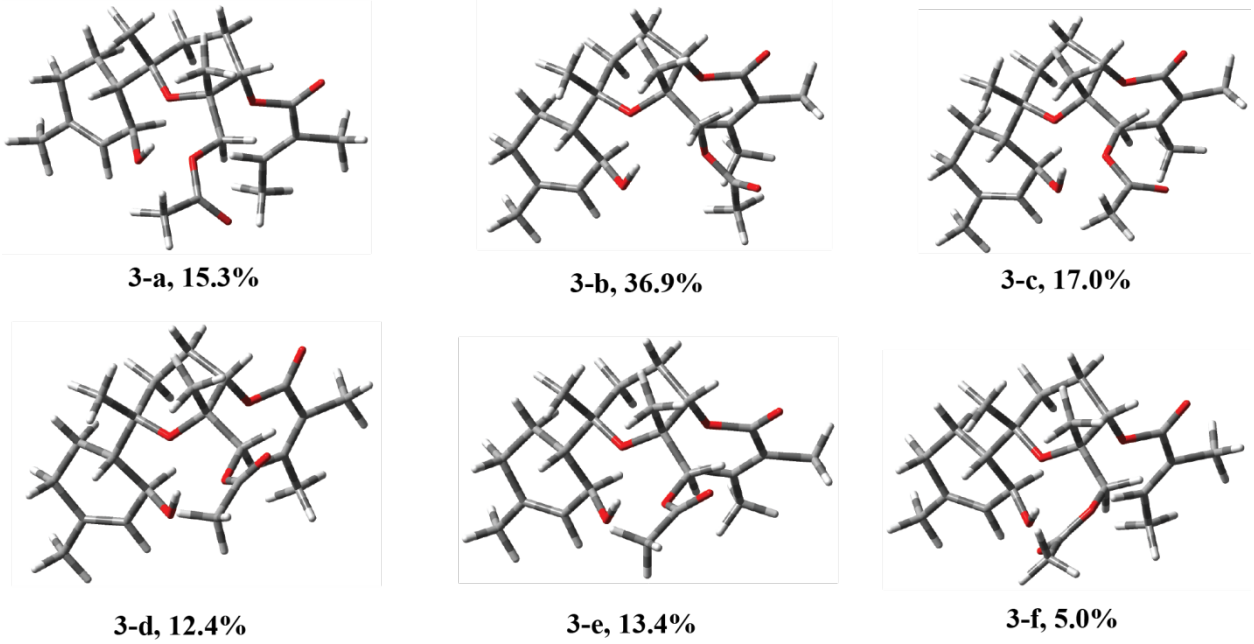

Figure S21. Minimized conformers of **3** in the gas phase using DFT at the B3LYP/6-31G∗ level: compound **3**, showing six conformers in 2 kcal/mol range from the global minimum.

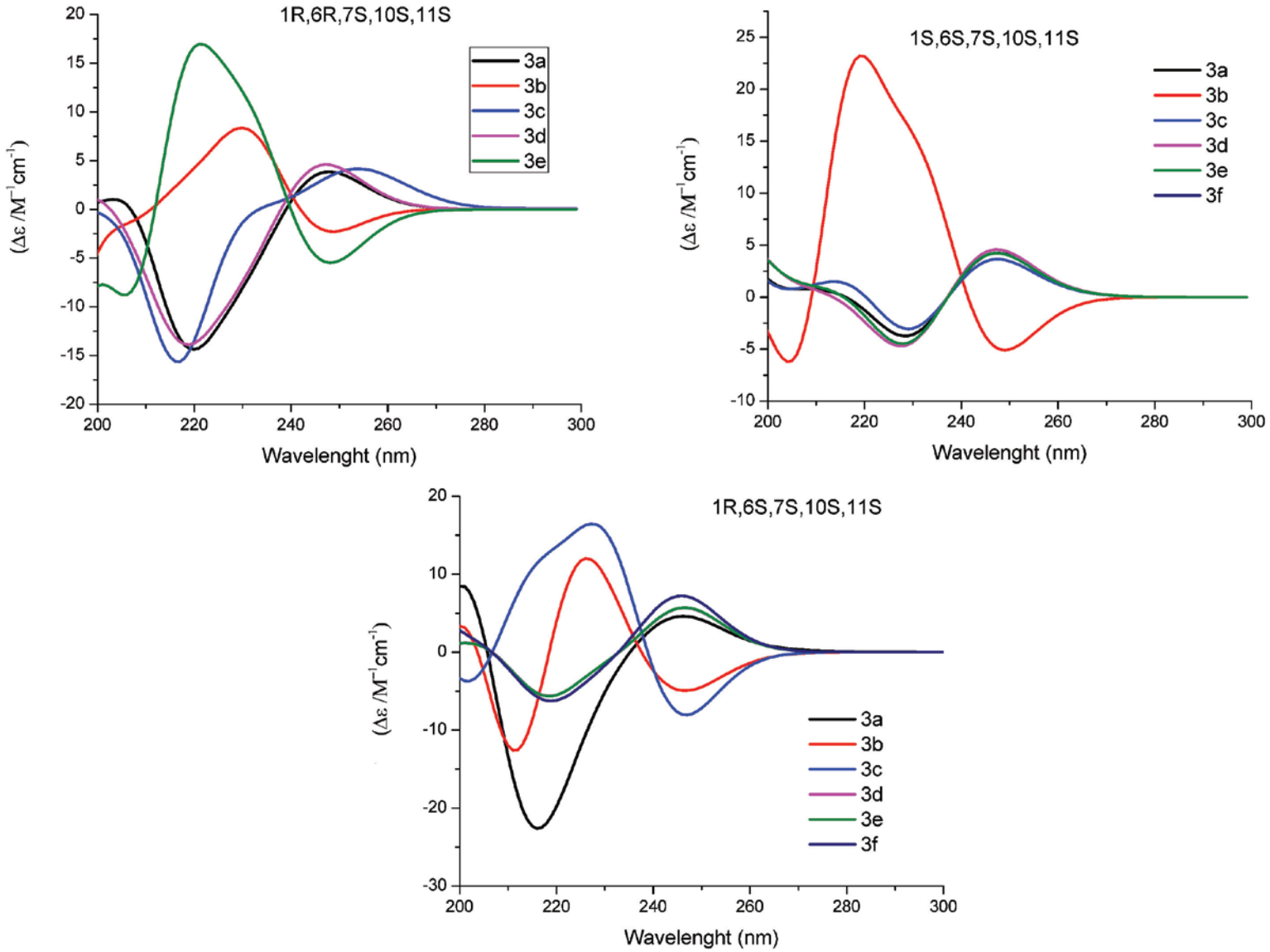

Figure S22. Calculated ECD spectra of the minimized conformers of **3** in MeOH (DFT/B3LYP/6-31G**)

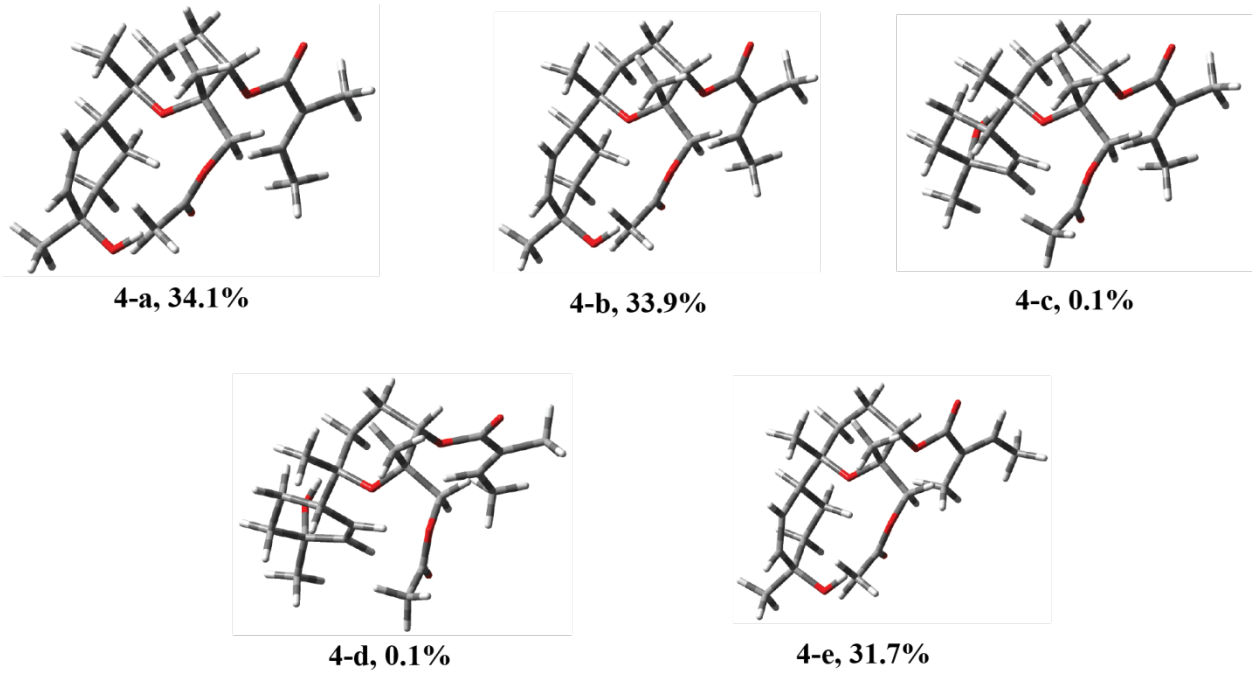

Figure S23. Minimized conformers of **4** in the gas phase using DFT at the B3LYP/6-31G∗ level: compound **4**, showing five conformers in 2 kcal/mol range from the global minimum.

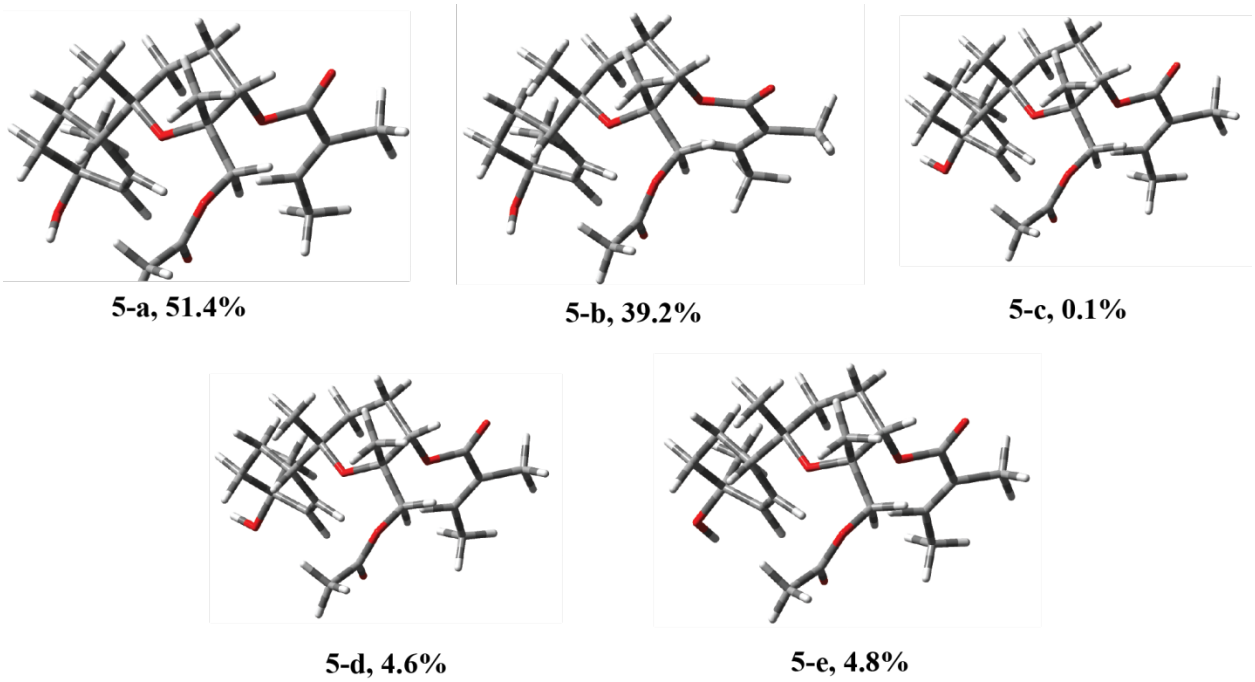

Figure S24. Minimized conformers of **5** in the gas phase using DFT at the B3LYP/6-31G∗ level: compound **5**, showing five conformers in 2 kcal/mol range from the global minimum

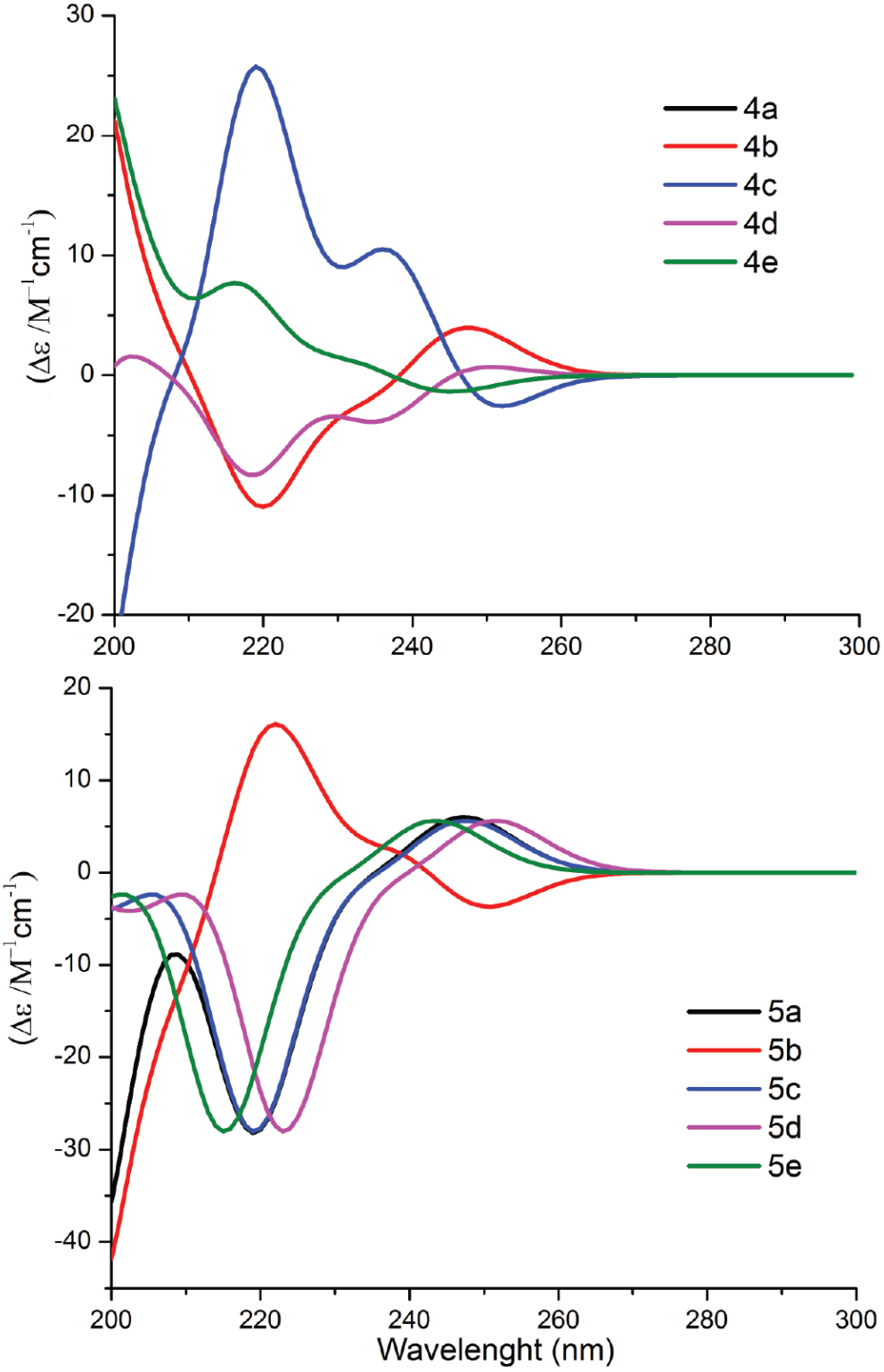

Figure S25. Calculated ECD spectra of the minimized conformers of **4** and **5** in MeOH (DFT/B3LYP/6-31G**)

3.3. Disesquiterpene and sesquiterpene coumarins from *Ferula pseudalliacea*, and determination of their absolute configurations

Dara Dastan, Peyman Salehi, Ahmad Reza Gohari , Stefanie Zimmermann, Marcel Kaiser, Matthias Hamburger, Hamid Reza Khavasi, Samad Nejad Ebrahimi

Phytochemistry 78 (2012) 170–178, doi:10.1016/j.phytochem.2012.02.016

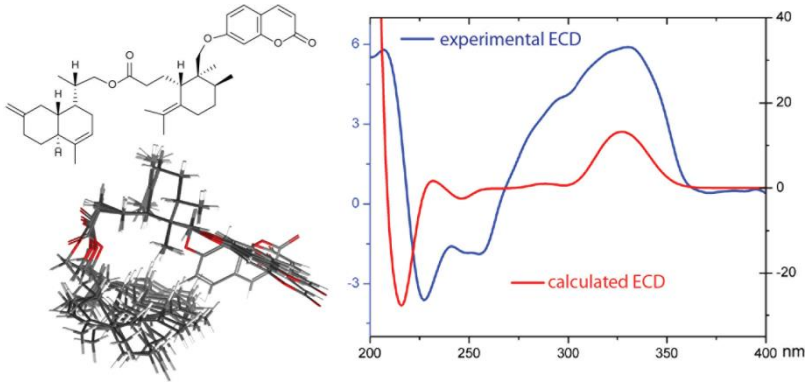

The first disesquiterpene coumarin, a new sesquiterpene coumarin, and four known sesquiterpene coumarins were isolated from the roots of *Ferula pseudalliacea*. The absolute configurations of four of the compounds were established by comparison of experimental and simulated ECD spectra using TDDFT.

Extraction of plant material for isolation, isolation of compounds, recording, and interpretation of analytical data for structure elucidation (mass spectrometry, microprobe NMR, optical rotation) were done by Dara Dastan. Experimental and quantum-chemical calculations of ECD spectra, contributing in writing of the manuscript, and preparation of some figures (Figure 2, 3, 6, 7, and 9) were my part to this publication. Antimalarial testing was done by Stefanie Zimmermann.

Samad Ebrahimi

Phytochemistry 78 (2012) 170–178

Contents lists available at SciVerse ScienceDirect

Phytochemistry

journal homepage: www.elsevier.com/locate/phytochem

Disesquiterpene and sesquiterpene coumarins from *Ferula pseudalliacea*, and determination of their absolute configurations

Dara Dastan [a], Peyman Salehi [a,*], Ahmad Reza Gohari [b,*], Stefanie Zimmermann [c,d], Marcel Kaiser [d,e], Matthias Hamburger [c], Hamid Reza Khavasi [f], Samad Nejad Ebrahimi [a,c]

[a] Department of Phytochemistry, Medicinal Plants and Drugs Research Institute, Shahid Beheshti University, G. C., Evin, Tehran, Iran
[b] Medicinal Plants Research Center, Faculty of Pharmacy, Tehran University of Medical Sciences, Tehran, Iran
[c] Division of Pharmaceutical Biology, University of Basel, Klingelbergstrasse 50, 4056 Basel, Switzerland
[d] Department of Medical Parasitology and Infection Biology, Swiss Tropical and Public Health Institute, 4002 Basel, Switzerland
[e] University of Basel, 4003 Basel, Switzerland
[f] Department of Chemistry, Shahid Beheshti University, G. C., Evin, Tehran, Iran

ARTICLE INFO

Article history:
Received 14 December 2011
Received in revised form 30 January 2012
Available online 20 March 2012

Keywords:
Ferula pseudalliacea
Apiaceae
Sesquiterpene coumarin
ECD
X-ray analysis
TDDFT
Plasmodium falciparum

ABSTRACT

The first disesquiterpene coumarin, sanandajin, five sesquiterpene coumarins, kamolonol acetate, fekrynol acetate, ethyl galbanate, methyl galbanate, farnesiferol B, and a sesquiterpene, aristolone, were isolated from a *n*-hexane extract of *Ferula pseudalliacea* roots. The structures were elucidated by 1D and 2D NMR, HR-ESIMS data, and kamolonol acetate was confirmed by single-crystal X-ray analysis. The absolute configuration of compounds was established by comparison of experimental and simulated ECD spectra using time dependence density function theory (TDDFT). *In vitro* antiplasmodial activity against *Plasmodium falciparum* K1 strain was determined. sanandajin, kamolonol acetate and methyl galbanate showed moderate antiplasmodial activity, with IC_{50} values of 2.6, 16.1 and 7.1 μM, respectively.

1. Introduction

The genus *Ferula* (Apiaceae) comprises about 180 species which grow mainly in central Asia, the Middle East, and central Europe (Pimenov and Leonov, 2004). Several species, such as *Ferula asafetida*, *Ferula gumosa* and *Ferula latisecta* have been used in folk medicine to treat stomachache, hysteria, infant colitis, and asthma (Eigner and Scholz, 1999; Zargari, 1997). The genus *Ferula* is known to be a rich source of biologically active compounds, such as sesquiterpenes (Abd El-Razek et al., 2001; Ahmed, 1999; Iranshahi et al., 2008; Kanani et al., 2011; Tamemoto et al., 2001) and coumarins (Abd El-Razek et al., 2001; Iranshahi et al., 2004, 2007, 2009; Zhou et al., 2000). *Ferula pseudalliacea* Rech.f. is an indigenous species of the Kurdistan (Sanandaj) mountains in western Iran. As part of a phytochemical study of endemic plants of Iran, and an ongoing screening for new antiprotozoal natural products (Adams et al., 2009a,b; Ślusarczyk et al., 2011), we investigated a *n*-hexane extract from roots of *F. pseudalliacea*. We here report on the identification of new disesquiterpene and sesquiterpene coumarins, along with known sesquiterpene coumarins, and on their *in vitro* antiplasmodial activity. Structures including their absolute configuration were established by a combination of methods, such as 1D and 2D NMR, high-resolution mass spectrometry, single-crystal X-ray analysis, and ECD spectroscopy.

2. Results and discussion

The *n*-hexane extract of *F. pseudalliacea* roots was separated by normal and reversed phase chromatography to give two new (**1** and **2**) and four known sesquiterpene coumarins (**3**–**6**), and a sesquiterpene (Scheme. 1), aristolone (**7**). Compound **1** was obtained as a colorless gum. Its molecular formula $C_{39}H_{52}O_5$ was deduced from HR-ESIMS (*m*/*z* 623.3722 $[M+Na]^+$, calc. 623.3712). The planar structure of **1** was established by analysis of the NMR spectral data. The ^{13}C NMR spectrum displayed 39 carbon signals (Table 1). A downfield resonance (δc 174.2) in the ^{13}C spectrum suggested the presence of an ester. Other carbon signals were six methyl groups (δc 10.4, 16.0, 20.1, 20.2, 22.4 and 23.8), eight aliphatic methylene carbons, an olefinic methylene and two primary oxygenated carbons (δc 68.3 and 71.6). The nine remaining downfield

* Corresponding authors. Tel.: +98 2122431621; fax: +98 2122431783.
E-mail addresses: p-salehi@sbu.ac.ir (P. Salehi), goharii_a@sina.tums.ac.ir (A. Reza Gohari).

0031-9422/$ - see front matter © 2012 Elsevier Ltd. All rights reserved.
doi:10.1016/j.phytochem.2012.02.016

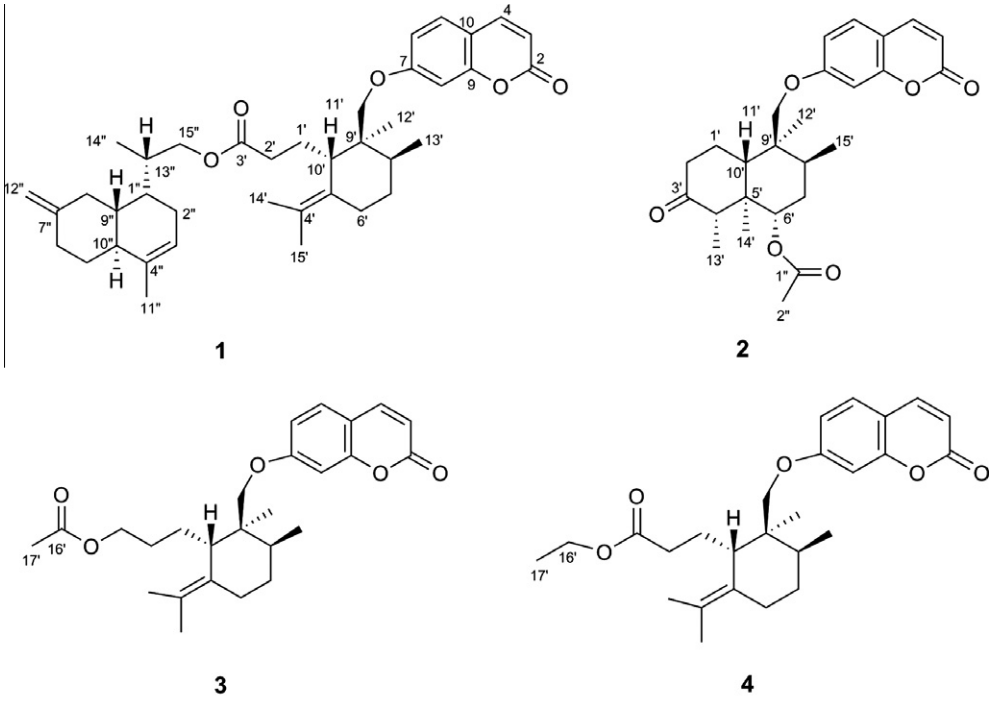

Scheme 1. Compounds **1**–**4**.

resonances were reminiscent of a 7-hydroxycoumarin, while the other thirty signals indicated an isoprenoid residue. The presence of an umbelliferyl moiety was confirmed by resonances at δ_H 6.22 (d, J = 9.5 Hz), 6.74 (d, J = 2.2 Hz), 6.8 (dd, J = 8.6, 2.3 Hz), 7.33 (d, J = 8.6 Hz) and 7.62 (d, J = 9.5 Hz) in the ^{1}H NMR spectrum.

Analysis of the COSY, HSQC and HMBC spectra suggested the presence of two discrete sesquiterpene residues (Fig. 1 and Table 1). The ^{1}H NMR spectrum exhibited resonances of four singlets corresponding to four tertiary methyl groups, and two doublets (3H each) of secondary methyl groups. An HMBC correlation from Me-13′ (δ_H 0.9) to C-9′ (δc 40.7) and C-8′ (δc 34.8), and a COSY correlation between H-8′ (δ_H 1.86) and Me-13′ (δ_H 0.9) confirmed a Me-13′ at C-8′. HMBC correlation of the Me-14″ (δ_H 0.81) with the resonance at δc 31.4 (C-13″), and COSY crosspeak between H-13″ (δ_H 2.38) and Me-14″ confirmed the attachment of Me-14″ at C-13″ (Table 1). The location of double bonds C-4′–C-5′, and C-7″–C-12″ was derived from HMBC connectivities. Me-14′ (δ_H 1.45) and Me-15′ (δ_H 1.61) showed correlations with C-4′ (δc 125.9) and C-5′ (δc 129.6), and H-12″a (δ_H 4.58) and H-12″b (δ_H 4.69) showed cross-peaks with resonances of C-6″ (δc 36.0) and C-7″ (δc 152.6), respectively. HMBC correlations of H-3″ (δ_H 5.5) with C-2″ (δc 30.4), C-10″ (δc 44.4) and C-11″ (δc 23.8) confirmed a double bond at C-3″–C-4″. Other important HMBC and COSY correlations are given in Fig. 1. The linkage of the three moieties was established by diagnostic HMBC connectivities. The methylene protons at C-11′ (δ_H 3.87 and 3.69) showed long-range correlation with C-7 (δc 161.9) and, thus, confirmed the attachment of the first sesquiterpene residue to the coumarin moiety. HMBC correlations of the H-1′, H-2′ and H-15″ signals (δ_H 1.86, 2.14, and 3.98, respectively) with the resonance at δc 174.2 (C-3′) revealed the location of the ester carbonyl group (C-3′), as well as the attachment of the second sesquiterpene unit. The relative configuration of the two sesquiterpene units was established by a NOESY spectrum (Fig. 1). NOESY crosspeaks of H-10′/H-11′, Me-13′/H-11′ and Me-12′/H-8′ confirmed that Me-12′ and H-8′ were located on the same face of the six-membered ring also H-10′ and Me-13′. NOESY crosspeaks between H-1″ and H-10″, and the $J_{9'',10''}$ = 11.2 Hz (*trans* orientation of H-9″ and H-10″) defined the relative configuration of the stereogenic centers at C-1″, C-9″ and C-10″ as depicted (Fig. 1).

The absolute configuration of **1** was investigated by comparison of experimental ECD spectra with calculated spectra using time dependent density functional theory (TDDFT). For this purpose, the 3D structure of **1** was submitted to a systematic conformational search in H_2O by Optimized Potential for Liquid Simulations (OPLS-2005) force field, within an energy window of 2 kcal/mol from particular global minima. A total of 28 conformational species were found. All conformers were subjected to geometrical optimization (DFT/B3LYP/6-31G*) in the gas phase combined with calculation of vibrational modes to confirm these minima. No imaginary frequencies were found. Conformational analysis using relative free energies indicated the presence of seven conformers, **1a** (72.94%), **1b** (8.54%), **1c** (6.79%), **1d** (3.91%), **1e** (2.94%), **1f** (2.55%), and **1g** (2.33%) in the gas phase (Fig 2). For these conformers, ECD spectra were calculated (TDDFT /B3LYP/6-31G*) in MeCN using the SCRF (self-consistent reaction field) method with the CPCM (conductor-like polarizable continuum) model. Calculated ECD spectra were assigned a Boltzmann weight according to the energy of the minimized conformers at 298.15 K and overlaid prior to comparison with the experimental ECD spectrum (Fig. 3). The calculated ECD spectrum of **1** closely matched with the experimental data, in particular positive Cotton effects (CE) in the 300–350 nm and 200–220 nm regions, a shoulder between 270–290 nm, and a negative CE in the region of 220–260 nm. Differences between calculated and experimental spectra were apparently due to minor difference between calculated and solution conformers of this flexible molecule (Zaugg et al., 2011). The positive CE between 270 and 350 nm in the experimental spectrum was likely due to a $\pi \rightarrow \pi^*$ transition in the extended π-system of coumarin moiety, while the weak $n \rightarrow \pi^*$ transitions were buried by strong $\pi \rightarrow \pi^*$ transition. On the basis of these data the absolute configuration of the inner sesquiterpene moiety was unambiguously established. For the second sesquiterpene residue, only the

Table 1
^{1}H and ^{13}C NMR spectroscopic data for compounds **1–4** ($CDCl_3$, 500 MHz for δ_H, 125 MHz for δc).[a]

Position	**1**		**2**		**3**		**4**	
	δ_C	δ_H (J in Hz)	δ_C	δ_H (J in Hz)	δ_C	δ_H (J in Hz)	δ_C	δ_H (J in Hz)
2	161.2		161.0		161.2		161.2	
3	112.7	6.22, d (9.5)	112.9	6.25, d (9.5)	112.7	6.22, d (9.5)	112.7	6.22, d (9.5)
4	143.4	7.62, d (9.5)	143.2	7.63, d (9.5)	143.4	7.62, d (9.5)	143.4	7.62, d (9.5)
5	128.5	7.33, d (8.6)	128.8	7.37, d (8.6)	128.5	7.33, d (8.5)	128.5	7.33, d (8.5)
6	113.1	6.80, dd (8.6, 2.3)	113.3	6.83, dd (8.6, 2.4)	113.0	6.80, dd (8.5, 2.0)	113.0	6.80, dd (8.5, 2.0)
7	162.8		161.9		162.8		162.8	
8	101.1	6.74, d (2.2)	101.3	6.79, d (2.3)	101.1	6.74, d (2.0)	101.1	6.74, d (2.0)
9	155.9		155.8		155.9		155.9	
10	112.2		112.7		112.2		112.2	
1′	22.2	1.86[b]	23.0	1.90	23.2	1.86[f]	22.2	1.86[g]
2′	32.3	2.14	41.1	2.36, α	26.7	1.40	32.3	2.14
				2.40, β				
3′	174.2		210.9		64.8	4.05	174.2	
4′	125.9		57.5	2.52, d (6.6)	125.1		125.9	
5′	129.6		45.4		130.0		129.6	
6′	24.4	2.50, d (13.8)	75.1	5.10, dd (11.1, 4.7)	24.4	2.50, d (12.5)	24.4	2.50, d (12.5)
7′	31.9	1.20, dd (13.1, 4.3)	32.1	1.70, α	31.9	1.20	31.9	1.20
				1.85, β				
8′	34.8	1.86[b]	36.2	1.99	34.8	1.86[f]	34.8	1.86[g]
9′	40.7		39.3		40.7		40.7	
10′	42.6	2.92	43.7	2.25, dd (11.5, 4.2)	42.9	2.92	42.6	2.92
11′	71.6	3.87, d (8.3)	75.2	3.78, d (9.1)	71.6	3.87, d (8.0)	71.6	3.87, d (8.0)
		3.69, d (8.3)		3.74, d (9.1)		3.69, d (8.0)		3.69, d (8.0)
12′	22.4	1.10, s	19.7	1.12, s	22.4	1.15, s	22.4	1.11, s
13′	16.0	0.90, d (7.0)	9.1	0.90, d (6.6)	16.0	0.90, d (7.0)	16.0	0.90, d (7.0)
14′	20.1	1.45, s	10.2	0.94, s	20.1	1.44, s	20.17	1.43, s
15′	20.2	1.61, s	15.1	1.13, d	20.2	1.60, s	20.19	1.60, s
16′					171.0		60.2	4.1, q (7.0)
17′					21.0	2.03, s	14.2	1.25, t (7.0)
1″	42.3	1.48[c]	170.3					
2″	30.4	2.02	21.7	2.02, s				
3″	121.8	5.50, s						
4″	135.3							
5″	27.0	1.67[d], α						
		1.23, β						
6″	36.0	2.06, α						
		2.40[e], β						
7″	152.6							
8″	25.6	1.50[c], α						
		1.96, β						
9″	44.1	1.70[d]						
10″	44.4	1.77						
11″	23.8	1.69[d]						
12″	103.6	4.69						
		4.58						
13″	31.4	2.38[e]						
14″	10.4	0.81, d (7.0)						
15″	68.3	3.98, dd (7.6, 6)						

[a] δ values were established from HMBC, COSY, HSQC and DEPT experiments.
[b–g] Overlapping signals.

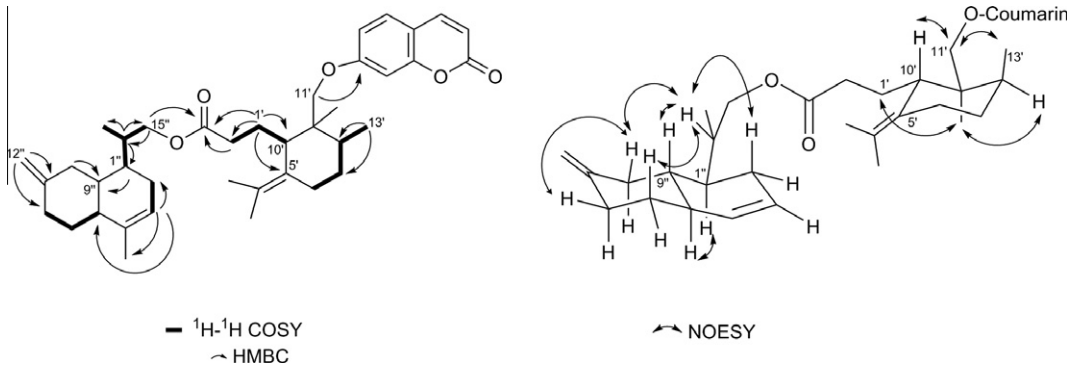

Fig. 1. Key COSY, HMBC and NOESY correlations of **1**.

relative configuration could be determined, due to the conformational flexibility of the linker and absence of diagnostic NOESY crosspeaks between the two moieties. Thus, the configuration of **1** was established as 8′*S*,9′*S*,10′*S*,1″*S*∗,9″*R*∗,10″*S*∗. Independent

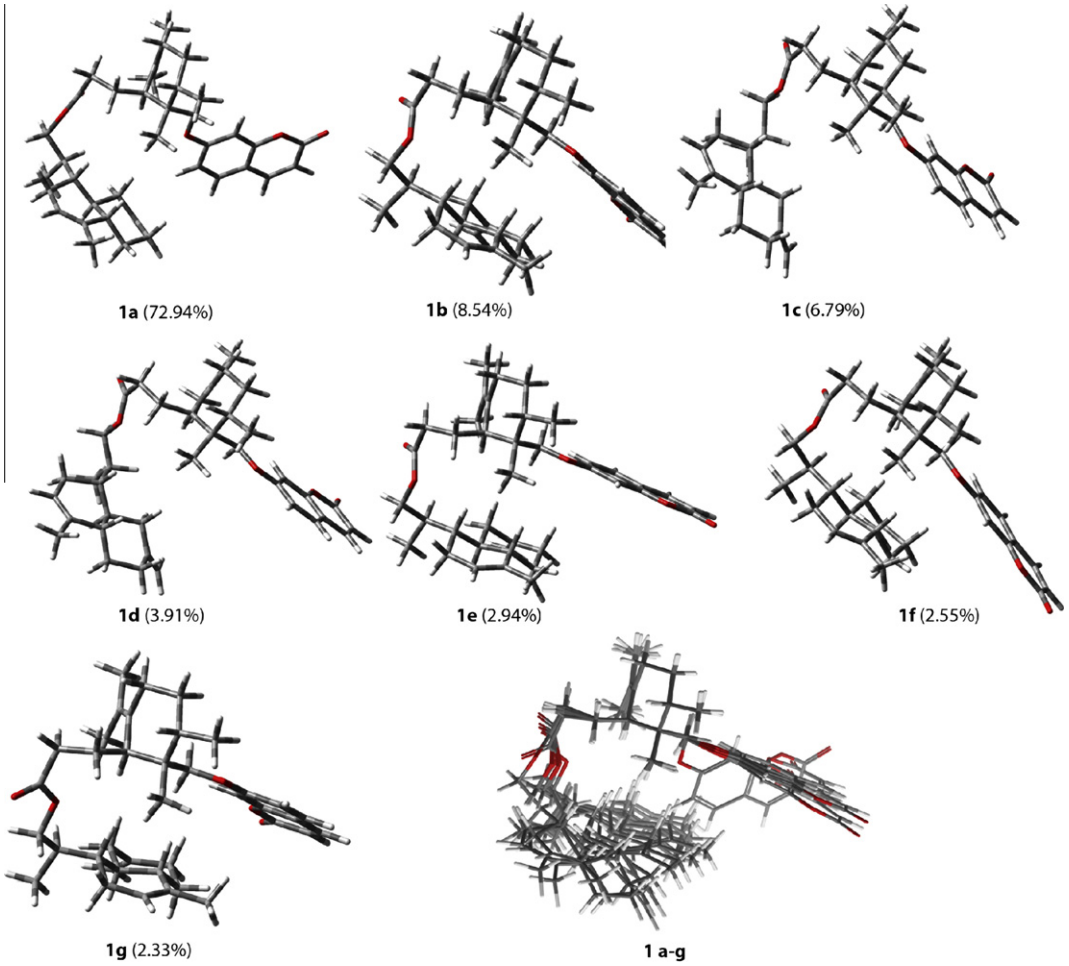

Fig. 2. Minimized conformers of **1** in the gas phase using DFT at the B3LYP/6-31G* level: compound **1**, showing seven conformers in 2 kcal/mol range from the global minimum.

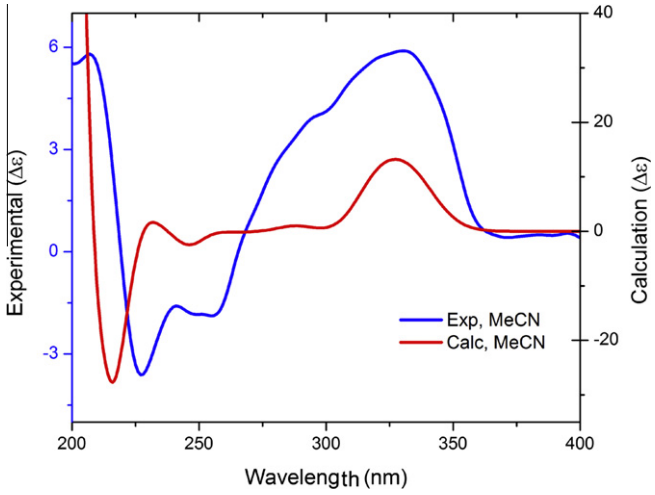

Fig. 3. Experimental (blue) and calculated (red) ECD spectra of **1**. Calculated spectra were obtained by using TDDFT at B3LYP/6-31G* level in MeCN. (For interpretation of the references to colour in this figure legend, the reader is referred to the web version of this article.)

evidence is needed to unambiguously determine the absolute configuration of the cadinene moiety in **1**.

Compound **2** was isolated as colorless crystals. A molecular formula $C_{26}H_{32}O_6$ was deduced from HR-ESIMS (*m*/*z* 463.2061 $[M+Na]^+$, calc 463.2097). Diagnostic signals in the ^1H and ^{13}C NMR spectra suggested a sesquiterpene coumarin. The ^{13}C NMR spectrum of **2** displayed 26 carbon signals (Table 1). Nine were indicative of an umbelliferyl moiety, while the remaining 17 signals suggested a sesquiterpene residue and an acetyl group. Resonances at δ_H 6.25 (d, *J* = 9.5 Hz), 6.79 (d, *J* = 2.3 Hz), 6.8 (dd, *J* = 8.6, 2.4 Hz), 7.37 (d, *J* = 8.6 Hz) and 7.63 (d, *J* = 9.5 Hz) in the ^1H NMR spectrum corroborated the coumarin portion.

The ^{13}C NMR signals were assigned to five methyl groups (δc 9.1, 10.2, 15.1, 19.7 and 21.7), three aliphatic methylenes (δc 23.0, 32.1 and 41.1), a primary oxygenated carbon (δc 75.2), a secondary oxygenated carbon (δc 75.1), and eight quaternary carbons including two carbonyl groups (δc 210.9 and 170.3) in the non-coumarin portion of **2**. The location of the carbonyl groups at C-3′ and C-1″ were determined by HMBC correlation: Me-13′ (δ_H 0.9), H-4′ (δ_H 2.52), H-2′ eq (δ_H 2.4) and H-2′ ax (δ_H 2.36) showed crosspeaks with C-3′ (δ_C 210.9), while Me-2″ (δ_H 2.02) and H-6′ (δ_H 5.1) were correlated to C-1″ (δ_C 170.3). Positions of methyl and carbonyl groups, and the attachment of the acetyl and sesquiterpene moieties were established by HMBC spectra (Fig. 4). The relative configuration of stereocenters at C-4′, C-5′, C-6′, C-8′, C-9′ and C-10′ was determined by NOESY data (Fig. 4). Crosspeaks of H-11′/H-10′, and H-8′/Me-12′ established an β-orientation for both H-10′ and Me-15′, and a α-orientation for Me-12′. Crosspeaks of H-10′ with H-4′ and H-6′ established α-orientation of Me-13′, Me-14′ and the acetyl group. The proposed structure

of **2** was corroborated by X-ray crystallographic analysis of the compound (Fig. 5).

The absolute configuration of **2** was established by comparison of experimental and calculated ECD spectra. A conformational search based on the X-ray relative configuration revealed eight conformers within a 2 kcal/mol energy window from the particular global minimum. These conformers were subjected to geometrical optimization and energy calculation using density function theory (DFT) with the B3LYP function and 6-31G* in the gas-phase combined with calculation of vibrational modes to confirm these minima. No imaginary frequencies were found. Conformational analysis using relative free energies indicated the presence of 6 stable conformers, **2a** (39.02%), **2b** (30.02%), **2c** (11.77%), **3d** (9.63%), **2e** (7.11%), and **2f** (2.45%) in the gas phase (Fig. 6). Calculation of the ECD spectra for these conformers were performed as described above. The weighted ECD spectrum in MeCN is shown in Fig 7. Experimental and calculated ECD spectra were in good agreement. Two negative CEs at 323 and 235 nm, two positive CEs at 290 and 210 nm, and a shoulder between 250 and 280 nm were also found in the calculated ECD spectrum. The differences between calculated and experimental spectra in the region 220–230 nm presumably resulted from an overestimation of the UV absorbance in the calculations, or from minor difference in solution conformation. Thus, the absolute configuration of **2** was established as 4′*S*,5′*R*,6′*S*,8′S,9′*S*,10′*R*.

Fekrynol acetate (**3**) and ethyl galbanate (**4**) had been previously reported from *Ferula krylovii* (Veselovskaya et al., 1981) and *Ferula gummosa* (Bednyak, 1962), respectively, but no spectral data were recorded at that time. We report here full NMR spectral assignments and determination of absolute configuration for these two compounds (Fig 8 and Table 1) which were obtained as a 1:1 mixture. The specific rotation for the mixture of compounds **3** and **4** was $[\alpha]_D^{20}$ − 17.0 (c = 1, $CHCl_3$).

The molecular models of **3** and **4** were built with the relative configuration represented in Scheme. 1, and the 3D structures subjected to conformational search using OPLS-2005 molecular mechanics force field. The conformational analysis afforded 21 conformers for **3** and 23 conformers for **4**. The DFT energy calculation at B3LYP/6-31G* level of theory yielding 15 relevant conformers for **3** and 12 conformers for **4** within an energy range of 2 kcal/mol from the global minimum. In both cases the conformers differed with respect to orientation of coumarin and ester moieties (Fig. 9A). ECD spectra were calculated for these conformers in MeCN (TDDFT/B3LYP/6-31G*/SCRF/CPCM). Each calculated ECD spectrum was assigned a Boltzmann weight according to the energy of the minimized conformers at 298.15 K and overlaid prior to comparison with the experimental ECD spectrum (Fig. 9B). The simulated ECD spectra showed very good agreement with the experimental spectrum. Two negative CEs were observed at 258 and 221 nm, along with two positive CEs at 322 and 246 nm. The difference between calculated and experimental spectra likely resulted from an overestimation of the UV absorbance in the calculations, or from minor conformational differences in solution. Calculated ECD spectra for **3** and **4** were similar. Hence, the ester

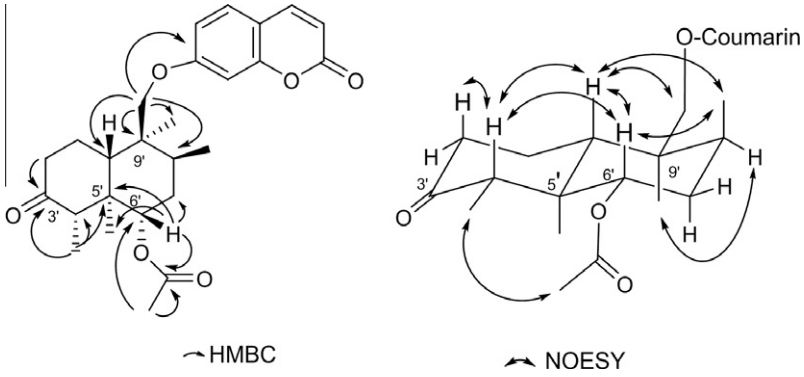

Fig. 4. Key HMBC and NOESY correlations of **2**.

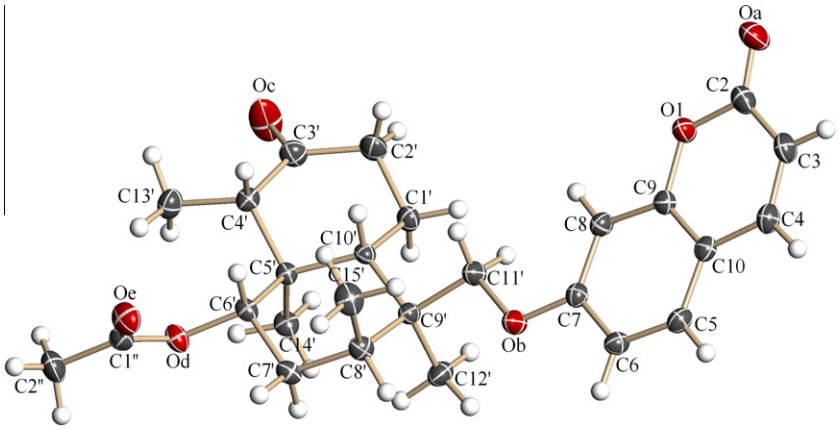

Fig. 5. Thermal ellipsoid plot of **2**.

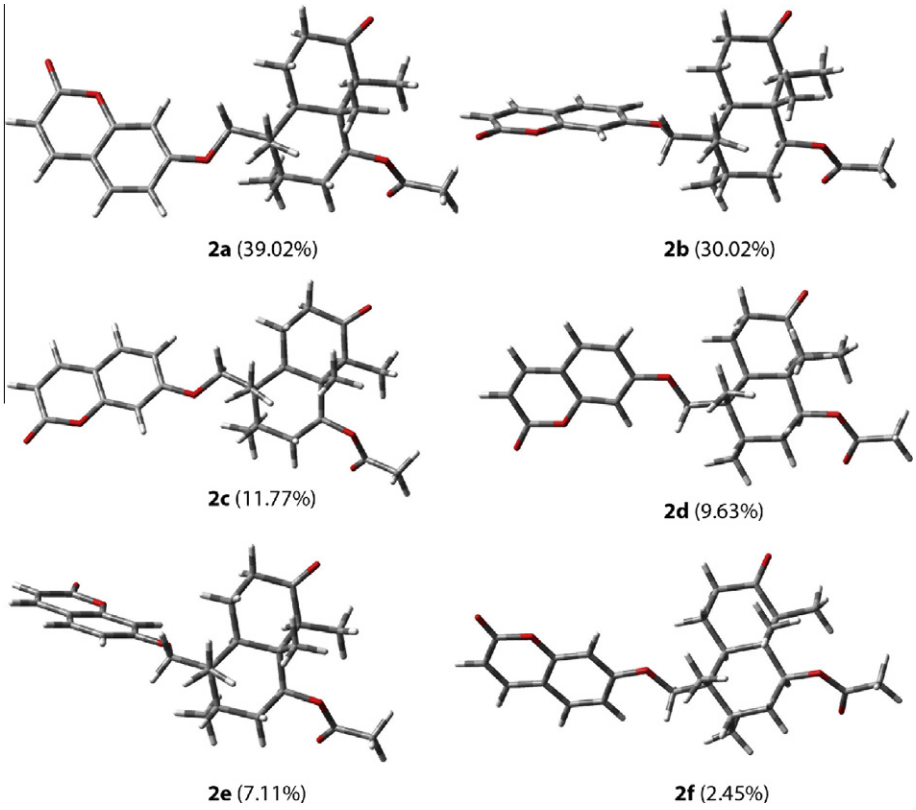

Fig. 6. Minimized conformers of **2** in the gas phase using DFT at the B3LYP/6-31G* level: compound **2**, showing six conformers in 2 kcal/mol range from the global minimum.

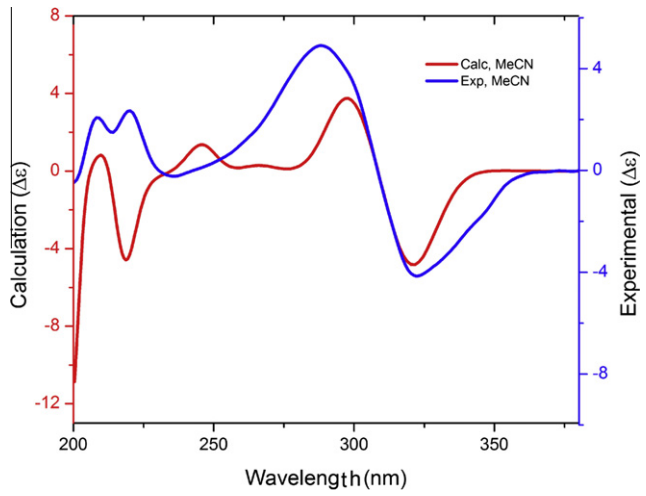

Fig. 7. Experimental (blue) and calculated (red) ECD spectra of **2**. Calculated spectra were obtained in MeCN using TDDFT at B3LYP/6-31G* level. (For interpretation of the references to colour in this figure legend, the reader is referred to the web version of this article.)

moiety had no effect on the ECD because of its distance from the stereogenic centers. Thus, we conclude that the absolute configuration of both compounds was 8′*S*,9′*S*,10′*S*.

Compounds **1**–**6** were tested for *in vitro* antiplasmodial activity (*Plasmodium falciparum* K1 strain) and for cytotoxicity in rat skeletal fibroblasts (L6-cell line) (Table 2). Disesquiterpene coumarin **1** showed moderate activity against *Plasmodium falciparum* (IC_{50} = 2.6 μM) with moderate selectivity index of 5.9 (selectivity index = IC_{50} of the L6 cells (cytotoxicity) divided by IC_{50} of the parasite), while compounds **2** and **5** were non-selectively cytotoxic. The IC_{50} values of compounds **3**, **4** and **6** were greater than 10 μM in the antiplasmodial assay. It seems that in the biosynthesis of the compounds, the key structure is compound **2** because cleavage of the C-3′/C-4′ bond provides entry into the same framework as compounds **1**, **3** and **4**.

3. Conclusions

The first disesquiterpene coumarin, a new sesquiterpene coumarin, four known sesquiterpene coumarins, and a sesquiterpene were isolated from the roots of *F. pseudalliacea*. The configurations of compound **1**–**4** were determined as 8′*S*,9′*S*,10′*S*,1″*S**,9″*R**,10″*S** (sanandajin), 4′*S*,5′*R*,6′*S*, 8′*S*,9′*S*,10′*R* (kamolonol acetate), 8′*S*,9′*S*,10′*S*, (fekrynol acetate) and 8′*S*,9′*S*,10′*S*, (ethyl galbanate), respectively. The occurrence of sesquiterpene coumarins in higher plants is essentially limited to the families Apiaceae and Asteraceae, where they have been reported from the genus *Ferula* (Murray et al., 1982; Nazari and Iranshahi, 2011), and *Artemisia*, *Achillea* and *Anthemis*, respectively (Hofer et al., 1983; Hofer and Greger, 1984). There have been reports on isolation of these compounds from other families, e.g., Euphorbiaceae (Fraga, 2005). Whether disesquiterpene coumarins are a unique feature of *F. pseudalliacea* remains to be clarified by a targeted search for such compounds. The sesquiterpene coumarins in Apiaceae and Asteraceae differ by the substitution pattern of the coumarin moiety. Umbelliferone derived sesquiterpene ethers are characteristic of Apiaceae, whereas isofraxidin (7-hydroxy-6,8-dimethoxycoumarin) and occasionally scopoletin (7-hydroxy-6-methoxycoumarin) are the typical coumarin residues in the Asteraceae. The absolute configuration of the sesquiterpene moiety has been established for

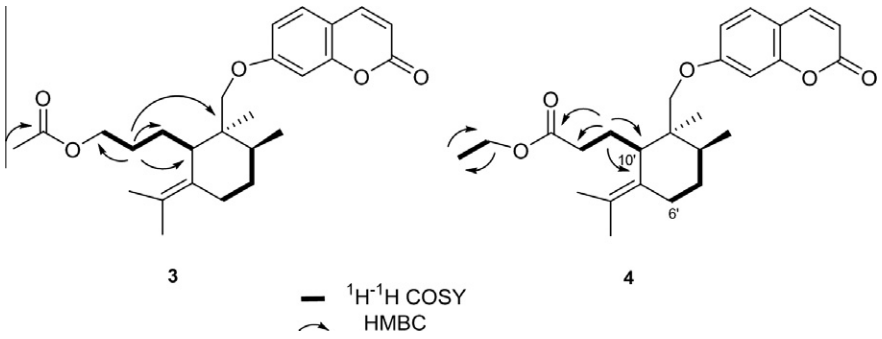

Fig. 8. Key COSY and HMBC correlations of **3** and **4**.

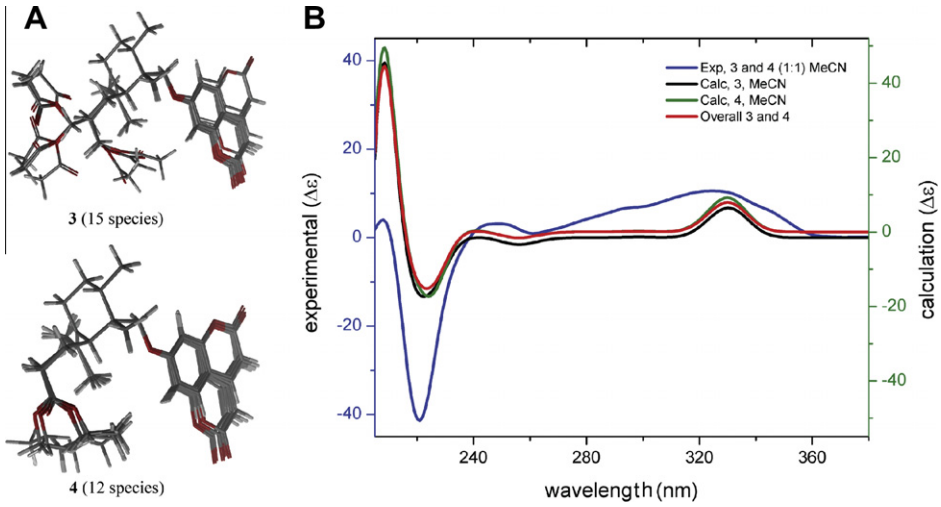

Fig. 9. (A) Minimized conformers of **3** and **4** in gas phase using DFT at the B3LYP/6-31G* level. (B) Experimental (blue) and calculated (black and green) ECD spectra of **3** and **4**. Calculated spectra were obtained via averaging of simulated spectra of compounds (ratio 1:1) by using TDDFT at B3LYP/6-31G* level in MeCN. (For interpretation of the references to colour in this figure legend, the reader is referred to the web version of this article.)

Table 2
Activity of compounds **1**–**6** against *Plasmodium falciparum* and L-6 cells.

Compound	IC_{50} (*P. falciparum* K1)	IC_{50} (L-6 cells)
Sanandajin (**1**)	2.6 ± 0.1[a]	9.4 ± 0.1[a]
Kamolonol acetate (**2**)	16.1 ± 0.4	7.5 ± 0.1
Fekrynol acetate (**3**)	NA[b]	ND[c]
Ethyl galbanate (**4**)	NA	ND
Methyl galbanate (**5**)	7.1 ± 0.1	4.3 ± 0.2
Farnesiferol B (**6**)	NA	35.7 ± 0.3
Artemisin	0.004	
Podophyllotoxin		0.02

[a] IC_{50} in μM with standard deviation.
[b] NA: not active (IC_{50} > 10 μM).
[c] ND: not determined.

selected sesquiterpene coumarin ethers, either by Horeau esterification, or by chemical degradation to compounds of known absolute stereochemistry (Hofer et al., 1983; Hofer and Greger, 1984). Earlier CD studies with non-derivatized sesquiterpene coumarin ethers to solely a CE in the 200 nm region into consideration seem questionable in conclusions (Miseeva et al., 1978).

Coumarins possess a broad range of biological activities, but data on antiplasmodial activity of coumarins are scarce (Argotte-Ramos et al., 2006; Lee et al., 2003; Muthaura et al., 2011; Oketch-Rabah et al., 2000). The reported *in vitro* activities so far showed moderate inhibition for these compounds (Ma et al., 2006; Ross et al., 2008; Subeki et al., 2005; Yenjai et al., 2000). Thus, compound **1** is among the most potent non-phototoxic coumarins.

4. Experimental

4.1. General experimental procedures

Melting points were determined on an Electrothermal melting point apparatus. Optical rotations were measured on a Perkin-Elmer 341 polarimeter. UV spectra were recorded on a Shimadzu UV-PC 2501 spectrometer. IR spectra were recorded on a Bruker Tensor 27 FT-IR spectrometer. ECD spectra of compounds **1**–**4** were recorded in MeCN on a AVIV CD spectrometer model 62ADS and analyzed with the AVIV 60DS V4.1 software. NMR spectra were measured on a Bruker DRX-500 spectrometer. HR-ESIMS spectra were acquired on a Bruker MicroTOF ESI-MS system. GPC separations were performed with a Knauer apparatus (Smartline pumps including a 50 mL pump (EA4301 V4), UV and RI detector). The column was Nucleogel 100-5 (300 × 7.7 mm; Macherey Nagel). $CHCl_3$ was used as eluent, and the flow rate was 1 mL/min. Semi-preparative HPLC was carried out with an Eurospher 100-7 RP C_{18} (250 × 20 mm; Macherey Nagel) column with a MeOH-H_2O gradient. Silica gel (70–230 and 230–400 mesh, Merck) and RP C_{18} (230–400 mesh, Fluka) were used for column chromatography. Silica TLC was performed on Merck F254 silica gel plates (10 × 10 cm).

4.2. Plant material

Roots of *F. pseudalliacea* were collected from Sanandaj (Senadezh) mountains, Kurdistan Province, Iran, in September 2008 at an altitude of 1500 m, and identified. A voucher specimen (MPH-1197) is deposited in the Herbarium of the Medicinal Plants and Drugs Research Institute, Shahid Beheshti University, Iran.

4.3. Extraction and isolation

The roots (1 kg) *F. pseudalliacea* were crushed and extracted with *n*-hexane (3 × 4 L, rt for 24 h). Evaporation of solvent at reduced pressure afforded 28 g of a light brown gum. A portion (25 g) was fractionated on a silica gel column eluted with *n*-hexane–$CHCl_3$–EtOAc mixtures of increasing polarity (100:0:0, 8:2:0, 5:5:0, 0:100:0, 0:9:1, 0:3:7, respectively) to give fractions 1–11. Fraction 4 (5 g) was further purified on a silica gel column [*n*-hexane–EtOAc (19:1) to EtOAc], to afford nine fractions (4.1–4.9). Silica gel chromatography [*n*-hexane–$CHCl_3$–EtOAc (12:7:1–2:9: 9)] of fraction 4.5 afforded five fractions (4.5.1–4.5.5). GPC of fraction 4.5.1 gave **1** (12 mg). Silica gel chromatography [*n*-hexane–$CHCl_3$–EtOAc (8:11:1–4:8:8)] of fraction 4.5.3 gave four fractions (4.5.3.1–4.5.3.4) together with aristolone (Rucker et al., 1984) (**7**, 8 mg). Methyl galbanate (Iranshahi et al., 2007) (**5**, 23 mg) was isolated from fraction 4.5.3.1 on a reversed-phase (C_{18}) column [C_3H_6O–H_2O (8:2)]. Fraction 4.8 was separated over a silica gel column [*n*-hexane–EtOAc (8:2–2:8)], to afford a mixture of fekrynol acetate and ethyl galbanate (**3** and **4**, 13 mg). Silica gel chromatography [*n*-hexane–EtOAc (7:3–4:6)] of fraction 8 (2.0 g) afforded five fractions (8.1–8.5). Farnesiferol B (Iranshahi et al., 2007) (**6**, 15 mg) was obtained from fraction 8.1 on a silica gel column [*n*-hexane–EtOAc (19:1–1:1)] and semi-preparative RP-HPLC (MeOH in H_2O (80–100% MeOH). Compound **2** (30 mg) was purified from fraction 8.4 on a silica gel column [*n*-hexane–$CHCl_3$ (8:2–1:9)].

4.4. Spectroscopic data of new compounds

4.4.1. Sanandajin (*1*)

Colorless gum; $[\alpha]_D^{25}$: +20.0 (*c* = 0.5, $CHCl_3$); UV ($CHCl_3$) λ_{max} (log ε) 324 (3.89), 238 (3.59) nm; IR (KBr) ν_{max} 2924, 2854, 1735, 1616, 1456, 1153–1069 cm^{-1}; ^1H NMR ($CDCl_3$, 500 MHz) and ^{13}C NMR ($CDCl_3$, 125 MHz), see Table 1; CD (MeCN, *c* = 0.183 mM, 0.1 cm patch length): $[\theta]_{233} = -10{,}396$, $[\theta]_{258} = -7053$, $[\theta]_{325} = 20{,}414$; HR-ESIMS *m/z* 623.3722 $[M+Na]^+$ (calcd for $C_{39}H_{52}O_5Na$, 623.3712).

4.4.2. Kamolonol acetate (*2*)

Colorless crystals ($CHCl_3$); mp 217–219 °C; $[\alpha]_D^{25}$: −8.0 (*c* = 1, $CHCl_3$); UV ($CHCl_3$) λ_{max} (log ε) 323 (4.01), 238 (3.5) nm; IR (KBr) ν_{max} 2924, 1726, 1612, 1510, 1426, 1236 cm^{-1} H NMR ($CDCl_3$, 500 MHz) and ^{13}C NMR ($CDCl_3$, 125 MHz), see Table 1; CD (MeCN, *c* = 0.9 mM, 0.1 cm patch length): $[\theta]_{215} = 2040$, $[\theta]_{290} = 5602$, $[\theta]_{322} = -5112$; HR-ESIMS *m/z* 463.2061 $[M+Na]^+$ (calcd for $C_{26}H_{32}O_6$ Na, 463.2097).

4.5. X-ray crystal structure analysis of kamolonol acetate (*2*)

The X-ray diffraction measurements were made on a STOE IPDS 2T diffractometer with graphite-monochromated Mo K_α radiation. For data collection, a colorless block crystal with dimensions of 0.40 × 0.25 × 0.23 mm was chosen and mounted on a glass fiber. Cell constants and an orientation matrix for data collection were obtained by least-squares refinement of diffraction data from 4804 unique reflections. Data were collected at a temperature of 298(2) K to a maximum 2θ value of 58.60° for **2** and in a series of ω scans in 1° oscillations and integrated using the Stoe X-AREA (Stoe and Cie, 2009) software package. The structures were solved by direct methods and subsequent difference Fourier maps, and refined on F^2 by a full-matrix least-squares procedure using anisotropic displacement parameters (Sheldrick, 1997). The compound crystallize in $P2_12_12_1$ space group of orthorhombic system with cell constants of *a* = 8.8921(18), *b* = 15.765(3) and *c* = 16.792(3). All hydrogen atoms were located in ideal positions and then refined isotropically. Subsequent refinement was converged with $R_1 = 0.0577$ $[I > 2.00\sigma(I)]$ and $wR_2 = 0.1168$. All refinements were performed using the X-STEP32 crystallographic software package (Stoe and Cie, 2000). Crystallographic data have been deposited with the Cambridge Crystallographic Data Center under CCDC 823135. These data can be obtained free of charge via www.ccdc.cam.ac.uk/deposit (or from the CCDC, 12Union Road, Cambridge CB2 1EZ, UK; fax: +44 1223 336033; deposit@ccdc.cam.ac.uk).

4.6. Conformational analysis, geometrical optimization, and ECD calculation

Conformational analysis of compounds **1**, **2**, **3**, and **4** were performed with Schrödinger MacroModel 9.1 software using the OPLS 2005 (Optimized Potential for Liquid Simulations) force field in H_2O. Conformers occurring within a 2 kcal/mol energy window from the global minimum were chosen for geometrical optimization and energy calculation using density function theory (DFT) with the B3LYP functional and the 6-31G* basis-set in the gas-phase with the Gaussian 09 program (Frisch et al., 2009). Vibrational analysis was done at the same level to confirm minima. TD-DFT/B3LYP/6-31G* in the gas phase and in MeCN using the SCRF (self-consistent reaction field) method with the CPCM (*Conductor*-like *polarizable* continuum) model, was employed to calculate excitation energy (denoted by wavelength in nm) and rotatory strength *R* in dipole velocity (R_{vel}) and dipole length (R_{vel}) forms. ECD curves were calculated based on rotatory strengths using a half bandwidth of 0.3 eV with conformers of **1**, **2**, **3**, and **4** using Gausssum 2.2 software (O'Boyle et al., 2009). The spectra were combined after Boltzmann weighting according to their population contribution.

4.7. Antiplasmodial assays

Tests of extracts and pure substances were done as previously described (Adams et al., 2009b). IC_{50} values were calculated from sigmoidal concentration inhibitions curves. Assays were run in two independent experiments in duplicate.

Acknowledgment

We are grateful to Shahid Beheshti University Research Council for partial support of this work.

Appendix A. Supplementary data

Supplementary data associated with this article can be found, in the online version, at doi:10.1016/j.phytochem.2012.02.016.

References

Abd El-Razek, M.H., Ohta, S., Ahmed, A.A., Hirata, T., 2001. Sesquiterpene coumarins from the roots of *Ferula assa-foetida*. Phytochemistry 58, 1289–1295.

Adams, M., Plitzko, I., Kaiser, M., Brun, R., Hamburger, M., 2009a. Anti-plasmodial flavonoid from *Pistacia atlantica*. Phytochem. Lett. 2, 159–162.

Adams, M., Zimmermann, S., Kaiser, M., Brun, R., Hamburger, M., 2009b. Protocol for HPLC-based activity profiling for natural products with activities against tropical parasites. Nat. Prod. Commun. 4, 1377–1381.

Ahmed, A.A., 1999. Sesquiterpene coumarins and sesquiterpenes from *Ferula sinaica*. Phytochemistry 50, 109–112.
Argotte-Ramos, R., Ramírez-Avila, G., Rodríguez-Gutiérrez, M.C., Ovilla-Muñoz, M., Lanz-Mendoza, H., Rodríguez, M.H., González-Cortazar, M., Alvarez, L., 2006. Antimalarial 4-phenylcoumarins from the stem bark of *Hintonia latiflora*. J. Nat. Prod. 69, 1442–1444.
Bednyak, A.E., 1962. Materialy l-go [Pervogo] Vseros. S'ezda Farmatsevtov (Moscow: Med.) Sb. 182-94.
Eigner, D., Scholz, D., 1999. *Ferula asa-foetida* and *Curcuma longa* in traditional medical treatment and diet in Nepal. J. Ethnopharmacol. 67, 1–6.
Fraga, B.M., 2005. Natural sesquiterpenoids. Nat. Prod. Rep. 22, 465–486.
Frisch, M.J., Trucks, G.W., Schlegel, H.B., Scuseria, G.E., Robb, M.A., Cheeseman, J.R., Scalmani, G., Barone, V., Mennucci, B., Petersson, G.A., Nakatsuji, H., Caricato, M., Li, X., Hratchian, H.P., Izmaylov, A.F., Bloino, J., Zheng, G., Sonnenberg, J.L., Hada, M., Ehara, M., Toyota, K., Fukuda, R., Hasegawa, J., Ishida, M., Nakajima, T., Honda, Y., Kitao, O., Nakai, H., Vreven, T., Montgomery, J.A., Peralta, J.E., Ogliaro, F., Bearpark, M., Heyd, J.J., Brothers, E., Kudin, K.N., Staroverov, V.N., Kobayashi, R., Normand, J., Raghavachari, K., Rendell, A., Burant, J.C., Iyengar, S.S., Tomasi, J., Cossi, M., Rega, N., Millam, J.M., Klene, M., Knox, J.E., Cross, J.B., Bakken, V., Adamo, C., Jaramillo, J., Gomperts, R., Stratmann, R.E., Yazyev, O., Austin, A.J., Cammi, R., Pomelli, C., Ochterski, J.W., Martin, R.L., Morokuma, K., Zakrzewski, V.G., Voth, G.A., Salvador, P., Dannenberg, J.J., Dapprich, S., Daniels, A.D., Farkas, O., Foresman, J.B., Ortiz, J.V., Cioslowski, J., Fox, D.J. 2009. Gaussian 09, Revision A.02, Gaussian, Inc., Wallingford CT.
Hofer, O., Weissensteiner, W., Widhalm, M., 1983. Absolute-configurations and circular-dichroism of sesquiterpene-coumarin ethers. Monatsh. Chem. 114, 1399–1411.
Hofer, O., Greger, H., 1984. Naturally-occurring sesquiterpene-coumarin ethers, 6. new sesquiterpene-isofraxidin ethers from *Achillea depressa*. Monatsh. Chem. 115, 477–483.
Iranshahi, M., Amin, G., Shafiee, A., 2004. A new coumarin from *Ferula persica*. Pharm. Biol. 42, 440–442.
Iranshahi, M., Arfa, P., Ramezani, M., Jaafari, M.R., Sadeghian, H., Bassarello, C., Piacente, S., Pizza, C., 2007. Sesquiterpene coumarins from *Ferula szowitsiana* and in vitro antileishmanial activity of 7-prenyloxycoumarins against promastigote. Phytochemistry 68, 554–561.
Iranshahi, M., Hosseini, S.T., Shahverdi, A.R., Molazade, K., Khan, S.S., Ahmad, V.U., 2008. Diversolides A–G, guaianolides from the roots of *Ferula diversivittata*. Phytochemistry 69, 2753–2757.
Iranshahi, M., Rezaee, R., Sahebkar, A., Bassarello, C., Piacente, S., Pizza, C., 2009. Sesquiterpene coumarins from the fruits of *Ferula badrakema*. Pharm. Biol. 47, 344–347.
Kanani, M.R., Rahiminejad, M.R., Sonboli, A., Mozaffarian, V., Kazempour Osaloo, S., Ebrahimi, S.N., 2011. Chemotaxonomic significance of the essential oils of 18 *Ferula* species (Apiaceae) from Iran. Chem. Biodivers. 8, 503–517.
Lee, K.H., Chai, H.B., Tamez, P.A., Pezzuto, J.M., Cordell, G.A., Win, K.K., Tin-Wa, M., 2003. Biologically active alkylated coumarins from *Kayea assamica*. Phytochemistry 64, 535–541.
Ma, C., Zhang, H.J., Tan, G.T., Hung, N.V., Cuong, N.M., Soejarto, D.D., Fong, H.H., 2006. Antimalarial compounds from *Grewia bilamellata*. J. Nat. Prod. 69, 346–350.
Miseeva, G.P., Saidkhodzhaev, A.I., Khasanov, T.K., 1978. Circular dichroism of farnesiferol A and some of its analogs. Chem. Nat. Compd. 14, 110–111.
Murray, R.D.H., Mendez, J., Brown, S.A., 1982. The Natural Coumarins, first ed. John Wiley & Sons Inc., New York, pp. 555–559.
Muthaura, C.N., Keriko, J.M., Derese, S., Yenesew, A., Rukunga, G.M., 2011. Investigation of some medicinal plants traditionally used for treatment of malaria in Kenya as potential sources of antimalarial drugs. Exp. Parasitol. 127, 609–626.
Nazari, Z.E., Iranshahi, M., 2011. Biologically active sesquiterpene coumarins from *Ferula species*. Phytother. Res. 25, 315–323.
O'Boyle, N.M., Tenderholt, A.L., Langner, K.M., 2009. Cclib: a library for package-independent computational chemistry algorithms. J. Comput. Chem. 29, 839–845.
Oketch-Rabah, H.A., Mwangi, J.W., Lisgarten, J., Mberu, E.K., 2000. A new antiplasmodial coumarin from *Toddalia asiatica* roots. Fitoterapia 71, 636–640.
Pimenov, M.G., Leonov, M.V., 2004. The Asian Umbelliferae biodiversity database (ASIUM) with particular reference to South-West Asian taxa. Turk. J. Bot. 28, 139–145.
Ross, S.A., Krishnaven, K., Radwan, M.M., Takamatsu, S., Burandt, C.L., 2008. Constituents of *Zanthoxylum flavum* and their antioxidant and antimalarial activities. Nat. Prod. Commun. 3, 791–794.
Rucker, G., Mayer, R., Breitmaier, E., Will, G., Kirfel, A., El, M., 1984. Oxidized aristolane sesquiterpenes from *Aristolochia debilis*. Phytochemistry 23, 1647–1649.
Sheldrick, G.M., 1997. SHELX97: Program for Crystal Structure Solution and Refinement. University of Göttingen, Göttingen, Germany.
Ślusarczyk, S., Zimmermann, S., Kaiser, M., Matkowski, A., Hamburger, M., Adams, M., 2011. Antiplasmodial and antitrypanosomal activity of tanshinone-type diterpenoids from *Salvia miltiorrhiza*. Planta Med. 77, 1594–1596.
Stoe, Cie, 2000. X-STEP32, Version 107b: Crystallographic Package. Stoe & Cie GmbH, Darmstadt, Germany.
Stoe, Cie, 2009. X-AREA, Version 1.31: Program for the Acquisition and Analysis of Data. Stoe & Cie GmbH, Darmstadt, Germany.
Subeki, S., Matsuura, H., Takahashi, K., Yamasaki, M., Yamato, O., Maede, Y., Katakura, K., Kobayashi, S., Trimurningsih, T., Chairul, C., Yoshihara, T., 2005. Anti-babesial and anti-plasmodial compounds from *Phyllanthus niruri*. J. Nat. Prod. 68, 537–539.
Tamemoto, K., Takaishi, Y., Chen, B., Kawazoe, K., Shibata, H., Higuti, T., Honda, G., Ito, M., Takeda, Y., Kodzhimatov, O.K., Ashurmetov, O., 2001. Sesquiterpenoids from the fruits of *Ferula kuhistanica* and antibacterial activity of the constituents of *F. kuhistanica*. Phytochemistry 58, 763–767.
Veselovskaya, N.V., Sklyar, Y.E., Savina, A.A., 1981. Fekrynol and its acetate from *Ferula krylovii*. Khim. Prir. Soedin. 17, 798–799.
Yenjai, C., Sripontan, S., Sriprajun, P., Kittakoop, P., Jintasirikul, A., Tanticharoen, M., Thebtaranonth, Y., 2000. Coumarins and carbazoles with antiplasmodial activity from *Clausena harmandiana*. Planta Med. 66, 277–279.
Zargari, A., 1997. Medicinal Plants, 2. Tehran University Publications, Tehran.
Zaugg, J., Ebrahimi, S.N., Smiesko, M., Baburin, I., Hering, S., Hamburger, M., 2011. Identification of GABA A receptor modulators in *Kadsura longipedunculata* and assignment of absolute configurations by quantum-chemical ECD calculations. Phytochemistry 72, 2385–2395.
Zhou, P., Takaishi, Y., Duan, H., Chen, B., Honda, G., Itoh, M., Takeda, Y., Kodzhimatov, O.K., Lee, K.-H., 2000. Coumarins and bicoumarin from *Ferula sumbul*: anti-HIV activity and inhibition of cytokine release. Phytochemistry 53, 689–697.

Supplementary Data

Disesquiterpene and Sesquiterpene Coumarins from *Ferula pseudalliacea*, and determination of their absolute configurations by quantum-chemical ECD calculations

Dara Dastan[a], Peyman Salehi[,a], Ahmad Reza Gohari*[,b], Stefanie Zimmermann[c, d], Marcel Kaiser[d,e] , Matthias Hamburger[c], Hamid Reza Khavasi[f] and Samad Nejad Ebrahimi[a,c]*

[a]*Department of Phytochemistry, Medicinal Plants and Drugs Research Institute, Shahid Beheshti University, G. C., Evin, Tehran, Iran*

[b]*Medicinal Plants Research Center, Faculty of Pharmacy, Tehran University of Medical Sciences, Tehran, Iran*

[c]*Division of Pharmaceutical Biology, University of Basel, Klingelbergstrasse 50, 4056 Basel, Switzerland*

[d]*Department of Medical Parasitology and Infection Biology, Swiss Tropical and Public Health Institute , 4002 Basel, Switzerland*

[e]*University of Basel, 4003 Basel, Switzerland*

[f]*Department of Chemistry, Shahid Beheshti University, G. C., Evin, Tehran, Iran*

*To whom correspondence should be addressed. Tel: +982129902679. Fax: +98 2122431783.

E-mail address: p-salehi@sbu.ac.ir (P. Salehi). goharii_a@sina.tums.ac.ir (A. R.Gohari).

List of the spectrum and Figure

S1. HR-ESIMS of **1**

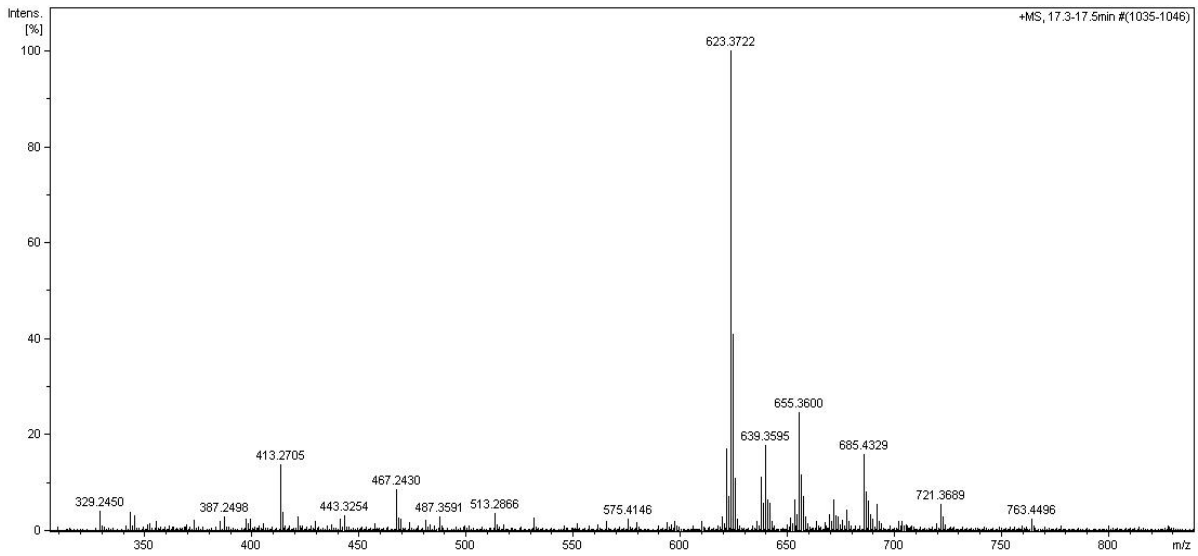

S2. ^{1}H NMR (500 MHz, CDCl3) of **1**

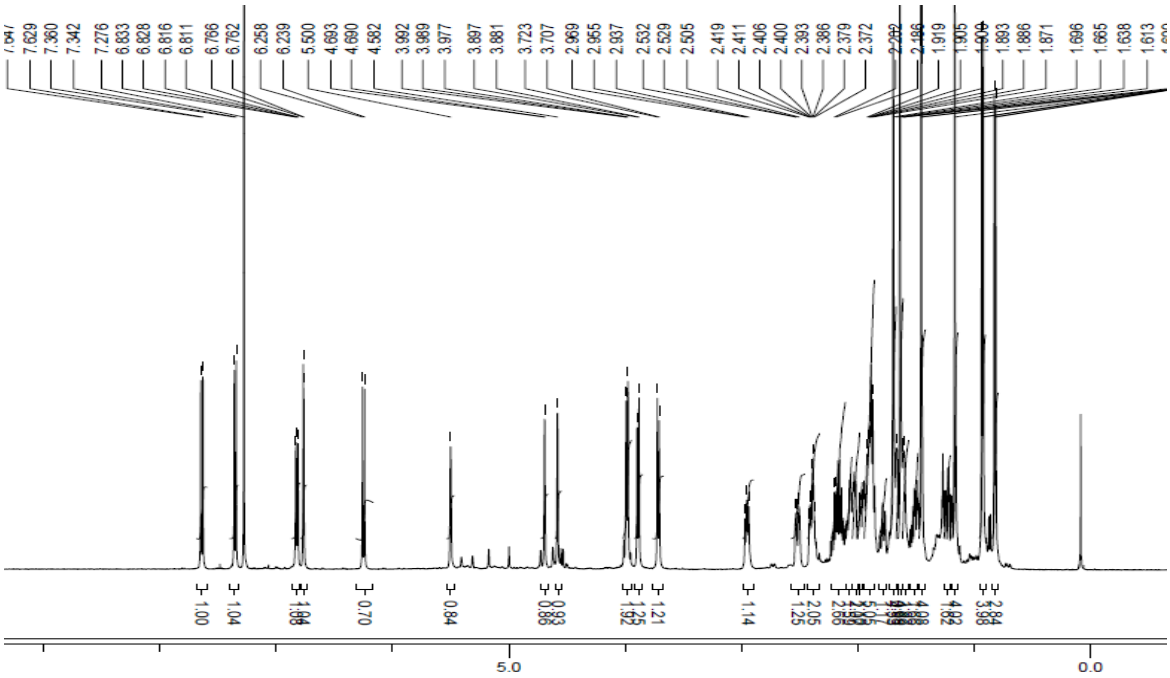

S3. Expansion of the ^{1}H NMR (500 MHz, CDCl3) of **1**

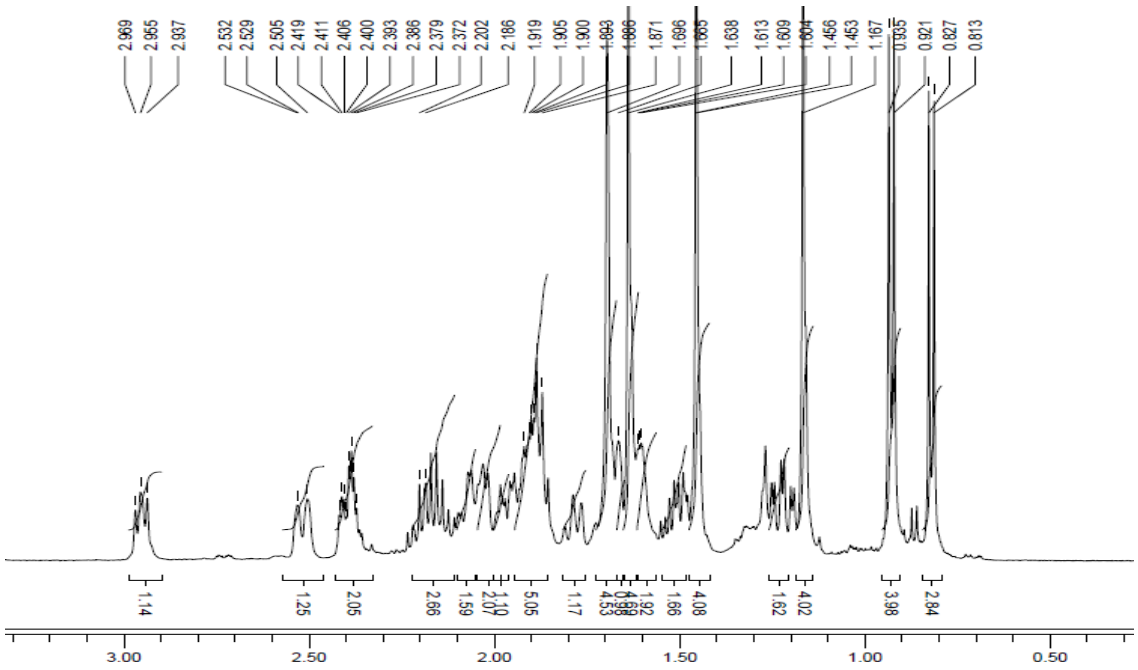

S4. ^{13}C NMR (125 MHz, CDCl3) of **1**

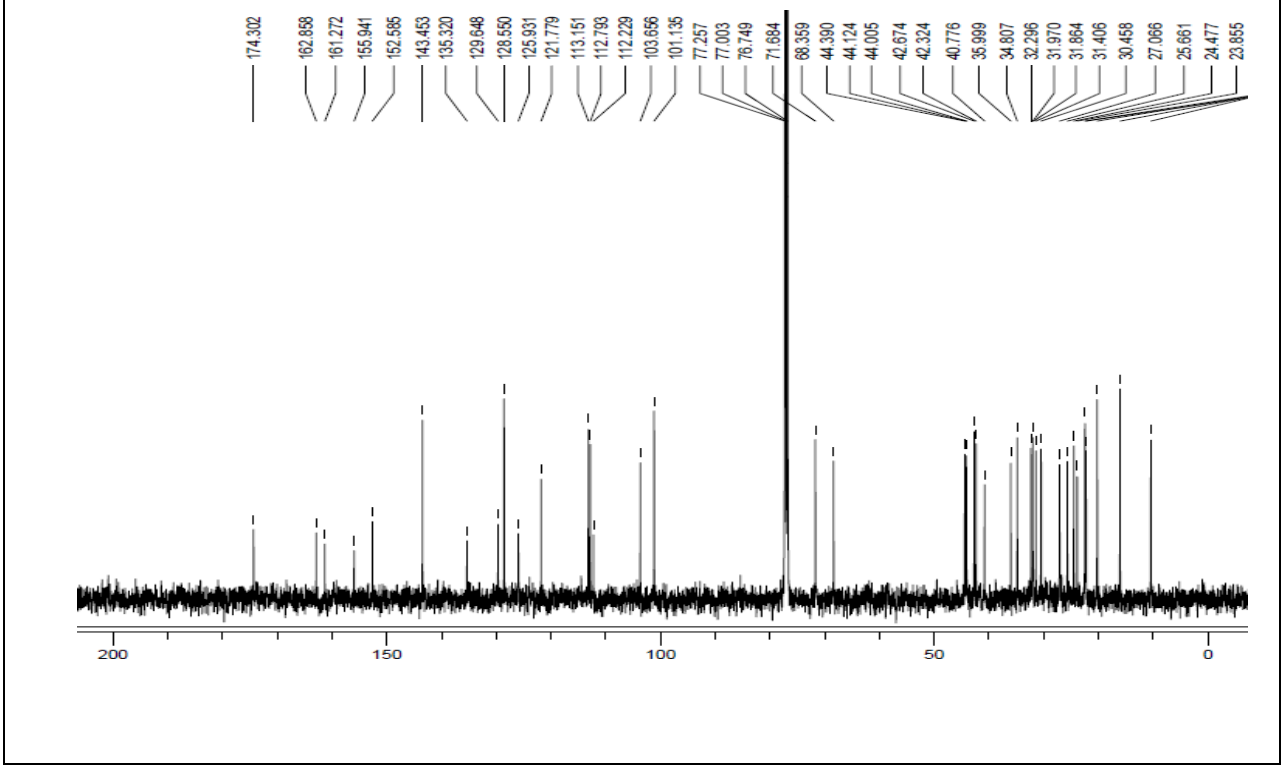

S5. DEPT 90 (500 MHz, CDCl3) of **1**

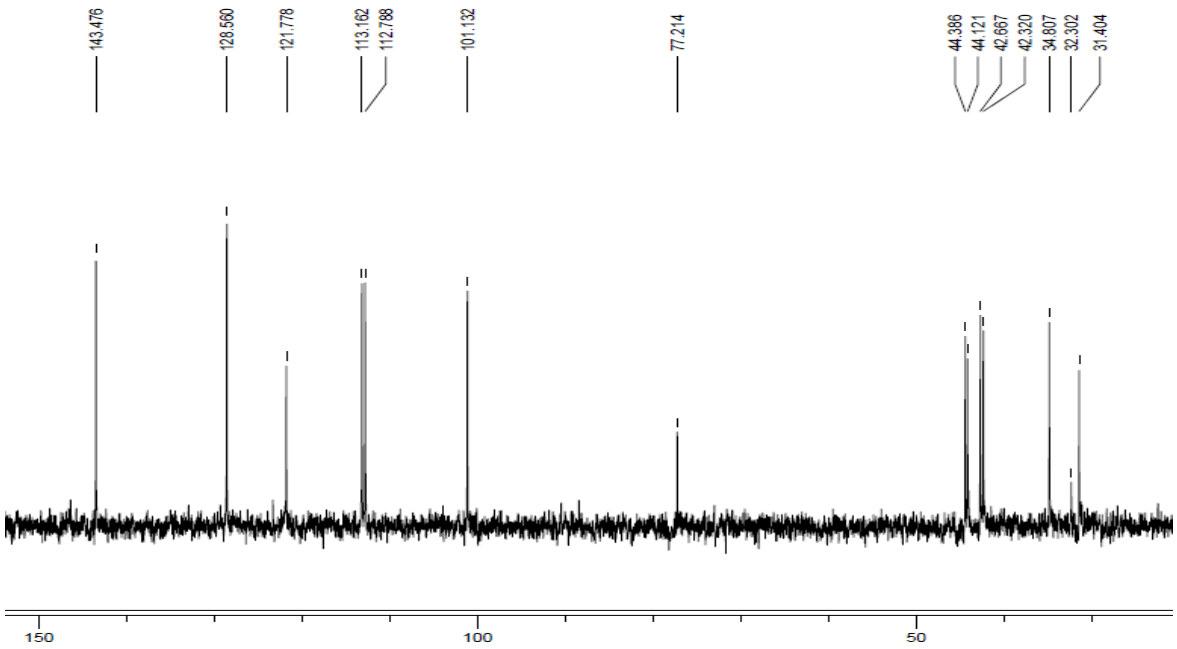

S6. DEPT 135 (500 MHz, CDCl3) of **1**

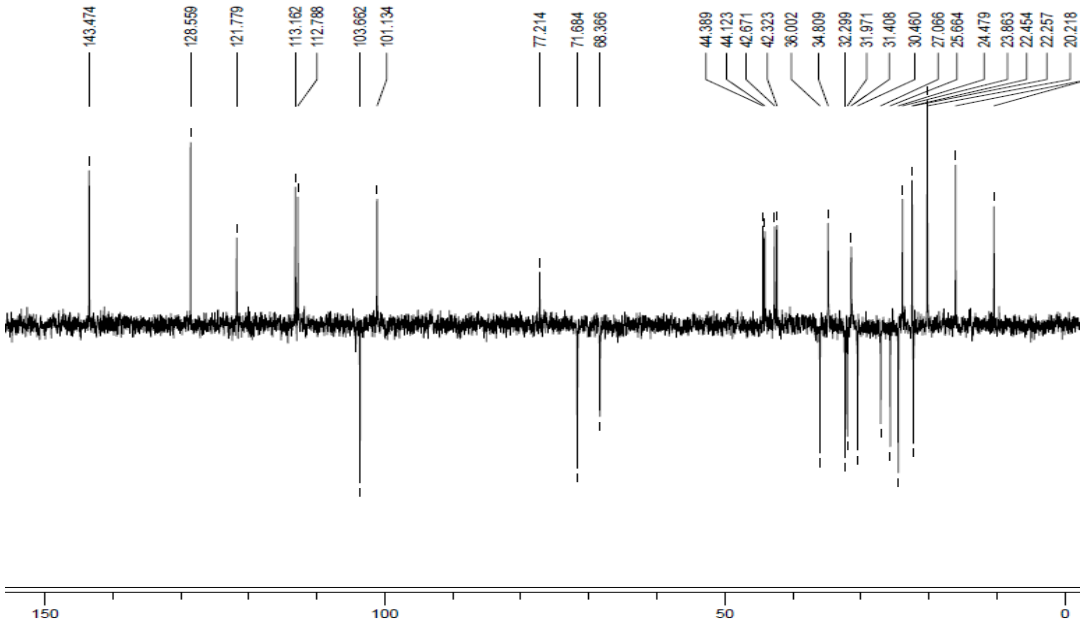

S7. COSY (500 MHz, CDCl3) of **1**

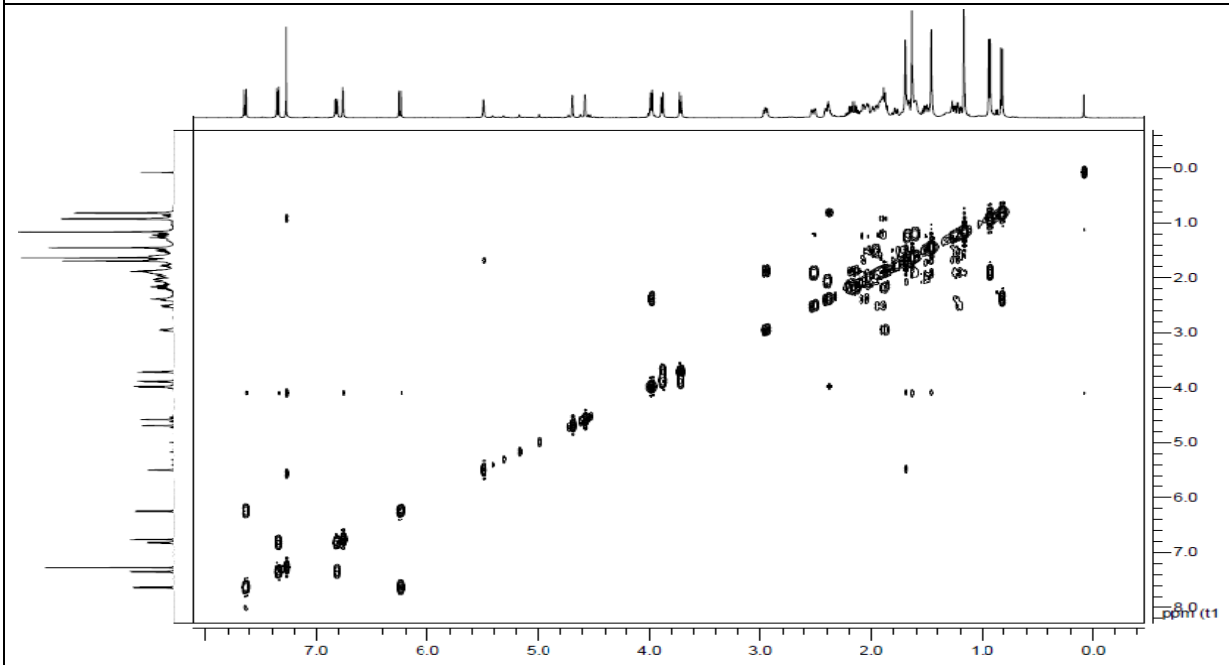

S8. Expansion of the COSY (500 MHz, CDCl3) of **1**

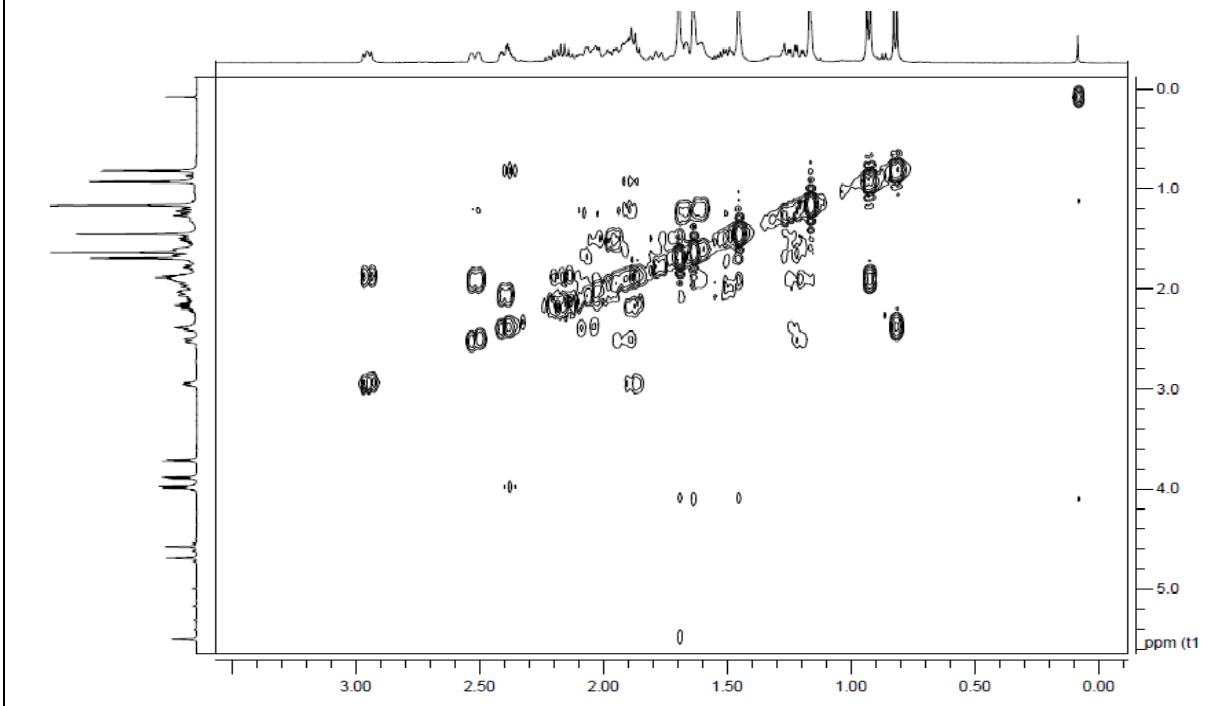

S9. HSQC (500 MHz, CDCl3) of **1**

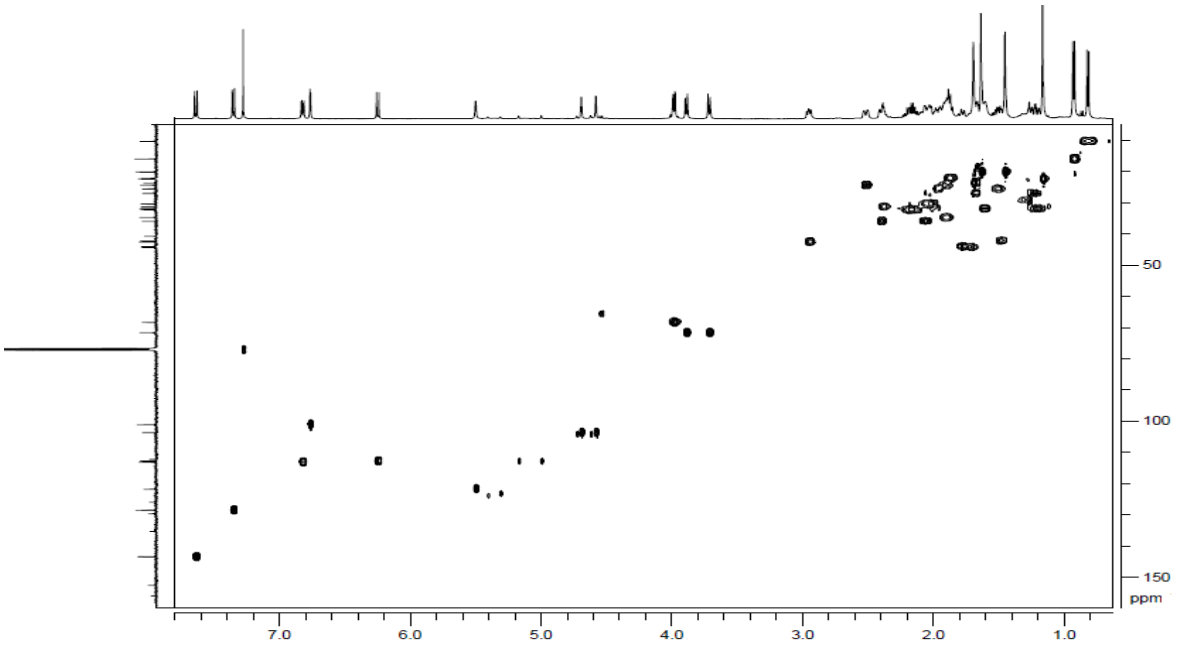

S10. Expansion of the HSQC (500 MHz, CDCl3) of **1**

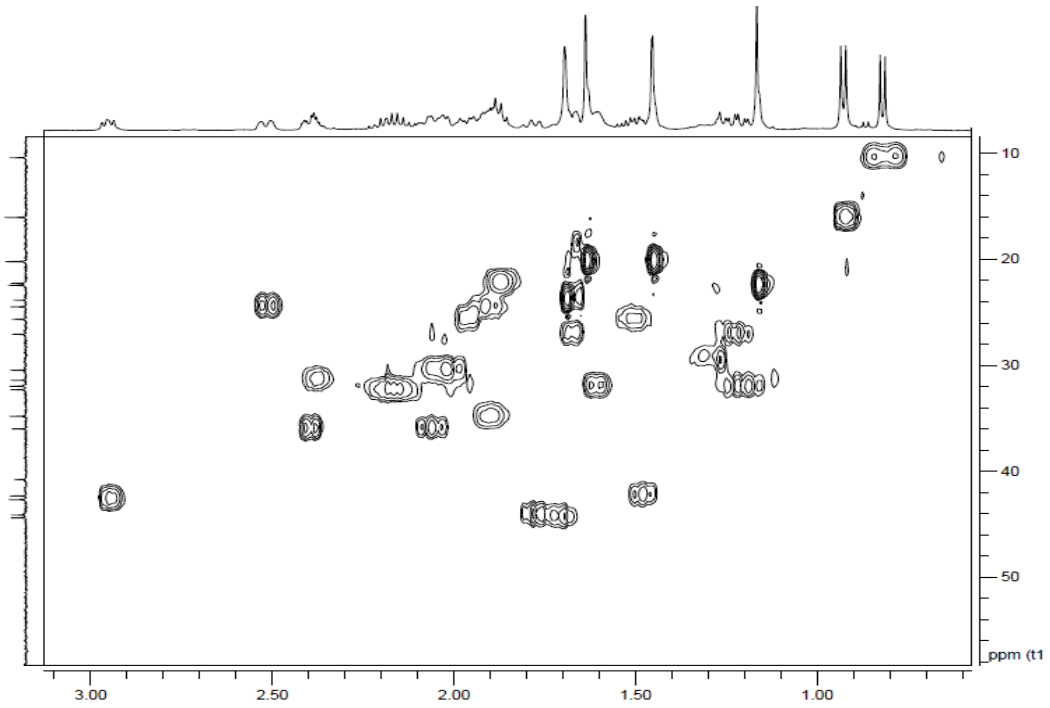

S11. HMBC (500 MHz, CDCl3) of **1**

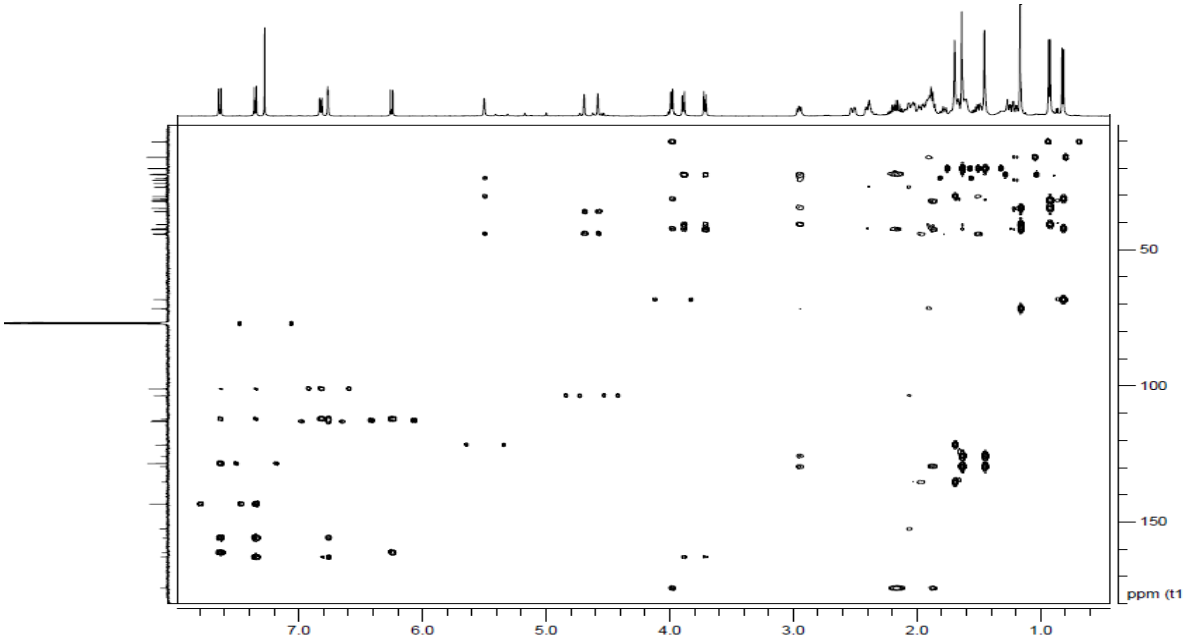

S12. Expansion of the HMBC (500 MHz, CDCl3) of **1**

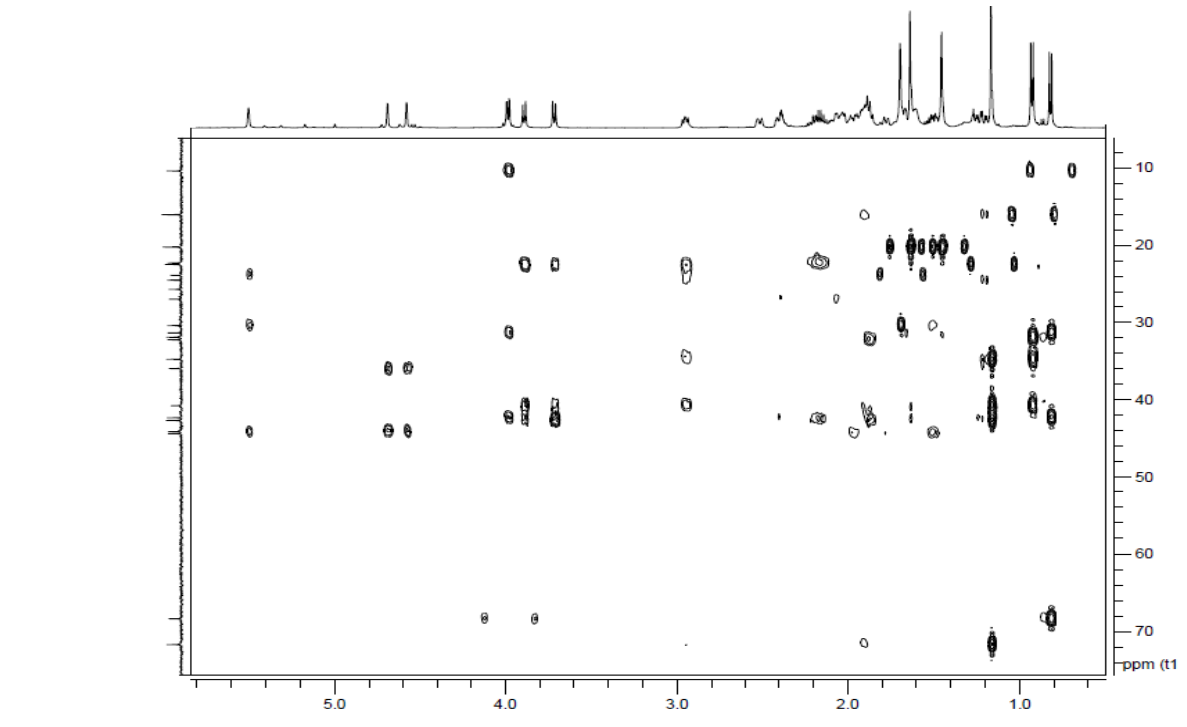

S13. NOESY (500 MHz, CDCl3) of **1**

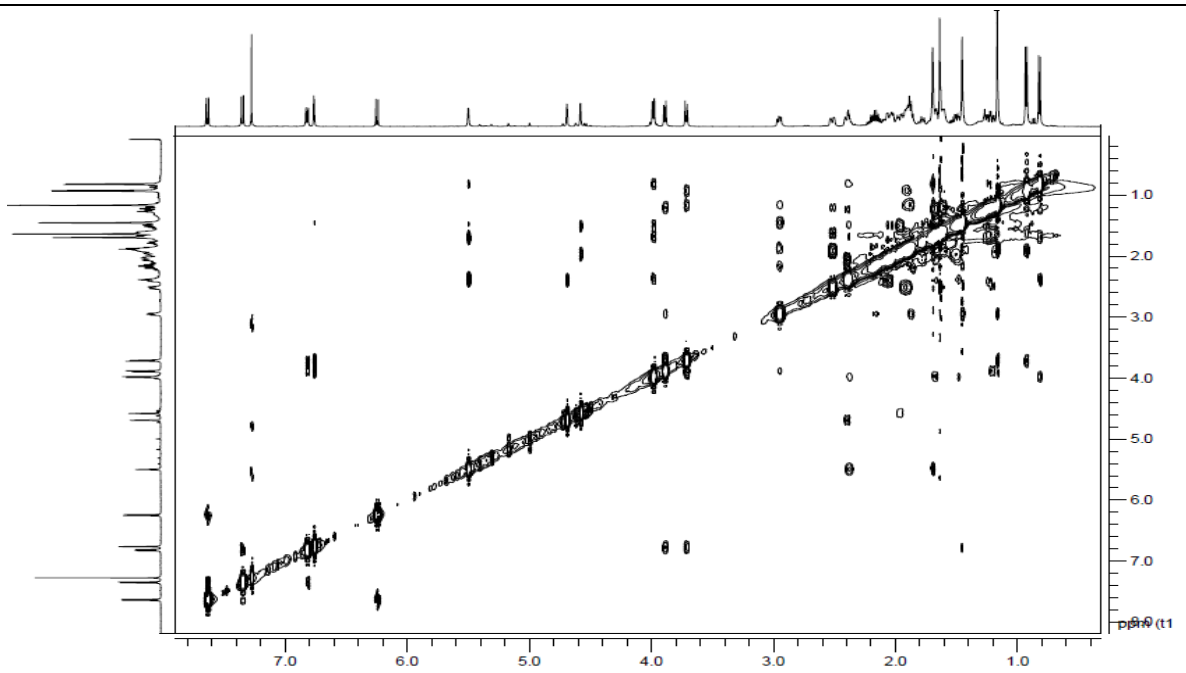

S14. Expansion of the NOESY (500 MHz, CDCl3) of **1**

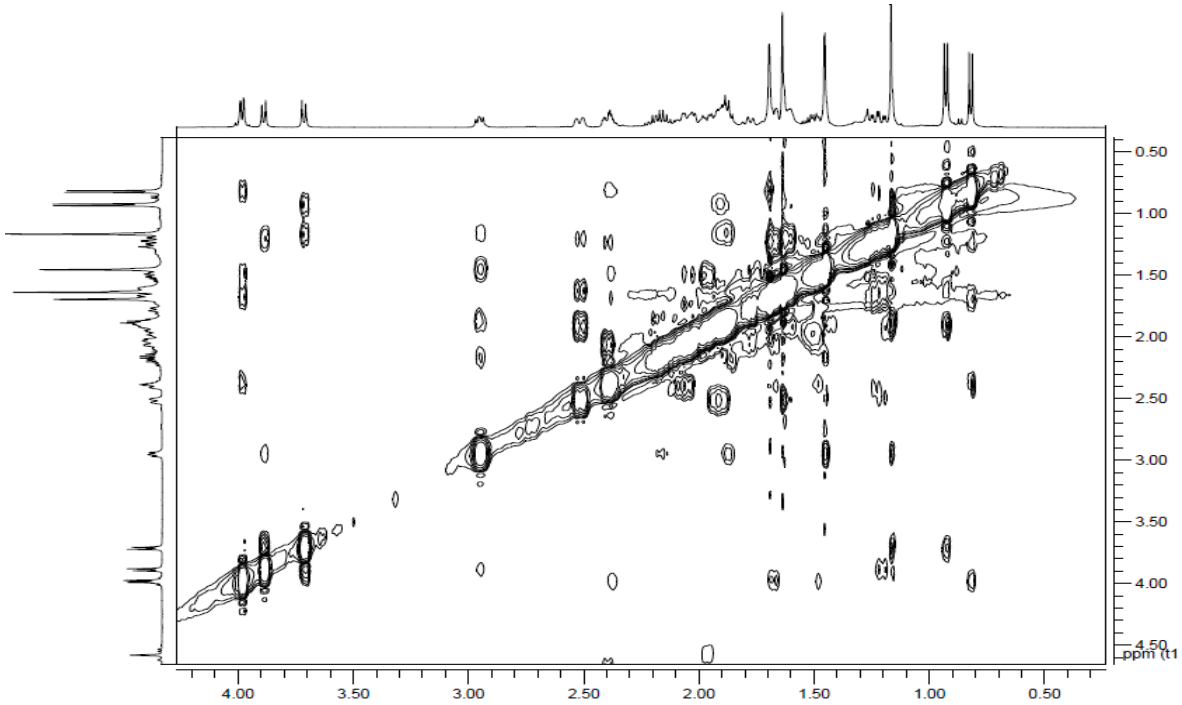

S15. HR-ESIMS of **2**

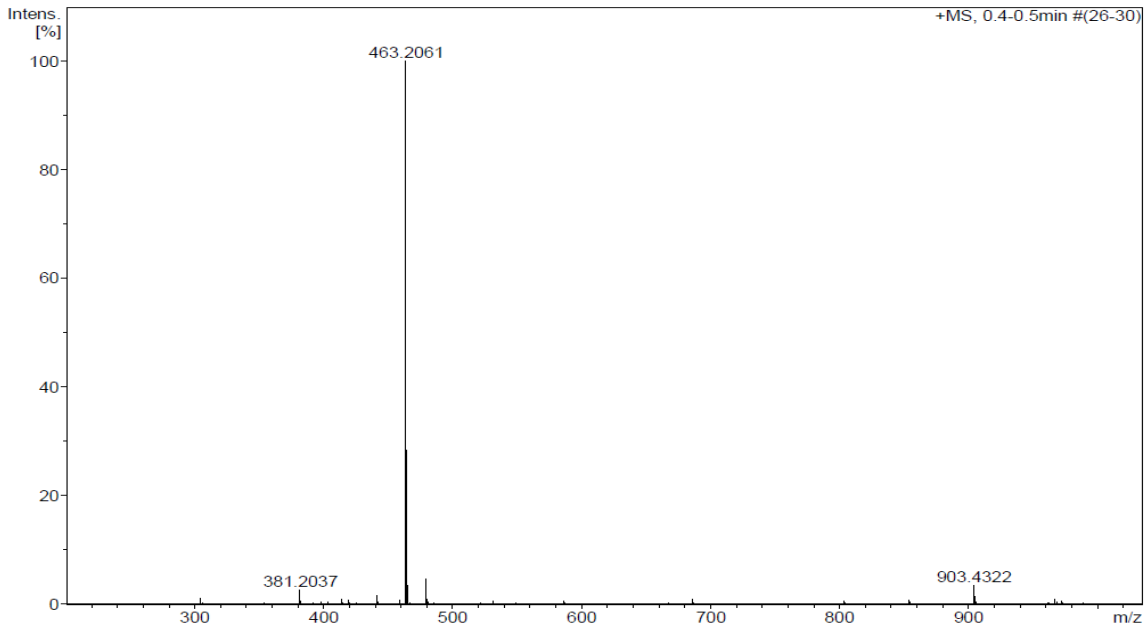

S16. ^{1}H NMR (500 MHz, CDCl3) of **2**

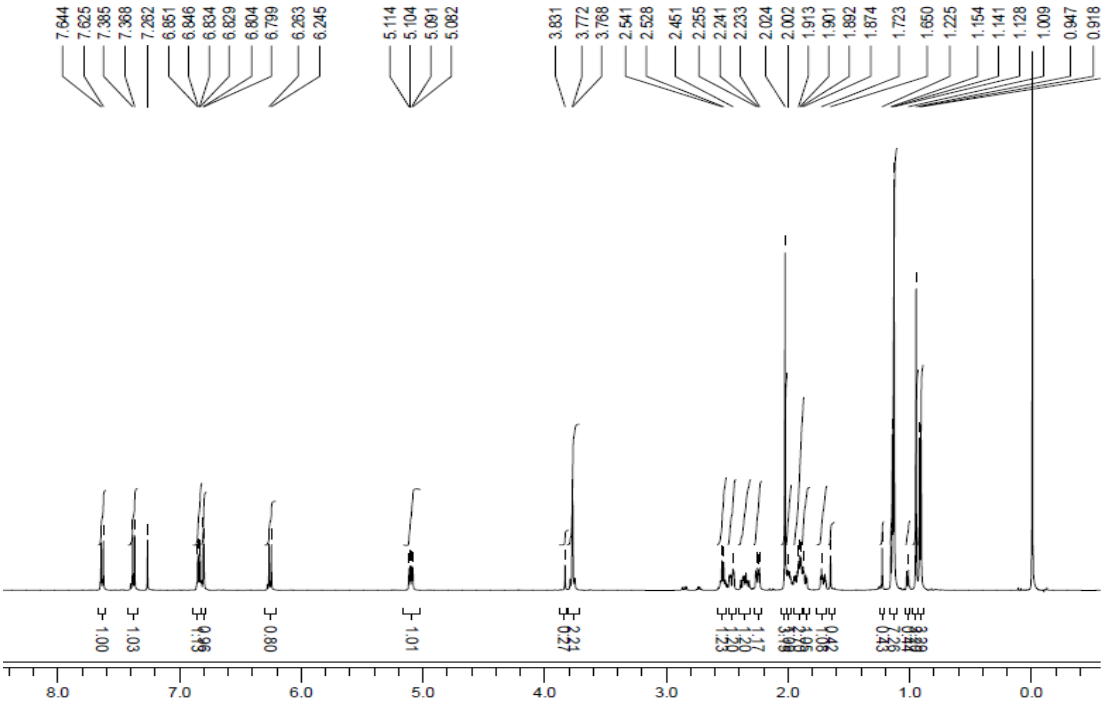

S17. Expansion of the ^{1}H NMR (500 MHz, CDCl3) of **2**

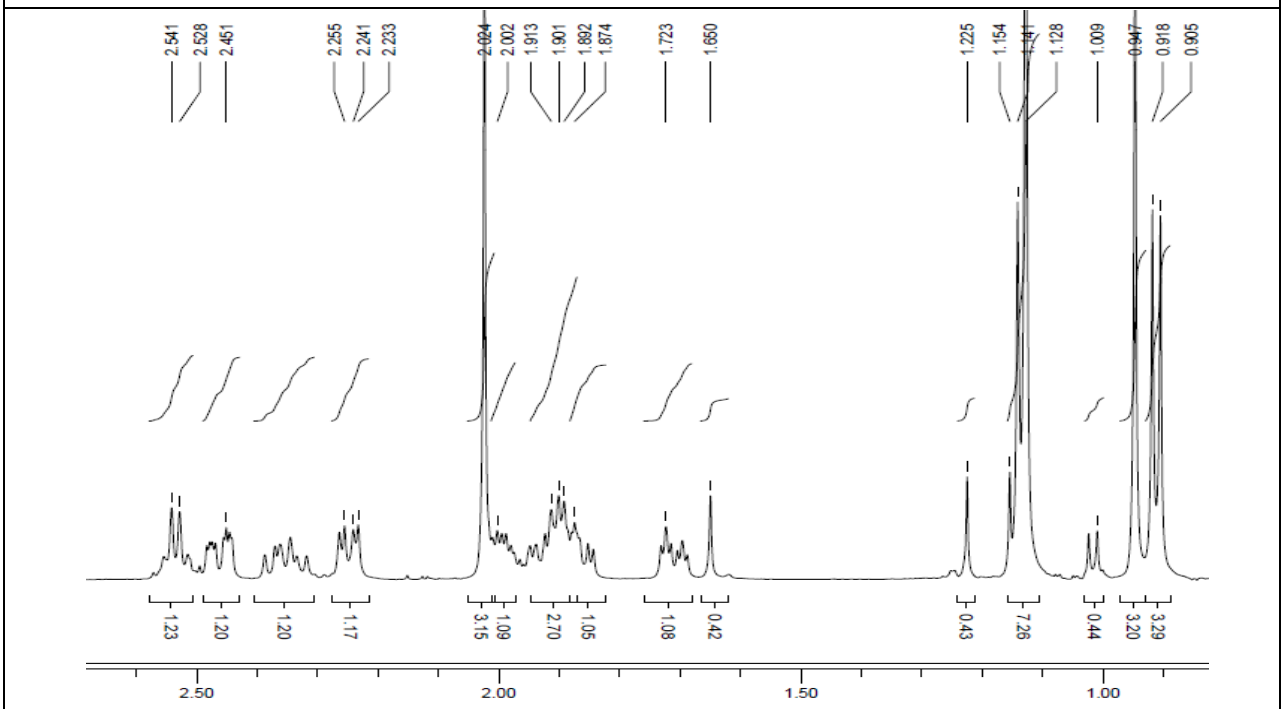

S18. ^{13}C NMR (125 MHz, CDCl3) of **2**

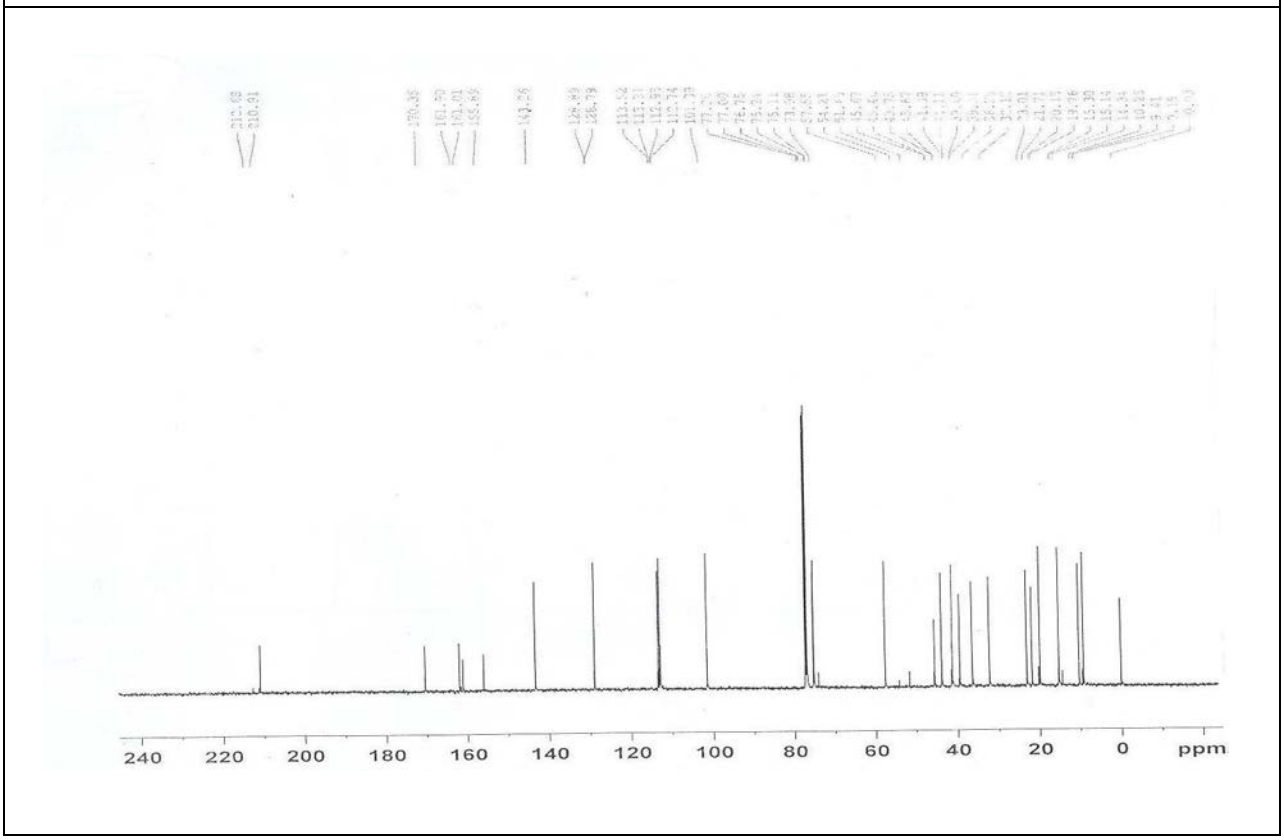

S19. DEPT 90 (500 MHz, CDCl3) of **2**

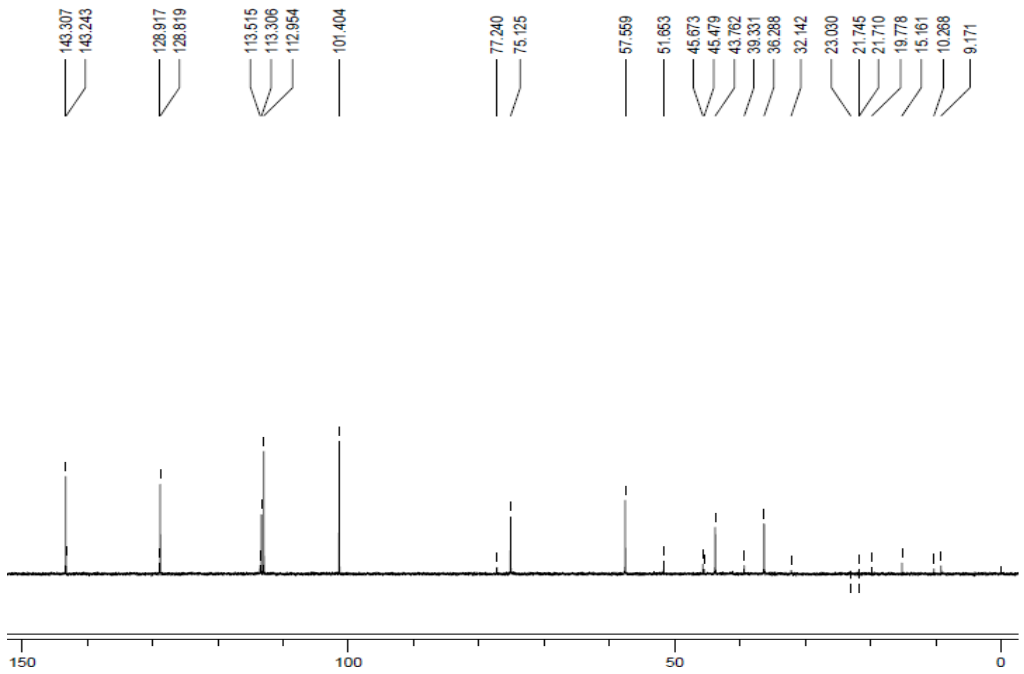

S20. DEPT 135 (500 MHz, CDCl3) of **2**

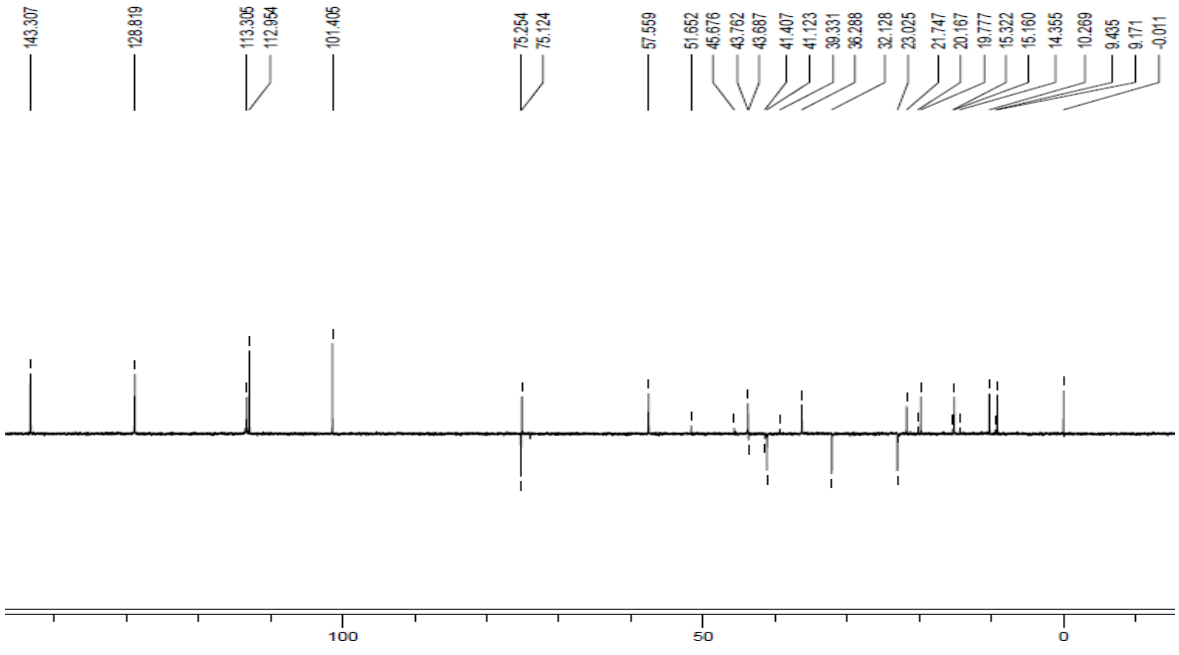

S21. HSQC (500 MHz, CDCl3) of **2**

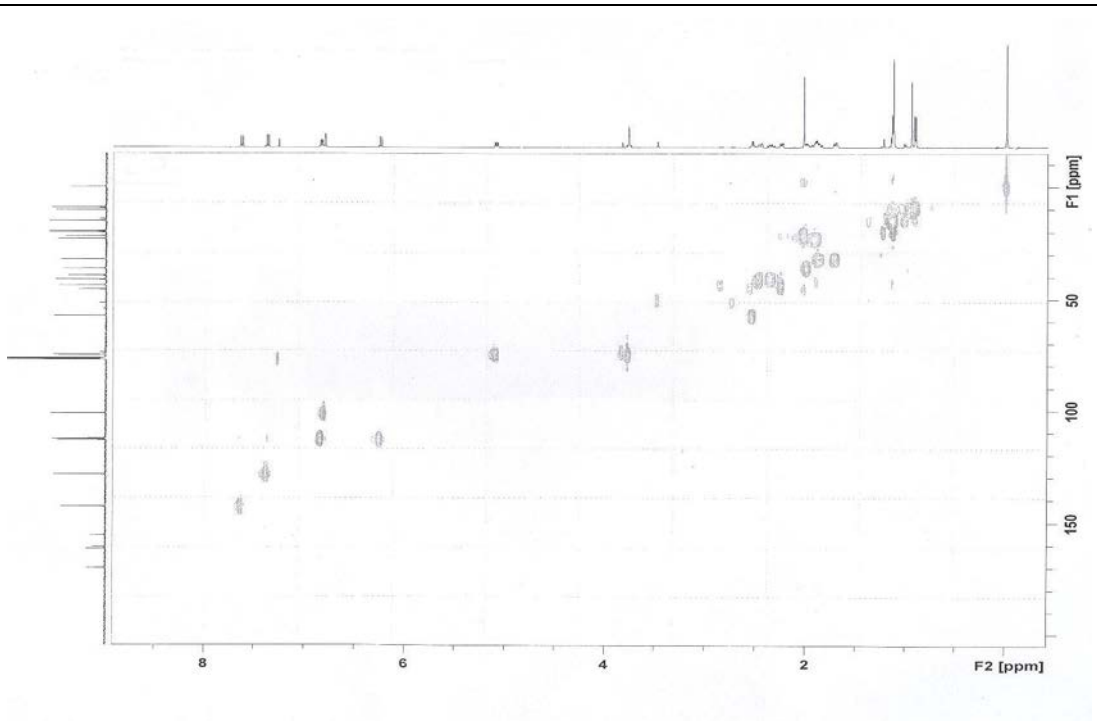

S22. Expansion of the HSQC (500 MHz, CDCl3) of **2**

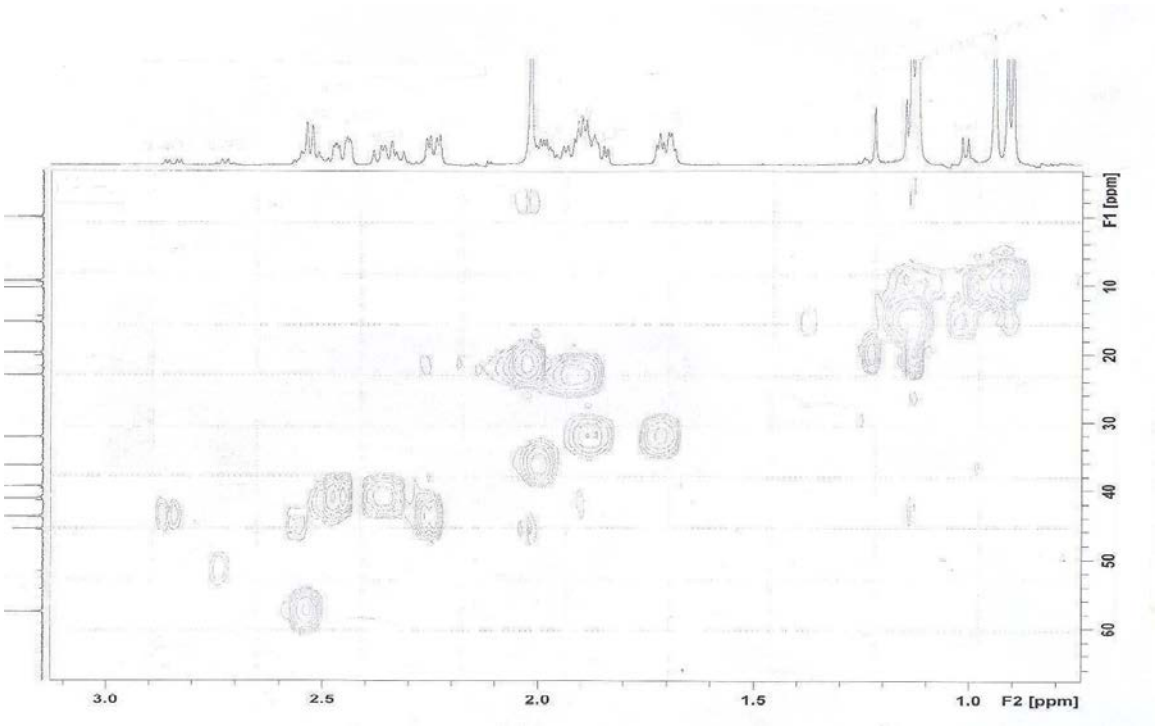

S23. HMBC (500 MHz, CDCl3) of **2**

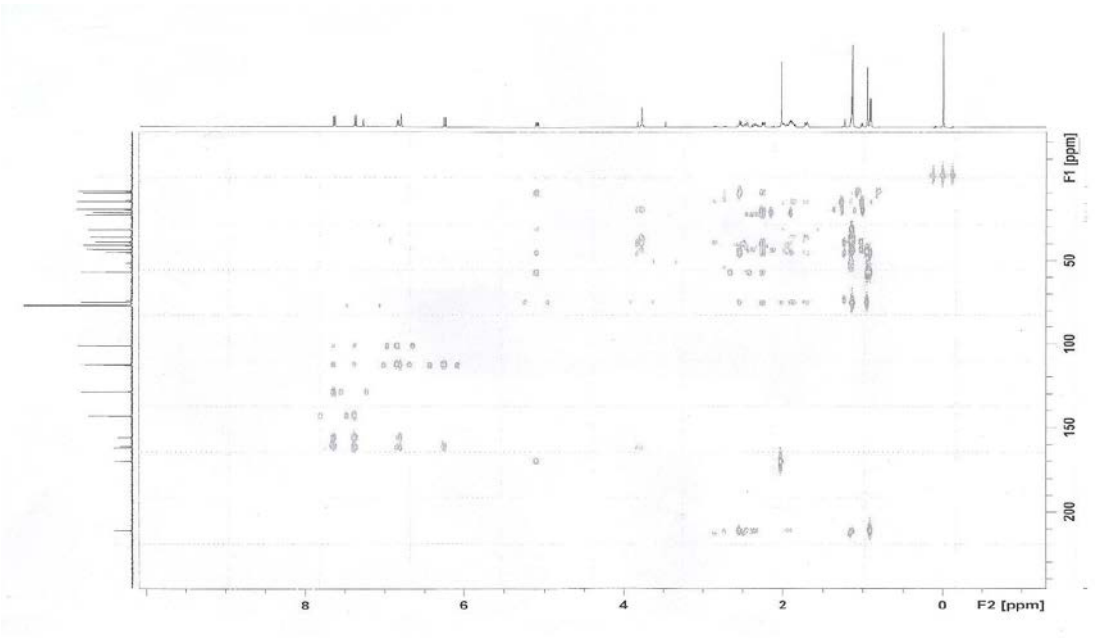

S24. Expansion of the HMBC (500 MHz, CDCl3) of **2**

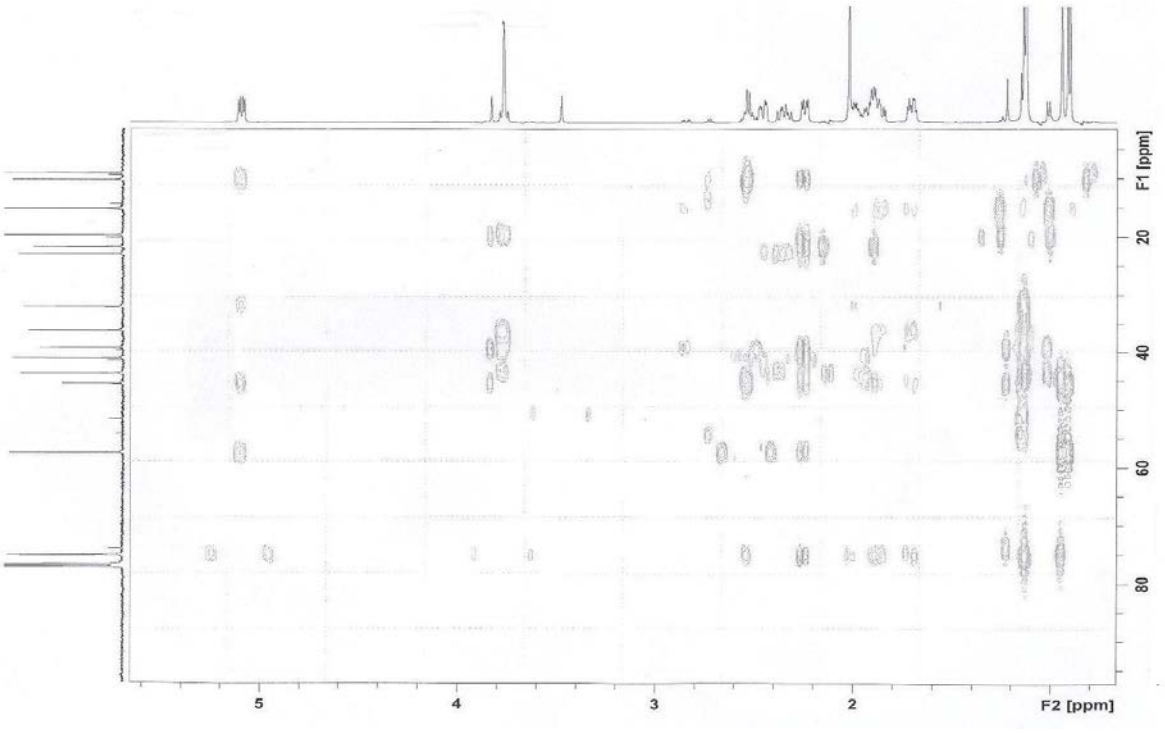

S25. NOESY (500 MHz, CDCl3) of **2**

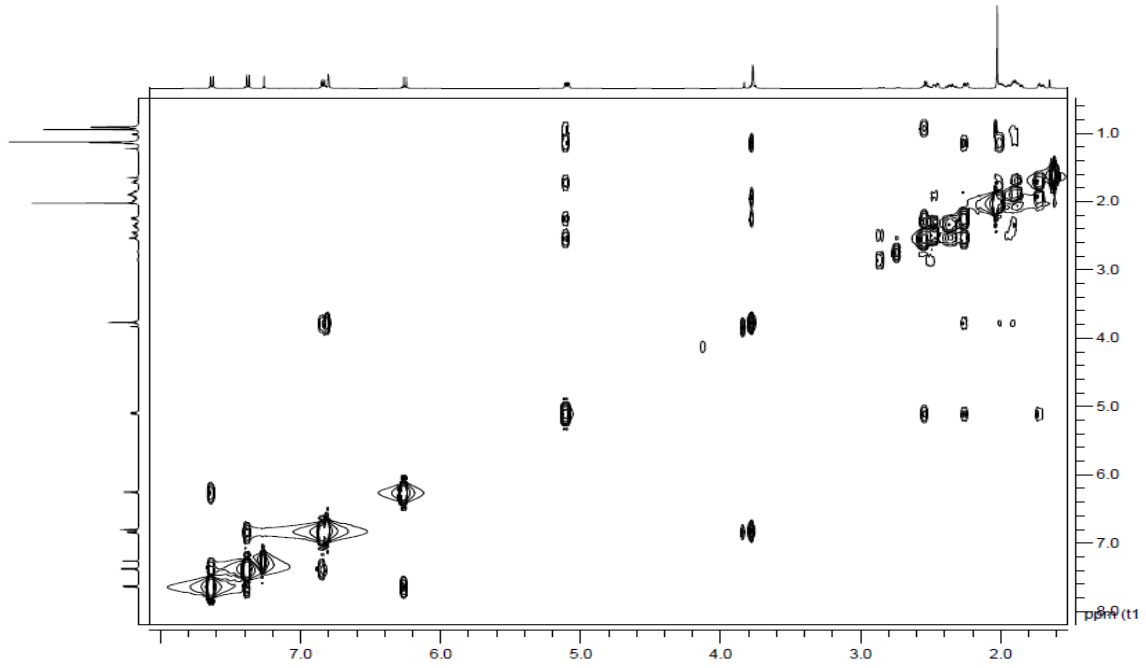

S26. Expansion of the NOESY (500 MHz, CDCl3) of **2**

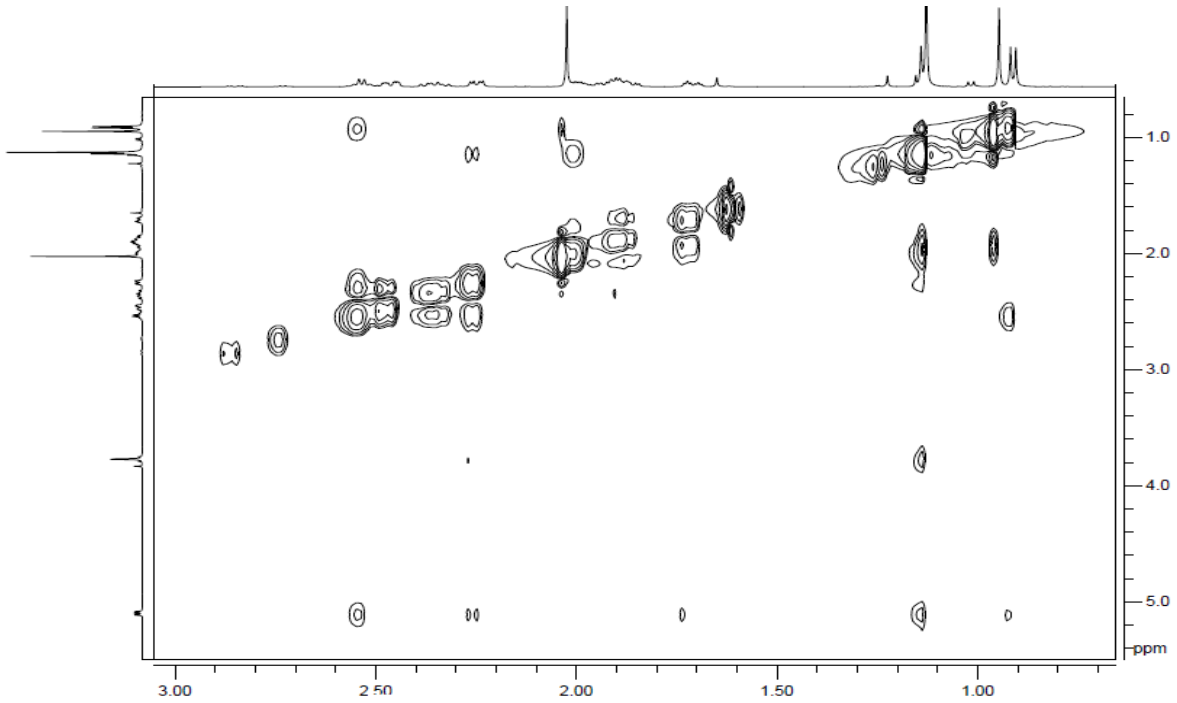

S27. ^{1}H NMR (500 MHz, CDCl3) of **3** and **4**

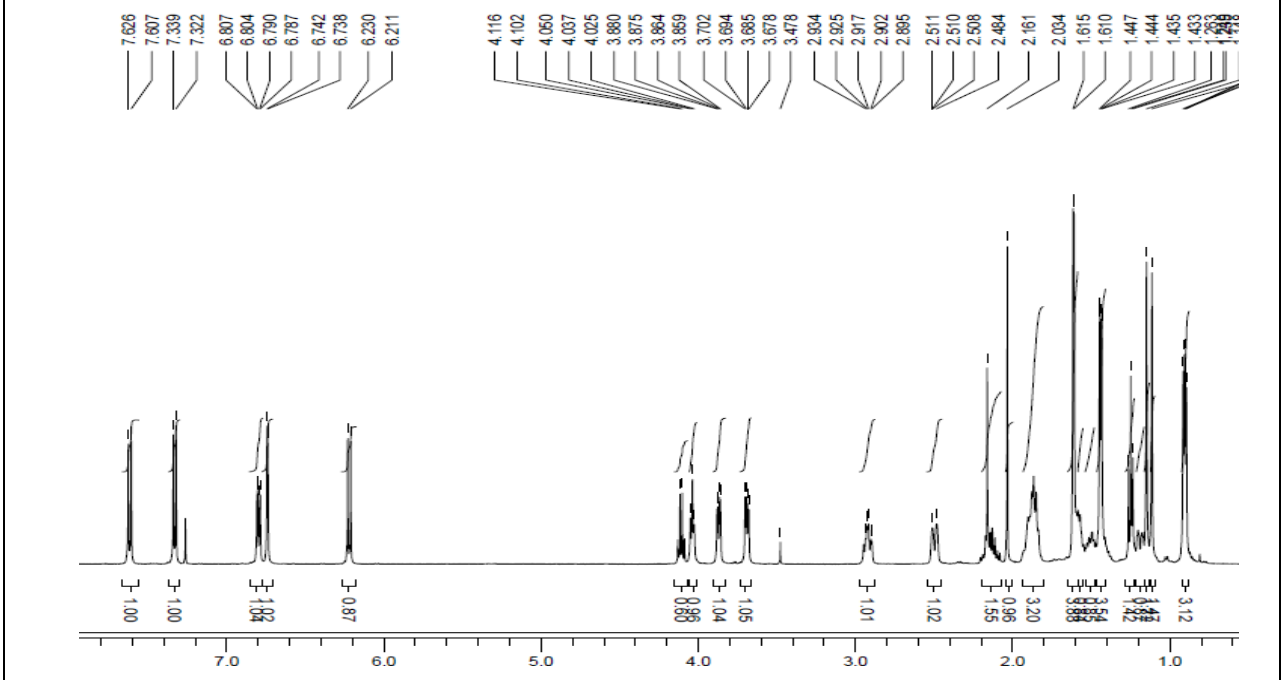

S28. Expansion of the ^{1}H NMR (500 MHz, CDCl3) of **3** and **4**

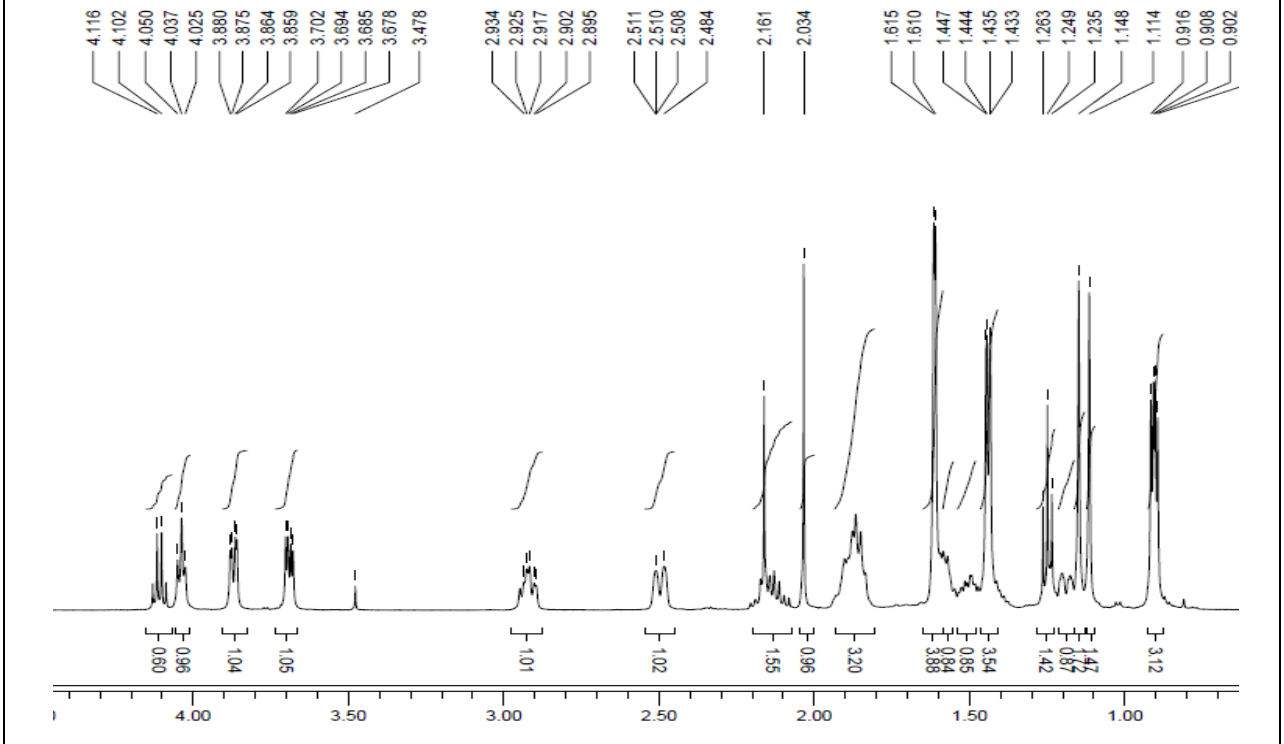

S29. ^{13}C NMR (125 MHz, CDCl3) of **3** and **4**

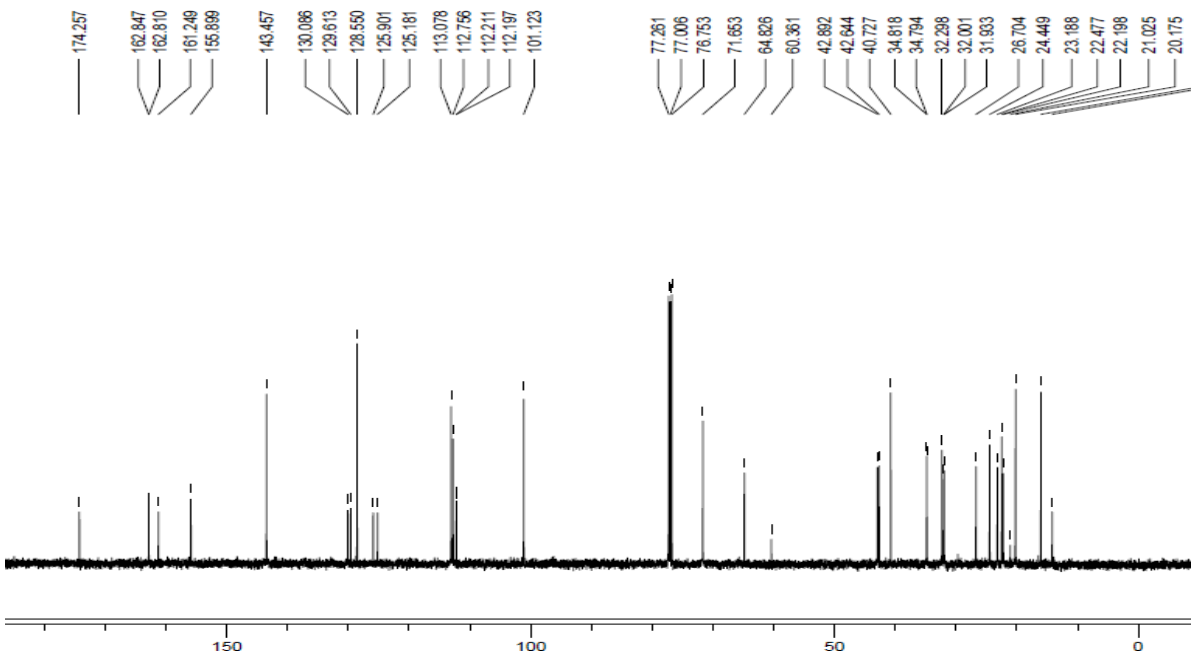

S30. Expansion of the ^{13}C NMR (125 MHz, CDCl3) of **3** and **4**

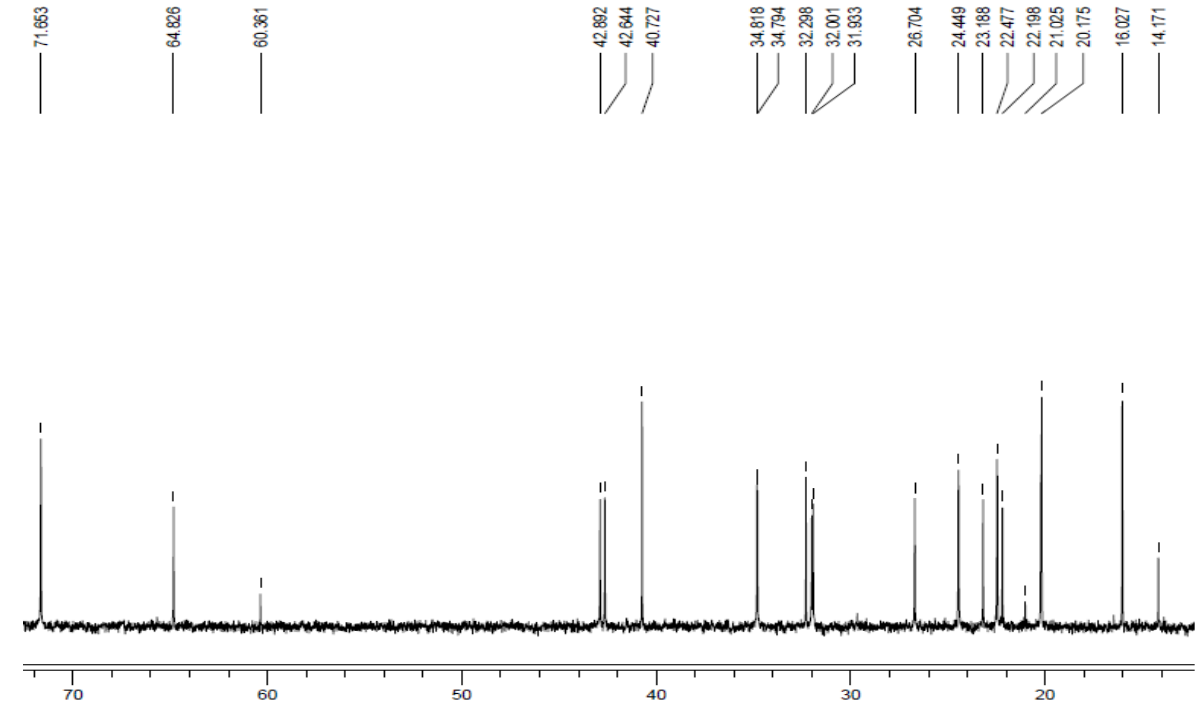

S31. DEPT 90 (500 MHz, CDCl3) of **3** and **4**

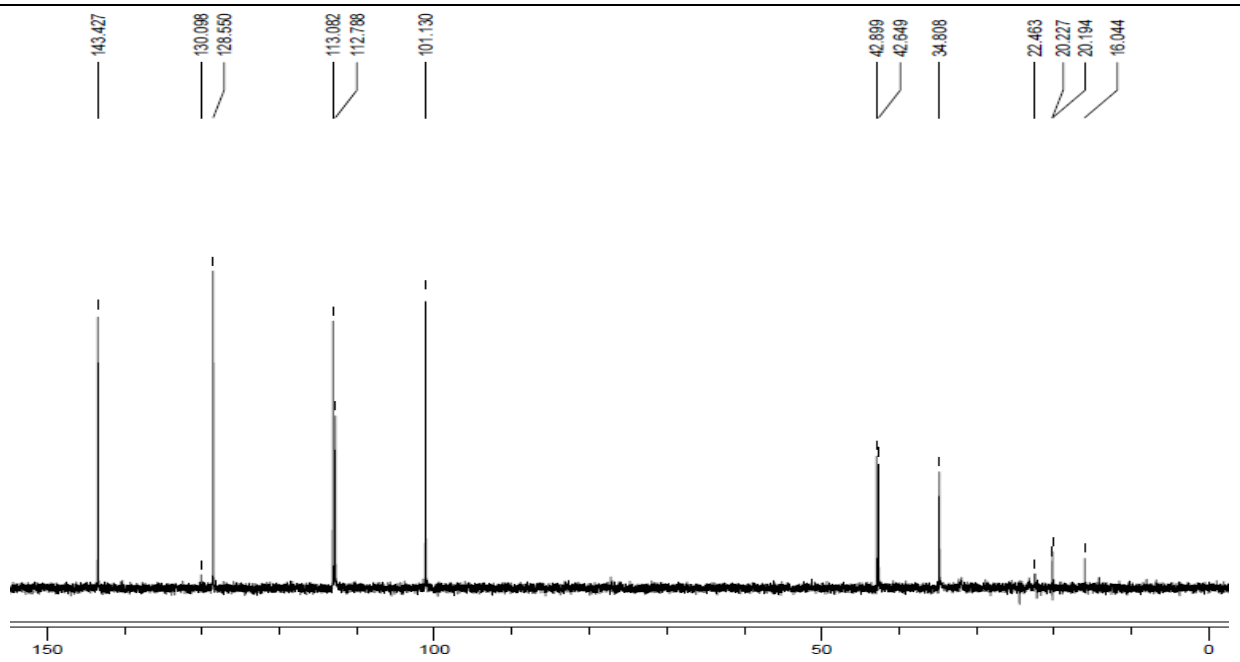

S32. DEPT 135 (500 MHz, CDCl3) of **3** and **4**

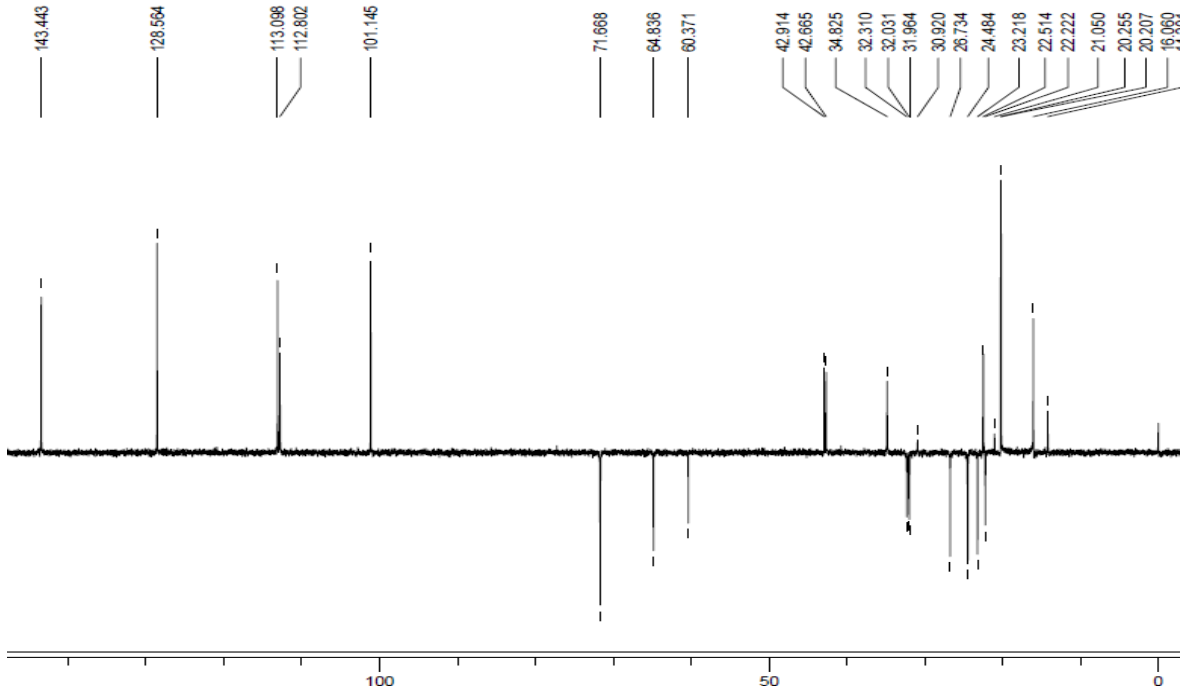

S33. COSY (500 MHz, CDCl3) of **3** and **4**

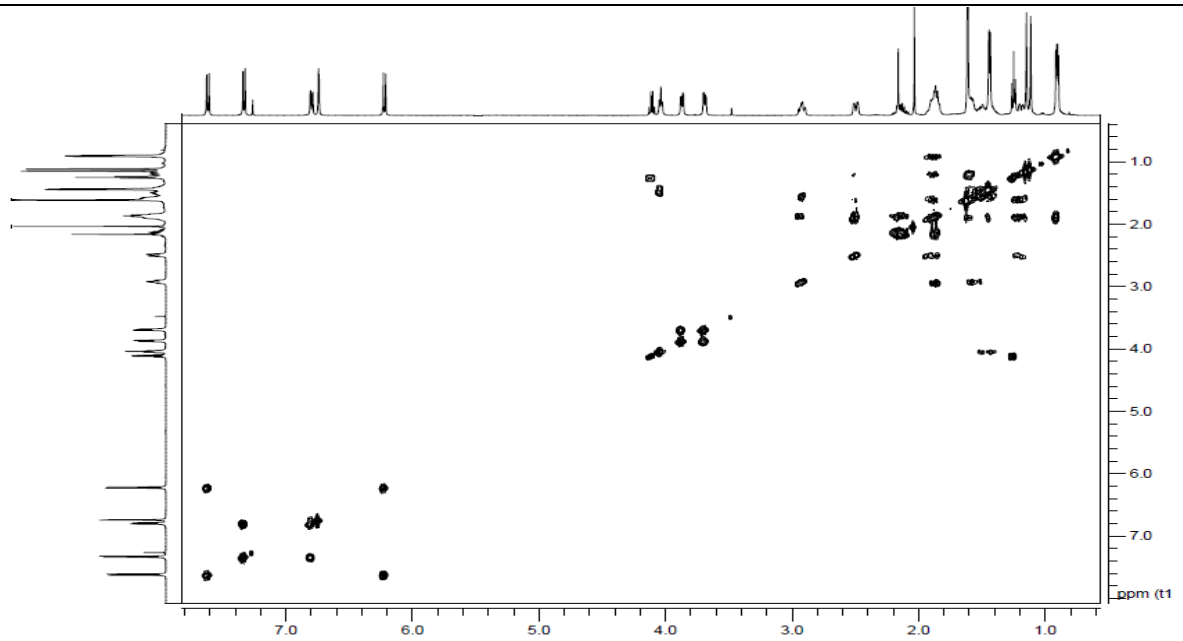

S34. Expansion of the COSY (500 MHz, CDCl3) of **3** and **4**

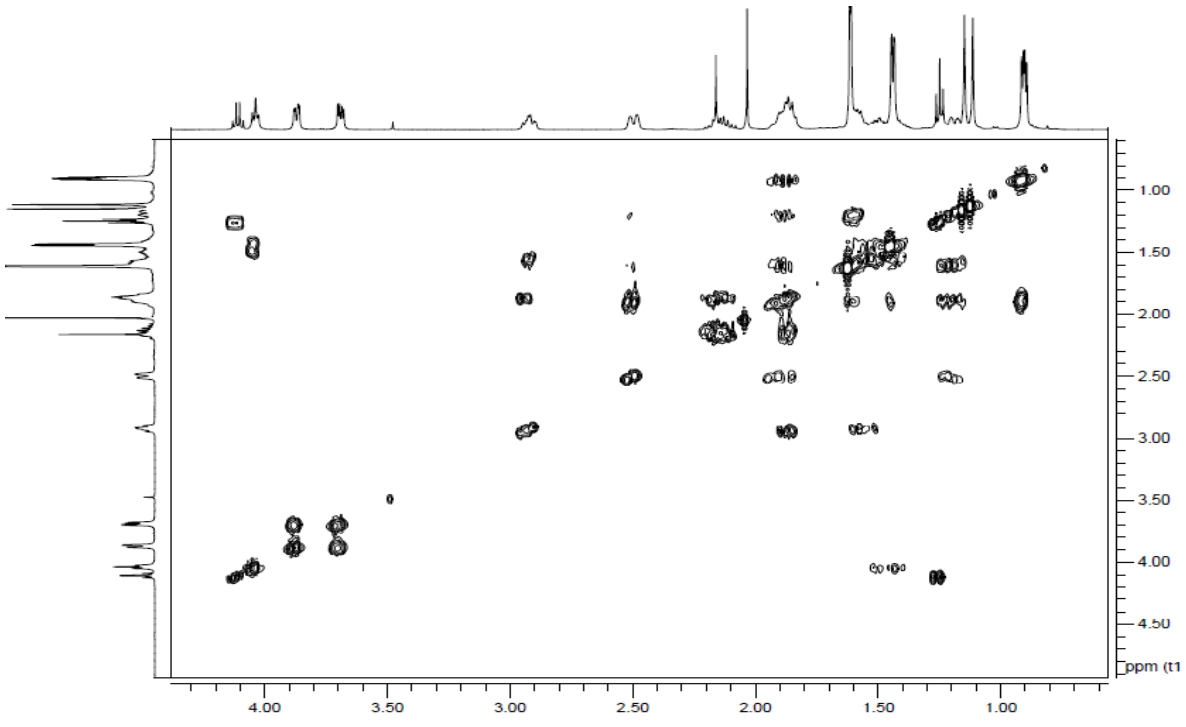

S35. HSQC (500 MHz, CDCl3) of **3** and **4**

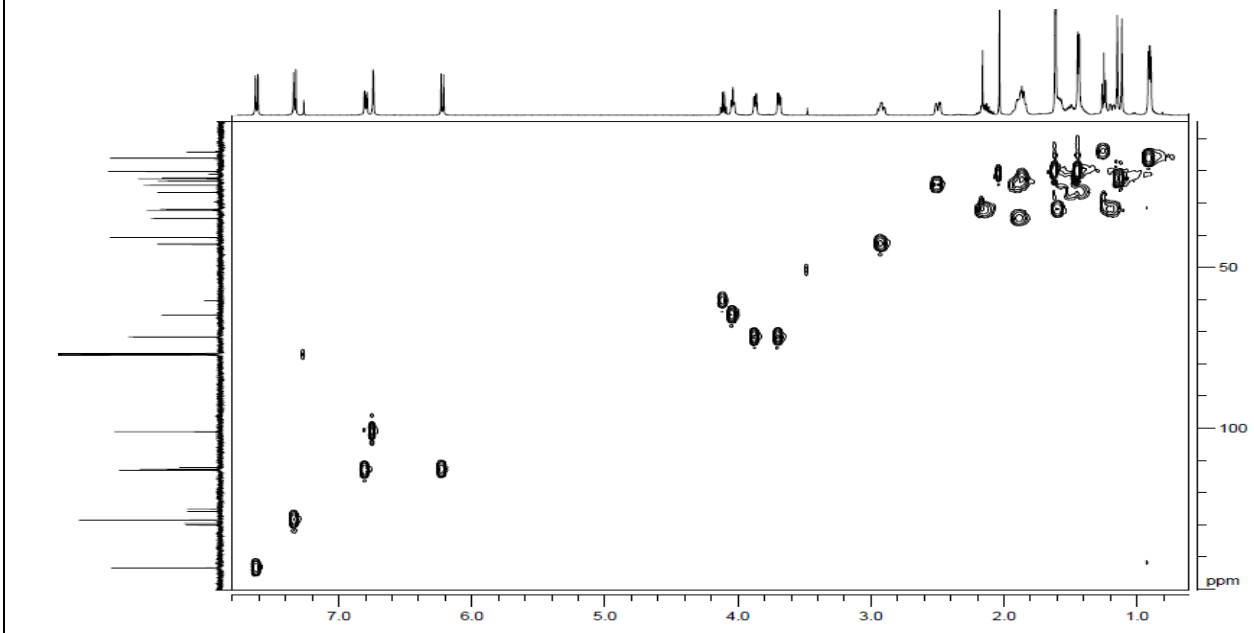

S36. Expansion of the HSQC (500 MHz, CDCl3) of **3** and **4**

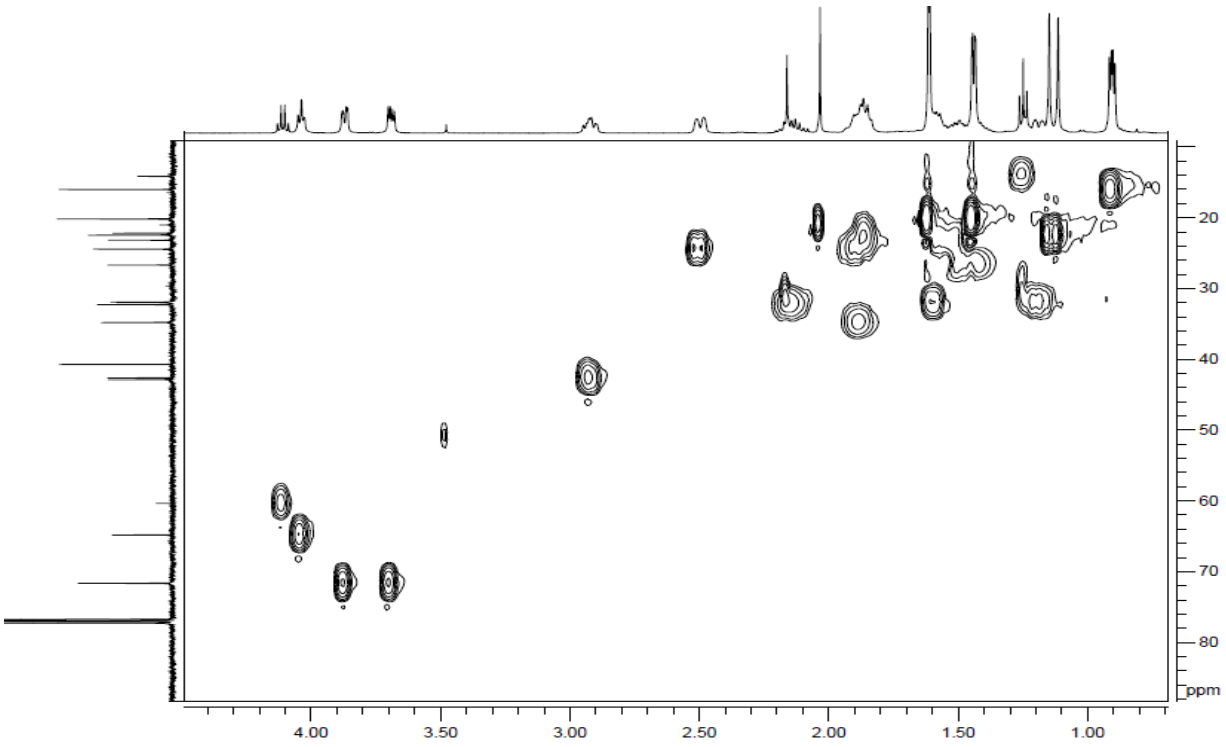

S37. HMBC (500 MHz, CDCl3) of **3** and **4**

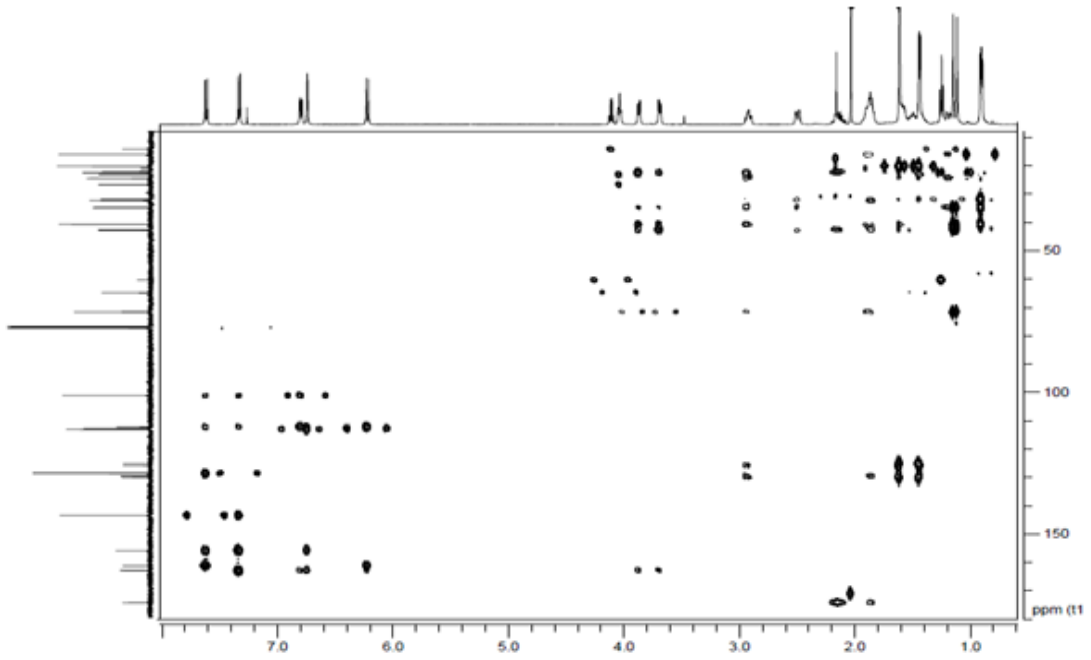

S38. Expansion of the HMBC (500 MHz, CDCl3) of **3** and **4**

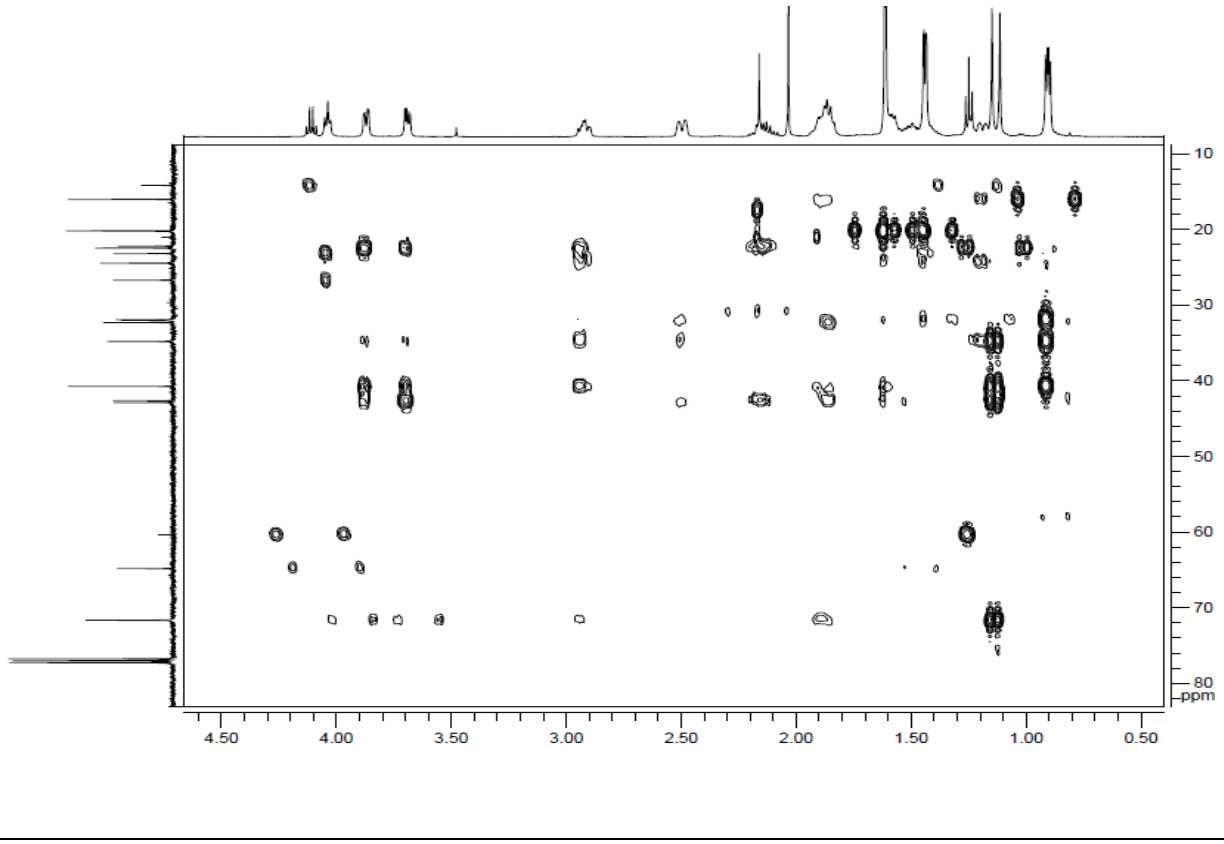

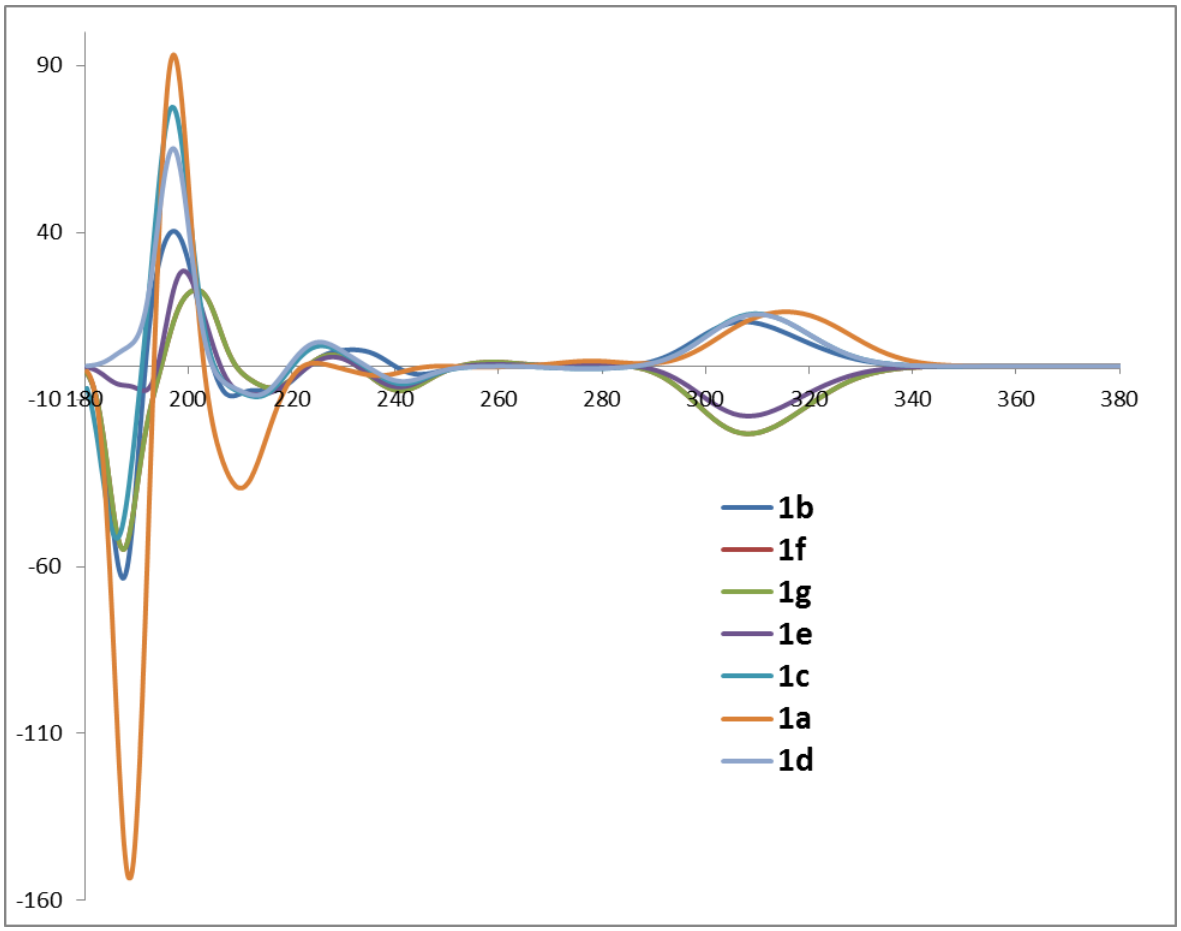

Figure S1. Calculated ECD spectra MeCN (CPCM) of each minimized conformer (DFT/B3LYP/6-31G*) of ***1*** occurring within an energy range of 2 kcal/mol from the global minimum.

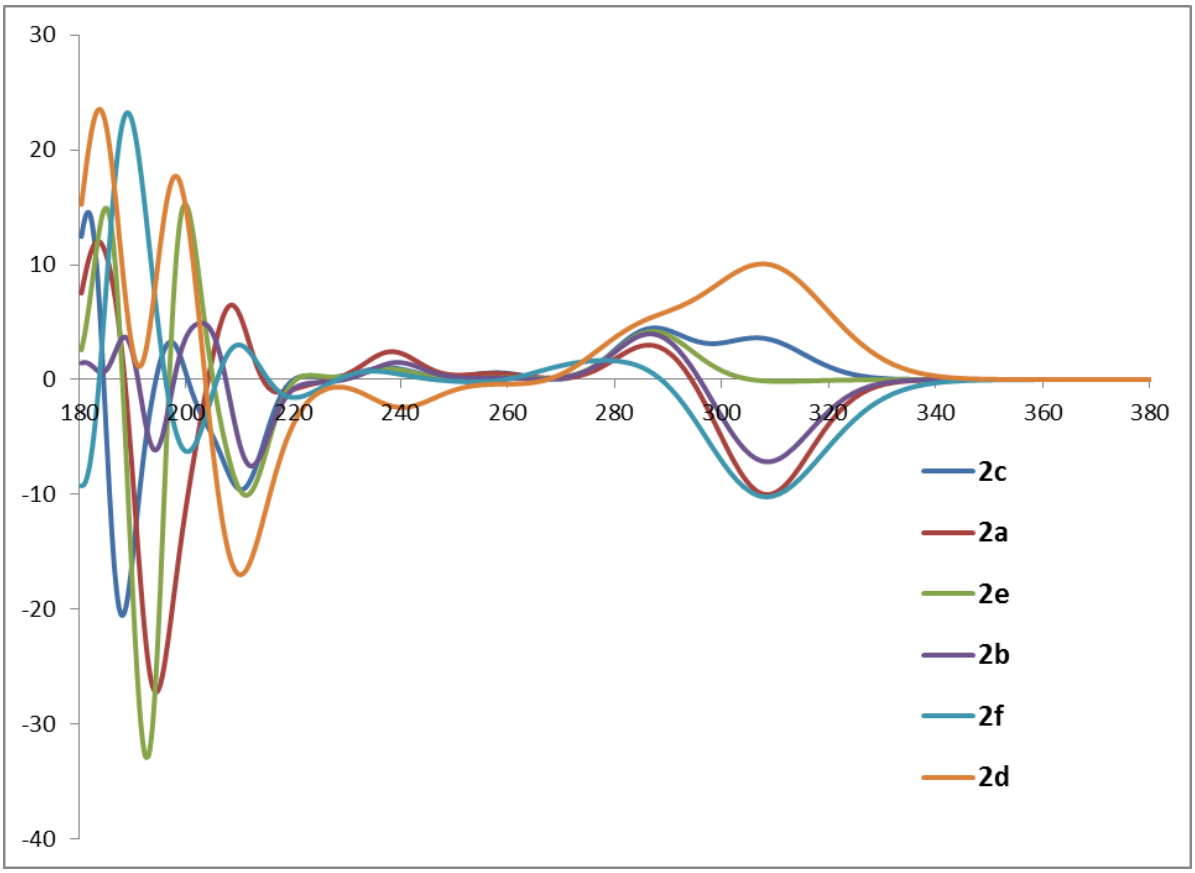

Figure S2. Calculated ECD spectra MeCN (CPCM) of each minimized conformer (DFT/B3LYP/6-31G*) of **2** occurring within an energy range of 2 kcal/mol from the global minimum.

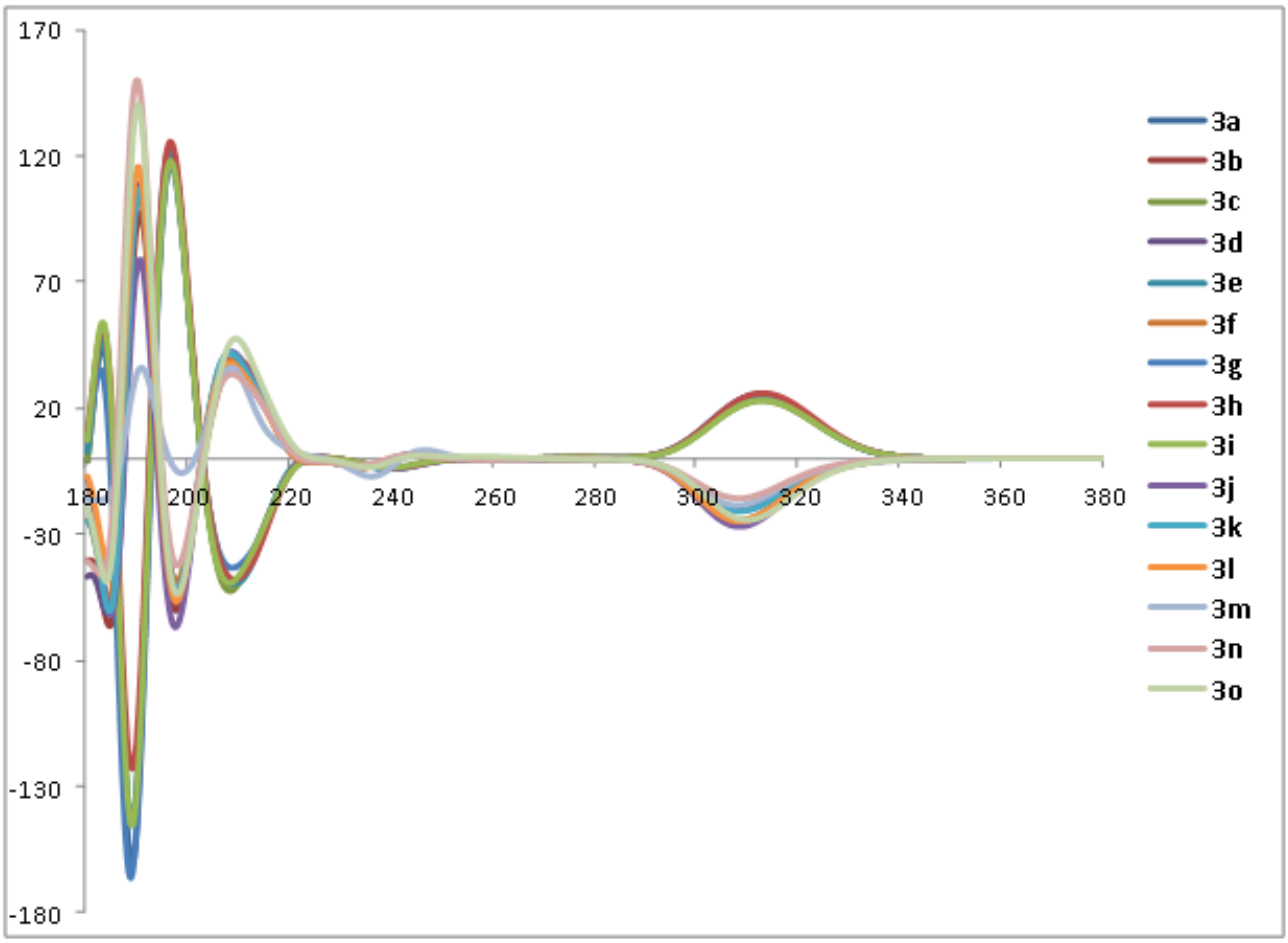

Figure S3. Calculated ECD spectra MeCN (CPCM) of each minimized conformer (DFT/B3LYP/6-31G*) of **3** occurring within an energy range of 2 kcal/mol from the global minimum.

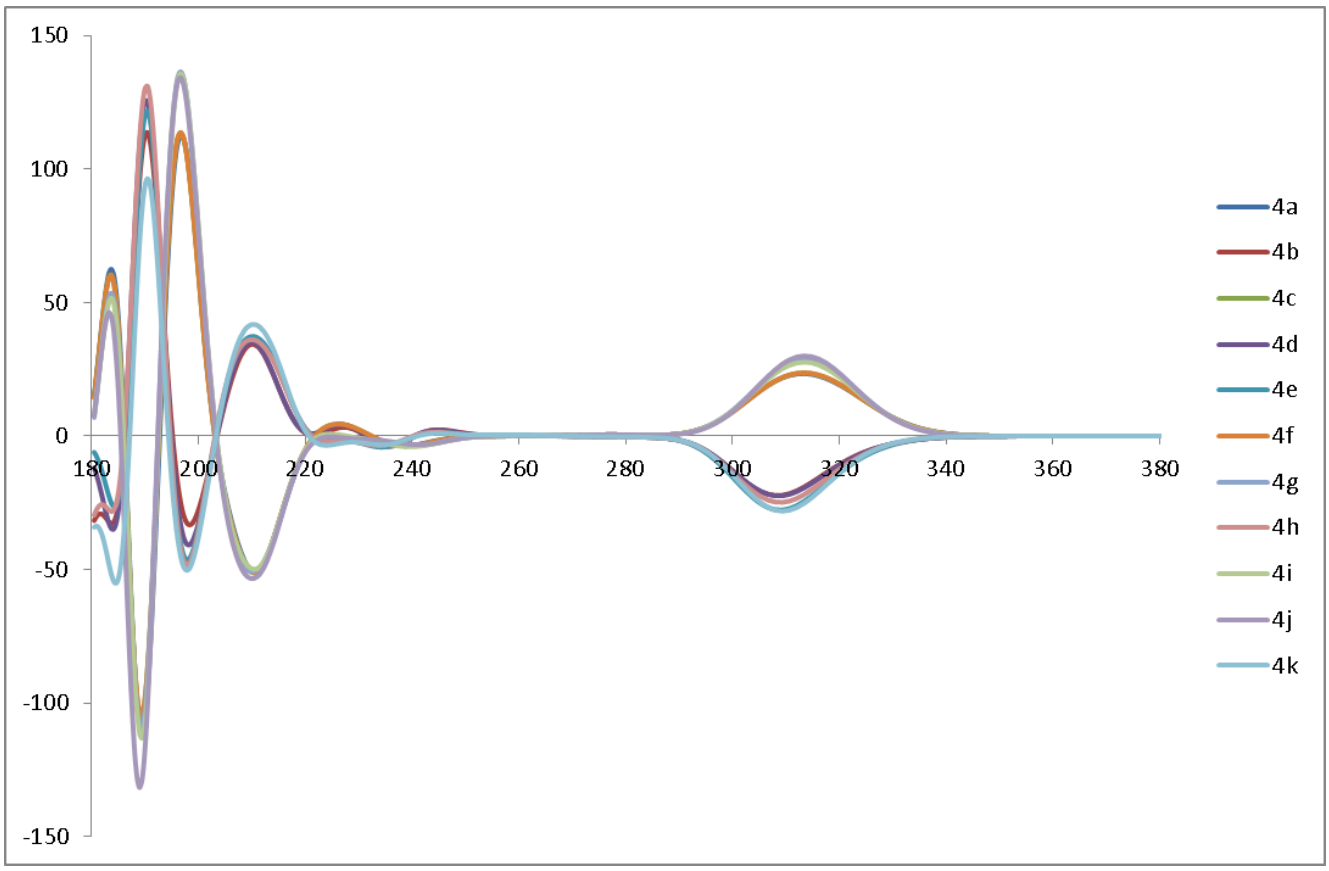

Figure S4. Calculated ECD spectra MeCN (CPCM) of each minimized conformer (DFT/B3LYP/6-31G*) of **4** occurring within an energy range of 2 kcal/mol from the global minimum.

3.4. Hydrangenone, a new isoprenoid with an unprecedented skeleton from *Salvia hydrangea*

Mehdi Moridi Farimani, Salman Taheri, Samad Nejad Ebrahimi, M. Babak Bahadori, Hamid Reza Khavasi, Stefanie Zimmermann, Reto Brun, and Matthias Hamburger

Org. Lett., 14, No. 1, 2012, 166-169, doi: 10.1021/ol202953b

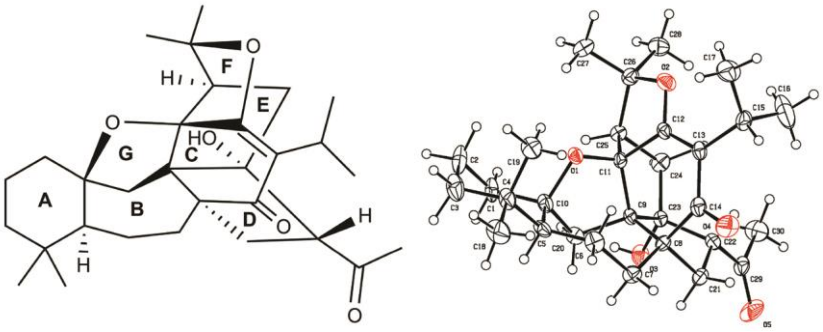

Hydrangenone, a new heptacyclic isoprenoid with a 6/7/6/5/5 membered carbon ring skeleton, was isolated from the aerial parts of *Salvia hydrangea*. The structure was established by extensive NMR spectroscopic methods. The relative and absolute configuration of **1** was assigned by NOESY and X-ray crystallographic analysis and by comparison of experimental and calculated electronic circular dichroism (ECD) spectra. Hydrangenone showed *in vitro* antiplasmodial activity, with an IC_{50} value of 1.4 μM against *P. falciparum*.

Extraction of plant material for isolation, recording, and interpretation of analytical data for structure elucidation (mass spectrometry, microprobe NMR, optical rotation) were done by Dr. Mehdi Moridi. Experimental and quantum-chemical calculations of ECD spectrum, contributing to writing of the manuscript, and preparation of some figures were my part to this publication. Antimalarial testing was done by Stefanie Zimmermann.

Samad Ebrahimi

ORGANIC LETTERS

2012
Vol. 14, No. 1
166–169

Hydrangenone, a New Isoprenoid with an Unprecedented Skeleton from *Salvia hydrangea*

M. Moridi Farimani,*,† Salman Taheri,‡ Samad N. Ebrahimi,†,§ M. Babak Bahadori,† Hamid R. Khavasi,∥ Stefanie Zimmermann,§,⊥ Reto Brun,⊥ and Matthias Hamburger§

Department of Phytochemistry, Medicinal Plants and Drugs Research Institute, Shahid Beheshti University, G. C., Evin, Tehran, Iran, Chemistry and Chemical Engineering Research Center of Iran, Tehran, Iran, Division of Pharmaceutical Biology, University of Basel, Klingelbergstrasse 50, 4056 Basel, Switzerland, Department of Chemistry, Shahid Beheshti University, G. C., Evin, Tehran, Iran, and Swiss Tropical and Public Health Institute, Socinstrasse 57, CH-4002 Basel, Switzerland

m_moridi@sbu.ac.ir

Received November 2, 2011

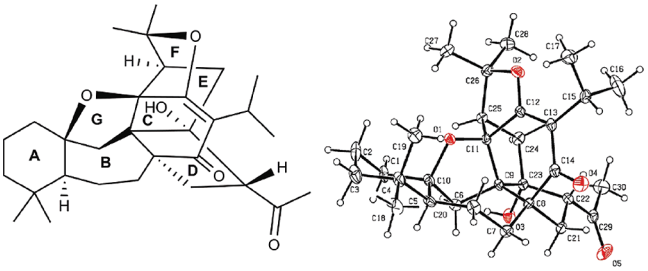

Hydrangenone, a new heptacyclic isoprenoid with a 6/7/6/5/5 membered carbon ring skeleton, was isolated from the aerial parts of *Salvia hydrangea*. The structure was established by extensive NMR spectroscopic methods. The relative and absolute configuration of 1 was assigned by NOESY and X-ray crystallographic analysis and by comparison of experimental and calculated electronic circular dichroism (ECD) spectra. Compound 1 showed in vitro antiplasmodial activity, with an IC_{50} value of 1.4 μM against *P. falciparum*. A plausible biosynthetic pathway of 1 was also proposed.

The genus *Salvia* is a rich source of structurally diverse terpenoids.[1] One of the most distinguishing features of *Salvia* species is their ability to synthesize isoprenoids with unusual scaffolds.[2] In a project directed at structurally interesting bioactive metabolites from Iranian Lamiaceae, we studied *Salvia hydrangea*. This species is popularly known in Persian as "Gol-e Arooneh". It grows widely in Iran, Anatolia, and Transcaucasia,[3] and its flowers are used in popular Iranian medicine as an anthelmintic and antileishmanial.[4] We recently identified two new antiplasmodial isoprenoids, perovskone B and salvadione C, from this plant.[5] Further examination of the *n*-hexane extract of

† Department of Phytochemistry, Shahid Beheshti University.
‡ Chemistry and Chemical Engineering Research Center of Iran.
§ University of Basel.
∥ Department of Chemistry, Shahid Beheshti University.
⊥ Swiss Tropical and Public Health Institute.

(1) Kintzios, S. E. *Sage: The Genus Salvia*; Harwood Academic Publishers: Amsterdam, 2000; pp 55−68.

(2) (a) Xu, G.; Hou, A. J.; Zheng, Y. T.; Zhao, Y.; Li, X. L.; Peng, L. Y.; Zhao, Q. S. *Org. Lett.* **2007**, *9*, 291–293. (b) Aoyagi, Y.; Yamazaki, A.; Nakatsugawa, C.; Fukaya, H.; Takeya, K.; Kawauchi, S.; Izumi, H. *Org. Lett.* **2008**, *10*, 4429–4432. (c) Ahmad, V. U.; Zahid, M.; Ali, M. S.; Ali, Z.; Jassbi, A. R.; Abbas, M.; Clardy, J.; Lobkovsky, E.; Tareen, R. B.; Iqbal, M. Z. *J. Org. Chem.* **1999**, *64*, 8465–8467. (d) Ahmad, V. U.; Zahid, M.; Ali, M. S.; Choudhary, M. I.; Akhtar, F.; Ali, Z.; Iqbal, M. Z. *Tetrahedron Lett.* **1999**, *40*, 7561–7564. (e) Moghaddam, F. M.; Moridi Farimani, M.; Seirafi, M.; Taheri, S.; Khavasi, H. R.; Sendker, J.; Proksch, P.; Wray, V.; Edrada, R. A. *J. Nat. Prod.* **2010**, *71*, 1601–1605. (f) Rustaiyan, A.; Masoud, S.; Anaraki, M. T. *Nat. Prod. Commun.* **2007**, *10*, 1031–1042.

(3) Rechinger, K. H. *Flora Iranica*; Akademische Druck- und Verlagsanstalt: Graz, 1987; pp 403−476.

(4) Amin, G. *Popular medicinal plants of Iran*; Ministry of Health Publications: Tehran, 1991; Vol. 1, p 41.

(5) Moridi Farimani, M.; Bahadori, M. B.; Taheri, S.; Ebrahimi, S. N.; Zimmermann, S.; Brun, R.; Amin, G.; Hamburger, M. *J. Nat. Prod.* **2011**, *74*, 2200–2205.

10.1021/ol202953b
Published on Web 12/01/2011

S. hydrangea led to the isolation of hydrangenone (**1**), an isoprenoid with an unprecedented skeleton which is characterized by an unusual arrangement of 6/7/6/5/5 membered carbon rings fused with two tetrahydrofuran rings.

The aerial parts of *S. hydrangea* DC. ex Benth. were collected from the Koohin region in Qazvin province, Iran, in May 2009. The dried plant material (4.5 kg) was extracted with *n*-hexane (3 × 25 L). Fractionation of the *n*-hexane extract (107 g) by column chromatography on silica gel (*n*-hexane/EtOAc step gradient) afforded 30 fractions. Fraction 20 (1.1 g) was separated on a silica gel column [$CHCl_3$/Me_2CO (97:3)] into 10 fractions (20a−20j). Fraction 20b was further purified by preparative TLC on silica gel [CH_2Cl_2/Me_2CO (97:3)] to afford **1** (6 mg, R_f = 0.45).

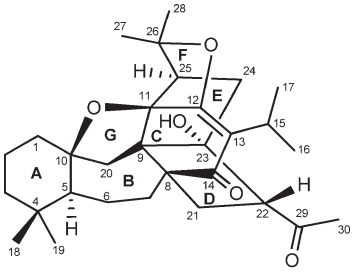

1

Hydrangenone (**1**) was obtained as colorless needles ($CHCl_3$).[6] A molecular formula of $C_{30}H_{42}O_5$ was established from its HR-ESIMS (*m*/*z* 505.2902 $[M+Na]^+$, calcd 505.2924). The molecular formula accounted for 10 degrees of unsaturation. Absorption bands at 3440, 1707, and 1611 cm^{-1} in the IR spectrum implied the presence of OH, carbonyl, and olefinic functionalities, respectively. The ^{13}C NMR spectrum showed resonances of 30 carbons attributable by the DEPT spectrum to seven methyl, eight methylene, four methine, and 11 quaternary carbons (Table 1). Thus, 41 hydrogen atoms could be accounted for, while the remaining one was likely from a hydroxyl group. ^{13}C NMR resonances at δ_C 202.1 (C), 123.3 (C), and 172.5 (C) suggested the presence of an α,β-unsaturated ketone moiety containing a trisubstituted double bond and an oxygen substituent at the β-position. The resonance at δ_C 212.0 (C) was indicative of a second carbonyl group. Four carbon signals at δ_c 87.9 (C), 90.0 (C), 90.9 (C), and 93.6 (C) suggested the presence of oxygen bearing sp^3 carbons. The absence of other sp or sp^2 carbon signals and the 10 degrees of unsaturation implied that **1** contained seven rings, including two cyclic ethers. The ^1H NMR spectrum (Table 1) showed resonances of five methyl singlets at δ_H 0.82, 0.84, 1.35, 1.66, and 2.11. Resonances of two additional methyl groups at δ_H 1.13 (d, J = 7.1 Hz) and 1.20 (d, J = 7.1 Hz), together with a signal at δ_H 3.24 (sept, J = 7.1 Hz) indicated the presence of an isopropyl moiety.

Comparison of the NMR data of **1** with those of isoprenoids previously isolated from *S. hydrangea* suggested structural similarities with perovskone B.[5] Notable differences in the NMR spectra of **1** and perovskone B were observed, suggesting a five-membered ring D in **1** instead of a six-membered ring as in perovskone B. Hence, structure determination mainly focused on confirmation of ring D and of its connectivity to rings B, C, and E.

Unambiguous assignment of NMR data was achieved by a combination of COSY, HSQC, and HMBC experiments in $CDCl_3$ and C_6D_6. HMBC data (correlations from H-20β to C-9, C-8, and C-23, and from H-24β to C-23, C-9, and C-25) revealed the connectivity between C_{20}−C_9−C_{23}−C_{24}−C_{25} (Figure 1). Correlations of H-7β and H-21β with C-8, C-9, and C-14, respectively, indicated that the tertiary carbon C-8 was a bridgehead between C-7, C-9, C-14, and C-21. HMBC correlations of H-22 with C-21, C-23, and C-29, and of H-21β with C-8, C-9, C-14, C-22, and C-23, respectively, confirmed the presence of a five-membered ring D. The acetyl group was located at C-22 according to the HMBC cross peaks of H-22 and H-21α with C-29, and also of H-30 with C-29 and C-22. HMBC correlations of H-25 with C-11, C-12, and C-26 confirmed the nature of ring E.

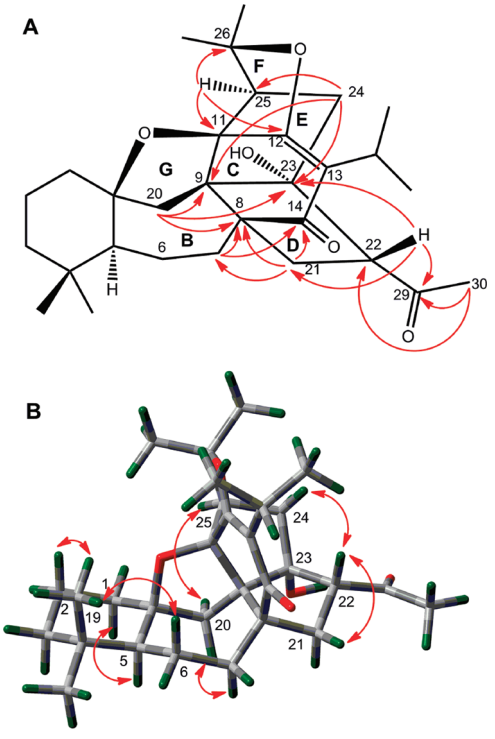

Figure 1. (A) Key HMBC and (B) NOESY correlations of **1**.

The relative configuration of **1** was deduced from a NOESY spectrum (Figure 1). NOESY correlations between H-5, H-1α, H-6α, and H-20α, as well as between Me-19, H-2β, and H-6β corroborated the linkage of rings A and B. Diagnostic cross peaks between H-22, H-21β, and H-24β were observed and confirmed their cofacial orientation. Equally, an NOESY cross-peak between

(6) Hydrangenone (**1**): Colorless crystal; $[\alpha]^{20}_D$ +51.9 (*c* 0.27, $CHCl_3$); IR (KBr) ν_{max} 3440, 2937, 1707, 1611, 1457, 1370, 1230, 1110 cm^{-1}; for ^1H and ^{13}C NMR data, see Table 1; CD (MeOH, $c = 1.0 \times 10^{-6}$ M, 0.1 cm path length): $[\theta]_{202}$ +4797, $[\theta]_{243}$ −29336, $[\theta]_{266}$ −33773, $[\theta]_{318}$ + 27521; $C_{30}H_{42}O_5$ was established from its HR-ESIMS (*m*/*z* 505.2902 $[M+Na]^+$, calcd 505.2924).

Table 1. ^{1}H and ^{13}C NMR Data of Compound **1**[a]

	$CDCl_3$		Benzene-d_6	
Position	δ_H (J in Hz)	δ_C	δ_H (J in Hz)	δ_C
1α	1.12[b]	42.7, t	1.17, dt (3.0, 13.5)	42.3, t
1β	1.37, br d (12.6)		1.39[b]	
2α	1.46[b]	20.1, t	1.48[b]	19.8, t
2β	1.60[b]		1.88, tq (3.5, 13.5)	
3α	1.64[b]	43.0, t	1.58[b]	42.5, t
3β	1.68[b]		1.70[b]	
4		34.5, s		33.9, s
5	1.01, m	53.6, d	0.88,[b] dd (4.5, 12.5)	53.0, d
6α	1.70[b]	22.8, t	1.65[b]	22.5, t
6β	1.33[b]		1.40[b]	
7α	1.75, br t (14.0)	44.1, t	1.67,[b] dd (11.5, 14.0)	44.1, t
7β	2.13,[b] dd (7.8, 14.5)		2.05,[b] dd (8.0, 14.0)	
8		66.3, s		66.1, s
9		55.4, s		54.8, s
10		90.0, s		89.3, s
11		93.6, s		93.1, s
12		172.5, s		170.9, s
13		123.3, s		122.8, s
14		202.1, s		200.6, s
15	3.24, sept (7.1)	24.6, d	3.70, sept (7.0)	24.7, d
16	1.20, d (7.1)	20.7, q	1.50, d (7.0)[b]	20.5, q
17	1.13,[b] d (7.1)	20.3, q	1.45,[b] d (7.0)	20.1, q
18	0.84, s	32.3, q	0.85,[b] s	31.8, q
19	0.82, s	21.6, q	1.01, s	21.3, q
20α	2.38, d (14.0)	43.1, t	2.08, d (14.0)	42.8, t
20β	2.18, d (14.0)		2.45, d (14.0)	
21α	2.00, dd (11.7, 13.8)	44.3, t	2.02,[b] dd (11.5, 14.0)	43.8, t
21β	2.63, dd (5.8, 11.7)		2.80, dd (5.0, 11.5)	
22	2.35[b]	62.7, d	2.42, dd (5.0, 14.0)	62.2, d
23		87.9, s		87.4, s
24α	1.47[b]	34.8, t	1.41[b]	34.5, t
24β	2.35[b]		2.62, dd (8.0, 12.5)	
25	2.77, dd (8.0, 11.5)	56.9, d	2.52, dd (8.0, 11.5)	56.5, d
26		90.9, s		89.7, s
27	1.35,[b] s	24.7, q	1.11, s	23.8, q
28	1.66,[b] s	27.4, q	1.57,[b] s	26.7, q
29		212.0, s		210.2, s
30	2.11,[b] s	30.8, q	1.72,[b] s	29.5, q
23-OH	3.86, s		6.36, s	

[a] Spectra were recorded at 500 MHz for ^{1}H and 125 MHz for ^{13}C. [b] Overlapping signals.

H-25 and H-20β confirmed their location on the same face of the molecule. However, we were not able to establish the relative configuration at C-23. A single-crystal X-ray study of **1** clarified the α-orientation of OH-23 and unambiguously confirmed the structure of **1** (Figure 2).[7]

Electronic circular dichroism (ECD) is a powerful chiroptical tool for determination of the absolute configuration in natural products.[8] The absolute configuration of **1** was established by measurement of the ECD spectrum and comparison with calculated ECD data. A conformational search based on the X-ray relative configuration revealed

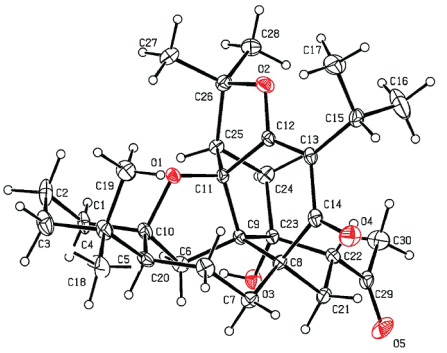

Figure 2. Single-crystal X-ray struture of **1**.

seven conformers within a 3 kcal/mol energy window from the particular global minimum. These conformers were subjected to geometrical optimization and energy calculation using density function theory (DFT) with the B3LYP function and 6-31G* in the gas phase combined with calculation of vibrational modes to confirm these minima. No imaginary frequencies were found. Conformational analysis using relative free energies indicated the presence of one predominant conformer (100%) in the gas phase. Theoretical calculation of ECD spectra of this conformer was performed by the time-dependent density function theory (TDDFT) method at B3LYP/6-31G* in MeOH using the SCRF (Self-consistent reaction field) method with the CPCM (*Conductor*-like *polarizable* continuum) model. The overall pattern of calculated ECD spectra was in good agreement with the experimental data (Figure 3). In particular, two negative Cotton effects (CE) were observed at 225, 279 nm, along with positive effect at 320 nm. Thus, the absolute configuration of **1** was established as 5*S*, 8*R*, 9*R*, 10*S*, 11*R*, 22*R*, 23*R*, 25*R*.

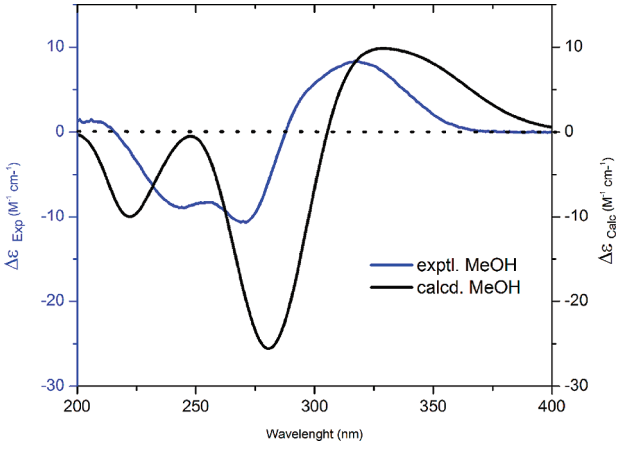

Figure 3. ECD spectra of **1**: experimental ECD (blue) and calculated ECD in MeOH(black).

Scheme 1. Plausible Biogenetic Pathway of **1**

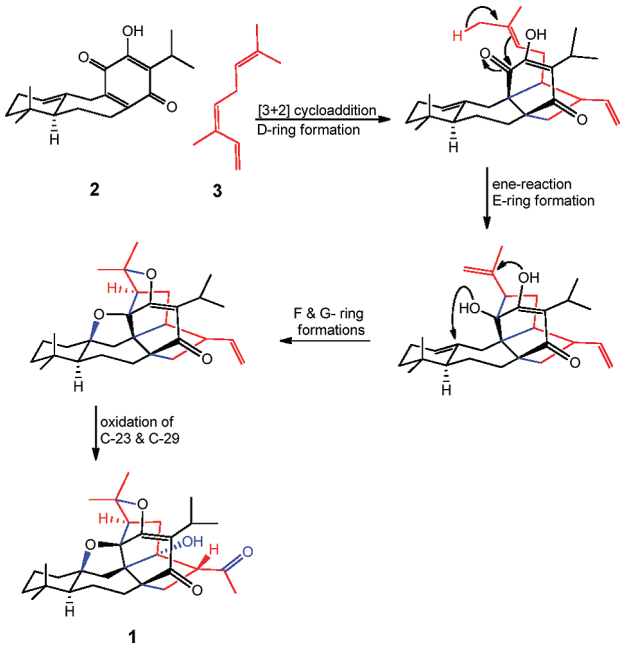

Hydrangenone (**1**) was tested for in vitro antiplasmodial activity against the *Plasmodium falciparum* K1 strain. The compound showed a moderate activity and selectivity index (IC_{50} 1.4 μM, SI = 6, cytotoxicity in rat myoblast (L6) cells). The positive control, artesunate, had an IC_{50} of 0.1 μM.

Hydrangenone (**1**) represents the first example of a new 6/7/6/5/5 membered carbon ring framework. A plausible biogenetic pathway toward this new skeleton bears close similarities to the proposed formation of some other rare isoprenoids in *Salvia* species (Scheme 1).[2c−2d,5,9] However, while these previously described isoprenoids could be explained by a Diels−Alder reaction between a monoterpene and a diterpenoid, hydrangenone (**1**) is probably formed via a [3 + 2] cycloaddition type reaction between a putative icetexone precursor (**2**) and *trans*-β-ocimene (**3**) to assemble the five-membered ring D. An intramolecular ene-type reaction[10] would then form the key C(11)−C(25) bond of carbocyclic ring E, and successive formation of the two tetrahydrofuran rings would complete the heptacyclic scaffold. Finally, two oxidation steps on C-23 and C-29 would lead to hydrangenone (**1**). The complex fusion of rings B−G confers a high degree of rigidity to the molecule.

Acknowledgment. Financial support by the Shahid Beheshti University Research Council is gratefully acknowledged.

Supporting Information Available. Experimental procedure, 1D and 2D NMR spectra, and X-ray data (CIF file) of hydrangenone (**1**). This material is available free of charge via the Internet at http://pubs.acs.org.

(7) Crystallographic data for **1**: $C_{30}H_{42}O_5$, MW = 482.64, orthorhombic, space group $P2_12_12_1$, a = 8.3674(5) Å, b = 10.8816(10) Å, c = 28.719(2) Å, V = 2614.9(3) Å^3, Z = 4, Dc = 1.229 g/cm^3, crystal dimensions 0.40 × 0.17 × 0.16 mm^3 were used for measurements on an STOE-IPDSII with a graphite monochromator (ω-scans, $2\theta_{max}$ = 56.36°), Mo Kα radiation. The total number of reflections measured was 12011, of which 6886 were unique. Final indices: R_f = 0.0691, R_w = 0.1090 for reflections with $I > 2\sigma(I)$. The crystal structure (**1**) was solved by direct methods using SHELX-97 (Sheldrich, G. M. University of Gottingen: Gottingen, Germany, 1990) and expanded using difference Fourier techniques, refined by SHELX-97 (Sheldrich, G. M. 1997). Crystallographic data for the structure of **1** have been deposited in the Cambridge Crystallographic Data Centre (deposition number: CCDC851279). Copies of these data can be obtained free of charge via the Internet at www.ccdc.cam.ac.uk/conts/retrieving.html (or from the Cambridge Crystallographic Data Centre, 12 Union Road, Cambridge CB21EZ, UK; fax (+44) 1223-336-033; or deposit@ccdc.cam.ac.uk).

(8) Li, X. C.; Ferreira, D.; Ding, Y. Q. *Curr. Org. Chem.* **2010**, *14*, 1678–1697.

(9) (a) Ahmad, V. U.; Zahid, M.; Ali, M. S.; Jassbi, A. R.; Ahmad, S.; Ali, Z. *Nat. Prod. Sci.* **2000**, *6*, 66–69. (b) Parvez, A.; Choudhary, M. I.; Akhter, F.; Noorwala, M.; Mohammad, F. V.; Hasan, N. M.; Zamir, T.; Ahmad, V. U. *J. Org. Chem.* **1992**, *57*, 4339–4340.

(10) Majetich, G.; Zhang, Y. *J. Am. Chem. Soc.* **1994**, *116*, 4979–4980.

Hydrangenone, a New Isoprenoid with an Unprecedented Skeleton from *Salvia hydrangea*

M. Moridi Farimani,*[,†] Salman Taheri,[‡] Samad N. Ebrahimi,[†,§] M. Babak Bahadori,[†] Hamid R. Khavasi,[⊥] Stefanie Zimmermann,[§,"] Reto Brun,["] and Matthias Hamburger,[§]

Department of Phytochemistry, Medicinal Plants and Drugs Research Institute, Shahid Beheshti University, G. C., Evin, Tehran, Iran, Chemistry and Chemical Engineering Research Center of Iran, Tehran, Iran, Division of Pharmaceutical Biology, University of Basel, Klingelbergstrasse 50, 4056 Basel, Switzerland, Department of Chemistry, Shahid Beheshti University, G. C., Evin, Tehran, Iran, Swiss Tropical and Public Health Institute, Socinstrasse 57, CH-4002 Basel, Switzerland.

*To whom correspondence should be addressed. Tel: +98 21 29902679. Fax: +98 21 22431783.

E-mail: m_moridi@sbu.ac.ir.

[†] Medicinal Plants and Drugs Research Institute, Shahid Beheshti University, G. C.

[‡] Chemistry and Chemical Engineering Research Center of Iran.

[§] University of Basel.

[⊥] Department of Chemistry, Shahid Beheshti University, G. C.

["] Swiss Tropical and Public Health Institute.

Supporting information

S1. General experimental procedures. Optical rotations were measured using a Perkin-Elmer 341 polarimeter. IR spectra were recorded on a Bruker Tensor 27 spectrometer. NMR spectra were recorded on Bruker DRX 500 and Avance III 500 spectrometers, using the residual $CDCl_3$ (δ_H 7.27/δ_C 77.0) and benzene-d_6 (δ_H 7.16/δ_C 128.0) signals as references. The 2D NMR experiments (^{1}H-^{1}H COSY, HMQC, HMBC, NOESY) were performed using standard Bruker software. HR-ESIMS spectra were acquired on a Bruker micrOTOF ESI-MS system. ECD spectra of compound **1** were recorded in MeOH (400 μg/ml) on an AVIV CD spectrometer model 62ADS and analyzed with the AVIV 60DS V4.1 software. Silica gel (70-230 and 230-400 mesh, Merck) were used for column chromatography. Preparative TLC was performed on silica gel 60 GF_{254} (Merck). Bands were detected on TLC under UV or by heating after spraying with 5% phosphomolybdic acid in EtOH.

S2. Conformational analysis, geometrical optimization, and ECD calculation

Conformational analysis of **1** was performed with Schrödinger MacroModel 9.1 software using the OPLS 2005 (Optimized Potential for Liquid Simulations) force field in H_2O. Conformers occurring within a 3 kcal/mol energy window from the global minimum were chosen for geometrical optimization and energy calculation using density function theory (DFT) with the B3LYP functional and the 6-31G* basis-set in the gas-phase with the Gaussian 03 program package.[1] Vibrational analysis was done at the same level to confirm minima. TD-DFT/B3LYP/6-31G* (in the gas phase and in MeOH using the SCRF (self-consistent reaction field) method with the CPCM (*Conductor*-like *polarizable* continuum) model, was employed to calculate excitation energy (denoted by wavelength in nm) and rotatory strength R in dipole velocity (R_{vel}) and dipole length (R_{vel}) forms. ECD curves were calculated based on rotatory strengths using a half bandwidth of 0.2 eV with conformers of **1**. The spectra were combined after Boltzmann weighting according to their population contribution.

S3. Antiplasmodial and antitrypanosomal assay. Tests of extracts and pure substances were done as previously described.[2] IC_{50} values were calculated from sigmoidal concentration inhibition curves. Assays were run in two independent experiments in duplicate.

(1) Frisch, M. J., Trucks, H. B., Schlegel, H. B., , M. J. Frisch, G. W. Trucks, H. B. Schlegel, G. E. Scuseria, M. A. Robb, J. R. Cheeseman, J. A. Montgomery, Jr., T. Vreven, K. N. Kudin, J. C. Burant, J. M. Millam, S. S. Iyengar, J. Tomasi, V. Barone, B. Mennucci, M. Cossi, G. Scalmani, N. Rega, G. A. Petersson, H. Nakatsuji, M. Hada, M. Ehara, K. Toyota, R. Fukuda, J. Hasegawa, M. Ishida, T. Nakajima, Y. Honda, O. Kitao, H. Nakai, M. Klene, X. Li, J. E. Knox, H. P. Hratchian, J. B. Cross, V. Bakken, C. Adamo, J. Jaramillo, R. Gomperts, R. E. Stratmann, O. Yazyev, A. J. Austin, R. Cammi, C. Pomelli, J. W. Ochterski, P. Y. Ayala, K. Morokuma, G. A. Voth, P. Salvador, J. J. Dannenberg, V. G. Zakrzewski, S. Dapprich, A. D. Daniels, M. C. Strain, O. Farkas, D. K. Malick, A. D. Rabuck, K. Raghavachari, J. B. Foresman, J. V. Ortiz, Q. Cui, A. G. Baboul, S. Clifford, J. Cioslowski, B. B. Stefanov, G. Liu, A. Liashenko, P. Piskorz, I. Komaromi, R. L. Martin, D. J. Fox, T. Keith, M. A. Al-Laham, C. Y. Peng, A. Nanayakkara, M. Challacombe, P. M. W. Gill, B. Johnson, W. Chen, M. W. Wong, C. Gonzalez, and J. A. Pople, Gaussian 03, Revision D.02; Gaussian, Inc., Wallingford CT., 2004.

(2) Adams, M.; Zimmermann, S.; Kaiser, M.; Brun, R.; Hamburger, M., *Nat. Prod. Commun.* **2009,** 4, 1377-1381

S4. Struture of Hydrangenone

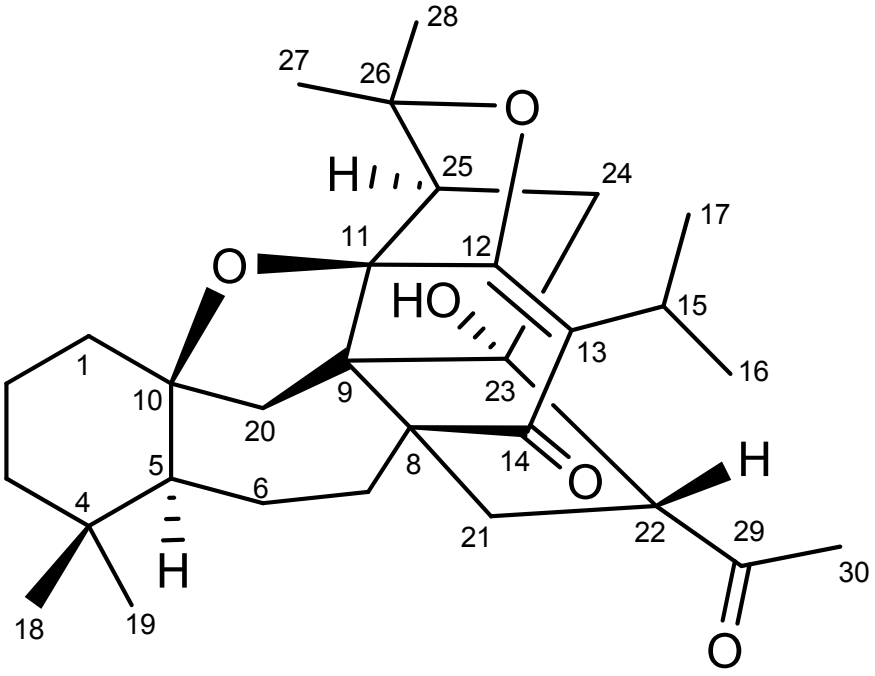

S5. Single-crystal X-ray struture of Hydrangenone

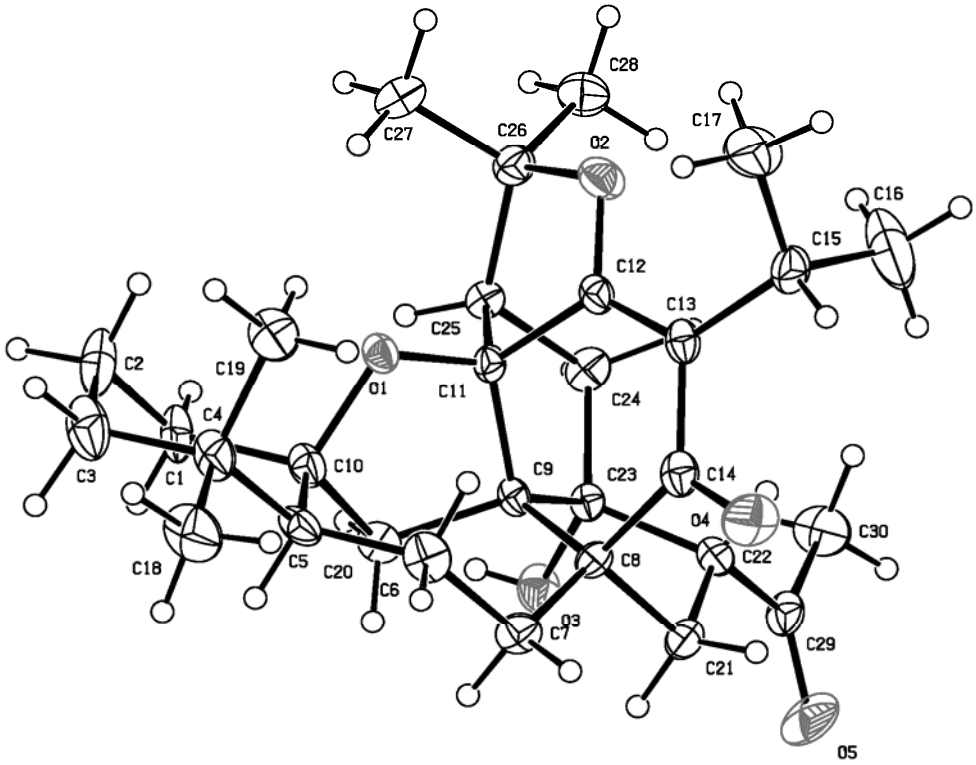

S6. ^{1}H NMR spectrum of Hydrangenone in C_6D_6

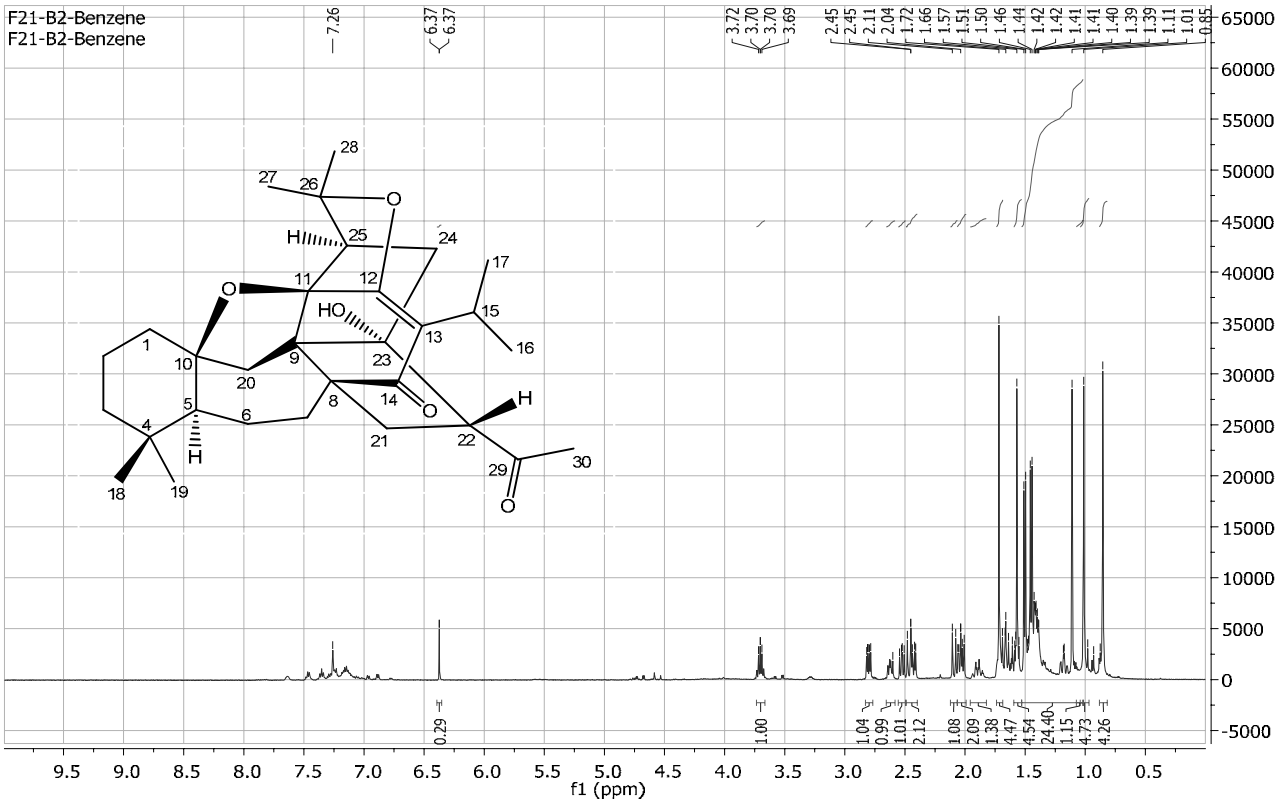

S7. Expanded ^{1}H NMR spectrum of Hydrangdione C in C_6D_6

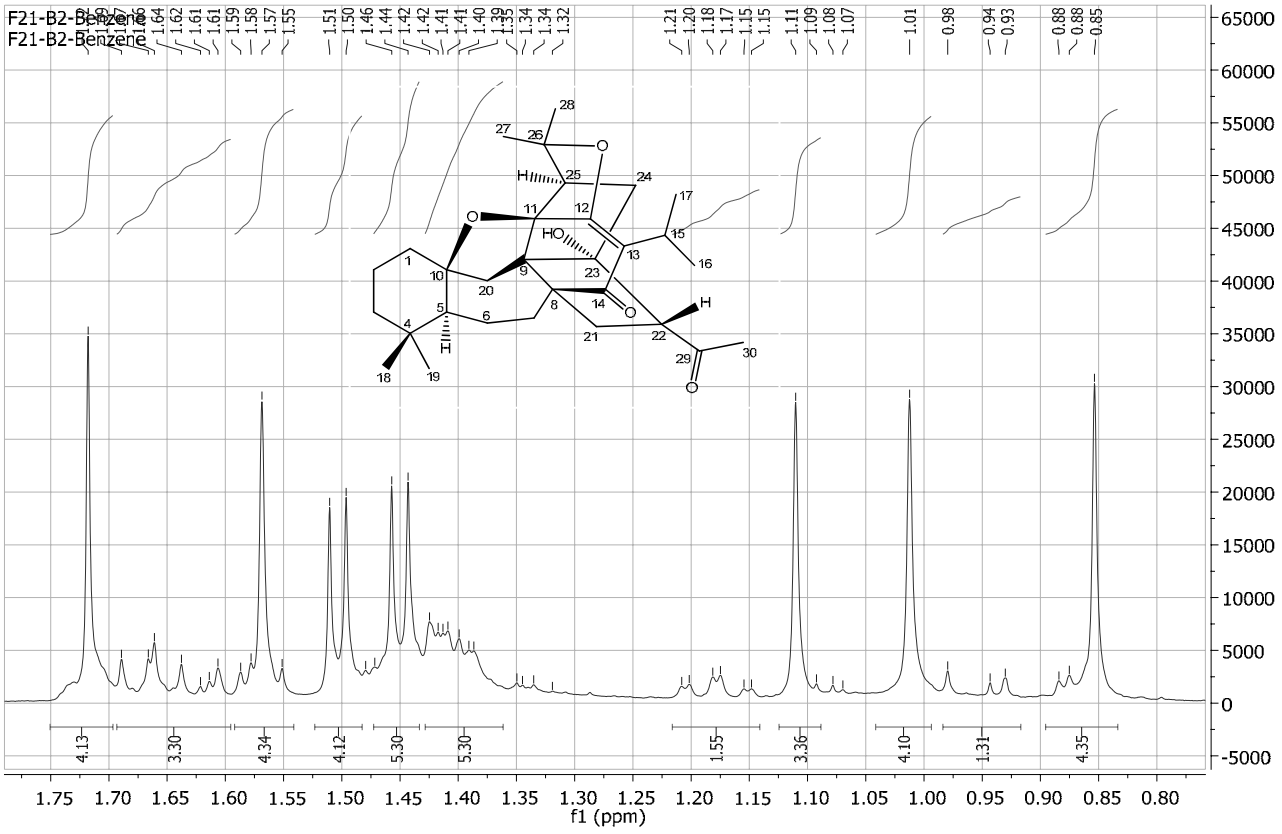

S8. Expanded ^{1}H NMR spectrum of Hydrangenone in C_6D_6

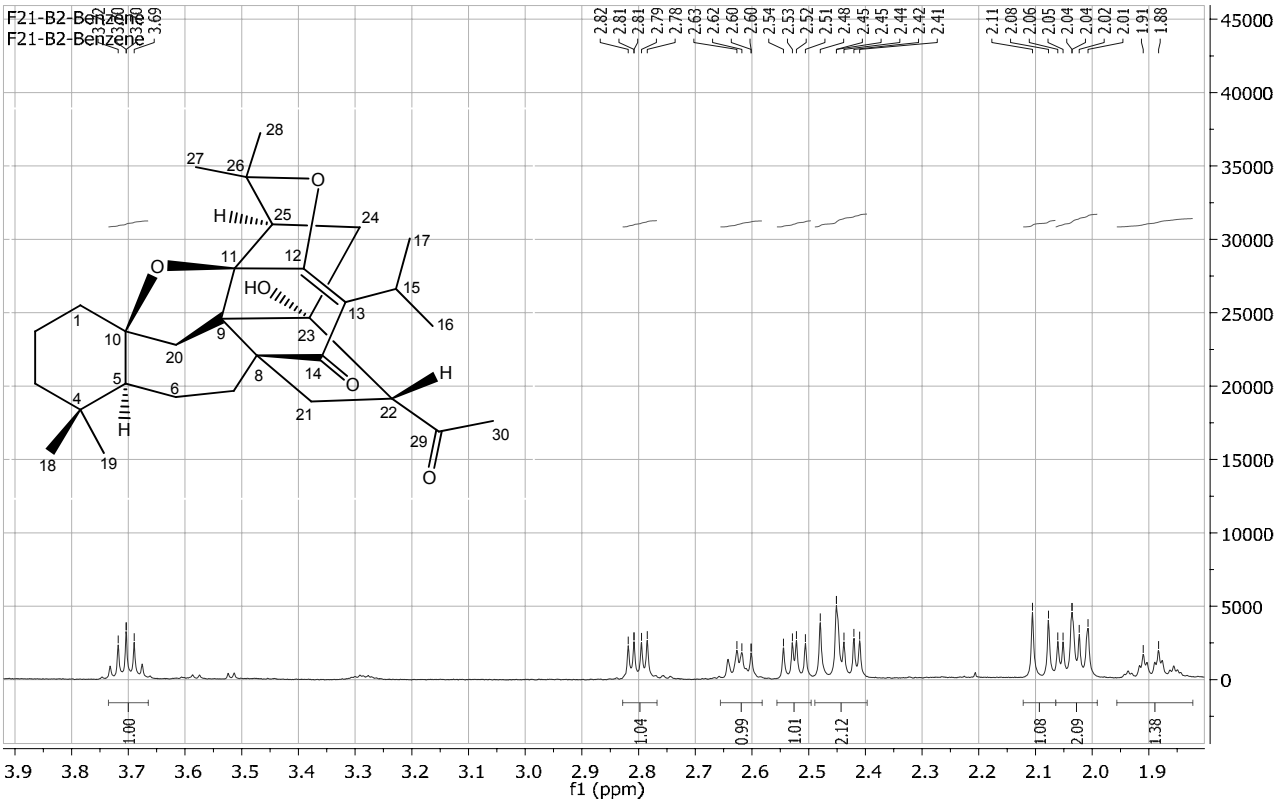

S9. ^{13}C NMR spectrum of Hydrangenone in C_6D_6

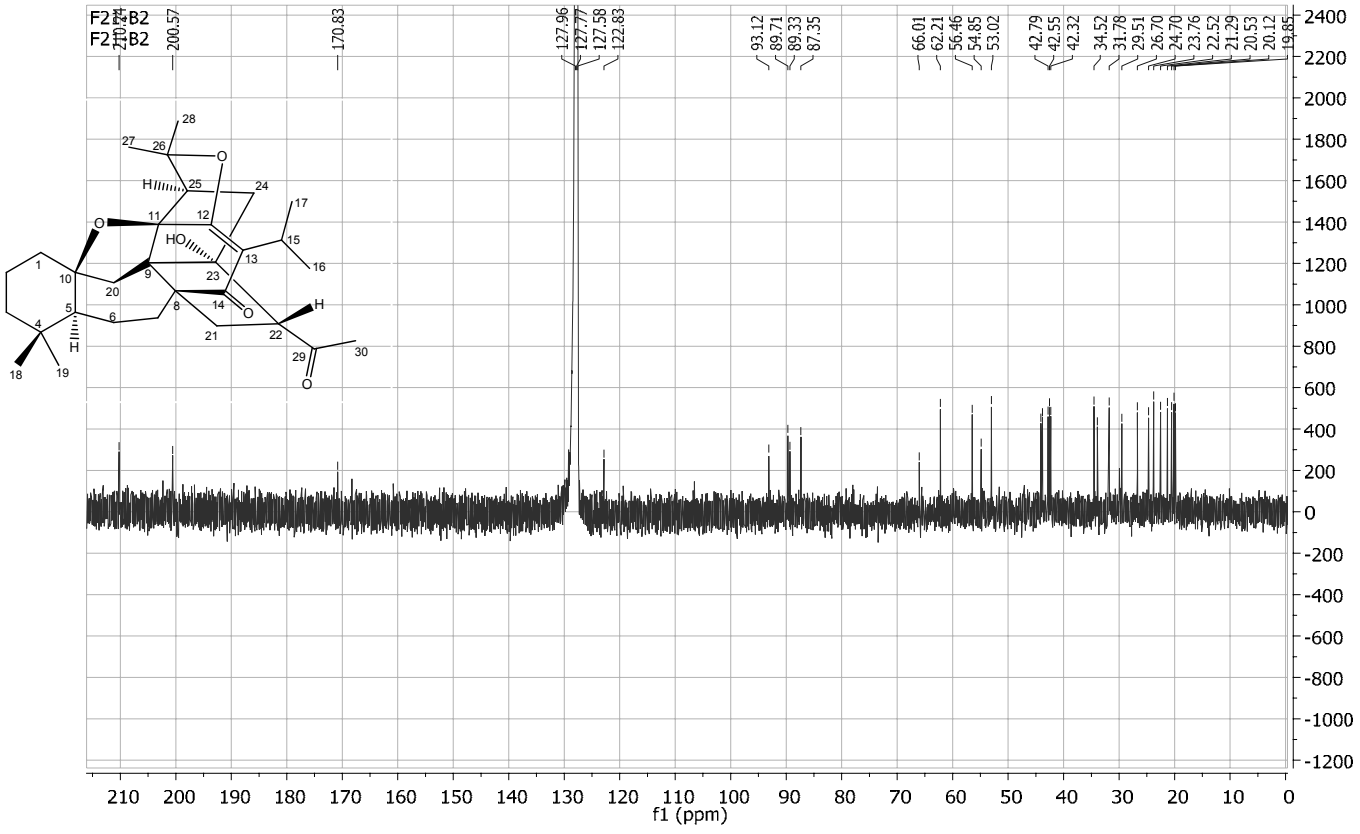

S10. Expanded ^{13}C NMR spectrum of Hydrangenone in C_6D_6

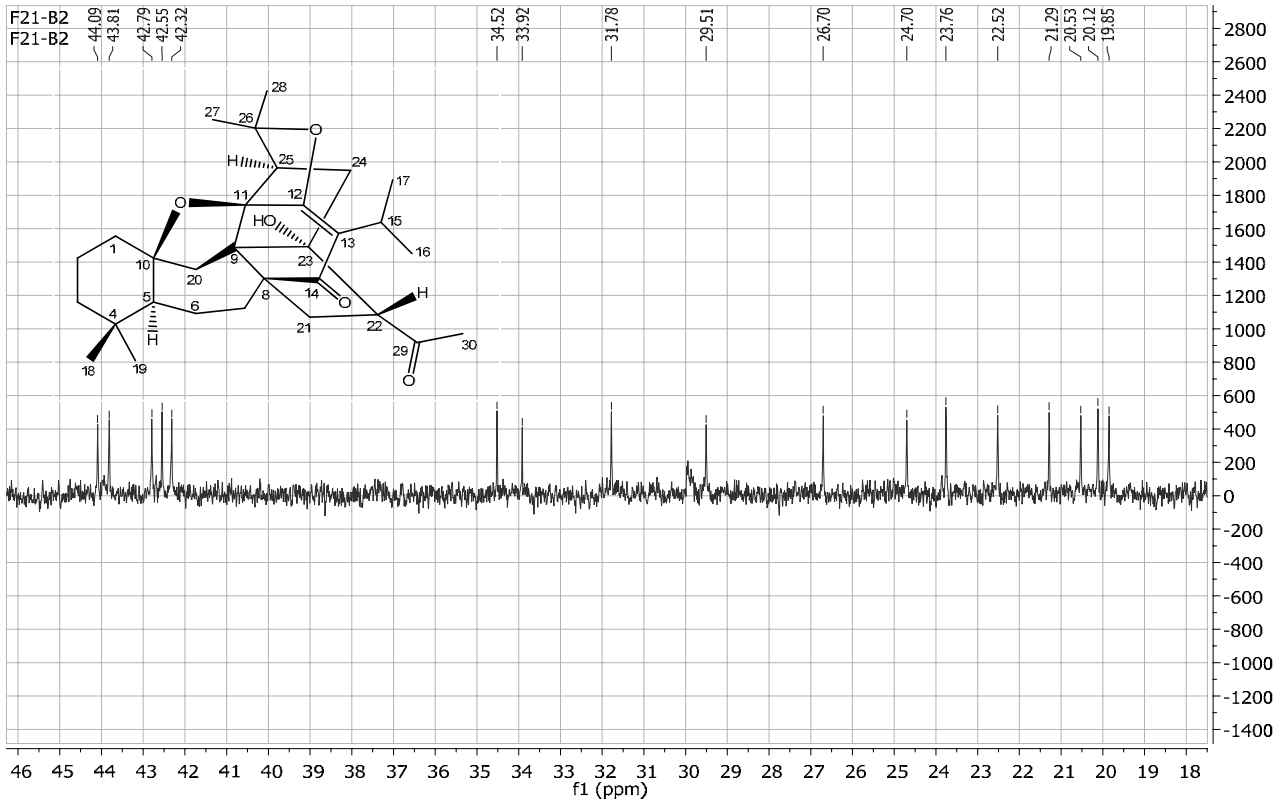

S11. Expanded ^{13}C NMR spectrum of Hydrangenone in C_6D_6

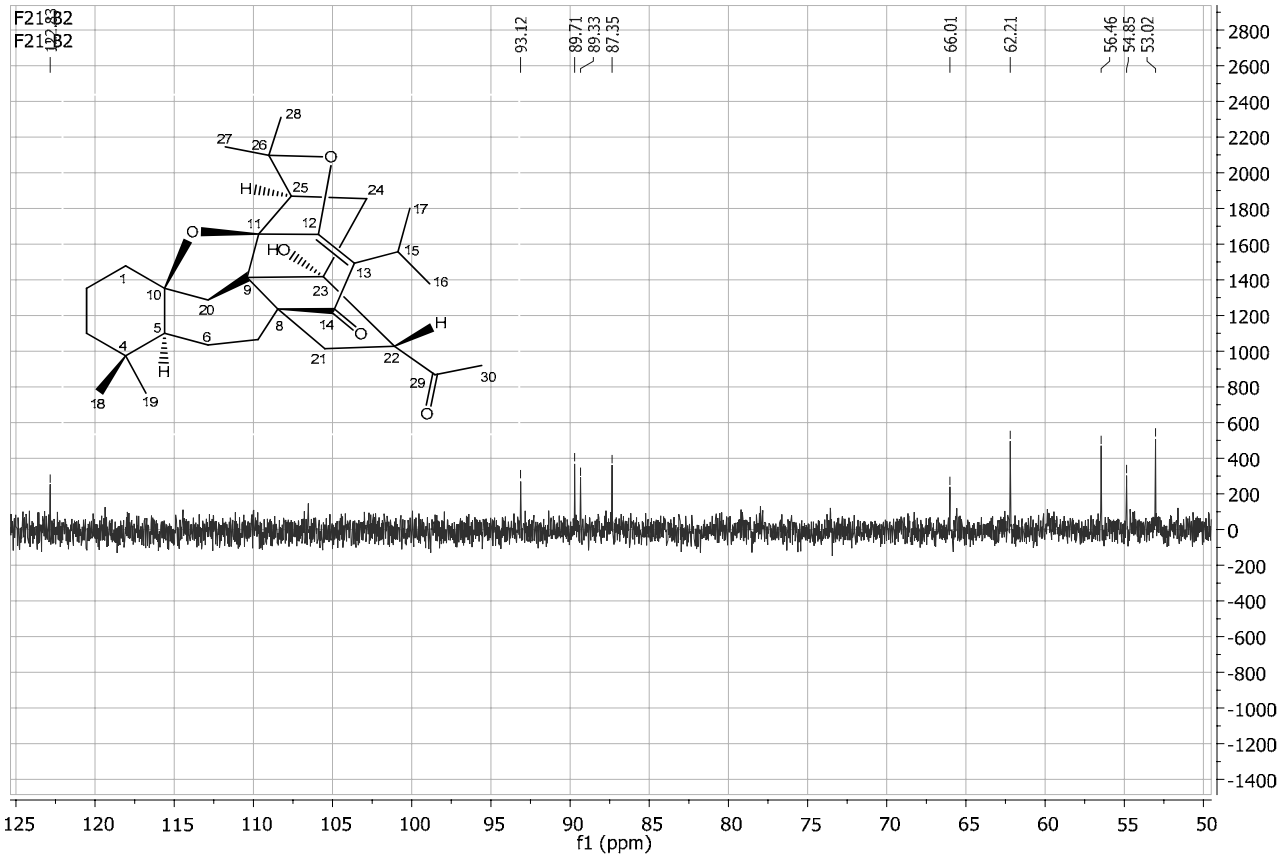

S12. DEPT135 spectrum of Hydrangenone in C_6D_6

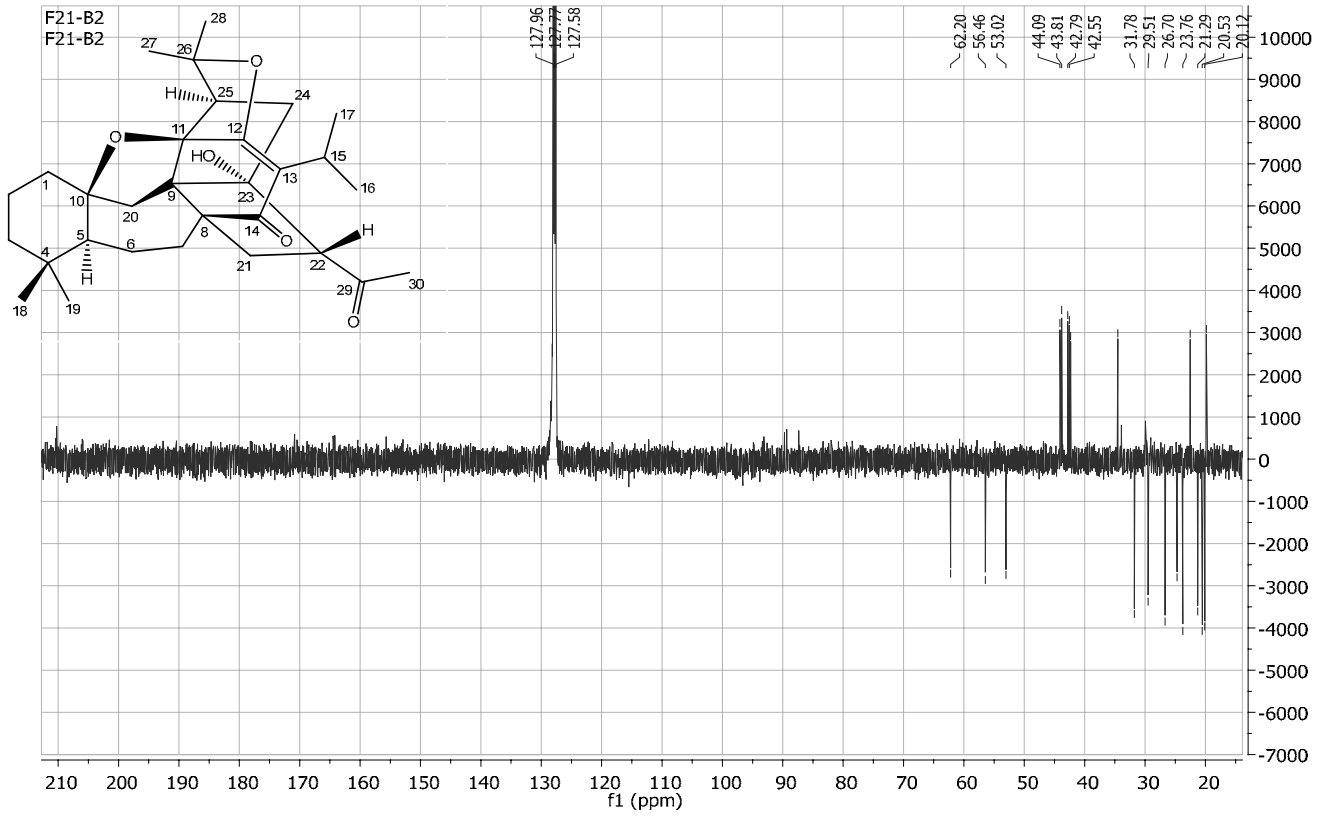

S13. Expanded DEPT135 spectrum of Hydrangenone in C_6D_6

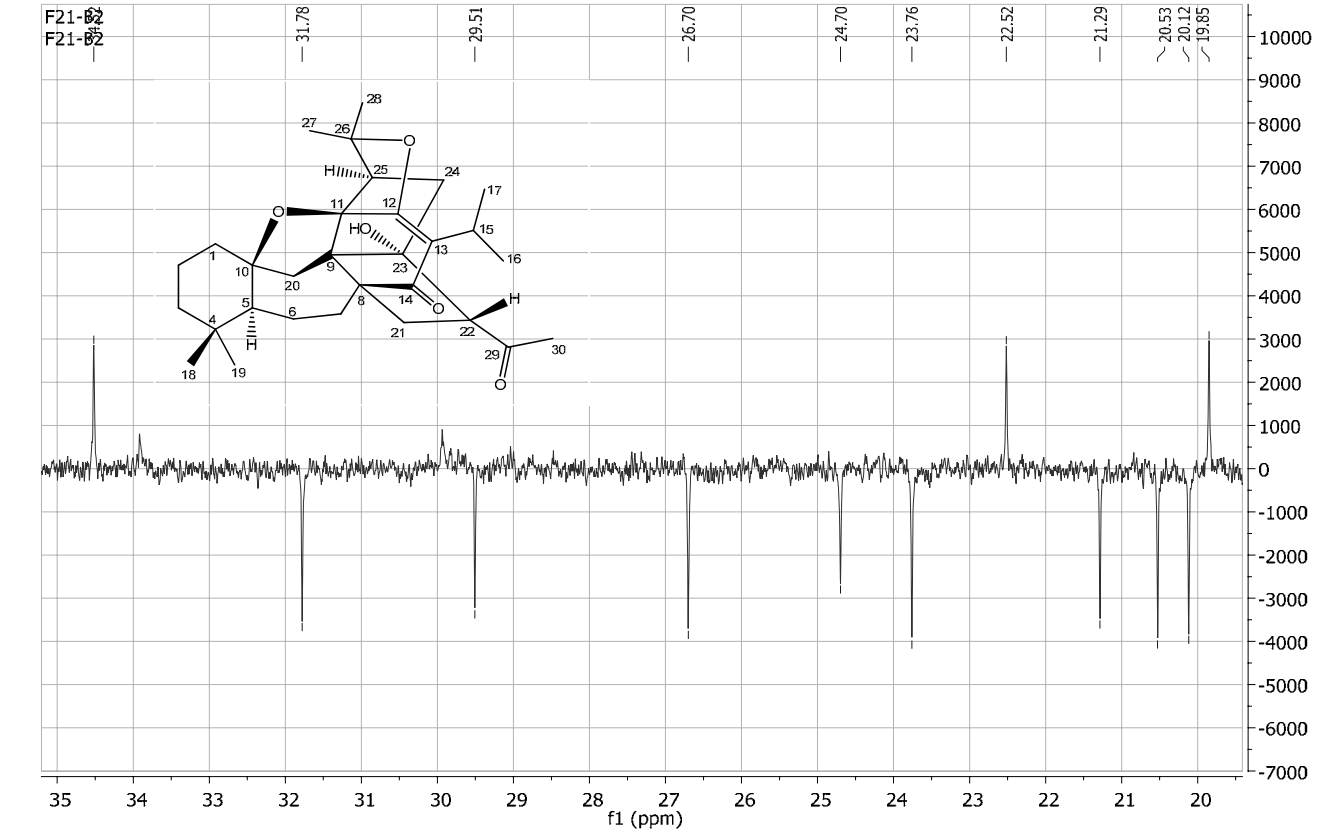

S14. Expanded DEPT135 spectrum of Hydrangenone in C_6D_6

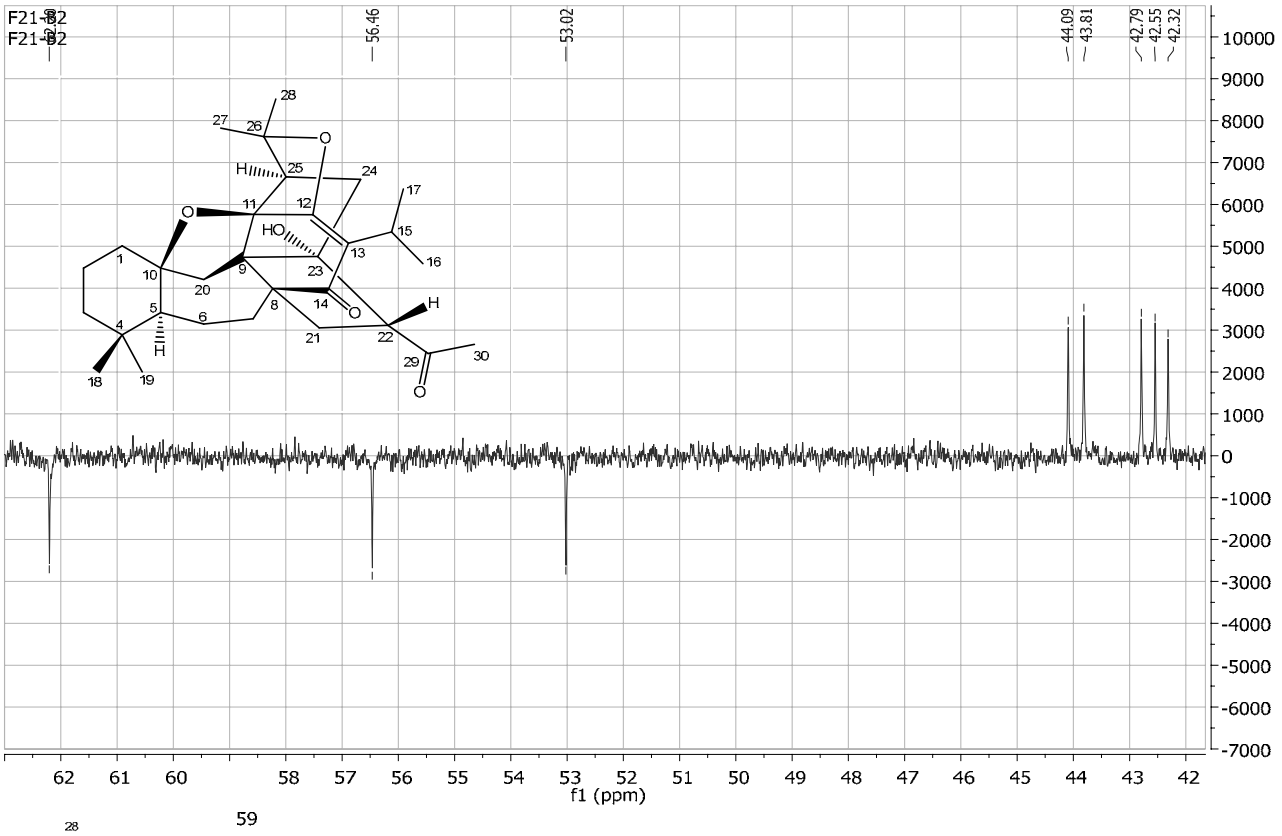

S15. ^1H ^1H COSY spectrum of Hydrangenone in C_6D_6

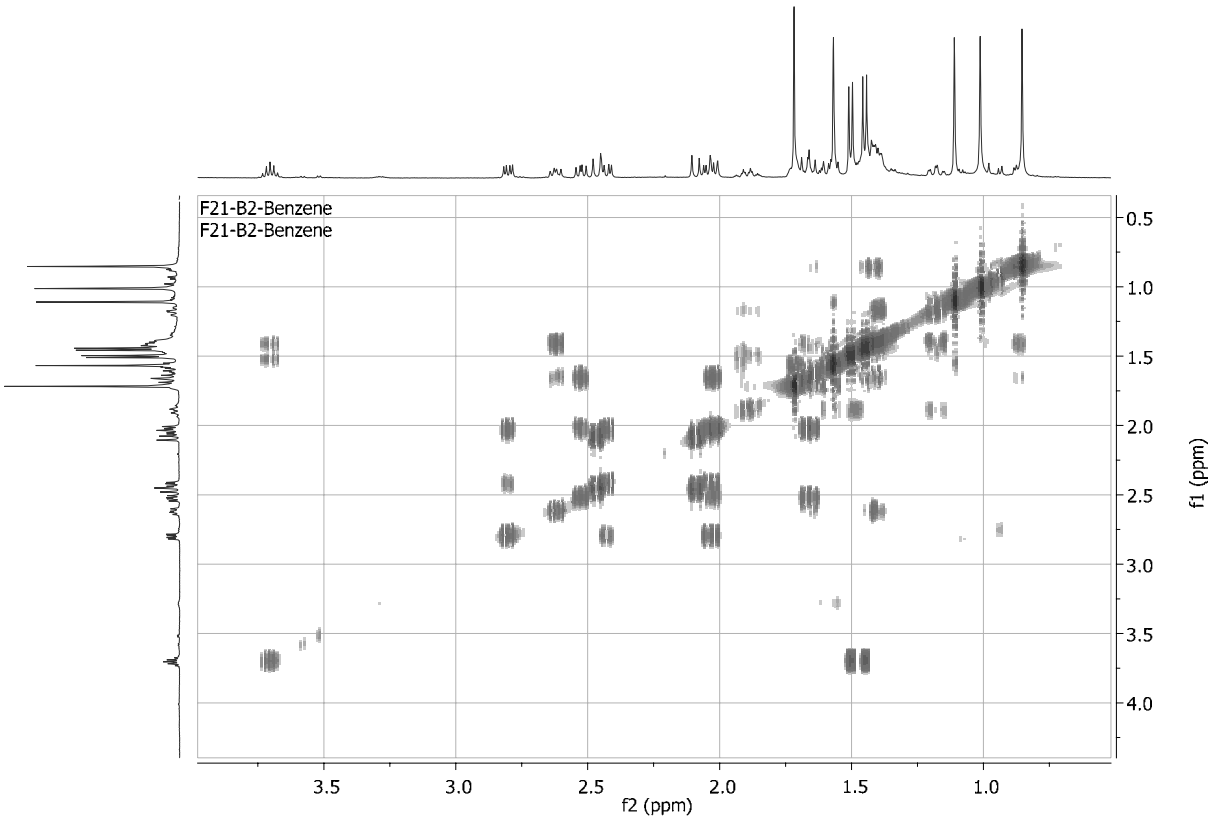

S16. HMQC spectrum of Hydrangenone in C_6D_6

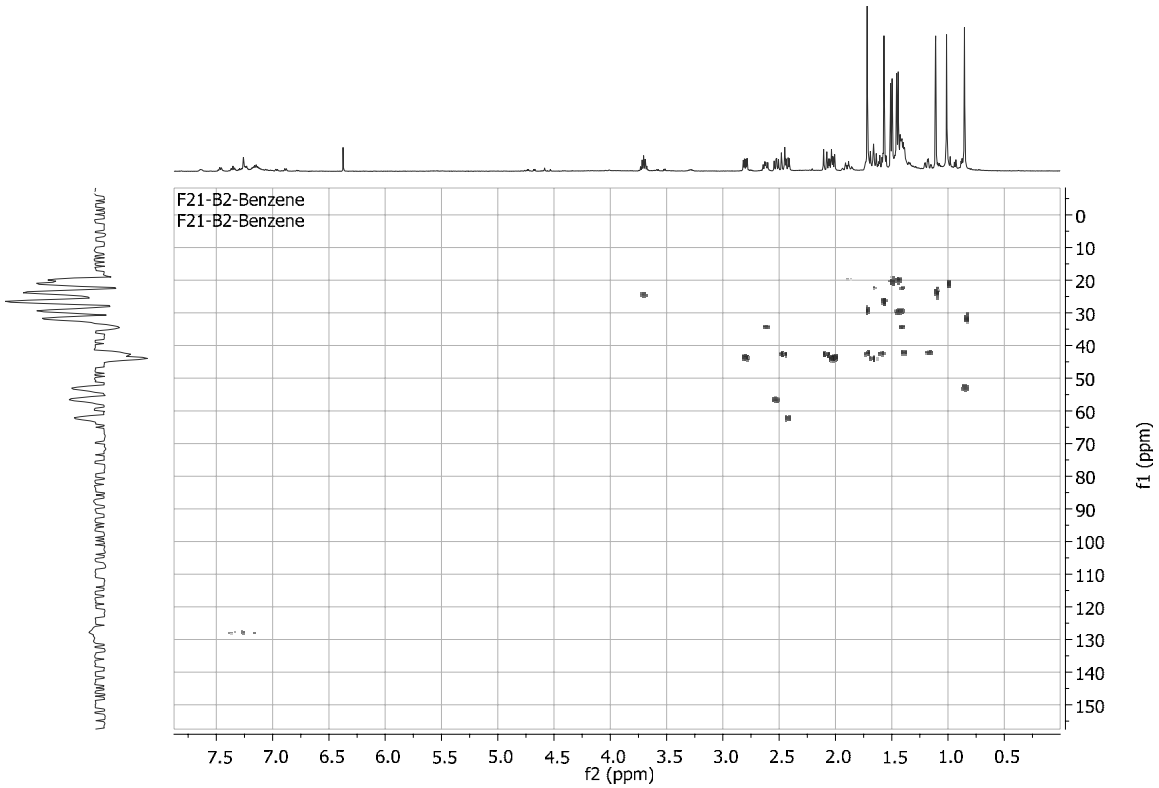

S17. Expanded HMQC spectrum of Hydrangenone in C_6D_6

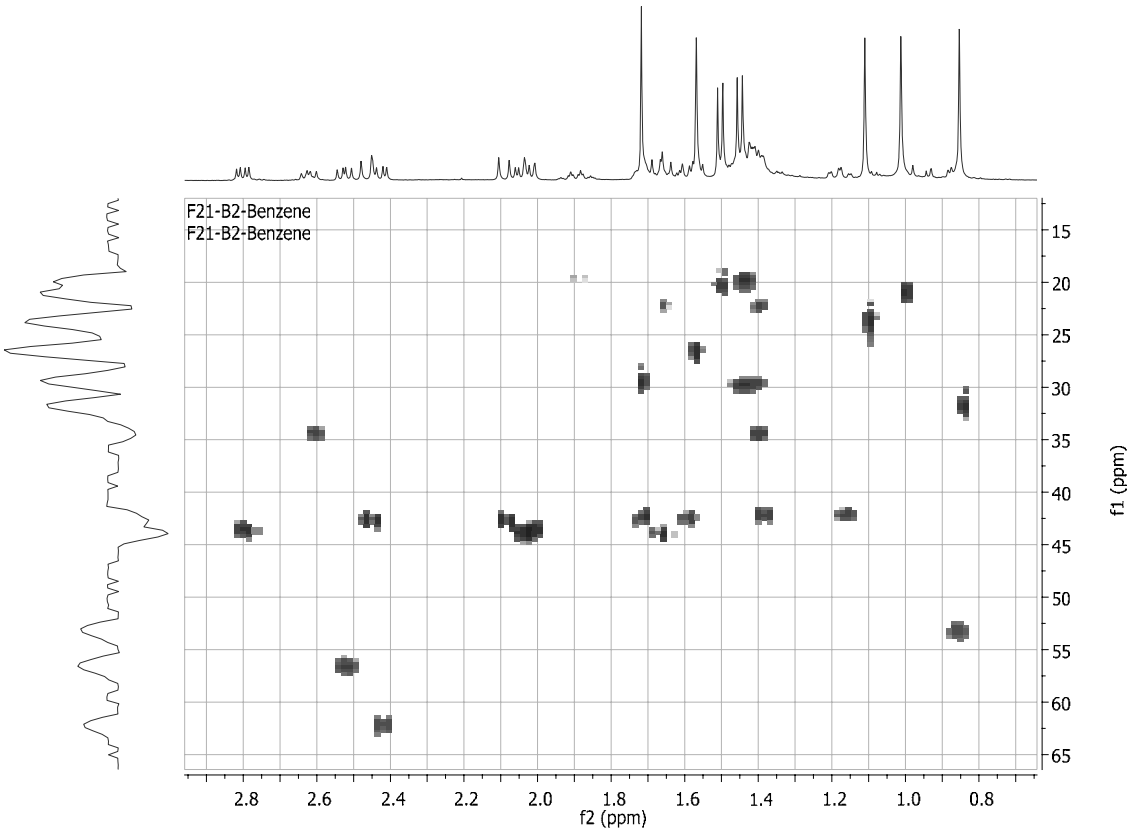

S18. HMBC spectrum of Hydrangenone in C_6D_6

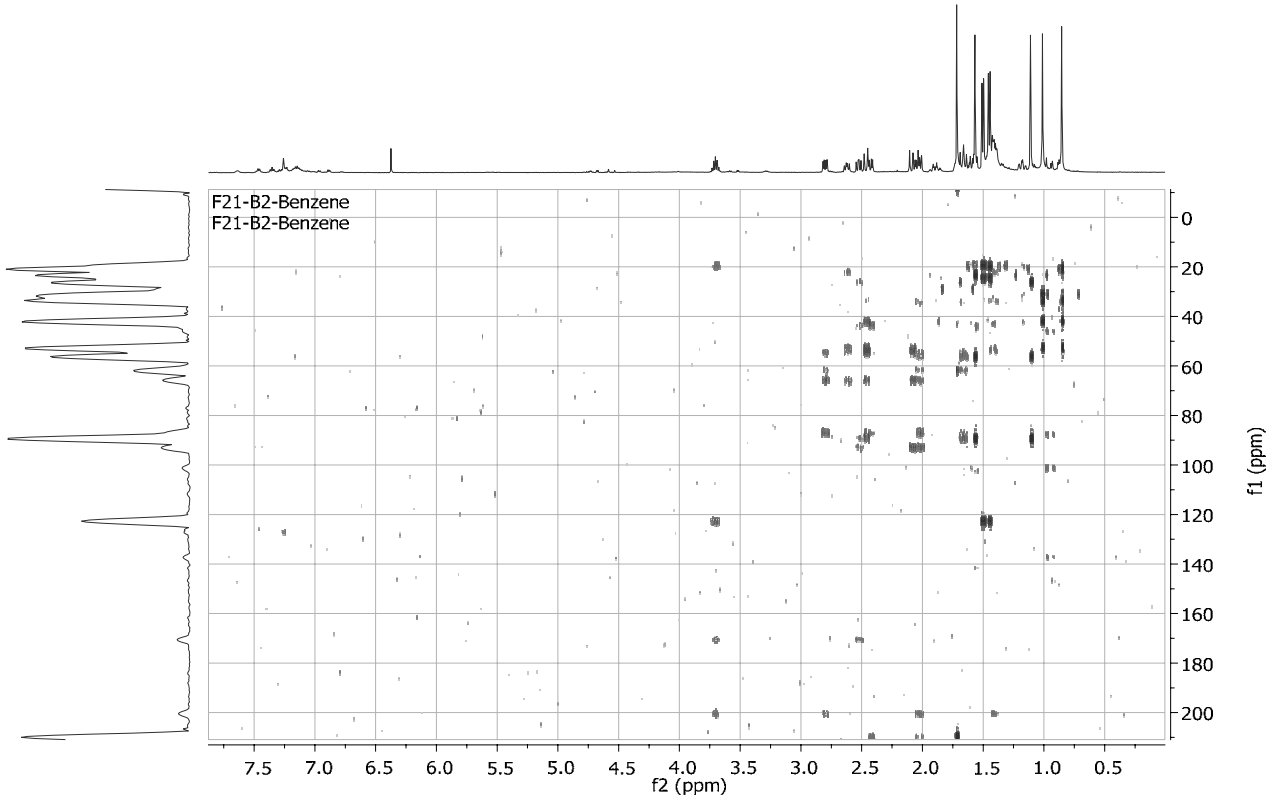

S19. Expanded HMBC spectrum of Hydrangenone in C_6D_6

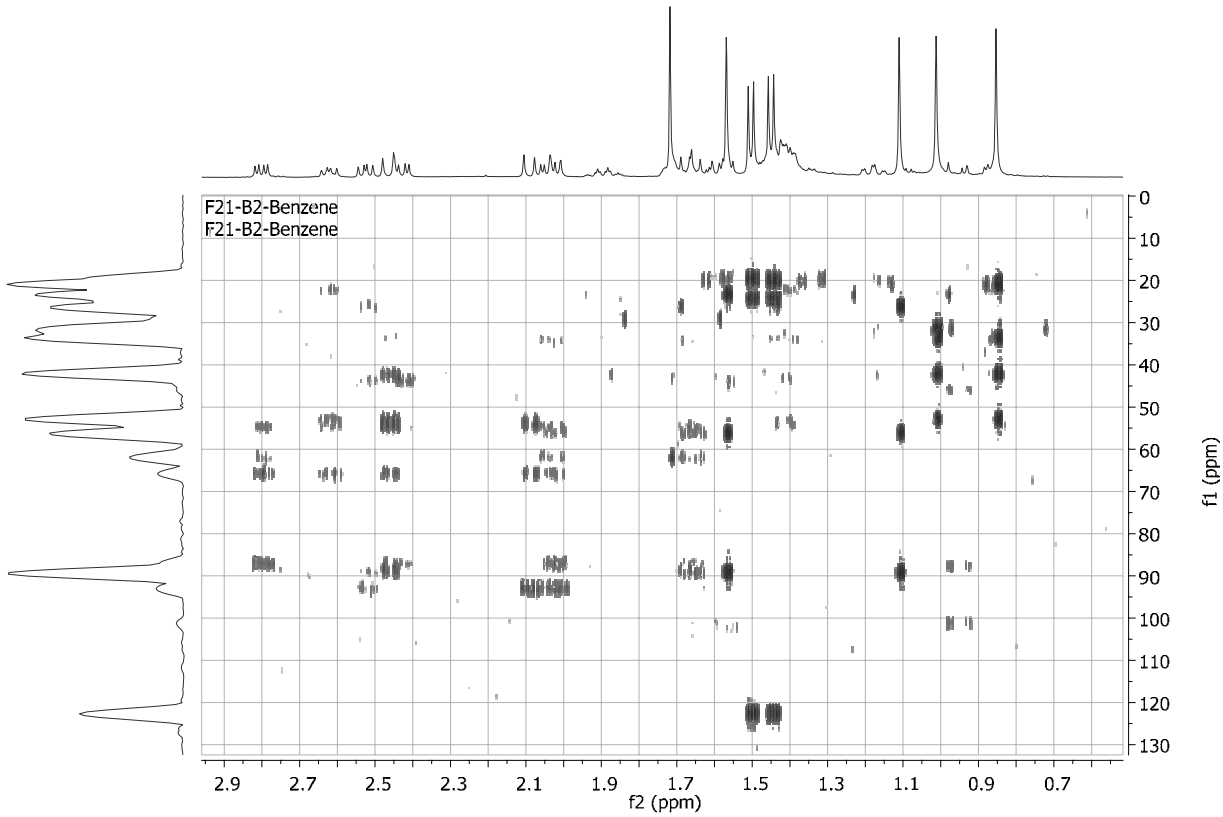

S20. NOESY spectrum of Hydrangenone in C_6D_6

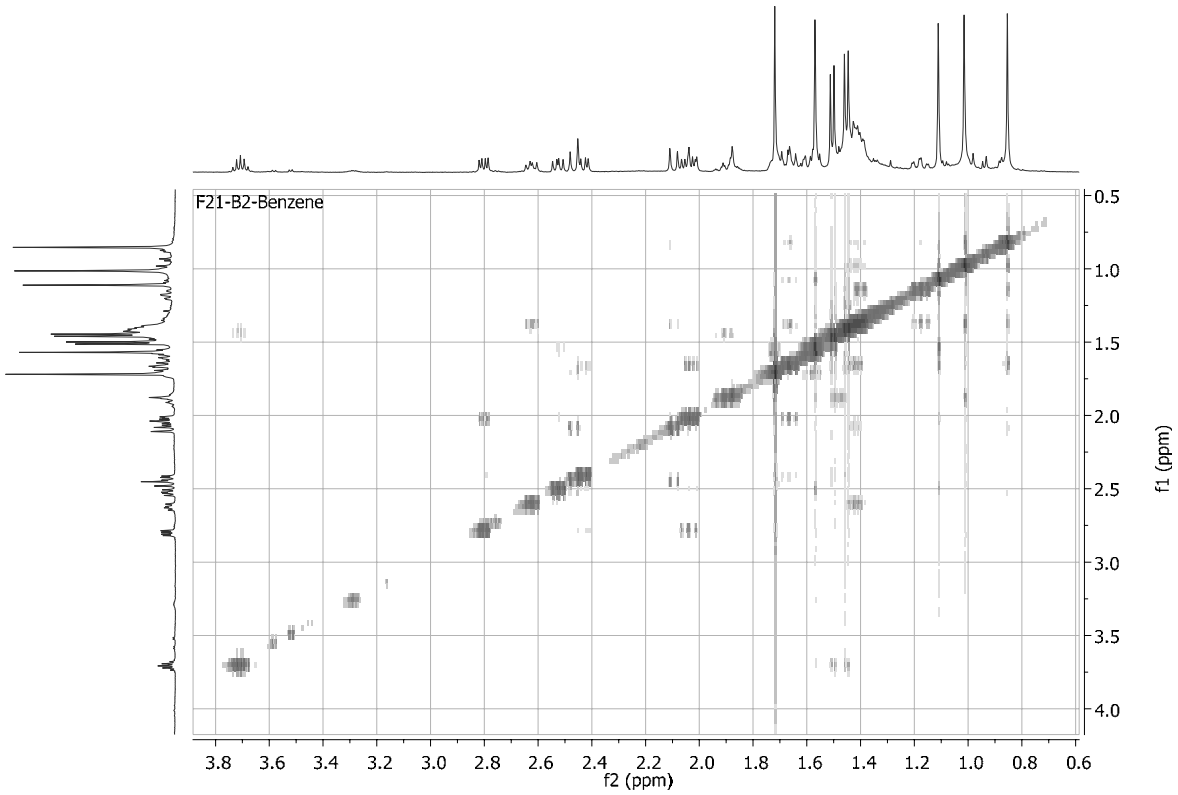

S21. Expanded NOESY spectrum of Hydrangenone in C_6D_6

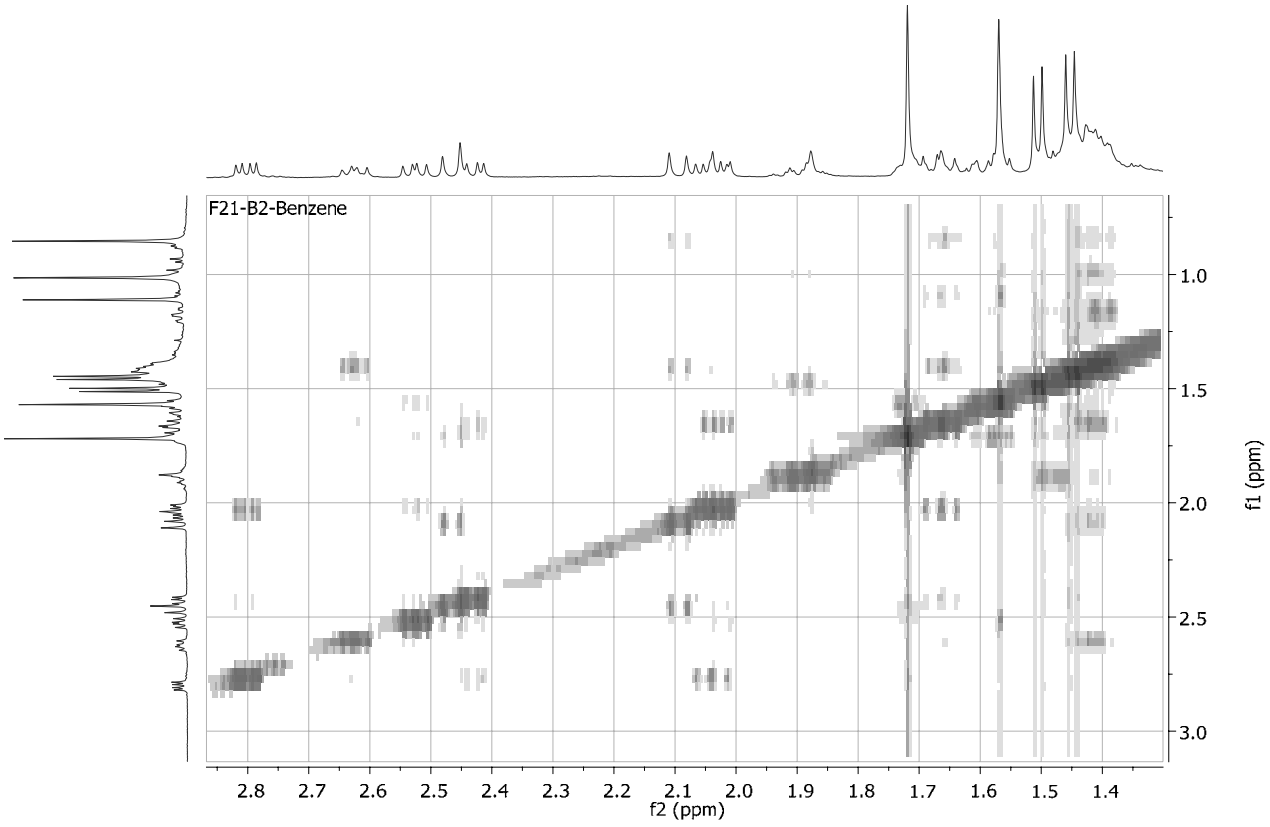

S22. ^{1}H NMR spectrum of Hydrangenone in $CDCl_3$

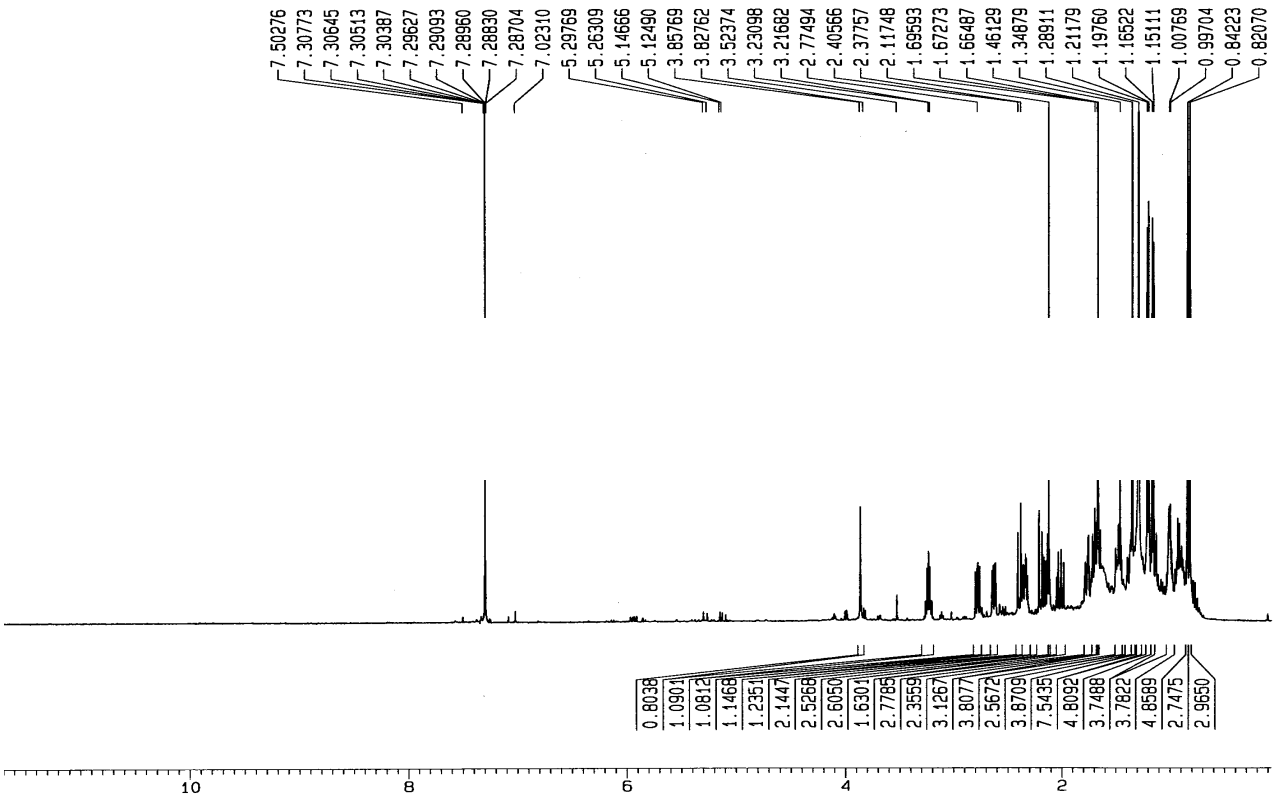

S23. Expanded ^{1}H NMR spectrum of Hydrangenone in $CDCl_3$

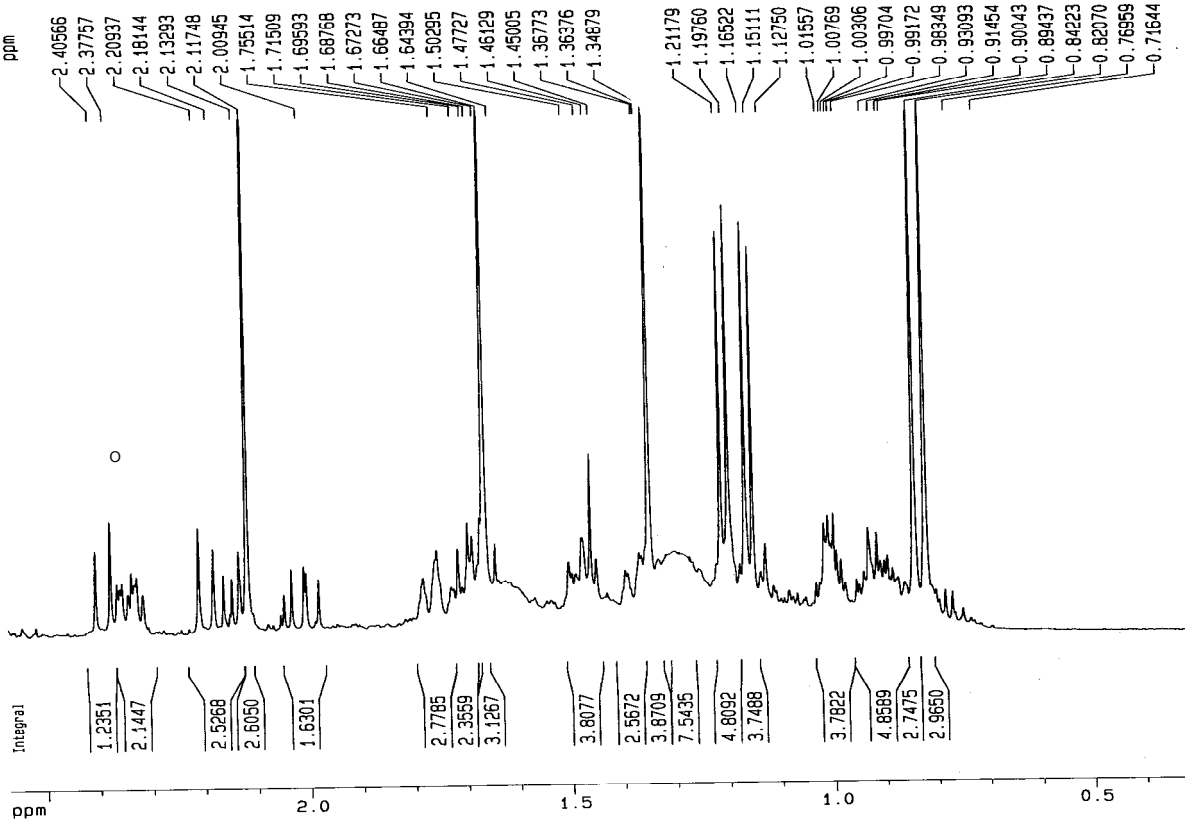

S24. Expanded ^{1}H NMR spectrum of Hydrangenone in $CDCl_3$

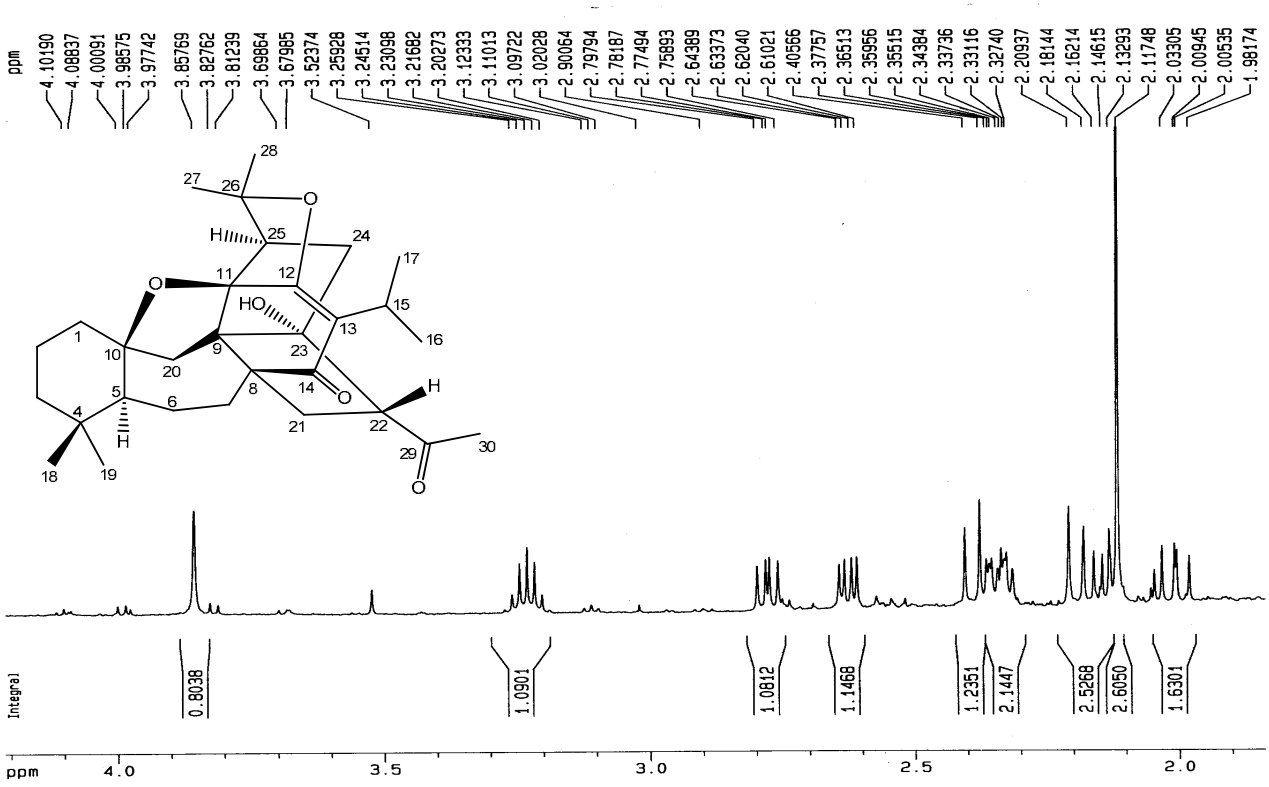

S25. ^{13}C NMR spectrum of Hydrangenone in $CDCl_3$

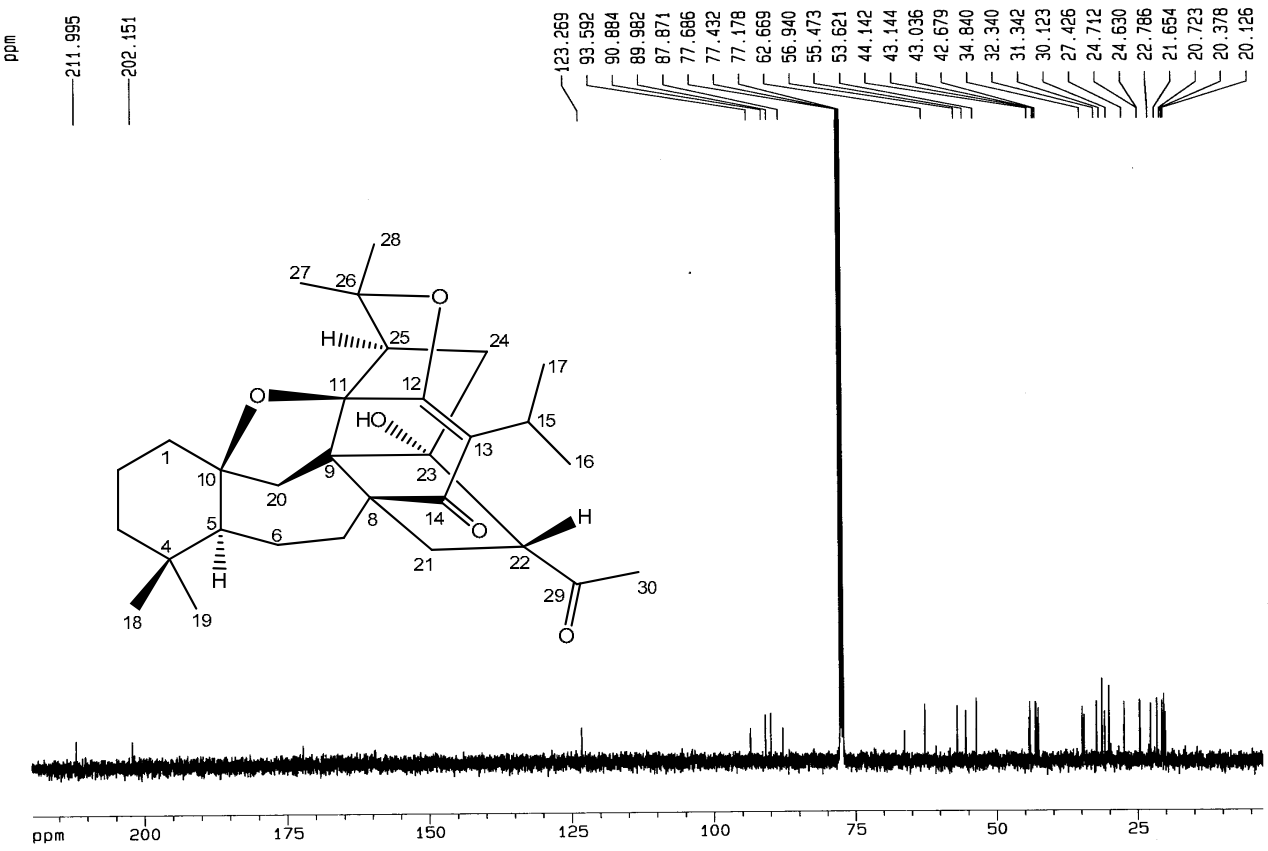

S26. Expanded ^{13}C NMR spectrum of Hydrangenone in $CDCl_3$

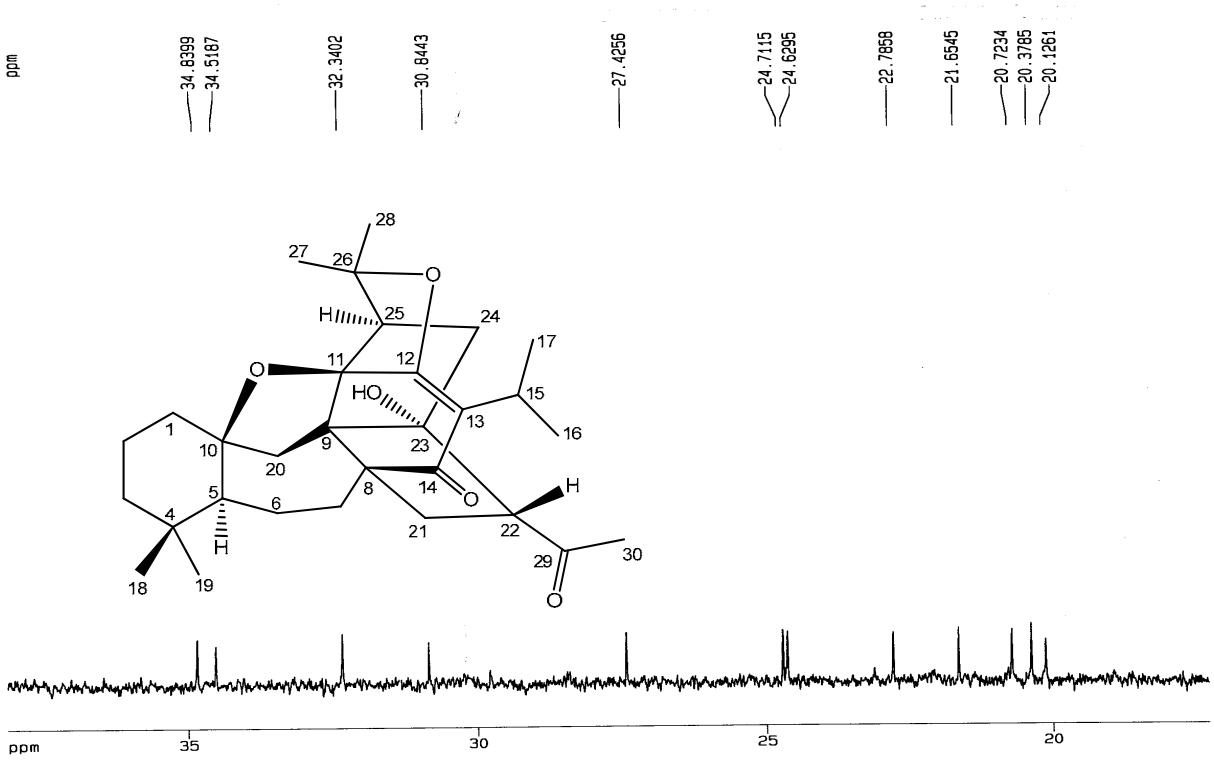

S27. Expanded ^{13}C NMR spectrum of Hydrangenone in $CDCl_3$

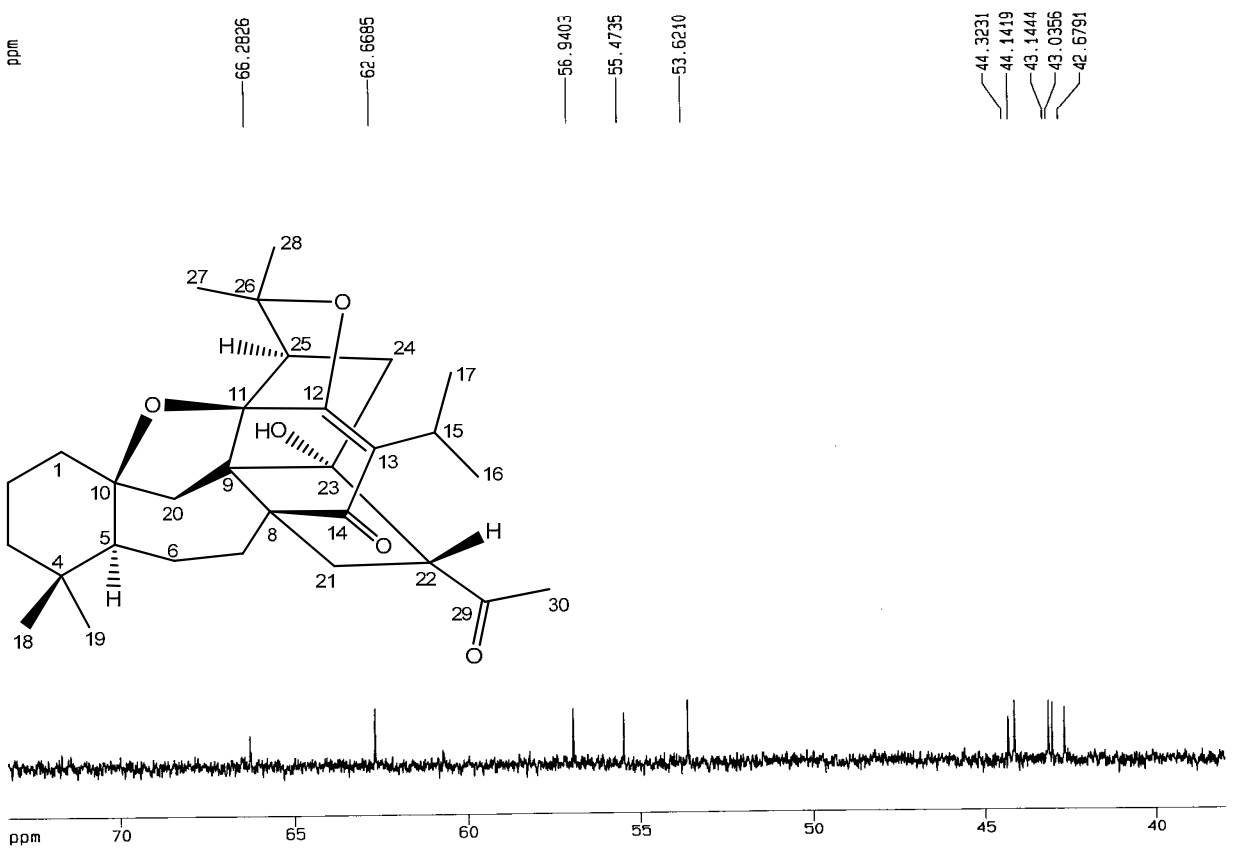

S28. DEPT135 spectrum of Hydrangenone in $CDCl_3$

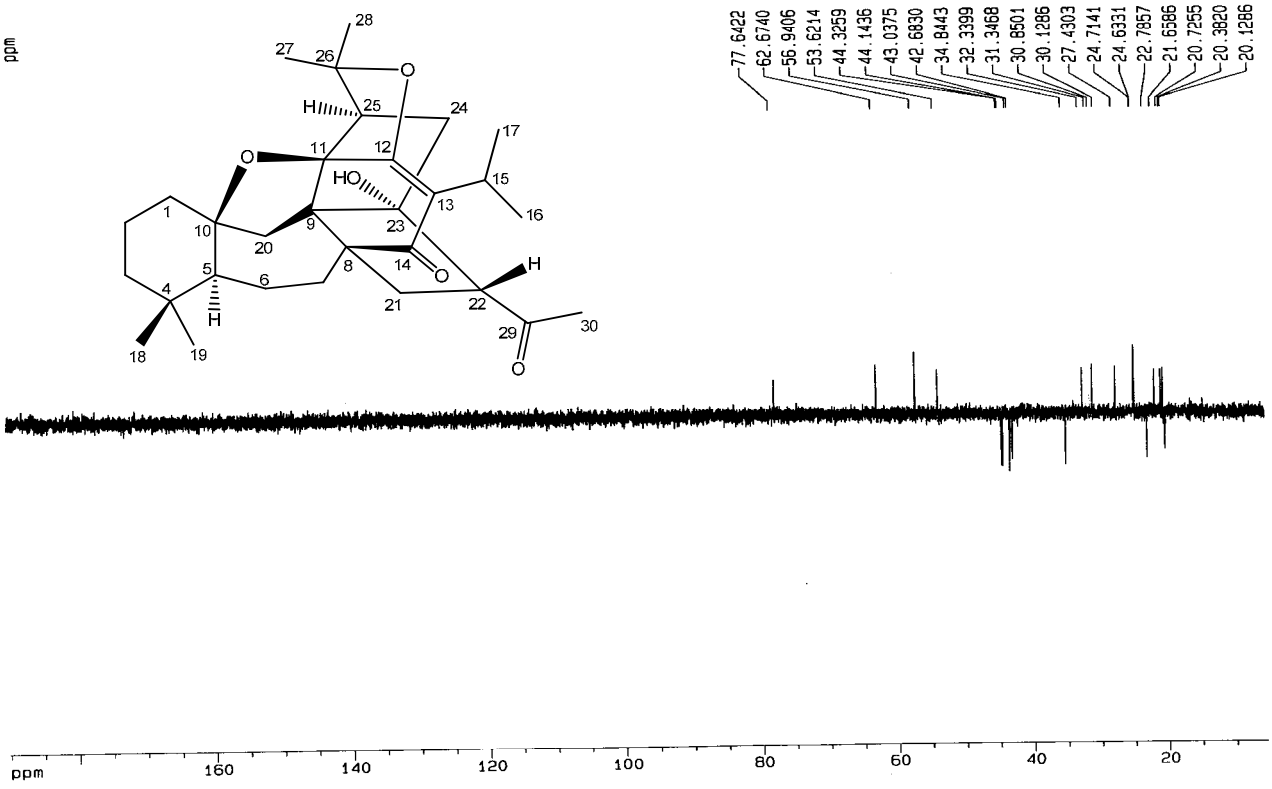

S29. Expanded DEPT135 spectrum of Hydrangenone in $CDCl_3$

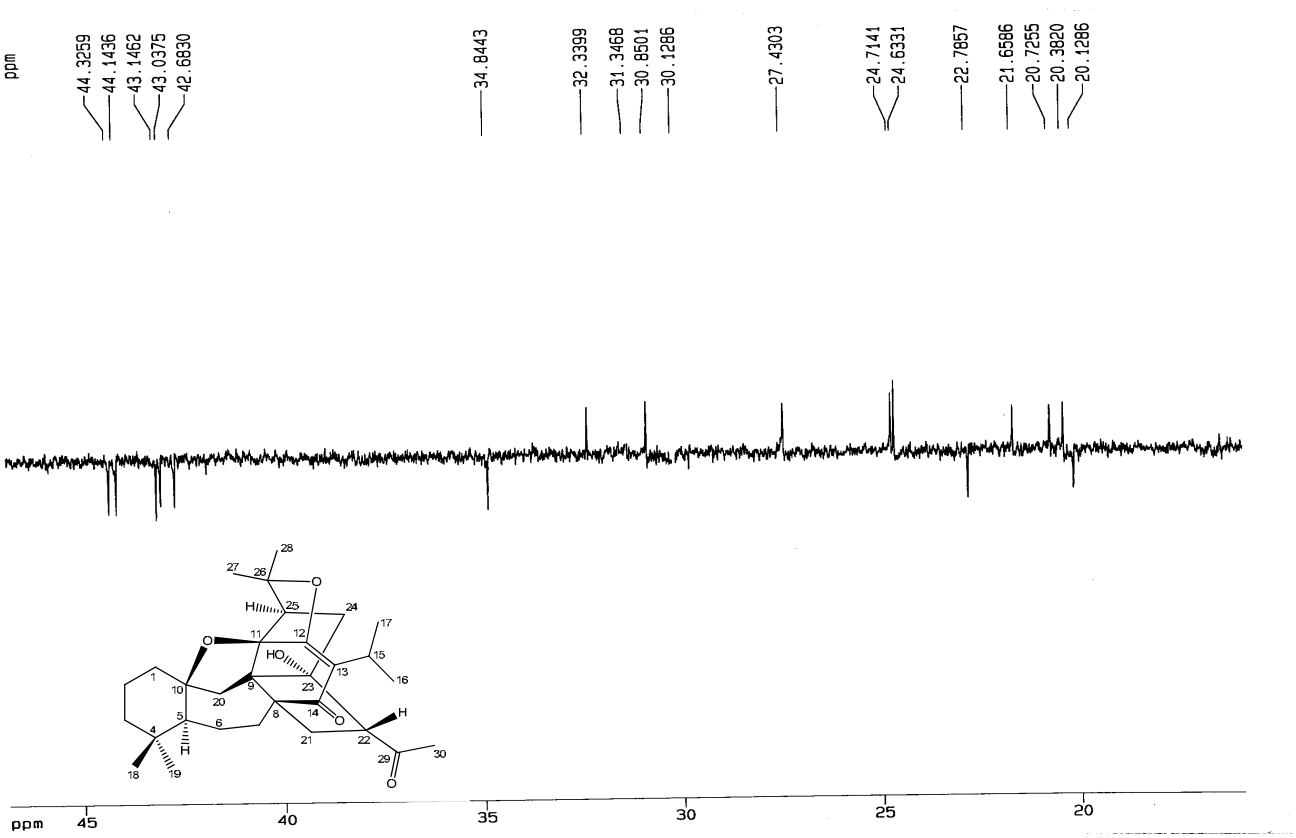

S30. HMQC spectrum of Hydrangenone in $CDCl_3$

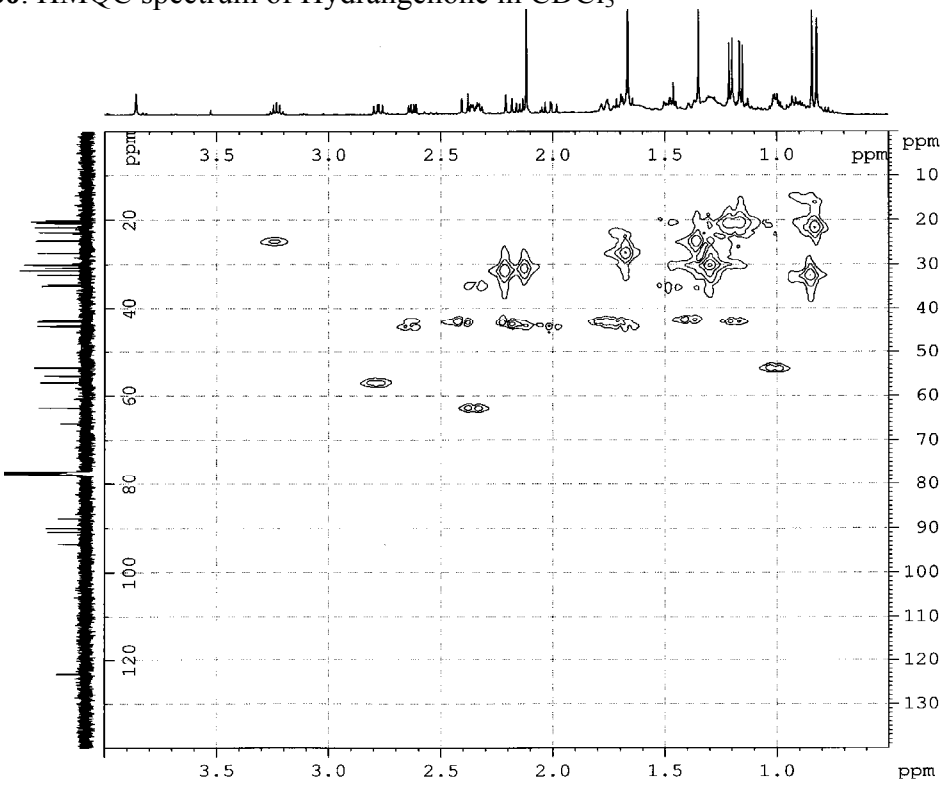

S31. Expanded HMQC spectrum of Hydrangenone in $CDCl_3$

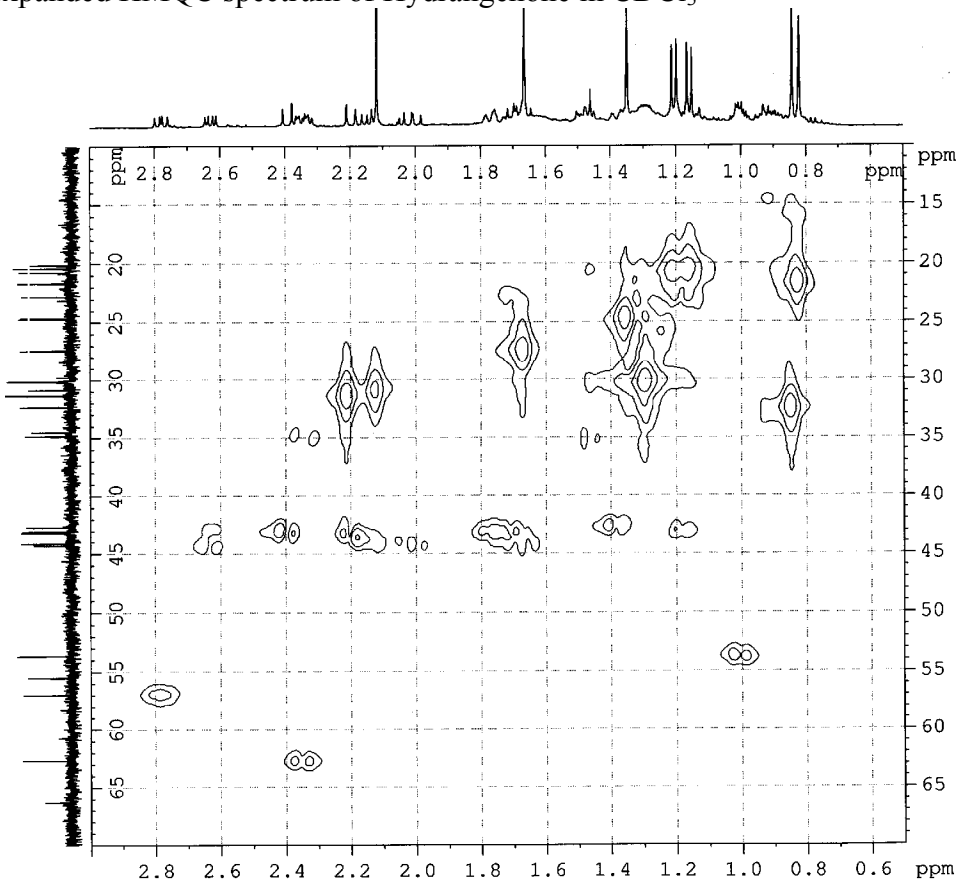

S32. HMBC spectrum of Hydrangenone in $CDCl_3$

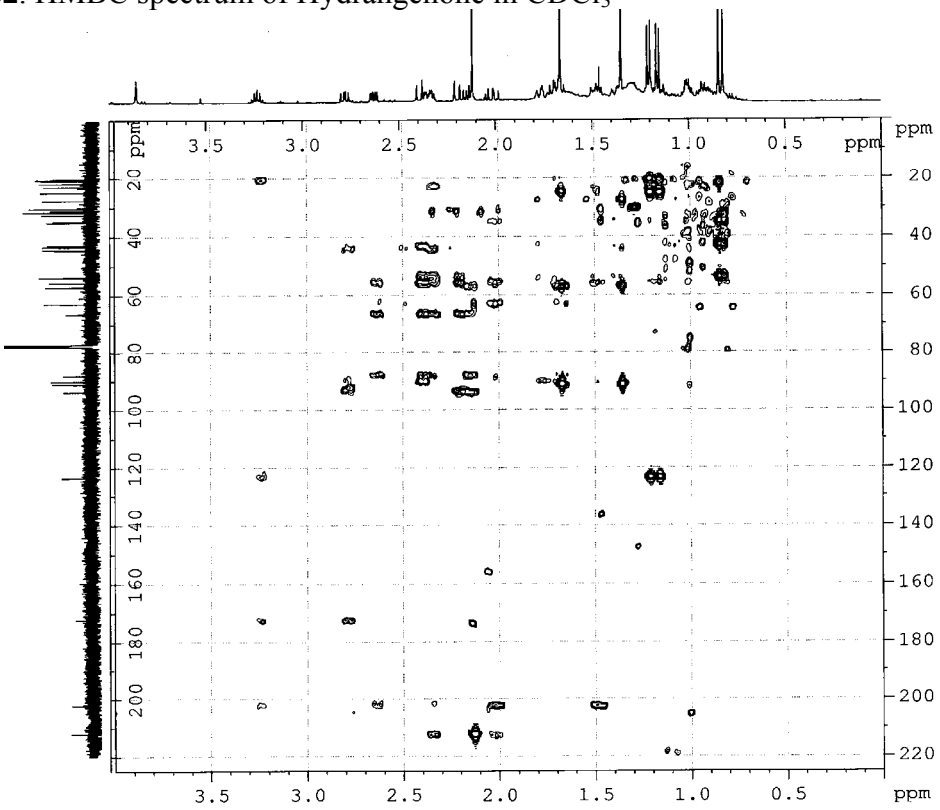

S33. Expanded HMBC spectrum of Hydrangenone in $CDCl_3$

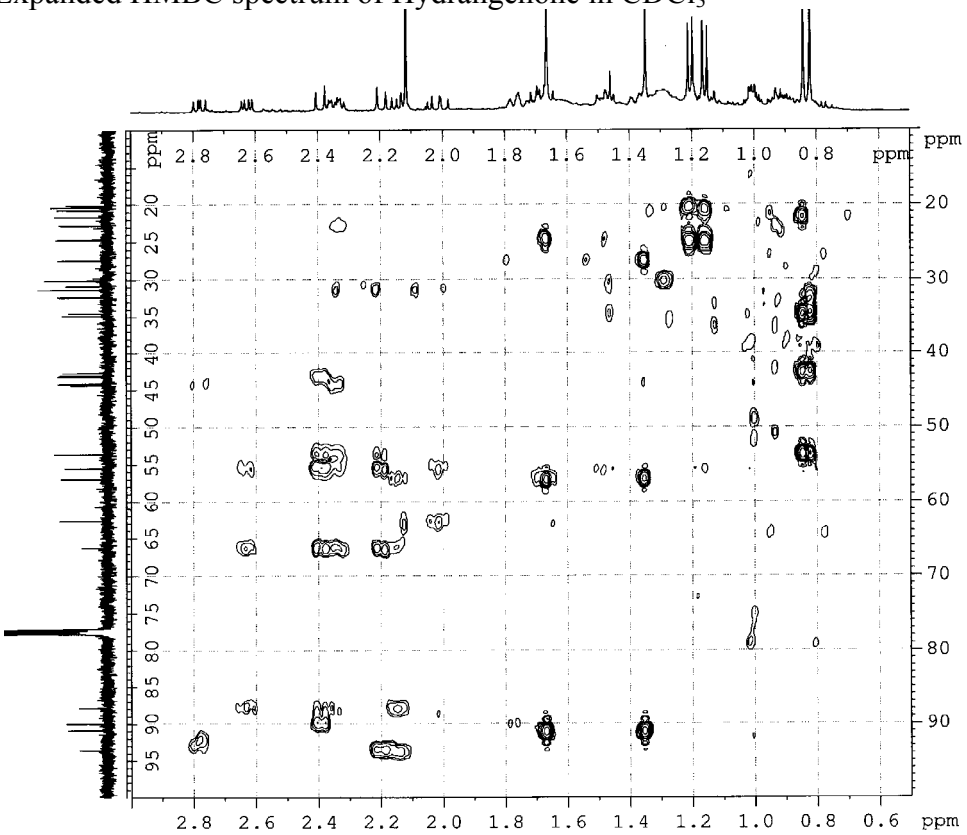

3.5. Triterpenoids with rare carbon skeletons from *Salvia hydrangea*: antiprotozoal activity and absolute configurations

Mehdi Moridi Farimani, M. Babak Bahadori, Salman Taheri, Samad Nejad Ebrahimi, Stefanie Zimmermann, Reto Brun, Gholamreza Amin , and Matthias Hamburger

J. Nat. Prod., 2011, 74 (10), pp 2200–2205 **DOI:** 10.1021/np200559c

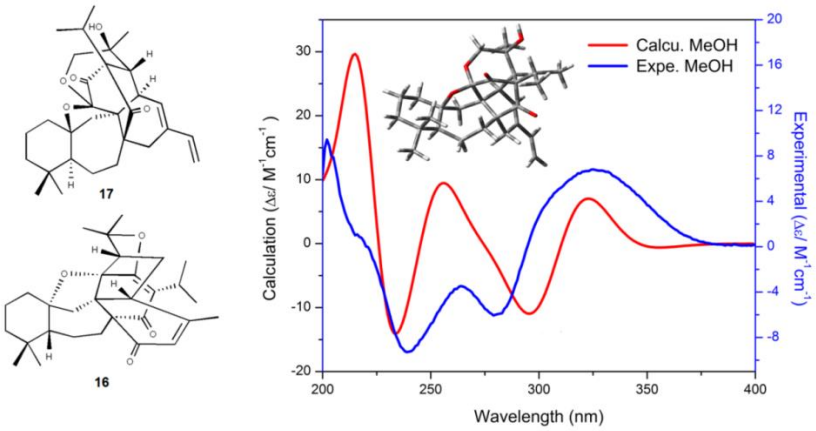

Salvadione C (**1**) and perovskone B (**2**), two new triterpenoids with rare carbon skeletons, were isolated from *n*-hexane extract of *Salvia hydrangea*. The absolute configuration was determined by comparison of experimental and calculated electronic circular dichroism (ECD) spectra. In vitro activity against *Plasmodium falciparum* K1 strain, *Trypanosoma brucei rhodesiense* STIB 900 strain, and cytotoxicity in rat myoblast (L6) cells were determined. Compounds **1** and **2** showed in vitro antiplasmodial activity, with IC_{50} values of 1.43 and 0.18 μM and selectivity indices (SI) of 86.2 and 69.6, respectively. IC_{50} values against *T. brucei rhodesiense* were found to be 4.33 and 15.92 μM, respectively.

Extraction of plant material, isolation, recording, and interpretation of analytical data for structure elucidation (mass spectrometry, microprobe NMR, optical rotation) were done by Dr. Mehdi Moridi. Experimental and quantum-chemical calculations of ECD spectra, contributing to writing of the manuscript, and preparation of some figures were my part to this publication. Antiprotozoal tests were done by Stefanie Zimmermann.

Samad Ebrahimi

JOURNAL OF NATURAL PRODUCTS

Article

pubs.acs.org/jnp

Triterpenoids with Rare Carbon Skeletons from *Salvia hydrangea*: Antiprotozoal Activity and Absolute Configurations

M. Moridi Farimani,*[,†] M. Babak Bahadori,[†] Salman Taheri,[‡] Samad N. Ebrahimi,[†,‡] Stefanie Zimmermann,[‡,§] Reto Brun,[§] Gholamreza Amin,[∥] and Matthias Hamburger[‡]

[†]Department of Phytochemistry, Medicinal Plants and Drugs Research Institute, Shahid Beheshti University, G. C., Evin, Tehran, Iran

[‡]Chemistry and Chemical Engineering Research Center of Iran, Tehran, Iran

[‡]Division of Pharmaceutical Biology, University of Basel, Klingelbergstrasse 50, 4056 Basel, Switzerland

[§]Swiss Tropical and Public Health Institute, Socinstrasse 57, CH-4002 Basel, Switzerland

[∥]Department of Pharmacognosy, Faculty of Pharmacy, Tehran University of Medical Sciences, Tehran, Iran

Supporting Information

ABSTRACT: Salvadione C (**1**) and perovskone B (**2**), two new triterpenoids with rare carbon skeletons, were isolated from an antiplasmodial *n*-hexane extract of *Salvia hydrangea*. The absolute configuration was determined by comparison of experimental and calculated electronic circular dichroism (ECD) spectra. In vitro activity against *Plasmodium falciparum* K1 strain, *Trypanosoma brucei rhodesiense* STIB 900 strain, and cytotoxicity in rat myoblast (L6) cells were determined. Compounds **1** and **2** showed in vitro antiplasmodial activity, with IC_{50} values of 1.43 and 0.18 μM and selectivity indices (SI) of 86.2 and 69.6, respectively. IC_{50} values against *T. brucei rhodesiense* were found to be 4.33 and 15.92 μM, respectively.

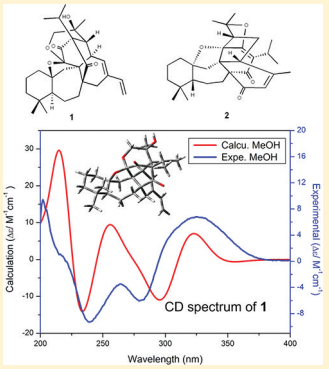

The genus *Salvia* comprises over 1000 species, being the largest genus of the Lamiaceae family. Several *Salvia* species, such as *S. officinalis*, *S. triloba*, *S. miltiorrhiza*, *S. hispanica*, and *S. sclarea*, are cultivated as medicinal plants, spices, and sources of essential oils for the perfume industry.[1] From a phytochemical viewpoint, the genus is characterized by the widespread occurrence of diterpenoids and triterpenoids. Rare classes of terpenoids in *Salvia* include sesterterpenoids[2,3] and some di- and triterpenoids with highly unusual carbon skeletons.[4−7]

In Iran, the genus *Salvia* consists of 58 annual and perennial species, 17 of which are endemic.[8] *S. hydrangea* DC. ex Benth. is a conspicuous aromatic plant that grows widely in Iran, Anatolia, and Transcaucasia.[8] Its common name in Persian is "Gol-e Arooneh", and the aerial parts of the plant have been used in Iranian folk medicine as anti-inflammatory, antispasmodic, carminative, and sedative compounds.[9] Infusions prepared from flowers serve as an anthelmintic and antileishmanial, especially in the Pars province of Iran.[10] Abietane-type diterpenoids have been reported from the roots of the plant. A moderate in vitro antiplasmodial effect of the flower extracts was attributed to a high content in pentacyclic triterpenes, mainly oleanolic acid.[11] *S. hydrangea* is taxonomically close to *S. bucharica*,[8] from which triterpenoids with novel carbon skeletons have been discovered.[6,7,12,13] This prompted us to investigate *S. hydrangea*. As part of an ongoing screening for new antiparasitic natural products,[14−17] an *n*-hexane extract of *S. hydrangea* was found active against *P. falciparum* and *T. b. rhodesiense*, with IC_{50} values of 3.2 and 18 μg/mL, respectively.

Herein, we report the isolation and structure elucidation of two active compounds, salvadione C (**1**) and perovskone B (**2**), including the determination of their absolute configuration by chiroptical methods.

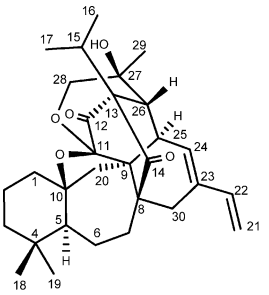

1

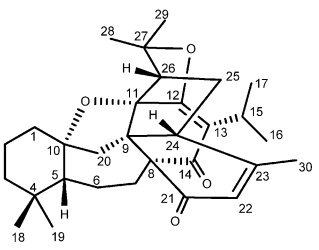

2

Received: June 29, 2011
Published: October 3, 2011

RESULTS AND DISCUSSION

Salvadione C (**1**) was isolated as a white, amorphous solid. The molecular formula of $C_{30}H_{40}O_5$ was deduced from HR-ESIMS at m/z 481.2949 $[M + H]^+$ (calcd 481.2965). The IR spectrum showed absorptions of hydroxy (3475 cm^{-1}), carbonyl (1713 cm^{-1}), and olefinic (1610 cm^{-1}) functionalities. The molecular formula accounted for 11 degrees of unsaturation. The ^{13}C NMR spectrum (Table 1) showed 30 carbon signals, which were resolved through a DEPT experiment into 5 methyl, 9 methylene, 6 methine, and 10 quaternary carbons. Thus, 39 hydrogen atoms could be accounted for, while the remaining atom was likely from a hydroxy group. ^{13}C NMR data (Table 1) showed signals for a monosubstituted double bond (δ_c 112.9, 138.5), a trisubstituted double bond (δ_c 131.2, 135.9), and two carbonyl carbons (δ_c 203.6, 209.1). Four carbon signals at δ_c 75.3 (CH_2), 76.8 (C), 92.0 (C), and 108.1 (C) indicated the presence of oxygen-bearing sp^3 carbons. The absence of other sp or sp^2 carbon signals implied that the structure of **1** contained seven rings, including two cyclic ethers, which is compatible with the molecular formula of $C_{30}H_{40}O_5$. The ^1H NMR spectrum (Table 1) showed resonances of three methyl singlets at δ_H 0.89, 1.04, and 1.31. Resonances of two additional methyl groups at δ_H 1.11 (d, J = 6.9 Hz) and 1.27 (d, J = 6.9 Hz), together with a signal at δ_H 2.29 (sept, J = 6.9 Hz) indicating the presence of an isopropyl moiety. Signals at δ_H 6.34 (dd, J = 17.5, 10.8 Hz), 5.23 (d, J = 17.5 Hz), and 5.05 (d, J = 10.8 Hz) were indicative of a vinyl group. Another olefinic methine signal appeared as a doublet at δ_H 5.68 (J = 6.1 Hz). Comparison of the NMR data of **1** with those of triterpenoids previously isolated from *S. bucharica* indicated that **1** likely had the same carbon skeleton as salvadiol.[7] Notable differences in the ^{13}C NMR spectra of **1** and salvadiol were observed, such as the resonance of an oxygen-bearing methylene carbon at δ_C 75.3 (C-28) replacing a methyl group at δ_C 29.8 in salvadiol. The chemical shifts of C-11, C-26, and C-27 in **1** were observed at δ_C 108.1, 54.9, and 76.8 and thus appeared downfield by ca. 8, 9, and 2 ppm, respectively. In contrast, C-25 in **1** was shifted upfield by ca. 15 ppm and appeared at δ_C 38.4. In the ^1H NMR spectrum, the methyl group at δ_H 1.24 (H-28) in salviadiol was replaced in **1** by an AB system (δ_H 3.85 and 3.74, 1H each, both d, J_{gem} = 14.7 Hz), reminiscent of an oxymethylene group attached to a quaternary sp^3 carbon. Along with the additional degree of unsaturation, these spectroscopic data suggested the presence of an oxepane ring through an oxygen bridge between C-11 and C-28. HMBC correlations (Figure 1) confirmed the carbon skeleton of **1**, and the heterocycle was corroborated by connectivities between H-28 (δ_H 3.85 and 3.74) and the C-11 and C-27 carbons (δ_C 108.1 and 76.8, respectively). Unambiguous assignment of ^1H and ^{13}C NMR data was achieved by a combination of HMQC, COSY, and HMBC experiments. The relative configuration of **1** was determined from a NOESY spectrum and NOE difference experiments (Figure 2) and was in accord with that of salvadiol, with exception of the newly formed heterocyclic ring.

The absolute configuration of **1** was established by measurement of the ECD spectrum and comparison with calculated ECD data. A conformational search based on the above established relative configuration revealed three conformers within a 3 kcal/mol energy window from the particular global minimum. These conformers were subjected to geometrical optimization and energy calculation using density functional theory (DFT) with the B3LYP function and 6-31G* in the gas phase combined with calculation of vibrational modes to confirm these minima. No imaginary frequencies were found. Conformation analysis using relative free energies indicated the presence of the two conformers **1a** (98.2%) and **1b** (1.8%) (Figure 3) in the gas phase. Theoretical calculation of ECD spectra of conformers was performed by the time-dependent density function theory (TDDFT) method at B3LYP/6-31G* in MeOH using the SCRF (self-consistent reaction field)

Table 1. ^1H and ^{13}C NMR Data of Compounds 1 and 2 ($CDCl_3$, 500 MHz for δ_H, 125 MHz for δ_C) [a]

1			2		
position	δ_H (J, Hz)	δ_C	position	δ_H (J, Hz)	δ_C
1	1.49[b]	41.7	1 α	1.18[b]	42.9
	2.00, br d (12.6)		1 β	1.40[c]	
2	1.28[c]	20.1	2	1.45[c]	20.9
	1.45[b]			1.69[d]	
3	1.47[b]	42.4	3	1.63[d]	42.2
	1.92[d]			1.81[e]	
4		36.4	4		34.1
5	1.27[c]	50.5	5	0.92, dd (3.3, 11.5)	53.7
6	1.88[d]	21.2	6	1.37[c]	19.9
				1.50[c]	
7	1.20[c]	42.0	7 α	2.60, dd (8.5, 15.5)	34.7
	1.88[d]		7 β	1.77[e]	
8		53.0	8		60.2
9		51.3	9		54.6
10		92.0	10		90.1
11		108.1	11		96.3
12		209.1	12		170.2
13		71.1	13		122.0
14		203.6	14		195.5
15	2.29, sept (6.9)	27.3	15	3.11, sept (7.0)	24.6
16	1.27, d (6.9)[c]	20.3	16	1.15, d (7.0)[b]	20.8
17	1.11, d (6.9)	18.8	17	1.08, d (7.0)	20.0
18	0.89, s	33.1	18	0.90, s	32.3
19	1.04, s	22.1	19	0.84, s	22.1
20 α	1.86[d]	42.0	20 α	1.74, d (13.7)	55.8
20 β	1.20[c]		20 β	2.64, d (13.7)	
21	5.05, d (10.8)	112.9	21		196.0
	5.23, d (17.5)				
22	6.34, dd (10.8, 17.5)	138.5	22	5.88, s	125.8
23		135.9	23		156.5
24	5.68, d (6.1)	131.2	24	2.74, br t (10.0)	49.7
25	3.76[e]	38.4	25 α	1.37[c]	34.2
			25 β	2.31, dt (7.4, 12.5)	
12.5)					
26	2.22, s	54.9	26	2.46, dd (7.0, 12.5)	54.8
27		76.8	27		90.3
28 α	3.85, d (14.7)	75.3	28	1.43, s	24.8
28 β	3.74, d (14.7)[e]				
29	1.31, s	26.7	29	1.72, s	27.4
30 α	2.44, d (17.0)	28.1	30	1.79, s	21.9
30 β	2.60, d (17.0)				

[a] δ values were established from HMBC, COSY, and HMQC experiments. [b,c,d,e] Overlapping signals.

dx.doi.org/10.1021/np200559c | J. Nat. Prod. 2011, 74, 2200–2205

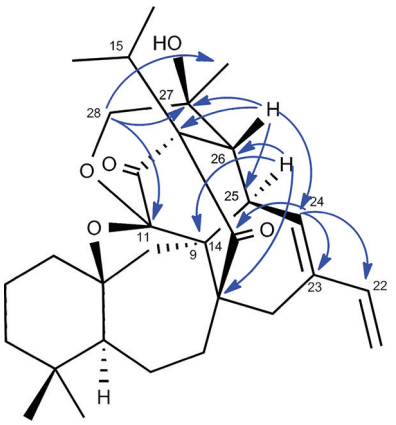

Figure 1. Key HMBC correlations of **1**.

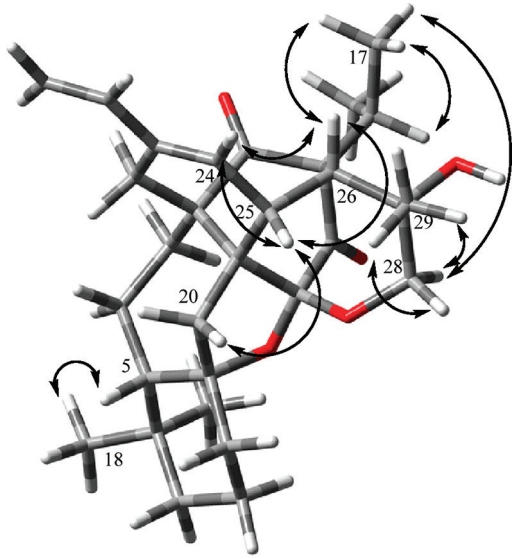

Figure 2. Key NOE correlations of **1**.

method with the CPCM (conductor-like polarizable continuum) model. The overall pattern of calculated ECD spectra was in good agreement with the experimental data (Figure 4). In particular, two negative Cotton effects (CE) were observed at 239 and 279 nm, along with positive effects at 205 and 325 nm. Thus, the absolute configuration of **1** was established as 5*S*,8*R*,9*S*,10*S*,11*R*,13*R*,25*R*,26*R*,27*S*. Salvadione C (**1**) is a new natural product with the same carbon skeleton as salvadiol.

Perovskone B (**2**) was isolated as an amorphous colorless powder. A molecular formula of $C_{30}H_{40}O_4$ was established from its HR-ESIMS (*m*/*z* 465.3040 $[M + H]^+$, calcd 465.3005). The IR spectrum showed absorption bands at 1673 and 1110 cm^{-1} indicative of α,β-unsaturated carbonyl and ether functionalities, respectively. The molecular formula accounted for 11 degrees of unsaturation. The ^{13}C NMR spectrum showed 30 carbon signals which originated, according to the DEPT spectrum, from 7 methyl, 7 methylene, 5 methine, and 11 quaternary carbons (Table 1). ^{13}C NMR resonances at δ_C 195.5 (C), 122.0 (C), and 170.2 (C) indicated the presence of an α,β-unsaturated carbonyl containing a trisubstituted double bond. A second α,β-unsaturated carbonyl moiety was characterized by resonances at δ_C 196.0 (C), 125.8 (CH), and 156.5 (C). Three oxygen-bearing quaternary carbons appeared at δ_C 90.1, 90.3, and 96.3. In the DEPT spectrum, all 40 hydrogens could be

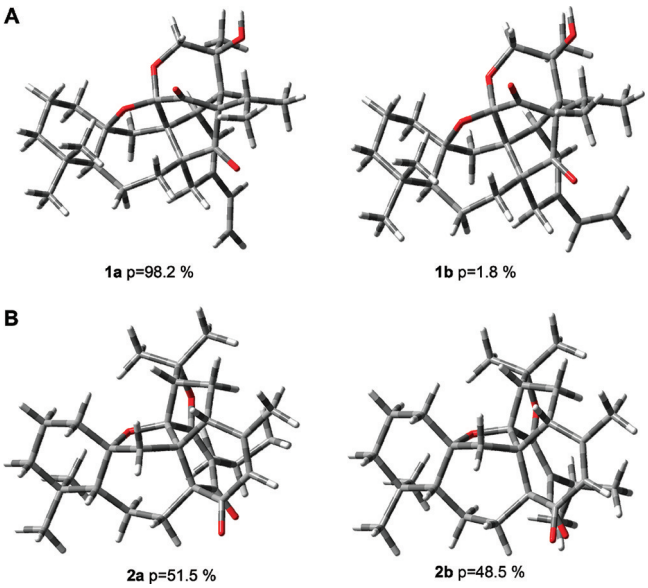

Figure 3. Minimized conformers of **1** and **2** in the gas phase using DFT at the B3LYP/6-31G* level: (A) compound **1**, showing the two conformers **1a**,**b** within a 3 kcal/mol range from the global minimum, differing only with respect to the orientation of the vinyl group: (B) compound **2**, showing the two major conformers **2a**,**b**, which according to Boltzmann weighing accounted for the total population and only differed in the orientation of the isopropyl moiety.

accounted for; therefore, the molecule did not contain free hydroxy groups. According to the degree of unsaturation, the structure of **2** was heptacyclic. In the ^1H NMR spectrum (Table 1), signals for a proton at δ_H 3.11 (sept, J = 7.0 Hz) and two methyl groups at δ_H 1.08 (d, J = 7.0 Hz) and 1.15 (d, J = 7.0 Hz) showed the presence of a vinylic isopropyl group. Five additional methyl groups appeared as singlets, among these a vinylic methyl resonating at δ_C 1.79. Only one olefinic proton was observed at δ_H 5.88 (s). The ^1H and ^{13}C NMR data strongly resembled those of perovskone, a triterpenoid from *Perovskia abrotanoides*,[18] indicating that the two compounds were structurally related. Inspection of the ^{13}C NMR spectra showed the lack of the C-21 methylene group in compound **2** but the presence of an additional carbonyl group (δ_C 196.0). This suggested that the methylene was replaced by a carbonyl group. Indeed, the signals of C-22 (δ_C 125.8) and C-23 (δ_C 156.5) were paramagnetically shifted ($\Delta\delta$ = +5.6 and +20.2 ppm, respectively) in comparison to those of perovskone. Also the resonances of neighboring H-23 (δ_H 5.88), H-30 (δ_H 1.79), and H-24 (δ_H 2.73) were shifted ($\Delta\delta$ = +0.56, +0.29, and +0.31 ppm, respectively). In comparison to perovskone, the C-14 resonance was shifted upfield by ca. 6 ppm and appeared at δ_C 195.5, while the signal of C-8 underwent a downfield shift of ca. 12 ppm (δ_C 60.2). These differences were in agreement with a 1,3-dicarbonyl moiety and suggested that the additional carbonyl group had to be located at C-21. HMBC correlations between H-22 (δ_H 5.88, s), H-30 (δ_H 1.79, s), H-7α (δ_H 2.60, dd), and H-7β (δ_H 1.77, m) and C-21, and between H-22 and C-8 (Figure 5) confirmed the location of the carbonyl group. Unambiguous assignments of NMR data were achieved by a combination of COSY, HMQC, and HMBC experiments, and the relative configuration was deduced from a NOESY spectrum (Figure 6). Diagnostic cross peaks between H-24, H-26, Me-30, H-25β, and H-20α were observed and confirmed their cofacial orientation. In addition, cross peaks between H-5,

dx.doi.org/10.1021/np200559c|*J. Nat. Prod.* 2011, 74, 2200–2205

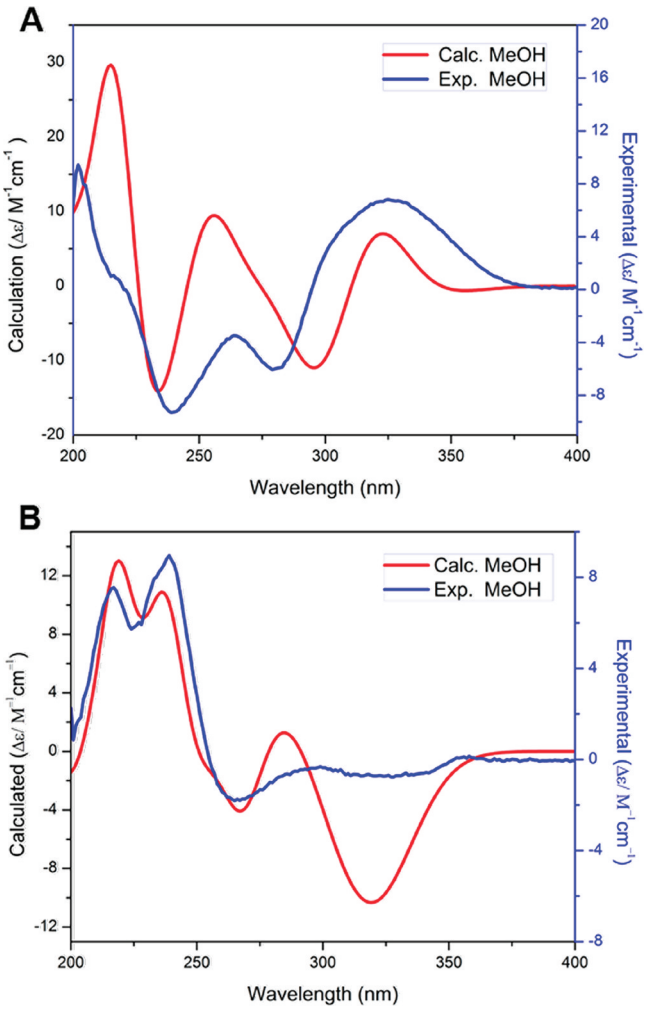

Figure 4. Experimental (blue) and calculated (red) ECD spectra of **1** (A) and **2** (B). Calculated spectra were obtained by using TDDFT at the B3LYP/6-31G* level in MeOH.

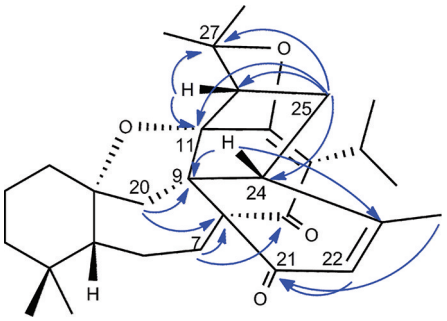

Figure 5. Key HMBC correlations of **2**.

H-20α and H-20β, and Me-18 corroborated the linkage of rings A and B and, hence, the same relative configuration is established as for perovskone.

The absolute configuration of **2** was established by comparison of experimental and calculated ECD spectra. The conformational analysis gave two conformers within a 3 kcal/mol energy window from the particular global minimum. They differed only in the orientation of the isopropyl group attached at C-13 (Figure 3). Conformers were subjected to geometrical optimization and energy calculation using the DFT-B3LYP 6-31G* theoretical level in the gas phase combined with

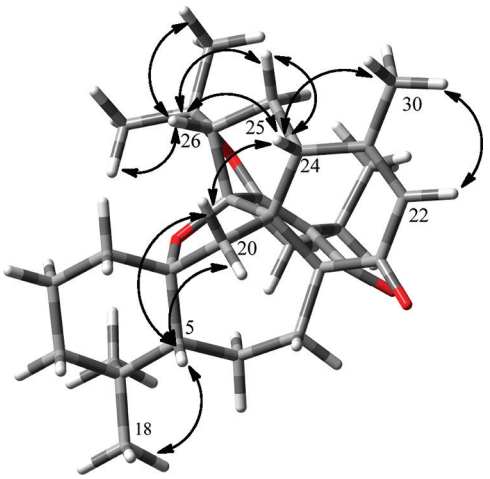

Figure 6. Key NOESY correlations of **2**.

calculation of vibrational modes to confirm these minima. No imaginary frequencies were found. Conformers **2a**,**b** contributed to 51.5 and 48.5% of the total, respectively. Calculation of the ECD spectra of the conformers was performed as described above. The weighted ECD spectrum in MeOH is shown in Figure 4. The overall patterns of experimental and calculated ECD spectra were in good agreement. Two positive Cotton effects (CE) at 215 and 238 nm along with two negative CEs around 266 nm and in the region 300−350 nm were also found in the calculated spectrum (Figure 4). Differences between calculated and experimental spectra presumably resulted from an overestimation of the UV absorbance in the calculations or may be due to minor differences between calculated and solution conformers.[19,20] Thus, the absolute configuration of compound **2** was established as 5*R*,8*R*,9*R*,10*R*,11*S*,12*R*,26*S*. This new natural product was named perovskone B.

Salvadione C (**1**) and perovskone B (**2**) were tested for in vitro antiplasmodial activity against *P. falciparum* K1 strain. The compounds showed fairly potent activity (IC_{50} values of 1.43 and 0.18 μM, respectively) and good selectivity indices (SI) of 86.2 and 69.6 (Table 2). Against *T. brucei rhodesiense* STIB 900,

Table 2. Activity (IC_{50} in μM with Standard Deviations (SD) and Selectivity Indices (SI)) against *Plasmodium falciparum* K1, *Trypanosoma brucei rhodesiense* STIB 900, and L6 Cells

compd	*P. falciparum*	SI	*T. b. rhodesiense*	SI[a]	L6 cells
1	1.43 ± 0.18	86.6	4.33 ± 0.24	43.2	>90.0
2	0.18 ± 0.002	69.6	15.92 ± 0.72	0.78	5.77 ± 0.41

[a]Selectivity index = IC_{50} of the L6 cells (cytotoxicity) divided by IC_{50} of the parasite.

they exhibited moderate potency (IC_{50} values of 4.33 and 15.92 μM, respectively).

Salvadione C and perovskone B both possess rare carbon skeletons that can be rationalized by a Diels−Alder type addition of an acyclic monoterpene (myrcene for salvadione C and *trans*-β-ocimene for perovskone B) to a diterpenoid[7,18] (Figure 7). The carbon skeletons found in **1** and **2** have been reported once from *S. bucharica* (salvadiol) and *Perovskia abrotanoides* (perovskone), but the scaffold of **1** is new and

dx.doi.org/10.1021/np200559c|*J. Nat. Prod.* 2011, 74, 2200−2205

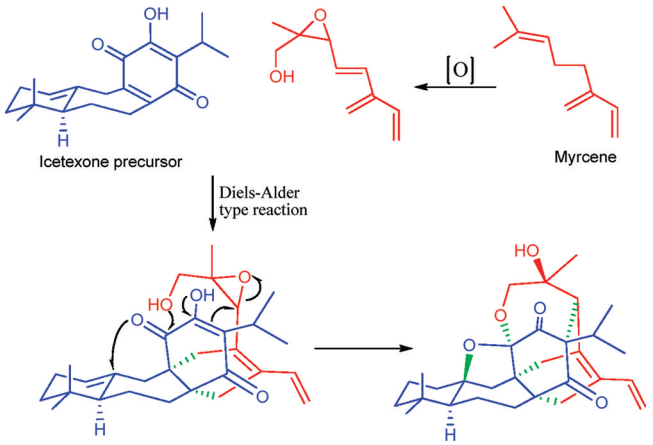

Figure 7. Proposed biogenetic pathway to salvadione C (**1**).

differs in the additional oxepane ring, which confers a high degree of rigidity to the molecule.

In conclusion, fractionation of the antiparasitic *n*-hexane extract of the aerial parts of *S. hydrangea* led to isolation of two new triterpenoids with rare skeletons. Perovskone B (**2**) showed in vitro antiplasmodial activity at submicromolar concentrations and good selectivity. Its druglike physicochemical properties warrant preliminary in vivo testing for exploration of the compound's potential for further investigation.

EXPERIMENTAL SECTION

General Experimental Procedures. Optical rotations were measured using a Perkin-Elmer 341 polarimeter. IR spectra were recorded on a Bruker Tensor 27 spectrometer. NMR spectra were recorded on Bruker DRX 500 and Avance III 500 spectrometers, using the residual $CDCl_3$ signal (δ_H 7.27/δ_C 77.0) as reference. The 2D NMR experiments (^{1}H–^{1}H COSY, HMQC, HMBC, NOESY) were performed using standard Bruker software. HR-ESIMS spectra were acquired on a Bruker micrOTOF ESI-MS system. ECD spectra of compounds **1** and **2** were recorded in MeOH (40 μg/mL) on an AVIV Model 62ADS CD spectrometer and analyzed with the AVIV 60DS V4.1 software. Silica gel (70–230 and 230–400 mesh, Merck) was used for column chromatography. Preparative TLC was performed on silica gel 60 GF_{254} (Merck). Bands were detected on TLC under UV or by heating after spraying with 5% phosphomolybdic acid in EtOH.

Plant Material. The aerial parts of *S. hydrangea* DC. ex Benth. were collected from the Koohin region in Qazvin province, Iran, in May 2009 and identified by Dr. G. R. Amin. A voucher specimen (6719-TEH) has been deposited at the herbarium of the Faculty of Pharmacy, Tehran University of Medical Sciences.

Extraction and Isolation. The air-dried, powdered aerial parts of *S. hydrangea* (4.5 kg) were extracted successively with *n*-hexane (3 × 25 L), EtOAc (3 × 25 L), and MeOH (3 × 25 L) by maceration at room temperature. Extracts were concentrated in vacuo, to afford dark gummy residues of *n*-hexane (107 g), EtOAc (110 g), and MeOH (280 g) extracts. The *n*-hexane extract was separated on a silica gel column (230–400 mesh, 900 g) with a gradient of *n*-hexane–EtOAc (100/0 to 0/100) as eluent, followed by increasing concentrations of MeOH (up to 5%) in EtOAc. On the basis of TLC analysis, fractions with similar composition were pooled to yield 30 combined fractions. The less polar fractions contained waxes and carotenoids compounds and were not further investigated. Fraction 16 (4.5 g) was separated on a silica gel column with CH_2Cl_2-Me_2CO (98:2), to afford seven fractions (16a–16g). Fraction 16d was further purified by preparative TLC (CH_2Cl_2–Me_2CO (100/3.5)) to afford **1** (11 mg, R_f = 0.72). Fraction 17 (2.2 g) was separated on a silica gel column with $CHCl_3$–Me_2CO (97/3) as eluent into seven fractions (17a–17g). Fraction 17a was recrystallized from $CHCl_3$–MeOH to yield 5-hydroxy-4′,7-dimethoxyflavone (6 mg). Fraction 18 (1.3 g) was separated over a silica gel column with $CHCl_3$–Me_2CO (97/3) as eluent, to afford oleanolic acid (25 mg). Fraction 19 (8.5 g) was triturated with Me_2CO and MeOH to give β-sitosterol (1 g). Fraction 21 (1.1 g) was separated on a silica gel column ($CHCl_3$–Me_2CO (97/3)) into 10 fractions (21a–21j). Fraction 21a was further purified by preparative TLC (CH_2Cl_2–Me_2CO (100/3.5)) to afford **2** (8 mg, R_f = 0.64). Fraction 22 (1.7 g) was triturated with Me_2CO, and the insoluble solid was recrystallized from Me_2CO to afford salvigenin (120 mg).

*Salvadione C (**1**):* white amorphous powder; $[\alpha]^{20}_D$ = +53° (*c* 1.0, $CHCl_3$); IR (KBr) ν_{max} 3475, 2940, 1713, 1610, 1460, 1375, 1225, 1137, 1064 cm^{-1}; ^{1}H and ^{13}C NMR data, see Table 1; CD (MeOH, *c* = 8.3 × 10^{-8} M, 1.0 cm path length) $[\theta]_{202}$ +31 128, $[\theta]_{216}$ +3592, $[\theta]_{229}$ +6677, $[\theta]_{239}$ −30 634, $[\theta]_{262}$ −12 305, $[\theta]_{279}$ −19 987, $[\theta]_{322}$ +22 008; positive HR-ESIMS *m*/*z* 481.2949 [M + H]$^+$ (calcd for $C_{30}H_{41}O_5$ 481.2965).

*Perovskone B (**2**):* white amorphous powder; $[\alpha]^{20}_D$ = +147° (*c* 0.9, $CHCl_3$); IR (KBr) ν_{max} 2935, 1673, 1455, 1372, 1233, 1110 cm^{-1}; ^{1}H and ^{13}C NMR data, see Table 1; CD (MeOH, *c* = 8.7 × 10^{-8} M, 1.0 cm path length): $[\theta]_{216}$ +24 711, $[\theta]_{239}$ +29 541, $[\theta]_{264}$ −5769, $[\theta]_{324}$ −2430; HR-ESIMS *m*/*z* 465.3040 [M + H]$^+$ (calcd for $C_{30}H_{41}O_4$ 465.3005).

Conformational Analysis, Geometrical Optimization, and ECD Calculation. Conformational analysis of **1** and **2** was performed with Schrödinger MacroModel 9.1 software using the OPLS 2005 (optimized potential for liquid simulations) force field in H_2O. Conformers occurring within a 3 kcal/mol energy window from the global minimum were chosen for geometrical optimization and energy calculation using density functional theory (DFT) with the B3LYP functional and the 6-31G* basis set in the gas phase with the Gaussian 03 program package.[21] Vibrational analysis was done at the same level to confirm minima. TD-DFT/B3LYP/6-31G*, in the gas phase and in MeOH using the SCRF (self-consistent reaction field) method with the CPCM (conductor-like polarizable continuum) model, was employed to calculate excitation energy (denoted by wavelength in nm) and rotatory strength *R* in dipole velocity (R_{vel}) and dipole length (R_{vel}) forms. ECD curves were calculated on the basis of rotatory strengths using a half-bandwidth of 0.18 eV with conformers of **1** and **2**. The spectra were combined after Boltzmann weighting according to their population contribution.

Antiplasmodial and Antitrypanosomal Assay. Tests of extracts and pure substances were done as previously described.[16] IC_{50} values were calculated from sigmoidal concentration inhibition curves. Assays were run in two independent experiments in duplicate.

ASSOCIATED CONTENT

Supporting Information

Figures giving 1D and 2D NMR spectra for salvadione C (**1**) and perovskone B (**2**). This material is available free of charge via the Internet at http://pubs.acs.org.

AUTHOR INFORMATION

Corresponding Author

*Tel: +98 21 29902679. Fax: +98 21 22431783. E-mail: m_moridi@sbu.ac.ir.

ACKNOWLEDGMENTS

Financial support by the Shahid Beheshti University Research Council is gratefully acknowledged.

REFERENCES

(1) Wu, C. Y.; Li, H. W. *Acta Bot. Yunn.* **1982**, *4*, 97–118.
(2) Moghaddam, F. M.; Farimani, M. M.; Seirafi, M.; Taheri, S.; Khavasi, H. R.; Sendker, J.; Proksch, P.; Wray, V.; Edrada, R. A. *J. Nat. Prod.* **2010**, *71*, 1601–1605.
(3) Rustaiyan, A.; Masoud, S.; Anaraki, M. T. *Nat. Prod. Commun.* **2007**, *10*, 1031–1042.

(4) Xu, G.; Hou, A. J.; Zheng, Y. T.; Zhao, Y.; Li, X. L.; Peng, L. Y.; Zhao, Q. S. *Org. Lett.* **2007**, *9*, 291−293.
(5) Aoyagi, Y.; Yamazaki, A.; Nakatsugawa, C.; Fukaya, H.; Takeya, K.; Kawauchi, S.; Izumi, H. *Org. Lett.* **2008**, *10*, 4429−4432.
(6) Ahmad, V. U.; Zahid, M.; Ali, M. S.; Ali, Z.; Jassbi, A. R.; Abbas, M.; Clardy, J.; Lobkovsky, E.; Tareen, R. B.; Iqbal, M. Z. *J. Org. Chem.* **1999**, *64*, 8465−8467.
(7) Ahmad, V. U.; Zahid, M.; Ali, M. S.; Choudhary, M. I.; Akhtar, F.; Ali, Z.; Iqbal, M. Z. *Tetrahedron Lett.* **1999**, *40*, 7561−7564.
(8) Rechinger, K. H. *Flora Iranica*; Akademische Druck- und Verlagsanstalt: Graz, Austria, 1987; pp 403−476.
(9) Iranian Herbal Pharmacopeia Committee. *Iranian Pharmacopeia*, 1st ed.; Ministry of Health and Medical Education: Tehran, Iran, 2002; Vol. *1*, pp 57−64.
(10) Amin, G. *Popular Medicinal Plants of Iran*; Ministry of Health Publications: Tehran, Iran, 1991; Vol. *1*, p 41.
(11) Sairafianpour, M.; Bahreininejad, B.; Witt, M.; Ziegler, H. L.; Jaroszewski, J. W.; Staerk, D. *Planta Med.* **2003**, *69*, 846−850.
(12) Ahmad, V. U.; Zahid, M.; Ali, M. S.; Jassbi, A. R.; Ahmad, S.; Ali, Z. *Nat. Prod. Sci.* **2000**, *6*, 66−69.
(13) Ahmad, V. U.; Zahid, M.; Ali, M. S.; Ali, Z.; Alam, N.; Tareen, R. B.; Iqbal, M. Z. *Z. Naturforsch., B* **1999**, *54*, 415−418.
(14) Adams, M.; Plitzko, I.; Kaiser, M.; Brun, R.; Hamburger, M. *Phytochem. Lett.* **2009**, *2*, 159−162.
(15) Adams, M.; Zimmermann, S.; Kaiser, M.; Brun, R.; Hamburger, M. *Nat. Prod. Commun.* **2009**, *4*, 1377−1381.
(16) Mokoka, T. A.; Zimmermann, S.; Julianti, T.; Hata, Y.; Moodley, N.; Cal, M.; Adams, M.; Kaiser, M.; Brun, R.; Koorbanally, N.; Hamburger, M., *Planta Med.* DOI: 10.1055/s-0030-1270932.
(17) Ślusarczyk, S.; Zimmermann, S.; Kaiser, M.; Matkowski, A.; Hamburger, M.; Adams, M., *Planta Med.* DOI: 10.1055/s-0030-1270933.
(18) Parvez, A.; Choudhary, M. I.; Akhter, F.; Noorwala, M.; Mohammad, F. V.; Hasan, N. M.; Zamir, T.; Ahmad, V. U. *J. Org. Chem.* **1992**, *57*, 4339−4340.
(19) Kamel, H. N.; Ding, Y.; Li, X. C.; Ferreira, D.; Fronczek, F. R.; Slattery, M. *J. Nat. Prod.* **2009**, *72*, 900−905.
(20) Tayone, W. C.; Honma, M.; Kanamaru, S.; Noguchi, S.; Tanaka, K.; Nehira, T.; Hashimoto, M. *J. Nat. Prod.* **2011**, *74*, 425−429.
(21) Frisch, M. J.; Trucks, H. B.; Schlegel, H. B.; Frisch, M. J.; Trucks, G. W.; Schlegel, H. B.; Scuseria, G. E.; Robb, M. A.; Cheeseman, J. R.; Montgomery, J. A., Jr.; Vreven, T.; Kudin, K. N.; Burant, J. C.; Millam, J. M.; Iyengar, S. S.; Tomasi, J.; Barone, V.; Mennucci, B.; Cossi, M.; Scalmani, G.; Rega, N.; Petersson, G. A.; Nakatsuji, H.; Hada, M.; Ehara, M.; Toyota, K.; Fukuda, R.; Hasegawa, J.; Ishida, M.; Nakajima, T.; Honda, Y.; Kitao, O.; Nakai, H.; Klene, M.; Li, X.; Knox, J. E.; Hratchian, H. P.; Cross, J. B.; Bakken, V.; Adamo, C.; Jaramillo, J.; Gomperts, R.; Stratmann, R. E.; Yazyev, O.; Austin, A. J.; Cammi, R.; Pomelli, C.; Ochterski, J. W.; Ayala, P. Y.; Morokuma, K.; Voth, G. A.; Salvador, P.; Dannenberg, J. J.; Zakrzewski, V. G.; Dapprich, S.; Daniels, A. D.; Strain, M. C.; Farkas, O.; Malick, D. K.; Rabuck, A. D.; Raghavachari, K.; Foresman, J. B.; Ortiz, J. V.; Cui, Q.; Baboul, A. G.; Clifford, S.; Cioslowski, J.; Stefanov, B. B.; Liu, G.; Liashenko, A.; Piskorz, P.; Komaromi, I.; Martin, R. L.; Fox, D. J.; Keith, T.; Al-Laham, M. A.; Peng, C. Y.; Nanayakkara, A.; Challacombe, M.; Gill, P. M. W.; Johnson, B.; Chen, W.; Wong, M. W.; Gonzalez, C.; Pople, J. A. *Gaussian 03, Revision D.02*; Gaussian, Inc., Wallingford, CT, 2004.

Triterpenoids with Rare Carbon Skeletons from Salvia hydrangea- Antiprotozoal Activity and Absolute Configurations

M. Moridi Farimani,[*,†] M. Babak Bahadori,[†] Salman Taheri,[‡] Samad N. Ebrahimi,[†,§] Stefanie Zimmermann,[§,⊥] Reto Brun,[⊥] Gholamreza Amin,[ǁ] and Matthias Hamburger,[§]

Department of Phytochemistry, Medicinal Plants and Drugs Research Institute, Shahid Beheshti University, G. C., Evin, Tehran, Iran, Chemistry and Chemical Engineering Research Center of Iran, Tehran, Iran, Division of Pharmaceutical Biology, University of Basel, Klingelbergstrasse 50, 4056 Basel, Switzerland, Swiss Tropical and Public Health Institute, Socinstrasse 57, CH-4002 Basel, Switzerland, Department of Pharmacognosy, Faculty of Pharmacy,Tehran University of Medical Sciences, Tehran, Iran.

*To whom correspondence should be addressed. Tel: +98 21 29902679. Fax: +98 21 22431783. E-mail: m_moridi@sbu.ac.ir.

[†] Shahid Beheshti University, G. C.

[‡] Chemistry and Chemical Engineering Research Center of Iran.

[§] University of Basel.

[⊥] Swiss Tropical and Public Health Institute.

[ǁ] Tehran University of Medical Sciences.

Supporting information

S1. ^{1}H NMR spectrum of Salvadione C in $CDCl_3$

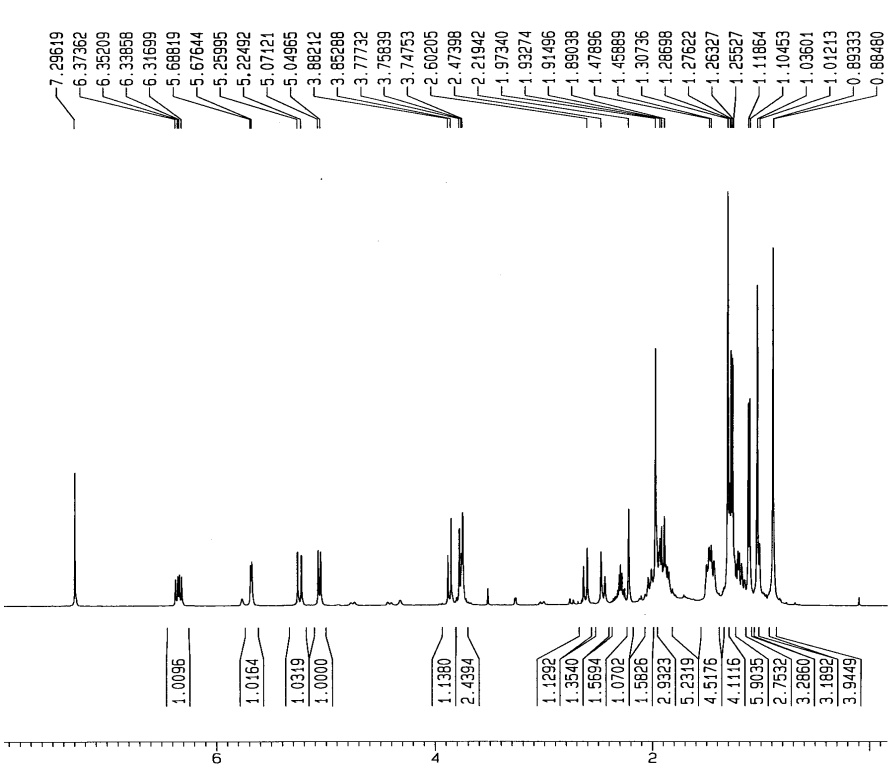


```
Current Data Parameters
NAME                  Dr.Moridi
EXPNO                         2
PROCNO                        1

F2 - Acquisition Parameters
Date_               20101028
Time                    10.43
INSTRUM                 spect
PROBHD     5 mm QNP 1H/13
PULPROG                 zg30
TD                      32768
SOLVENT                 CDCl3
NS                          8
DS                          0
SWH                 10330.578 Hz
FIDRES              0.315264 Hz
AQ                  1.5860696 sec
RG                      161.3
DW                     48.400 usec
DE                      6.50 usec
TE                     298.0 K
D1                  6.00000000 sec
MCREST              0.00000000 sec
MCWRK               0.01500000 sec

======== CHANNEL f1 ========
NUC1                        1H
P1                      10.50 usec
PL1                     -3.00 dB
SFO1                500.1330885 MHz

F2 - Processing parameters
SI                      32768
SF                  500.1300049 MHz
WDW                         EM
SSB                         0
LB                      0.30 Hz
GB                          0
PC                      1.00

1D NMR plot parameters
CX                     20.00 cm
CY                      9.09 cm
F1P                   10.515 ppm
F1                  5259.05 Hz
F2P                   -0.161 ppm
F2                    -80.74 Hz
PPMCM                0.53384 ppm/cm
HZCM               266.98962 Hz/cm
```

S2. Expanded ^{1}H NMR spectrum of Salvadione C in $CDCl_3$

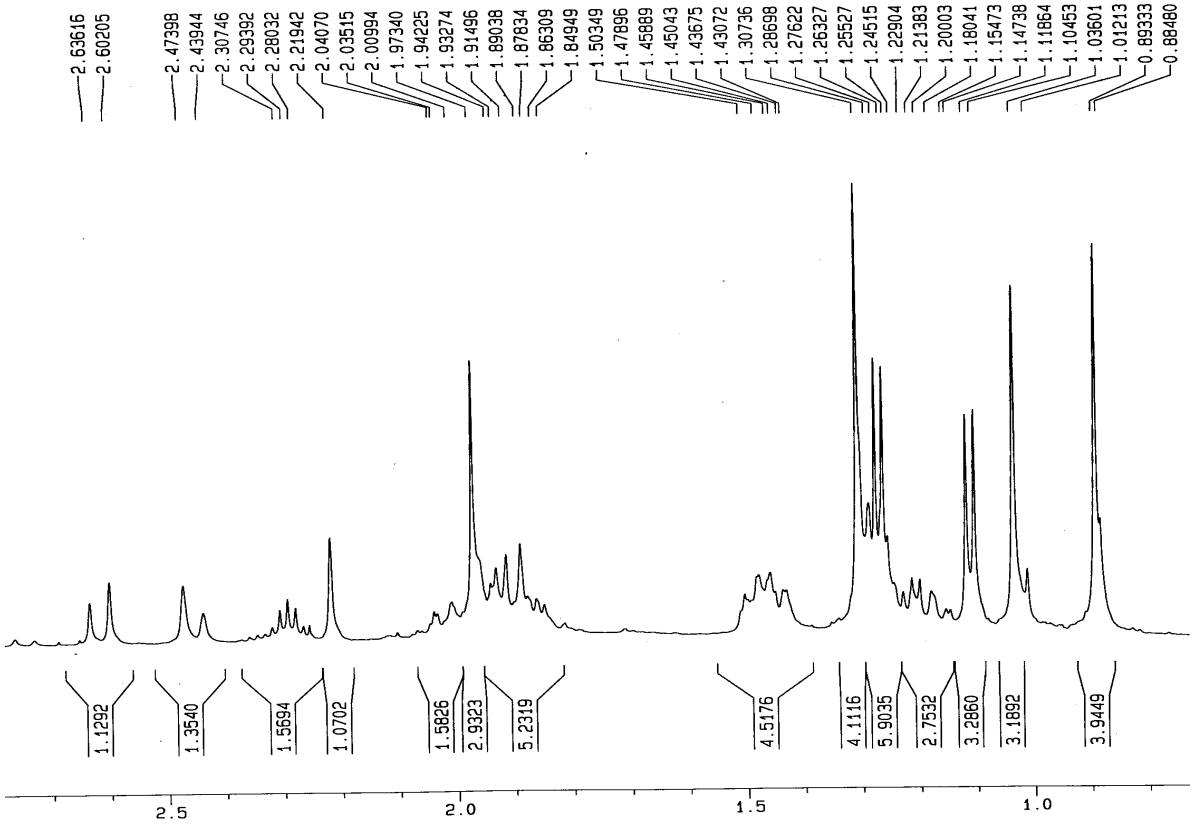

S3. Expanded ^{1}H NMR spectrum of Salvadione C in $CDCl_3$

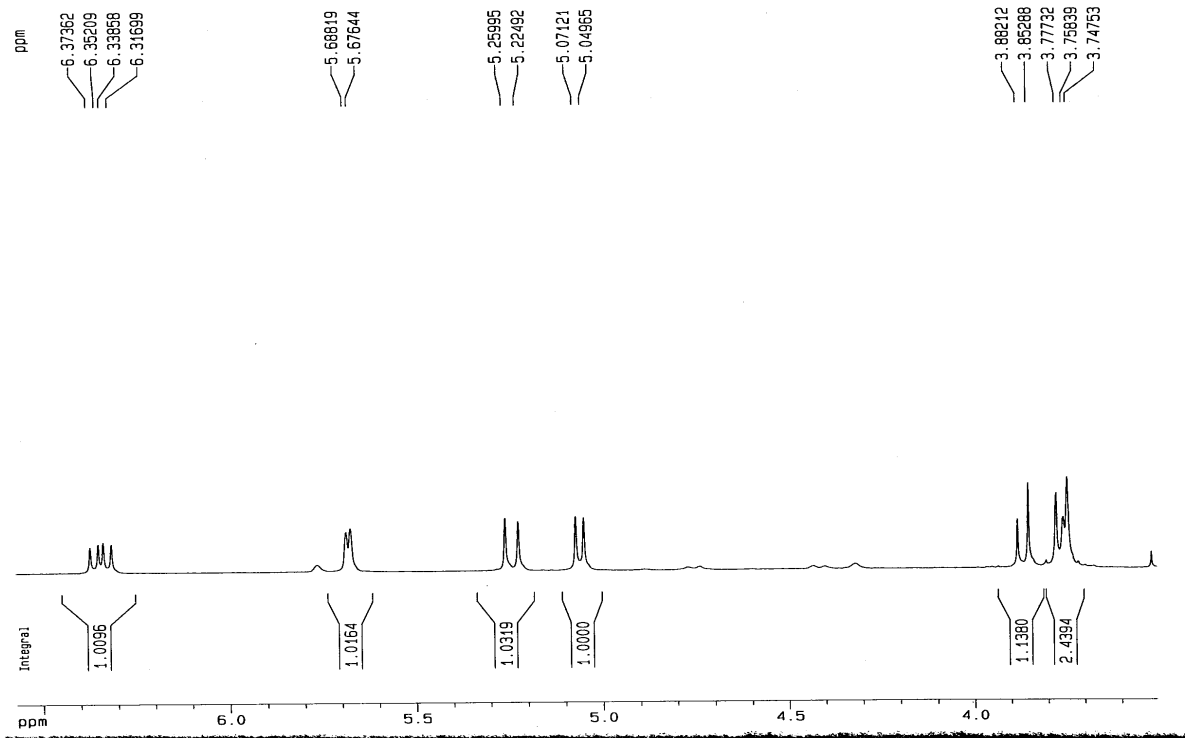

S4. ^{13}C NMR spectrum of Salvadione C in $CDCl_3$

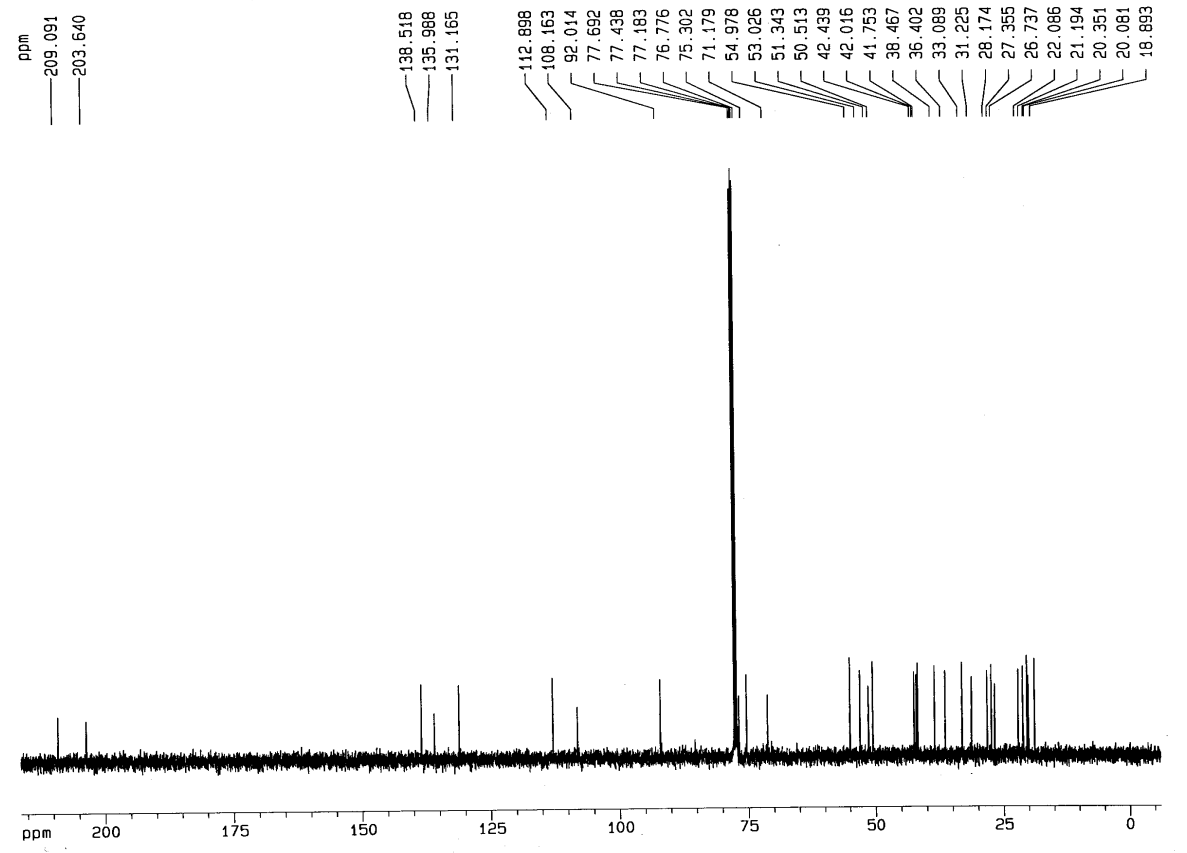

S5. Expanded ^{13}C NMR spectrum of Salvadione C in $CDCl_3$

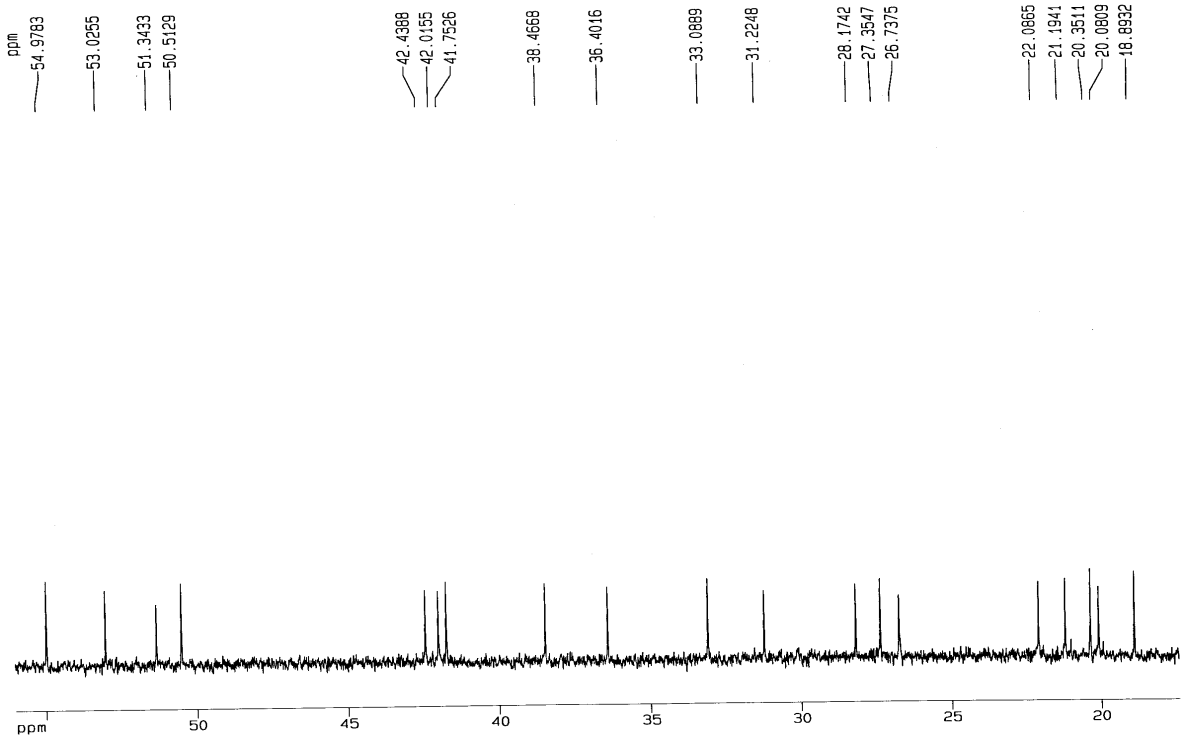

S6. DEPT135 spectrum of Salvadione C in $CDCl_3$

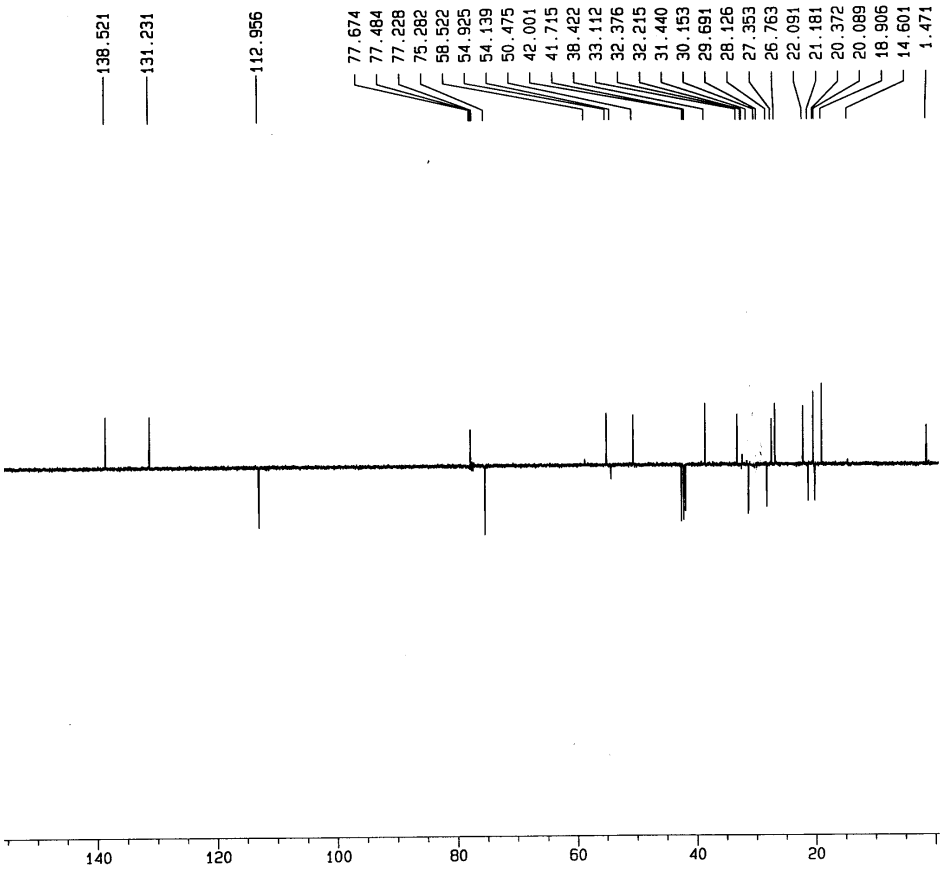


```
NAME                 Dr.Moridi
EXPNO                       17
PROCNO                       1

F2 - Acquisition Parameters
Date_               20100930
Time                   10.18
INSTRUM                spect
PROBHD   5 mm GNP 1H/13
PULPROG              dept135
TD                     65536
SOLVENT                CDCl3
NS                      4096
DS                         4
SWH                30030.029 Hz
FIDRES             0.458222 Hz
AQ                 1.0912410 sec
RG                    4597.6
DW                   16.650 usec
DE                    6.50 usec
TE                   290.3 K
CNST2              145.0000000
D1                 12.00000000 sec
d2                  0.00344828 sec
d12                 0.00002000 sec
DELTA               0.00001159 sec
MCREST              0.00000000 sec
MCWRK               0.01500000 sec

======== CHANNEL f1 ========
NUC1                       13C
P1                       9.10 usec
p2                      18.20 usec
PL1                      3.00 dB
SF01               125.7703643 MHz

======== CHANNEL f2 ========
CPDPRG2                waltz16
NUC2                       1H
P3                      13.00 usec
p4                      26.00 usec
PCPD2                   80.00 usec
PL2                      0.00 dB
PL12                    15.50 dB
SF02               500.1320005 MHz

F2 - Processing parameters
SI                         32768
SF                 125.7577390 MHz
WDW                           EM
SSB                            0
LB                          1.00 Hz
GB                             0
PC                          1.40

1D NMR plot parameters
CX                         20.00 cm
CY                          3.17 cm
F1P                       181.529 ppm
F1                      22828.69 Hz
F2P                        -0.550 ppm
F2                        -69.21 Hz
PPMCM                   9.10397 ppm/cm
HZCM                 1144.89490 Hz/cm
```

S7. DEPT90 spectrum of Salvadione C in $CDCl_3$

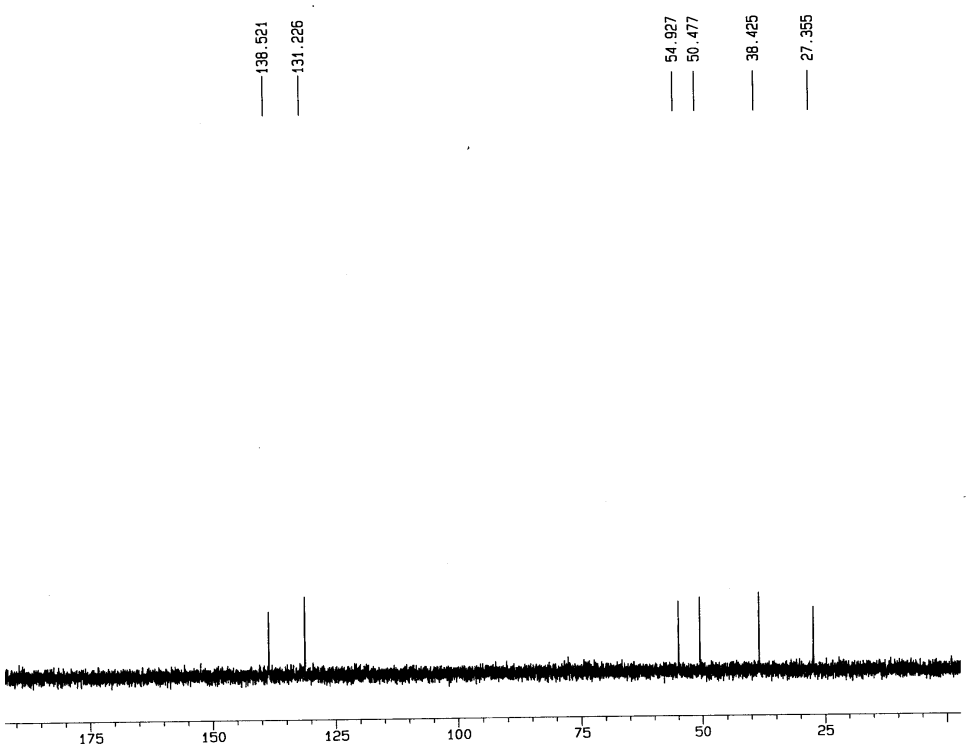


```
Current Data Parameters
NAME            Dr.Moridi
EXPNO                  18
PROCNO                  1

F2 - Acquisition Parameters
Date_          20101014
Time              11.39
INSTRUM           spect
PROBHD   5 mm QNP 1H/13
PULPROG          dept90
TD                65536
SOLVENT           CDCl3
NS                  484
DS                    4
SWH           30030.029 Hz
FIDRES        0.458222 Hz
AQ            1.0912410 sec
RG                 6502
DW               16.650 usec
DE                6.50 usec
TE                290.6 K
CNST2        145.0000000
D1             2.00000000 sec
d2             0.00344828 sec
d12            0.00002000 sec
DELTA          0.00001159 sec
MCREST         0.00000000 sec
MCWRK          0.01500000 sec

======== CHANNEL f1 ========
NUC1                13C
P1                 9.10 usec
p2                18.20 usec
PL1               3.00 dB
SFO1         125.7703643 MHz

======== CHANNEL f2 ========
CPDPRG2         waltz16
NUC2                1H
P3                13.00 usec
p4                26.00 usec
PCPD2             80.00 usec
PL2                0.00 dB
PL12              15.50 dB
SFO2         500.1320005 MHz

F2 - Processing parameters
SI                 32768
SF           125.7577390 MHz
WDW                  EM
SSB                   0
LB                 1.00 Hz
GB                    0
PC                 1.40

1D NMR plot parameters
CX                20.00 cm
CY                 1.86 cm
F1P              205.408 ppm
F1               25831.69 Hz
F2P               -2.721 ppm
F2               -342.21 Hz
PPMCM            10.40648 ppm/cm
HZCM          :308.69519 Hz/cm
```

S8. HMQC spectrum of Salvadione C in $CDCl_3$

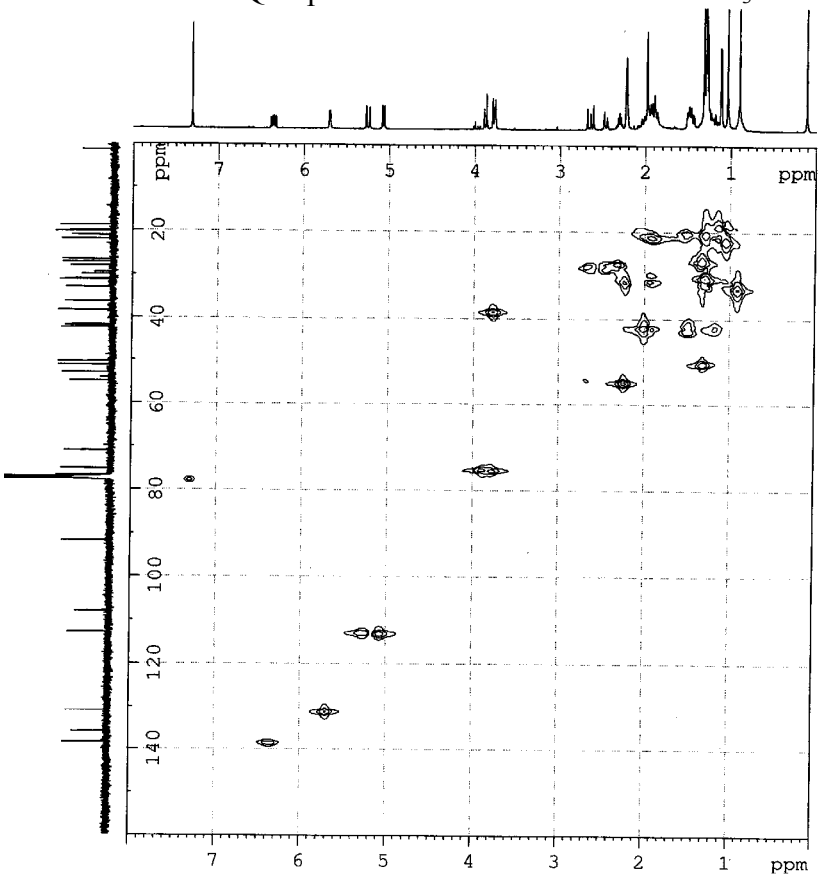

S9. Expanded HMQC spectrum of Salvadione C in $CDCl_3$

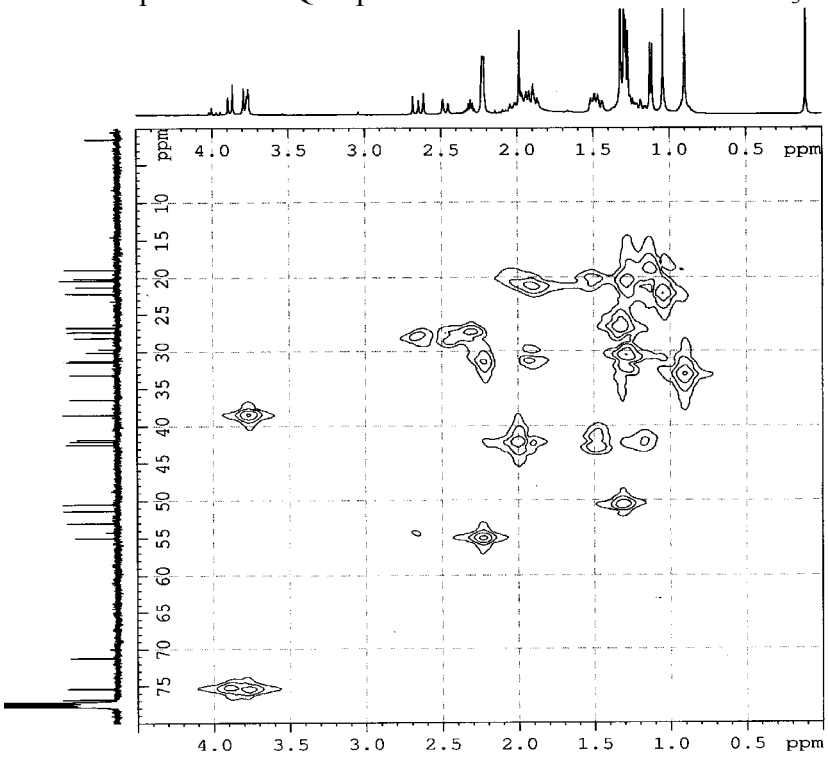

S10. HMBC spectrum of Salvadione C in $CDCl_3$

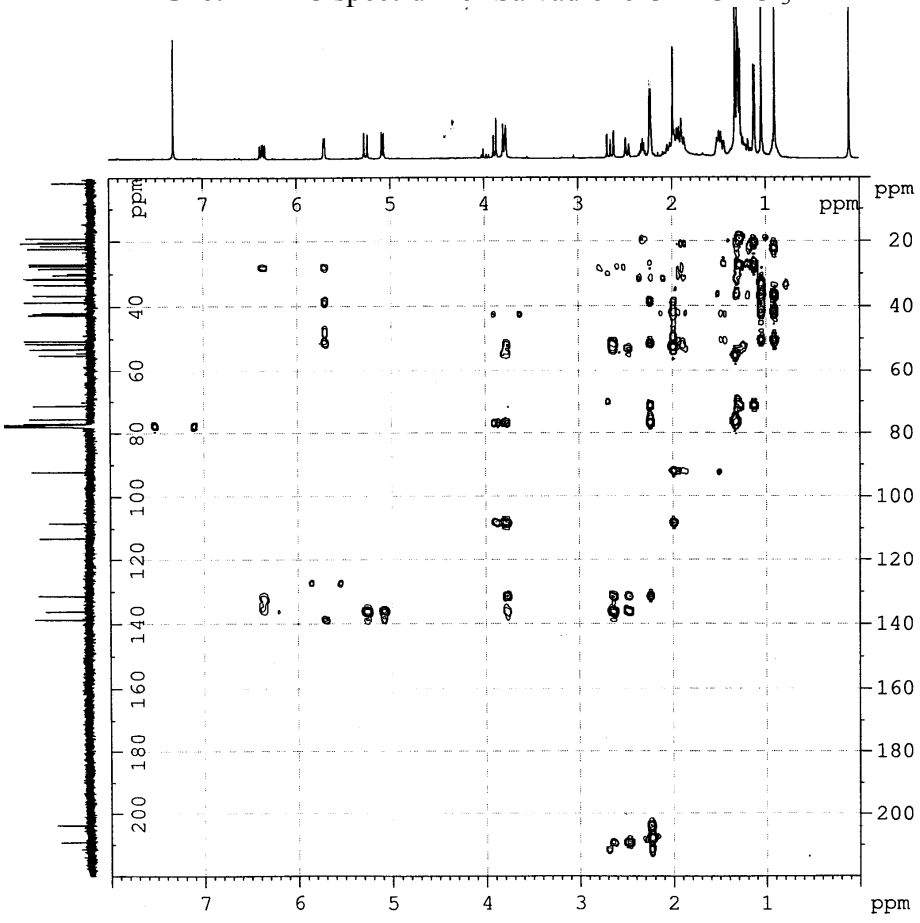

S11. Expanded HMBC spectrum of Salvadione C in $CDCl_3$

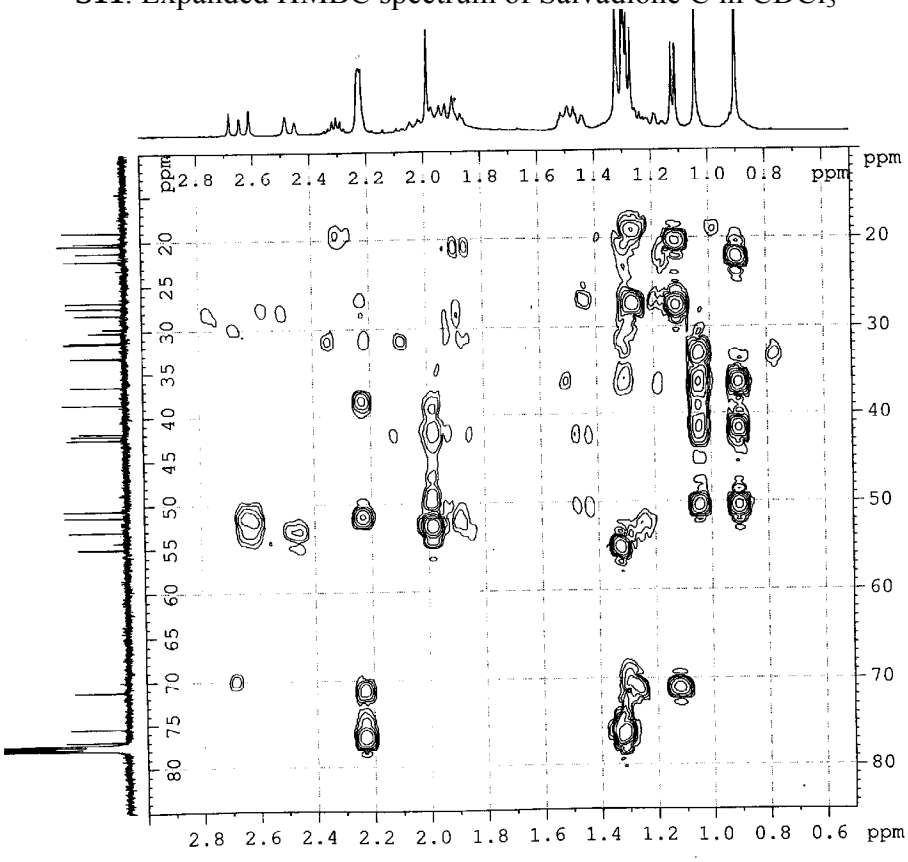

S12. ^{1}H-^{1}H COSY spectrum of Salvadione C in $CDCl_3$

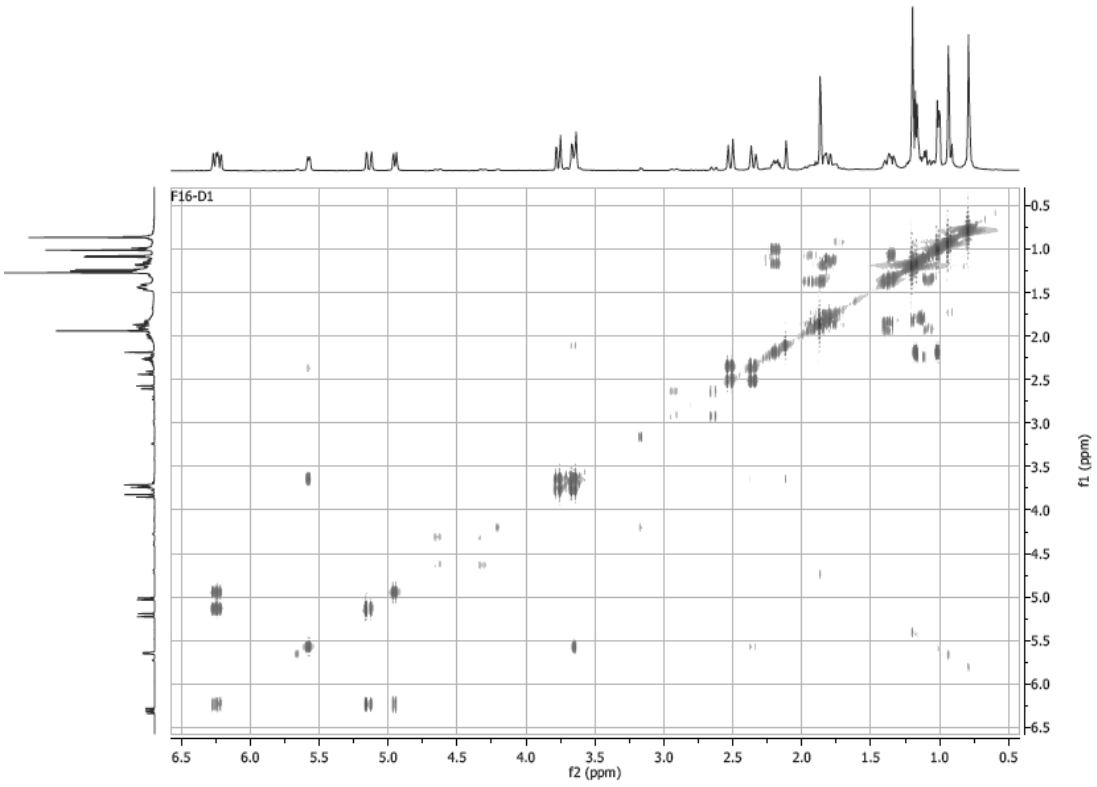

S13. NOESY spectrum Salvadione C in $CDCl_3$

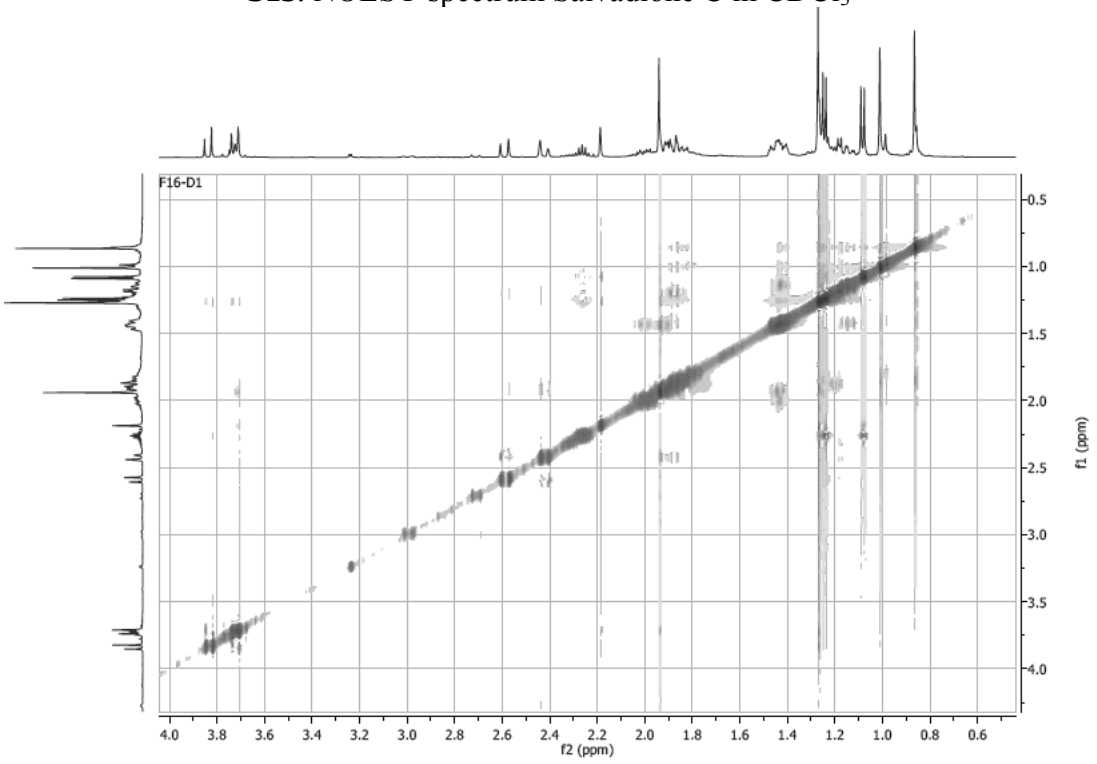

S14. ^1H NMR spectrum of Perovskone B in $CDCl_3$

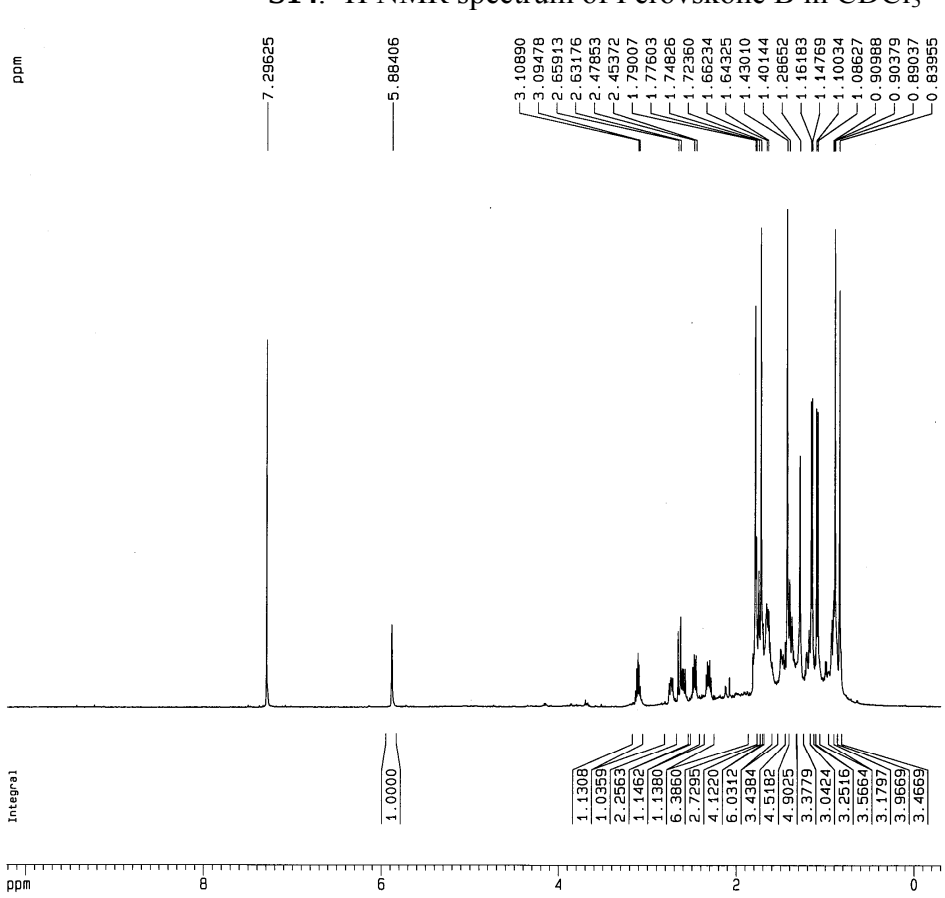


```
Current Data Parameters
NAME            Dr.Moridi
EXPNO                   5
PROCNO                  1

F2 - Acquisition Parameters
Date_           20101028
Time                11.17
INSTRUM             spect
PROBHD   5 mm QNP 1H/13
PULPROG             zg30
TD                 32768
SOLVENT            CDCl3
NS                     16
DS                      1
SWH           10330.578 Hz
FIDRES         0.315264 Hz
AQ             1.5860696 sec
RG                 287.4
DW                48.400 usec
DE                 6.50 usec
TE                 298.0 K
D1             5.00000000 sec
MCREST         0.00000000 sec
MCWRK          0.01500000 sec

======== CHANNEL f1 ========
NUC1                   1H
P1                 10.50 usec
PL1                -3.00 dB
SFO1          500.1330885 MHz

F2 - Processing parameters
SI                 32768
SF            500.1300049 MHz
WDW                   EM
SSB                    0
LB                  0.30 Hz
GB                     0
PC                  1.00

1D NMR plot parameters
CX                 20.00 cm
CY                  9.43 cm
F1P               10.213 ppm
F1                5107.81 Hz
F2P                -0.301 ppm
F2                -150.54 Hz
PPMCM           0.52570 ppm/cm
HZCM          262.91788 Hz/cm
```

S15. Expanded ^{1}H NMR spectrum of Perovskone B in $CDCl_3$

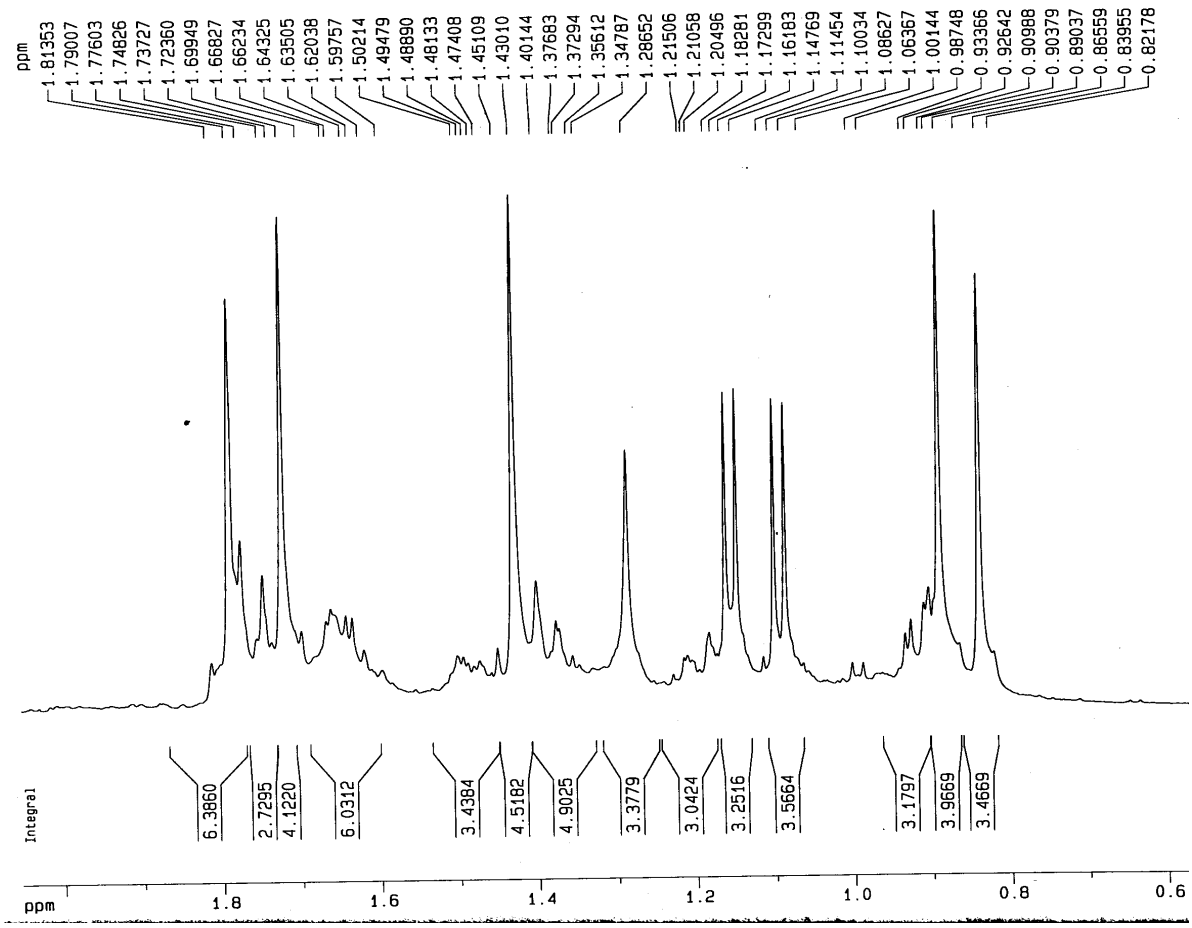

S16. Expanded ^{1}H NMR spectrum of Perovskone B in $CDCl_3$

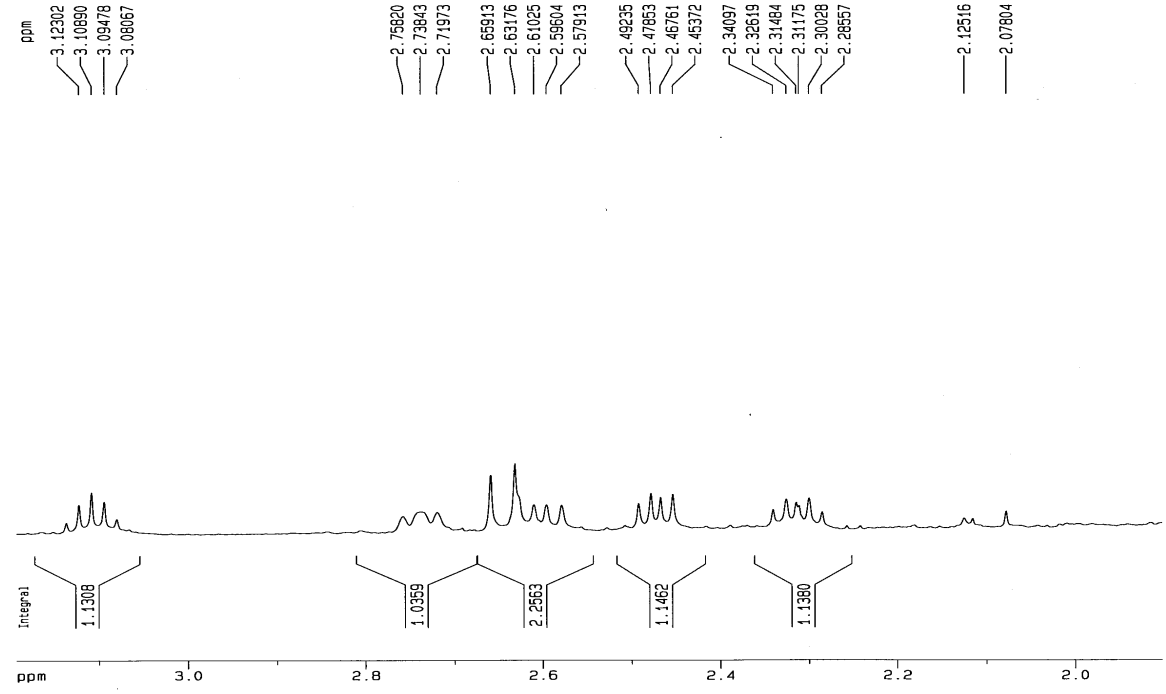

S17. ^{13}C NMR spectrum of Perovskone B in $CDCl_3$

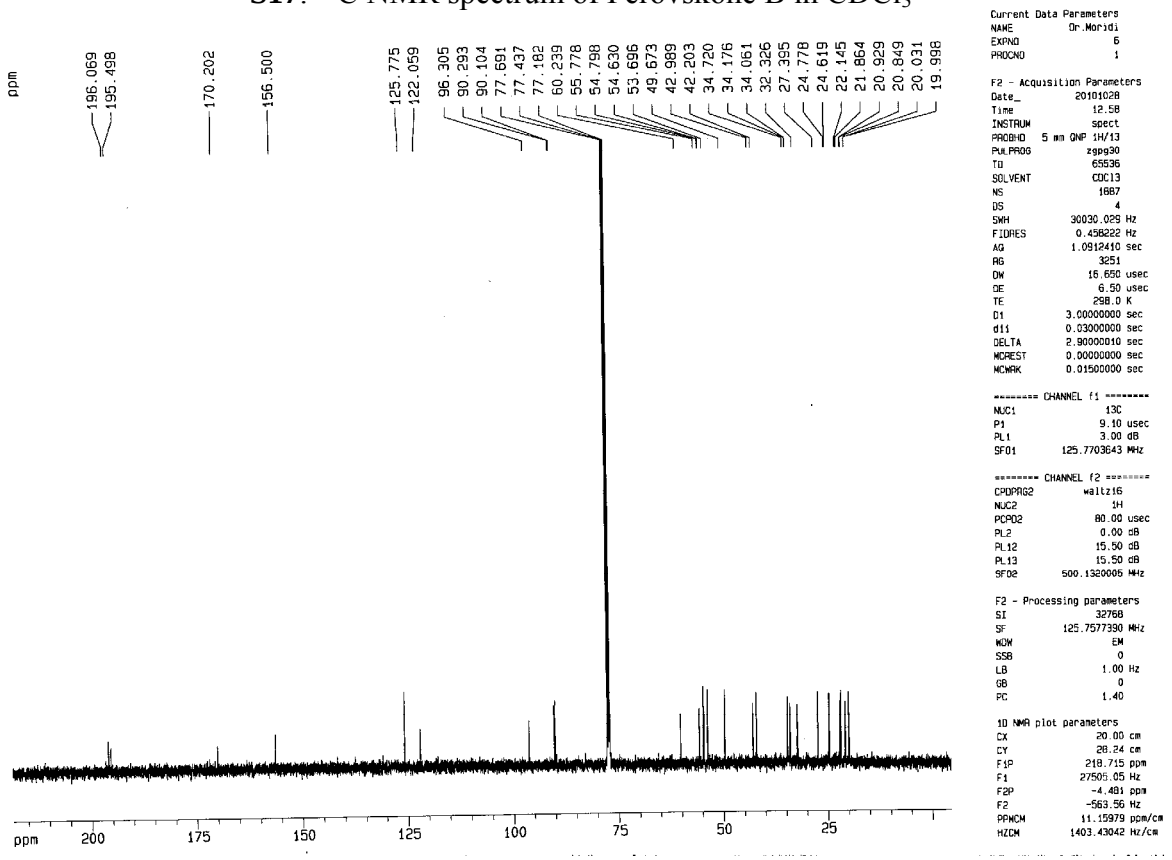

S18. Expanded ^{13}C NMR spectrum of Perovskone B in $CDCl_3$

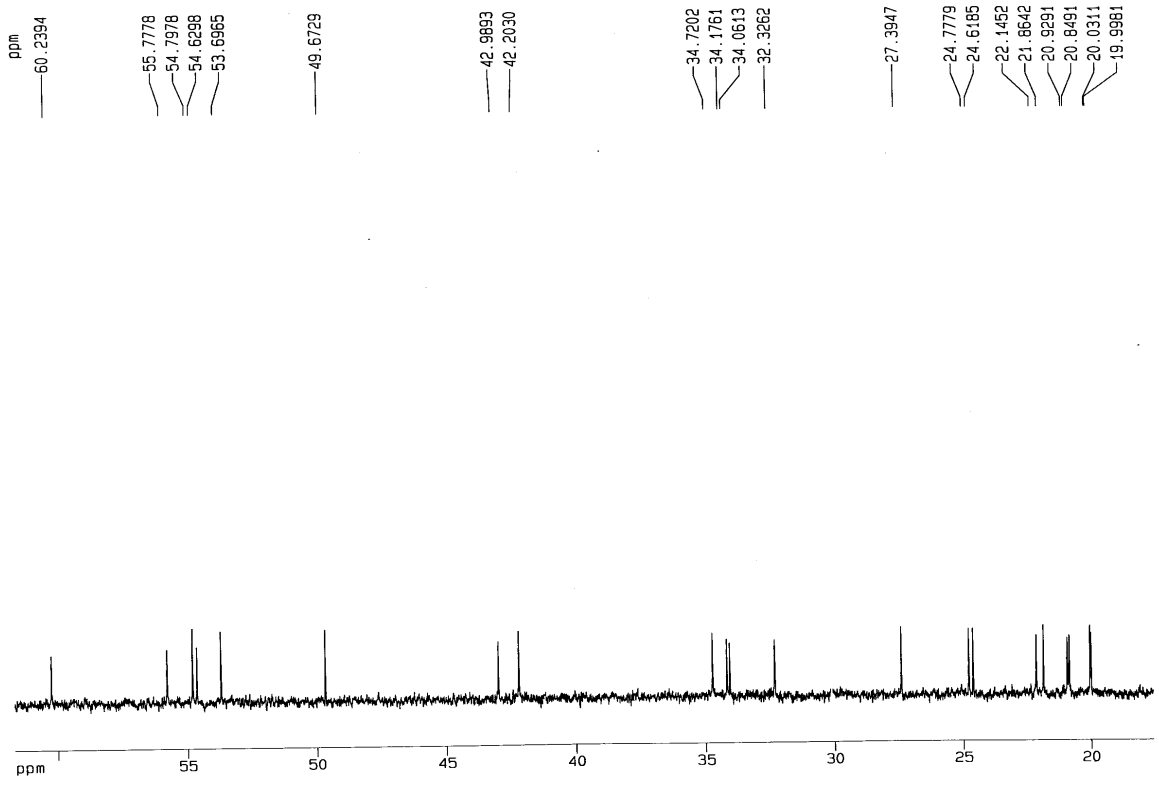

S19. DEPT135 spectrum of Perovskone B in $CDCl_3$

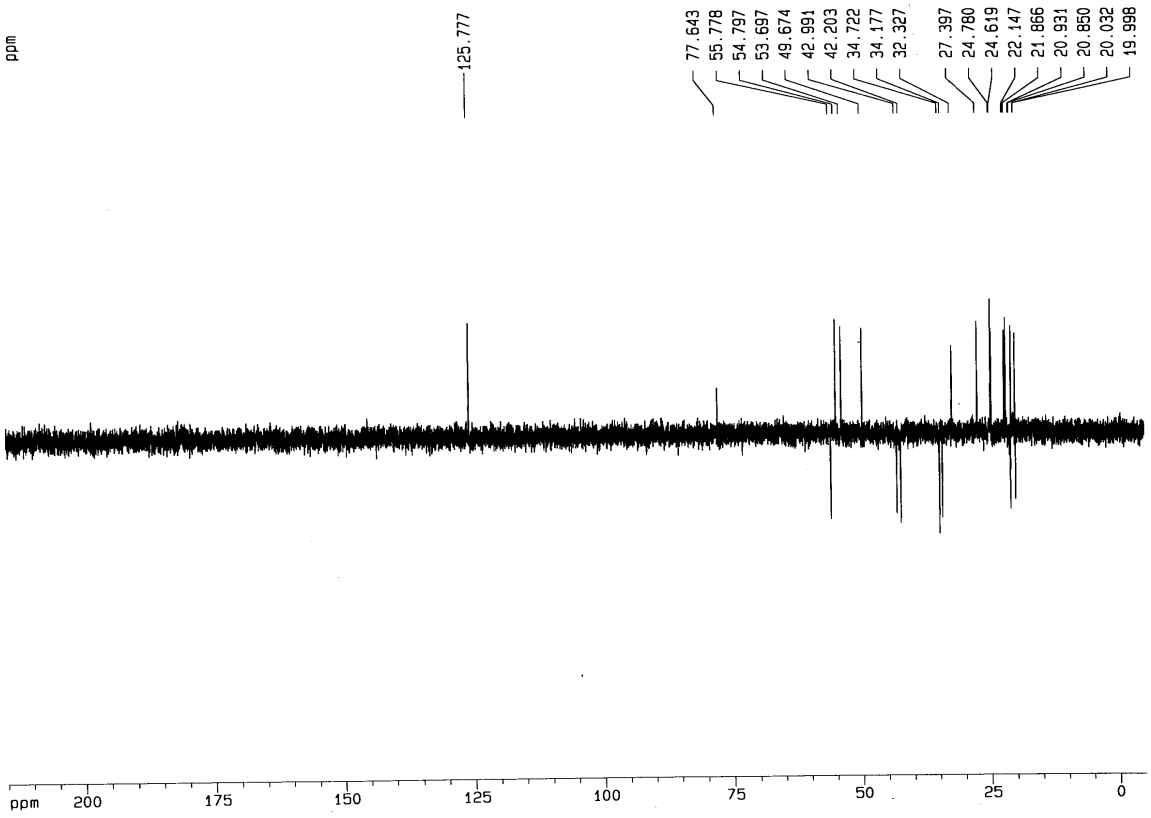

S20. Expanded DEPT135 spectrum of Perovskone B in $CDCl_3$

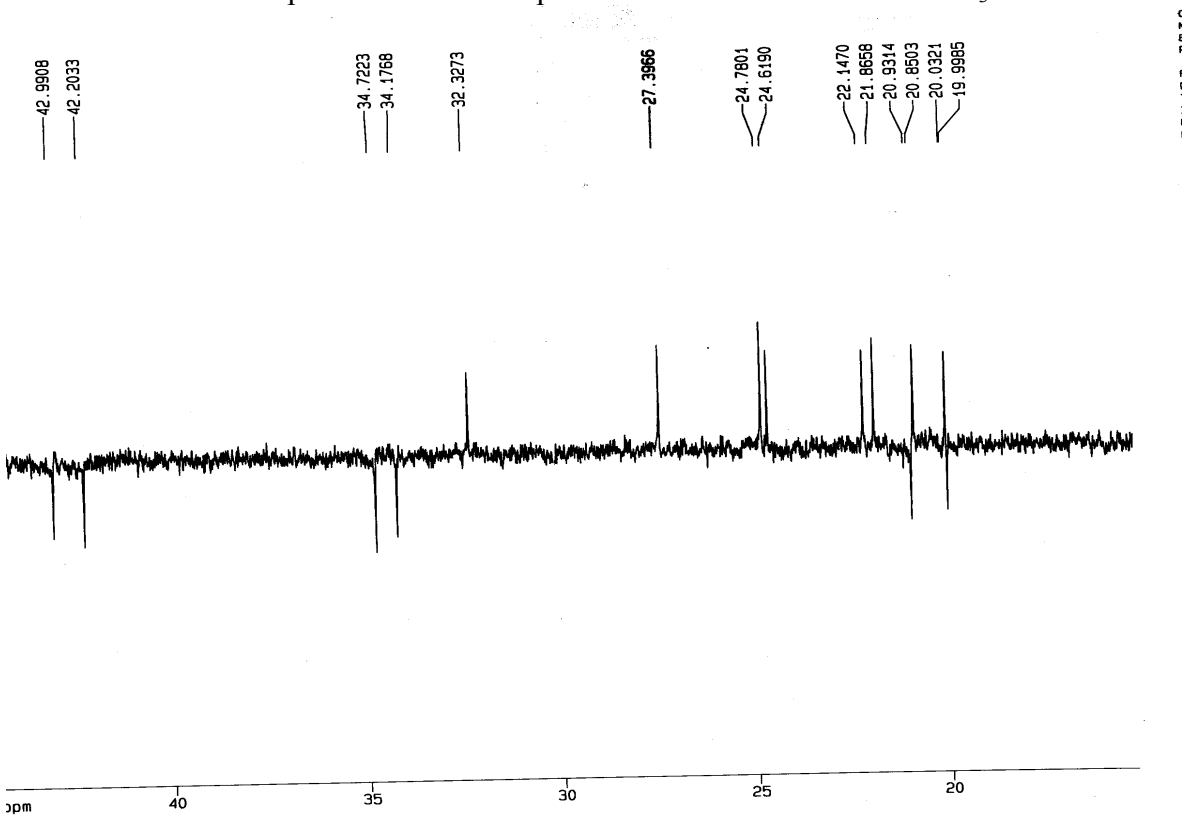

S21. ^{1}H ^{1}H COSY spectrum of Perovskone B in $CDCl_3$

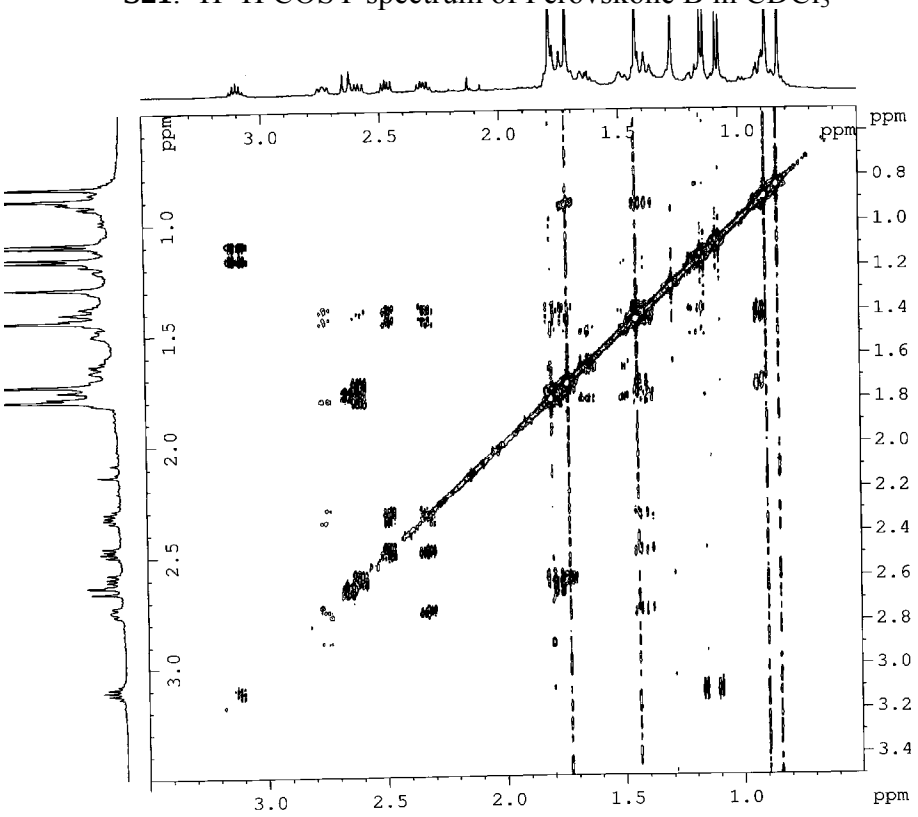

S22. HMQC spectrum of Perovskone B in $CDCl_3$

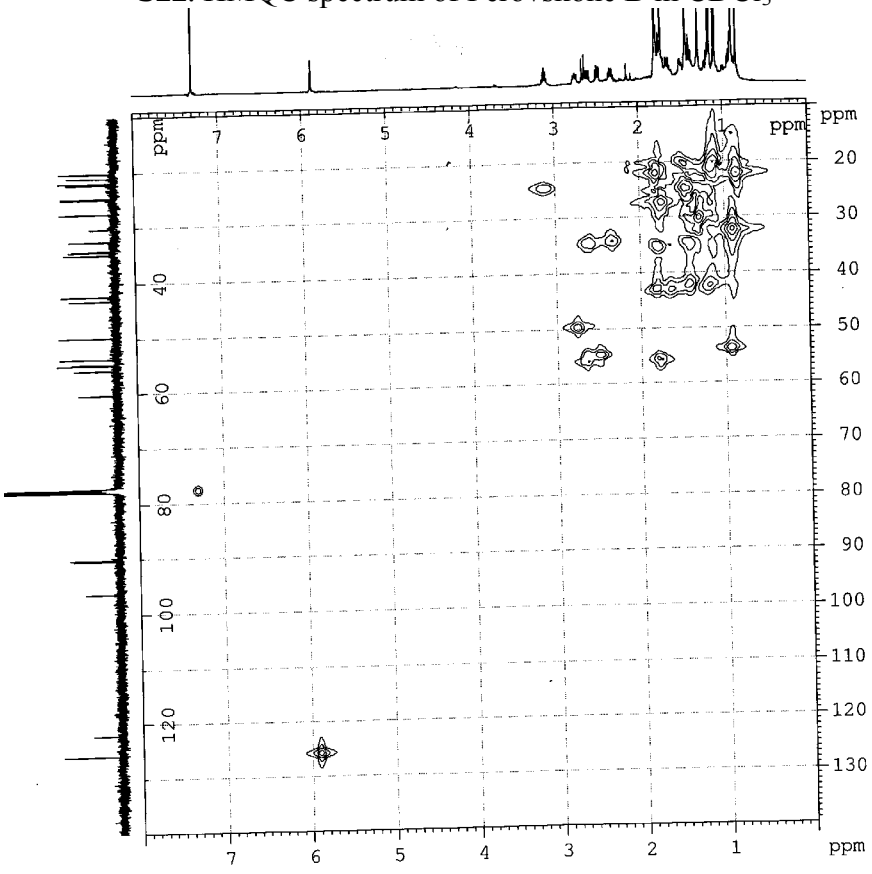

S23. Expanded HMQC spectrum of Perovskone B in $CDCl_3$

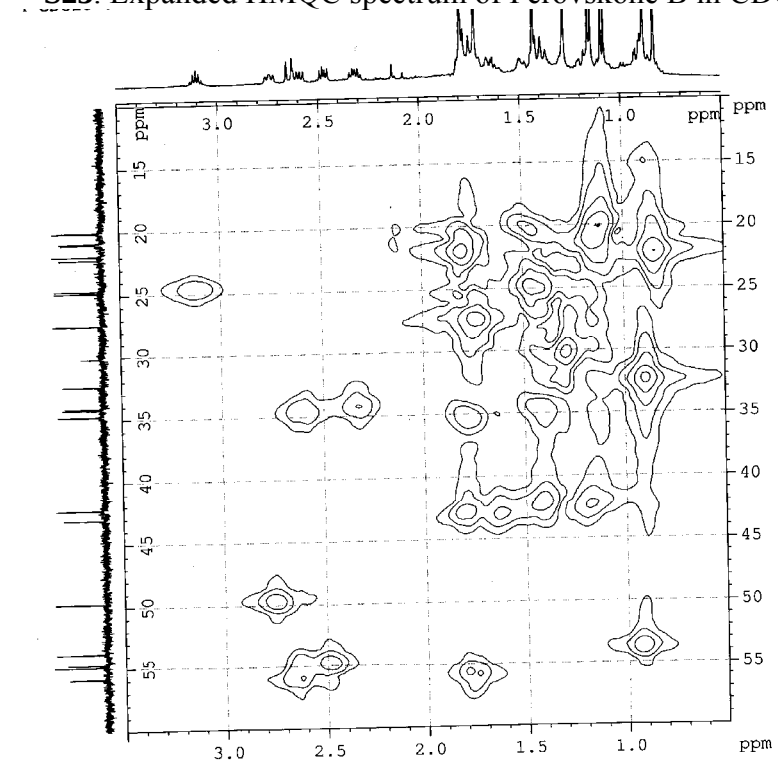

S24. HMBC spectrum of Perovskone B in $CDCl_3$

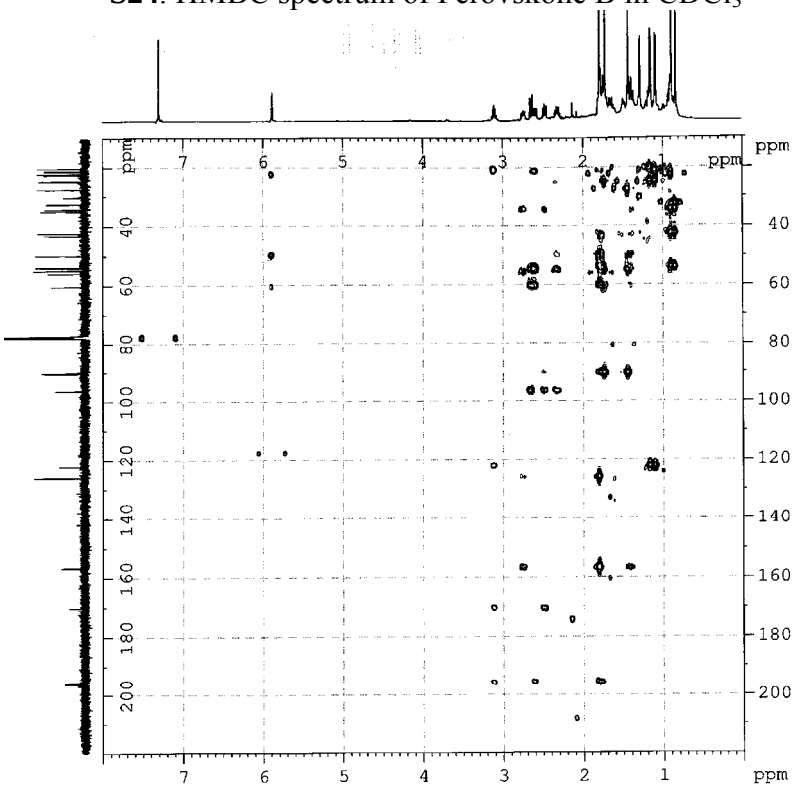

S25. Expanded HMBC spectrum of Perovskone B in $CDCl_3$

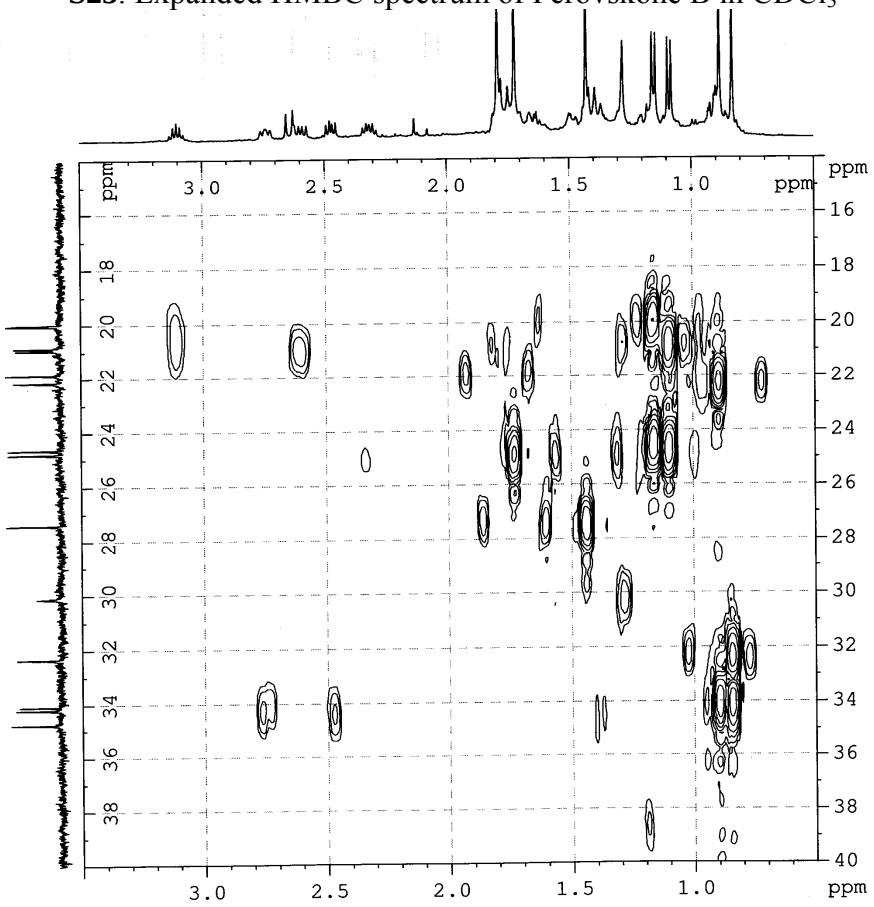

S26. NOESY spectrum of Perovskone B in $CDCl_3$

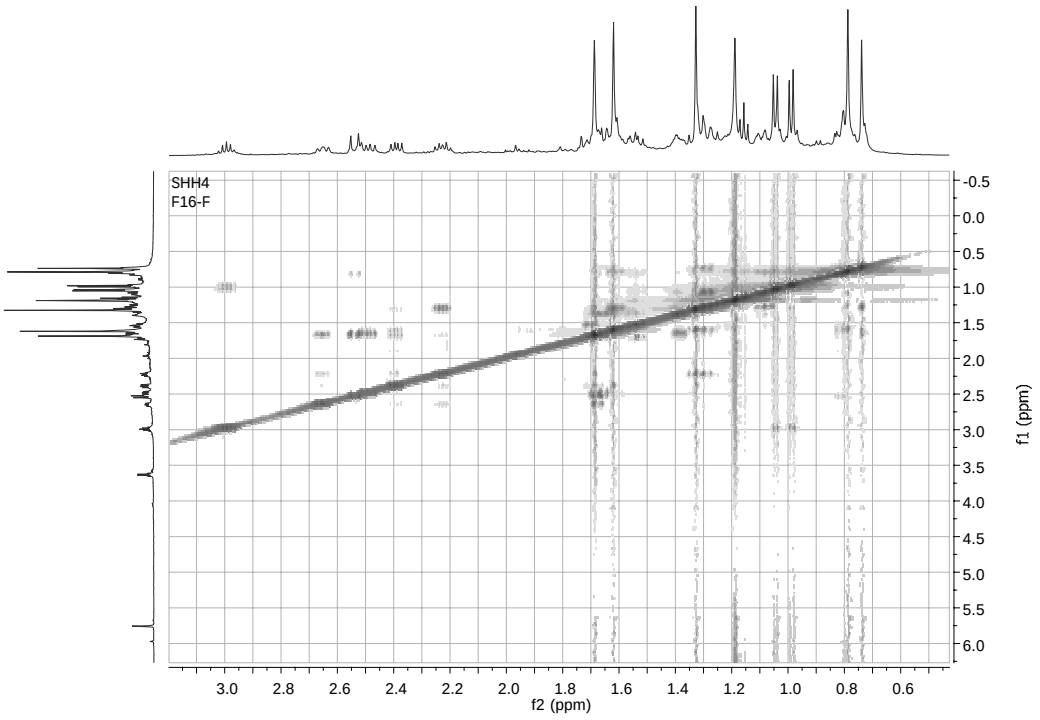

3. Conclusions and outlook

Iran has a highly diverse flora, and a high number of endemic plant species which are to be considered as a potentially rich source for novel phytochemicals. We investigated anti-parasitic activity against *P. falciparum* of selected Iranian medicinal plants. Several plant extracts mainly from species belonging to the Lamiaceae and Asteraceae families exhibited noticeable *in vitro* activity. Bioactivity guided phytochemical investigation of the extracts resulted in purification of several antiprotozoal compounds. A great number of the isolated compounds (almost 50%) had new structures, and we discovered several novel natural product scaffolds. This indicates that the diverse and unique flora of Iran has a great potential as a source of new natural compounds with sometimes unique skeletons. Although numerous plants of Iran have been phytochemically investigated, they have remained uninvestigated with respect to their bioactivity. Hence, they are a vast natural source for discovery of leads structure with new scaffold for a given target.

Moreover, establishment of an in-house extract library from Iranian plants will accelerate discovery of new bioactive molecules through high-throughput screening campaigns. We suggest that the plant collection be carried out based on ethnobotanical and taxonomical considerations.

Importance of sterochemical relevance on biological activity has made determination of the absolute configurations critical to understanding the behavior and interaction of chiral drugs with the biological environments. It is always a challenge for chemist to establish AC of chiral molecules by straightforward, nondestructive, and reliable methods. During the last decade quantum chemical calculations of chiroptical properties such as ECD, OR, and VCD have been established as reliable approaches for determination of the absolute configuration of optically active compounds. The interest in CD spectroscopy for determination of the AC of natural products has been steadily increasing (Figure 24). CD spectroscopy plays a significant role in the determination of ACs when their 3D structures cannot be elucidated by classical methods.

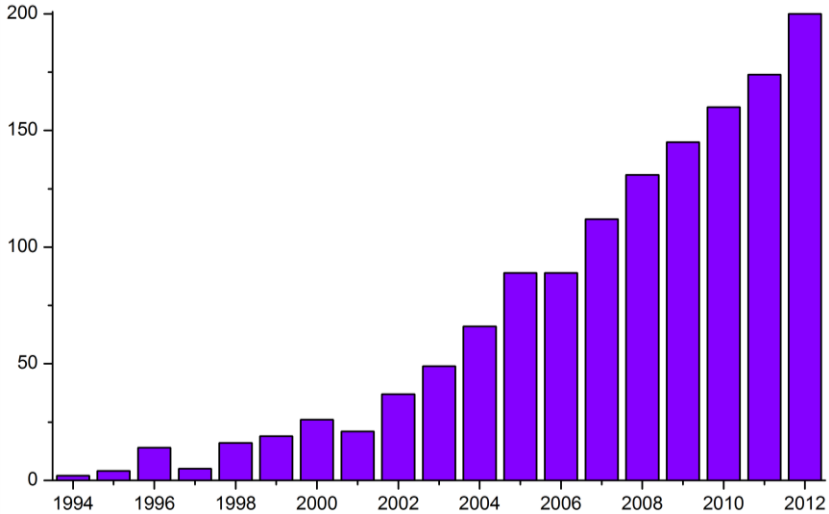

Figure 24: The number of annual published ECD related papers, the keyword was "circular dichroism + DFT". Source: SciFinder® database

In the course of this study, the AC of a wide range of new natural products was determined by calculation of ECD spectra and comparison with experimental data. We successfully applied this methodology to a diverse spectrum of conformationally rigid or flexible natural products, including abruquinones, acetylated furanocoumarins, terpenoids of various types, such as myrcene type monoterpenoids, bisabololoxide sesquiterpene diesters, abietane and labdane diterpenoids, manoloxide sesterterpenoids, ursane triterpenoids, as well as cardenolide glycosides, sesquiterpene coumarins, and complex isoprenoids with novel scaffolds. These compounds possess one to several stereogenic centers.

Undoubtedly, the application of quantum-chemically calculated chiroptical properties such as ECD, VCD, and OR, in combination with experimental data, has become an accepted means for fast, straightforward, and nondestructive assignment of AC in chiral compounds. By this approach the AC of compounds can be established within reasonable time. ECD is highly sensitive, but possesses low signal resolution. It works perfectly with rigid structures, but flexible molecules pose difficulties due to the simultaneous presence of several conformers with different population and optical contribution. Therefore, a careful conformational analysis is a very critical step in the prediction of ECD spectra.

A case in point of highly flexible bisaboloxides (**5**–**9**) (chapter 3.2), the relative stereochemistry of the entire molecule could not be established by NMR experiments due to a freely rotating bond between two discrete portions of the molecules. We demonstrated here that the absolute configuration could be established with the aid of ECD calculation in cases where relative stereochemical correlation of two portions of a molecule was not known. The assignment of AC was achieved through a careful conformational analysis of all relevant stereoisomers, followed by simulation of ECD spectra.

In some molecules the differences between ECD spectra of stereoisomers are not distinct enough to establish their AC. In these cases ECD data have to be combined with additional methods, such as calculation of optical rotation. In the case of the abietane diterpene sahandone (**4**) (chapter 3.1), for example, the AC was revised by calculation and comparison of the optical rotation values rather than ECD calculation.

Comparison of simulated ECD spectra with experimental data of a broad spectrum of new natural products revealed that TDB3LYP/6-31g** is a reliable approach for calculation of excitation states. Assignment of the AC of a compound is based on the comparison between calculated and experimental ECD spectra: the better they match, the more reliable conclusions can be drawn. However, conclusions for unambiguous configurational assignments can be drawn even if the calculated ECD spectra do not perfectly match with the experimental data. Comparison of ECD curves obtained for individual conformers of a compound showed that even subtle conformational differences may lead to substantial changes of the chiroptical properties. Consequently, the quality of predicted ECD data critically depends on a careful conformational analysis, and on the computational method used for prediction of CD spectra.

There are several examples in literature concerning revision of previously reported stereo structures. Consequently, ACs of some NP in the literature needs re-establishment by quantum chemical calculations of chiroptical properties.

Application of ECD spectra in establishing an AC requires existing of at least one UV-vis-NIR range chromophore, which enables correlation between 3D structure and the sign of spectrum. In case of lacking appropriate chromophore, VCD technique can be used as an alternative chiroptical tool for determination of molecular structure of chiral compounds (such as sanandajin, chapter 3.3). Also, in case of high conformational flexibility in solution, the novel solid-state CD method should be considered as an important tool for the determination of AC.

Acknowledgments

I would like to thank, first and foremost, Prof. Matthias Hamburger who gave me opportunity to join his research group and doing my PhD here in Basel. I thank him for his support, encouragement, and excellent advices during my entire PhD program.

I would like to express my gratitude to Prof. Jean-Luc Wolfender and Prof. Angelo Vedani whom accepted to be co-referee and chair in PhD examination.

I want to express my sincere appreciation to Dr. Michele Adams and Dr. Mouhssin Oufir, Christian Abbet, and Dr. Fahimeh Moradi whom edited my thesis with amazing patience and perception. To Steffi, for her fantastic work and great help in biological parts of my thesis and for all the exciting scientific works we published together. Also I would like to thank Prof. Reto Brun and Mr. Marcel Kaiser from Swiss Tropical and Public Health Institute for excellent collaborations.

Thanks are due to PD Dr. Olivier Potterat for his help and great support during my PhD time. Orlando and Manuela thank you so much for your assistance in laboratory and administration issues, you are great!

I thank Dr. Martin Smiesko because of great support I had during my PhD in application ab initio techniques. Also my best thanks to Dr. Janine Zaugg where we started together this exciting topic in chirality where I learned a lot from you.

Thanks to Dr. Inken Plitzko, Dr. Maria de Meri and Dr. Melanie Raith for your assistance in measuring NMR spectra and structure elucidation of natural compounds.

I would like to acknowledge my collogues in Iran, Dr. Moridi, Prof. Salehi, Dr. Sonboli, Dr. Ghassempour, Mr. Bahdori and Mr. Dastan for their help and support.

My warm thanks to all current and former colleagues from the Division of Pharmaceutical Biology in Basel. It was and it still is a pleasure to work with you.

I would like to thank Iranian Scholarship office for financial support of my PhD program.

Finally, very special thanks are extended to members of my family, especially my wife, Eli, for her love and constant support, understanding and encouragement.